CERN/1050
14 JANUARY 1972

THE 300 GeV PROGRAMME

CERN EUROPEAN ORGANIZATION FOR NUCLEAR RESEARCH

THE 300 GeV PROGRAMME

CERN/1050
14 JANUARY 1972

THE 300 GeV PROGRAMME

CERN

EUROPEAN ORGANIZATION
FOR NUCLEAR RESEARCH

CERN - Service d'Information scientifique - H/487 - 4000 - janvier 1972

Index

Chapter 1

INTRODUCTION

Towards the end of 1970, a report was issued covering the design of experimental facilities for nuclear particle physics research in Europe at a proton energy level of 300 GeV (report MC/60 Vols I and II). This report was the result of studies undertaken at CERN during 1970 by a group of people called the "300 GeV Machine Committee". The group consisted of staff of the European national accelerator laboratories and staff of CERN. Apart from three CERN staff, all the members of the group worked part-time on the design studies and they involved in the work many of their own staff in the national laboratories and at CERN. Thus the studies were carried out and the report was written by people who at that time had no idea whether the programme they proposed would ever be carried out nor whether they themselves would take part in it.

The accelerator and its auxiliary equipment described in report MC/60, although providing almost the same experimental facilities as proposed in several previous reports, did so in a way fundamentally different from the ways previously proposed. Previously the idea had always been to build a complete set of experimental facilities and an entirely new laboratory quite separate from the existing CERN laboratory at Meyrin and somewhere else in Europe. Report MC/60 presented a programme based on the idea of building the new accelerator next door to the CERN-Meyrin laboratory and of using major equipment already existing or being constructed at the Meyrin laboratory as an integral part of the new facilities. This idea, which was first put forward in the spring of 1970, enabled the cost of the 300 GeV Programme to be reduced to nearly half the cost of the programme put forward in 1964 (see report CERN/563) and it enabled research to start using the new facilities about three years earlier than previously forseen.

In February 1971, the Council of CERN approved the programme described in MC/60 and immediately work began. The first task was to build up a design and construction staff who would see the programme through to its conclusion. Once sufficient staff were in post, the job of the detailed design of the accelerator and its component parts began in earnest.

Some of the staff who joined the 300 GeV Programme after its approval took part in the studies which resulted in report MC/60 and that report naturally formed the basis of the work carried out in 1971. However, the design was now being carried out by people who were responsible for the machine components which they and their staff would be building during

the course of the programme. Not only was the general design of the accelerator and its parameters completely reviewed, but each component part was examined in great detail both with regard to its technical practicability and with an eye to possible cost reductions. The result is this report.

Comparing this report on the European 300 GeV facilities with its predecessor MC/60, the similarities are far more evident than the differences. In fact a cursory reading of the two reports will hardly reveal their differences. This, in a sense, is a comforting fact since it means that a further year's study by the final project team has not revealed any major shortcomings of the 1970 study. Certainly there are some differences, for example the choice of a window frame magnet design rather than the H magnet design which was favoured in MC/60, but generally the overall design and that of the component parts are not greatly changed.

As far as the experimental facilities provided by the 300 GeV Programme are concerned, the basic specification remains unaltered although there are many detailed changes incorporated as a result of a dialogue between machine builders and experimental physicists which went on during the whole of 1971 and is still continuing.

The programme still envisages that a beam of protons of 200 GeV energy will be available to feed experiments in the West Hall of the existing laboratory in the sixth year of the programme, that is to say 1976, and 300 GeV protons will be fed to the North Experimental Area on the new site at the end of the programme, that is in 1979. As described in MC/60 and in this report, there are many alternative options to this particular programme which have to be taken up or abandoned at different times during the course of the programme. For example, towards the end of 1973, it must be decided whether to order another set of iron-cored bending magnets, identical to the first set which will give 200 GeV energy and which will be ordered towards the end of 1972, or whether to order a set of superconducting bending magnets.

However, due to the dialogue between experimental physicists and machine builders already mentioned, the beam layout in the West Hall has been completely revised. Previously it was proposed simply to bring the beam of 200 GeV protons up to the entrance of the West Hall and, from targets placed in the ante-rooms of the West Hall, to generate all secondary beams required for experimentation. Now it is proposed to construct a switchyard deep underground near the ejection system of the machine in which can be generated an r.f. separated beam for BEBC and, if required, a neutrino beam also using BEBC as the detector. The r.f. separated beam and the 200 GeV proton beam now share the tunnel from the switchyard up to the West Hall. These and other modifications improve the range of experimentation possible in the West Hall but inevitably they cost money and one of the major problems in the years ahead will be how many of the experimental possibilities described in this report can be built within the annual budgets now agreed for the two laboratories of CERN.

It is impossible to end an introduction to a report of this kind without reference to the two limiting factors which beset all projects, namely time and money.

During the evolution of the 300 GeV Programme there have been two pressures which inevitably have moulded the programme. One has been the natural desire of the Member States to reduce programme cost to the bare minimum which will satisfy the requirements. As a result of this pressure the budgets now allocated only just cover the necessary items of the programme and much will depend on the tender prices that European industry will offer for the component parts in the next few years. The other pressure, acting in the opposite direction, comes from the experimental physicists who, just as naturally, want the programme to provide them with facilities as extensive as possible as fast as possible.

The 300 GeV Programme as it now stands is a compromise which has been reached as a result of the interplay of these two pressures. The budget of 1150 MSF at 1970 costs now agreed for the programme should, with reasonable good fortune and careful management, cover the programme as it is described. Any modifications or options arising in the course of the programme can only be adopted if they do not increase the costs of the programme. The time schedules are extremely tight; five years from a start from zero to 200 GeV is a very ambitious programme, especially when it is remembered that it took six years to build the CERN 28 GeV proton synchrotron which is less than a tenth the size. If this schedule is to be realised it is clear that only modifications to the programme which are not time consuming can be entertained.

The European 300 GeV Programme has now run one year and so far there have been no unpleasant surprises. The staff recruitment has gone according to plan; the first two major contracts for civil engineering work have been placed at costs within the estimates. Such modifications to the programme as have been suggested and adopted can be contained within the project costs and time scales. It can only be hoped that these early favourable experiences will continue throughout the programme.

Chapter 2

THE MACHINE LATTICE

2.1 General Description

The lattice is of separated function type and FODO configuration. This is in contrast to the first generation of alternating gradient synchrotrons which were of combined function type and in which magnets with hyperbolic poles bent and at the same time focused the proton beam. In the separated function type of machine bending is provided by simple dipole magnets, focusing by relatively few quadrupole magnets. The two types of lattice have been compared in considerable detail. There seems to be no difference in cost but the separated function lattice has a number of other advantages.

One of these advantages is that the simple dipole magnets can run at a field of 1.8 Tesla. This is 50% higher than, for example, the field at the equilibrium orbit in the CPS magnets, and leads to a compact ring. It is this feature that makes it possible to construct a machine of up to 400 GeV within a mean radius of 1100 m, the maximum possible on the CERN II site. The FODO configuration in which focusing and defocusing quadrupoles are equally spaced around the ring, as well as being the cheapest of the many alternatives studied, is also the most compact.

Another advantage of the separated function lattice is that the long straight sections necessary for injection, ejection, r.f. etc. can simply be provided by omitting bending magnets from the lattice. The regular focusing properties of the machine are therefore uninterrupted and there is no need for special matched insertions.

This independence of focusing and bending systems makes it particularly simple to use the missing-magnet principle which allows one to develop the energy of the machine by leaving out some bending magnets in each period initially and adding them later.

2.2 The Missing Magnet Concept

2.2.1 The three stages with conventional magnets

The machine may be equipped with conventional magnets in three stages:

Table 2.2

Stage	Energy (GeV)	Magnets per semi-period*
A	200	2
B	300	3
C	400	4

Stage A (200 GeV) is the machine with only half the bending magnets installed. This machine can be completed in about five years and leaves open the option of filling the remaining half of the machine with superconducting magnets. These by themselves would raise the energy to above 500 GeV (assuming a field of 4.5 T) or 700 GeV if both superconducting and conventional magnets were powered together.

Should it become clear later in the construction period that there is no reasonable hope of using superconducting magnets within the timescale and should the physics interest make the extra 100 GeV important one could decide to order and install a third magnet in each semi-period (Stage B). The decision will be taken in the third year of the construction period so that the date of completion of either stage is not delayed beyond the limit already set by the expenditure profile. Stage B, being more expensive than Stage A, would be completed about a year later, i.e. towards the end of the sixth year. The remaining two years of the Programme will be devoted to completing and equipping the North Experimental Area. Stage B, 300 GeV, is the nominal design matched to the Programme budget. It is not possible within the budget to fill the whole of the 2.2 km diameter ring with magnets unless magnet prices or those of other components turn out to be less than we have estimated but if this proved to be the case a fourth magnet per semi-period could be installed giving Stage C, 400 GeV.

2.2.2 Geometry

The principal parameters of the lattice are given in Table 2.1. In each of the 216 semi-periods there is room between adjacent quadrupoles for the four conventional bending magnets 6.26 m long of Stage C. This is shown in Fig. 2.1. Also shown dotted in this figure are the two magnets of Stage A. In changing from A to C only a slight realignment of the outer pair of magnets is needed. The sagittal distance $x \simeq R\,(\pi/N)^2/16 = 5.8$ cm.

A semi-period of the Stage B machine will contain two B1 magnets and one B2. The realignment necessary on adding the second B1 magnet is less than 5.8 cm but because of the asymmetry introduced the D quadrupoles must be moved sideways.

---

* The circumference of the machine is divided into 216 semi-periods nearly all of which contain bending magnets.

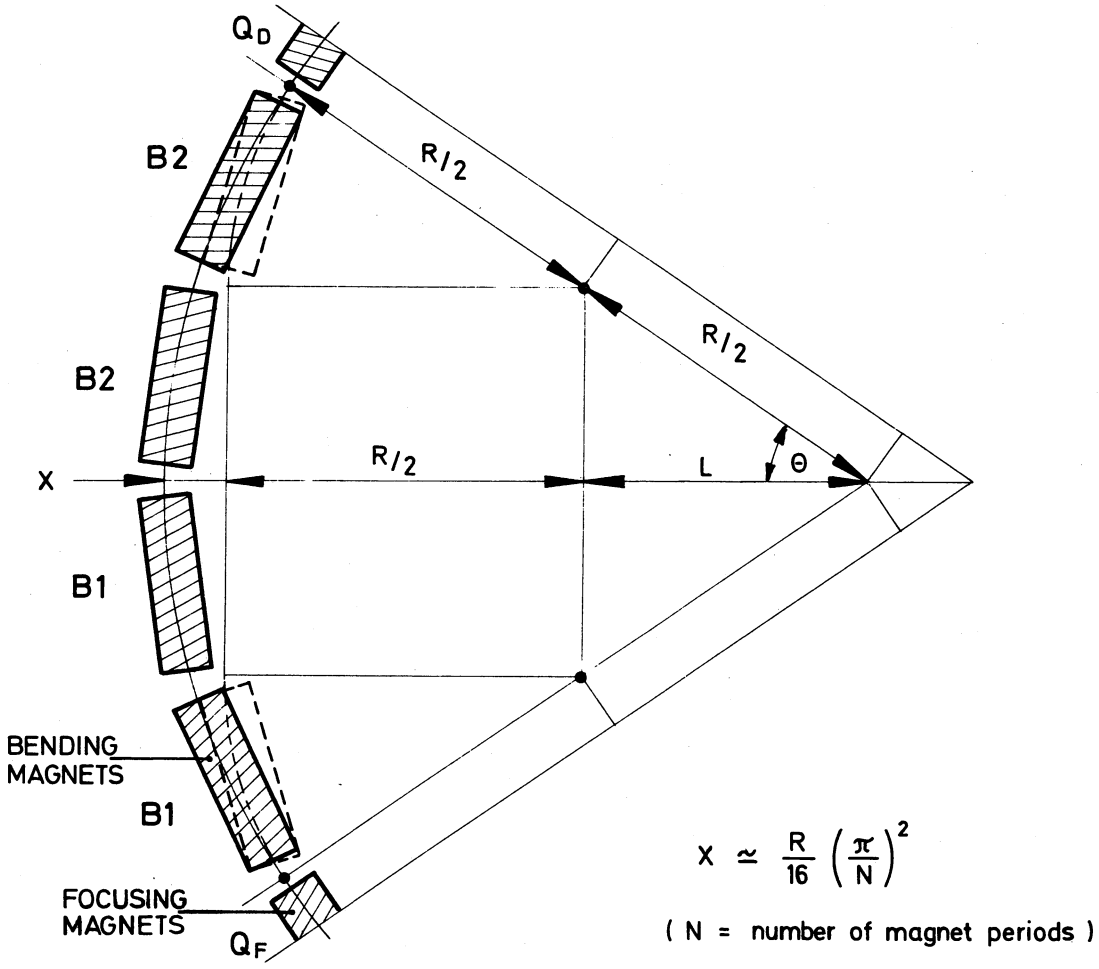

Fig. 2.1 Missing magnet geometry (one half period)

Table 2.1

Lattice and Orbit Parameters

		A	B	C	
Maximum momentum		200	300	400	GeV/c
Maximum bending field		1.8	1.8	1.8	T
Magnetic bending radius		370.6	555.9	741.3	m
Mean radius		1100	1100	1100	m
Injection momentum		10	10	10	GeV/c
Injection field		0.090	0.060	0.045	T
Number of bending magnets per normal period		4	6	8	
Quadrupole gradient for Q = 28.75	F	9.95	14.93	19.90	T/m
	D	9.94	14.91	19.89	T/m
Quadrupole gradient for Q = 27.75	F	9.68	14.53	19.37	T/m
	D	9.67	14.51	19.36	T/m
Nominal length of quadrupoles				3.22	m
Nominal length of bending magnet				6.26	m
Length of inter-magnet gap				0.40	m
Length of short straight section				2.225	m
Free length in empty semi-period				28.78	m
Length of period				63.99	m
Structure of a period				FODO	
Number of periods	(N)			108	
Number of superperiods	(S)			6	
Nominal working point	(Q)			27.75	
Lattice functions for Q = 27.75					
Phase advance/period	(μ)			92.5	°
Maximum β value in F quadrupole	($\hat{\beta}_H$)			108.9	m
Maximum β value in D quadrupole	($\hat{\beta}_V$)			109.0	m
Minimum β value in D quadrupole	($\check{\beta}_H$)			18.0	m
Minimum β value in F quadrupole	($\check{\beta}_V$)			18.0	m
Maximum of momentum compaction function	($\hat{\alpha}_p$)	4.25	4.36	4.25	m
Minimum of momentum compaction function	($\check{\alpha}_p$)			-0.028	m
Total transition energy/rest energy	(γ_{tr})	23.78	23.33	24.08	

Now that the geometry of the machine is fixed, any change in the distribution of magnets around the ring occasioned by the missing magnet scheme must be applied evenly around the ring. It is not possible to either increase or decrease the extent of the long straight sections and keep the machine figure within the confines of the tunnel.

2.2.3 Superconducting conversion procedure

Removing nearly 1000 conventional magnets from a ring of this size and replacing them with superconducting magnets would be a long procedure lasting more than a year. During this time experiments would stop. Suggestions for superconducting conversion of the machine avoid this problem either by building an autonomous superconducting ring mounted above the conventional machine or in a separate tunnel, or by implementing a missing-magnet conversion procedure.

In the missing-magnet scheme the superconducting magnets might be wheeled in in multiples of six during the normal shut-down periods, installed in position but left dead. Once there and tested, both superconducting and conventional magnets would be moved a few centimetres to their new positions and realigned. This might take as little as a month. The superconducting machine would then be ready for commissioning. Should any unforeseen operational difficulty be experienced it is even possible to return to the old alignment positions and run the machine as before.

As far as one can predict, it will not be easy to construct a superconducting magnet whose aperture has a very high aspect ratio. It may also be an advantage to reduce the number of individual cryostats. For these reasons we have omitted in Stage A the two adjacent magnets which lie near the centre of the semi-period rather than the outer pair.

The final conversion to a fully superconducting machine would, of course, require a long interruption in the operation of the machine but at a time when one would have considerable experience of the problems of manufacturing and operating pulsed superconducting magnets. If the conventional magnets and quadrupoles were all replaced the energy at 4.5 Tesla would be above 1000 GeV.

2.2.4 Quadrupole strength

The strength of the quadrupoles is sufficient for Stage C. If in the third year it is decided to complete the machine at Stage A to leave space for superconducting magnets, an estimate will then be made of the extra quadrupole strength needed to cover the superconducting option. Probably the existing quadrupoles would be of sufficient strength to tune the superconducting machine to Q = 21.75 instead of 27.75 and this might be tolerated as a working point. Failing this an additional quadrupole could be placed beside the existing one. In order to make room for this, B1 and B2 could be moved somewhat closer together. The space for the superconducting magnets would then become somewhat shorter.

2.3 The Normal Period

The 108 focusing periods of the lattice are identical and have a FODO configuration. They each contain two quadrupoles (F and D) followed by equal drift lengths (0). In 84 of the periods each of the drift lengths contains a full complement of bending magnets. These are the normal periods. Figure 2.2 shows the arrangement of magnets in a normal period together with the betatron amplitude, β, and the phase advance, μ, in both horizontal and vertical planes. Also shown are the beam envelopes, a/2, at a point in the lattice where they are largest. The orbit functions are not significantly different for the A, B and C stages.

The FODO configuration has been chosen because it requires the least amount of focusing strength and hence, in a separated-function machine, results in the smallest radius. Another advantage of the FODO configuration is that the betatron amplitude is very different at the F and D quadrupoles so that correcting elements in the short straight sections which precede the quadrupoles act almost independently on the horizontal and vertical dynamics. Since a large value of β naturally occurs in the normal period it is unnecessary to use a special focusing insertion to inflate β at the ejection septum where a large β contributes to a high ejection efficiency.

A consequence of the large β_{max}/β_{min} ratio is that the width and height of the beam vary considerably throughout the period and at least two bending magnet types, B1 and B2, are required if aperture and stored energy are not to be wasted. The savings in stored energy and in magnet power supply cost are made by specifying two magnet types rather than one and outweigh the increase in development cost but this proves not to be the case if more than two magnet types are specified. B1 close to the F quadrupole has a large horizontal aperture and a narrow gap. B2 close to the D quadrupole has more square aperture. The sequence of magnets B1, B1, B2, B2 in the FD semi-period is reversed in the DF semi-period.

Although the aspect ratios of the beam at the F and D quadrupoles are quite different, both beam profiles fit conveniently into the same quadrupole aperture. The F and D quadrupoles are therefore identical, are powered in series and have a trim winding for independent adjustment of F and D strengths. This enables Q to be adjusted during the cycle. The F and D quadrupoles on either side of the ejection magnet will be of slightly different design to facilitate the passage of the extracted beam. This will pass just outside the good field region of the F quadrupole and between the coils. It will graze the yoke of the D quadrupole.

The number of periods and the betatron phase advance per period were free parameters in the lattice design and were therefore made the subject of an optimization study. It was first established by designing a number of lattices that there was a very flat cost optimum in phase advance between $\mu = 70^{\circ}$ and 100° and in periodicity of between 90 and 130. Increasing the

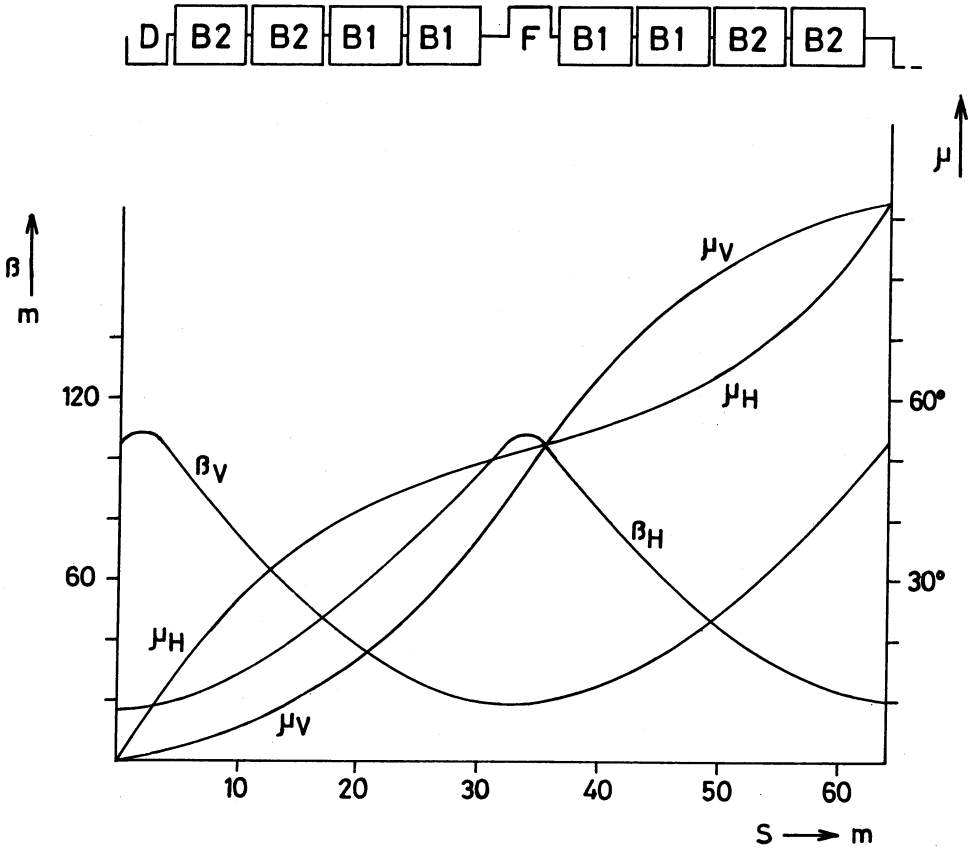

Fig. 2.2 a) Lattice functions in a period

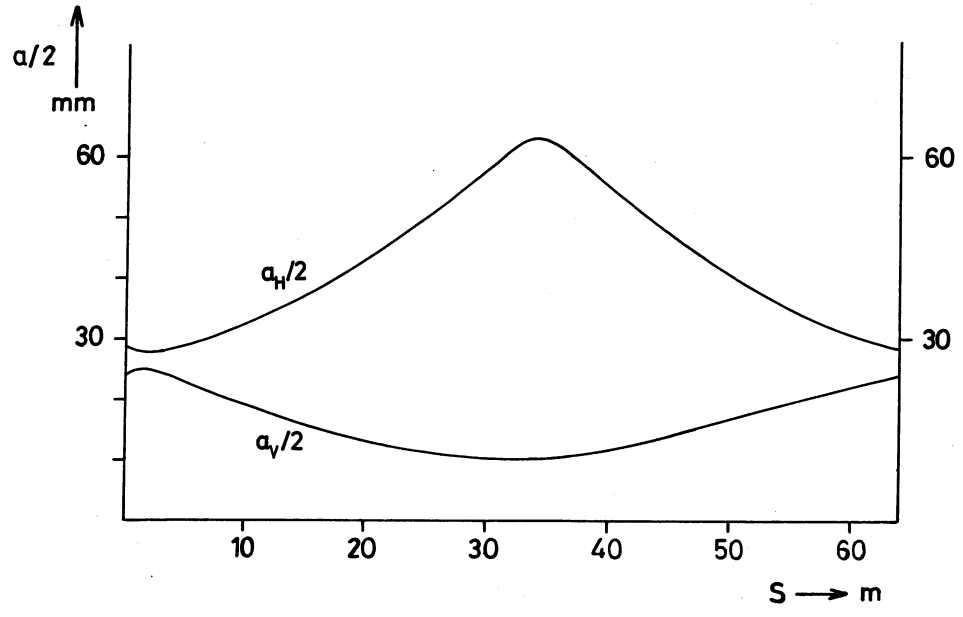

Fig. 2.2 b) Semi-apertures in period with $\alpha_{p,max}$

periodicity, N, reduces α_p and increases γ_{tr}. Both of these tendencies are desirable from the point of view of transfer from the CPS since acceptance of the main ring is limited at transition by the large momentum spread. Increasing N also had a general tendency to reduce apertures and stored energy.

On the other hand, a large number of periods imply a small β_{max} and a short distance between quadrupoles, features which hamper efficient slow ejection. The lattices with higher N contain more magnet units and also tend to demand higher field from the bending magnets since a larger proportion of the ring must be devoted to focusing magnets.

Fortunately, a small range of periodicities which includes N = 108 and 114 was found to satisfy these constraints and finally N = 108 was chosen since it is in this narrow range, it lies in the cost optimum and it is a number with many factors, an important consideration for the location of correcting elements.

A phase advance close to 90° was thought desirable since it simplified many of the correction procedures, notably closed-orbit correction. The quantization of Q dictated by structure resonances (Section 2.6) leads to a number of possible working points. 26.25, 27.75 and 28.75 have phase advances close to 90° and are remote from first and second order stop bands. Of these 27.75 ($\mu = 92.5^\circ$) has been chosen as the nominal value although quadrupoles are strong enough to drive Q to 28.75 for reasons which are discussed later in Section 2.6.

The 0.4 m gap between magnets is sufficient only for a vacuum connection and bellows and to leave room for the coil overhangs. All correction and diagnostic equipment together with special quadrupoles, sextupoles and dipoles for ejection will be placed in the short straight section, 2.2 m long, preceding each quadrupole. Even in the special periods this space will be reserved for these components.

2.4 Long Straight Section Insertions

The machine is divided into six identical superperiods. Each superperiod is composed of fourteen normal periods and a sequence of four special periods which form the long straight section insertion (Fig. 2.3a). Some or all of the bending magnets are omitted from the special periods to make room for the bulky components of the machine but the regular spacing of quadrupoles is preserved throughout the superperiod.

The six long straight sections of the machine are equally spaced around the ring. Straight section number 1 is assigned to the injection system for the input beam from the CPS, the second to an extraction system to the North Experimental Area, a third to the r.f. accelerating system, a fourth to a beam dump and the fifth reserved for future developments. Straight section 6 is used for the extraction system to the West Hall.

Numbers in diagonal box give n° of bends
in each semi-period.
4/4 = normal period (N.P.)

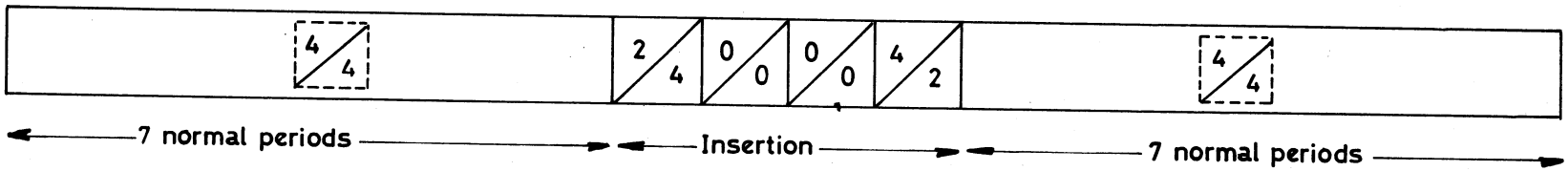

Fig. 2.3 a) Composition of the super-period

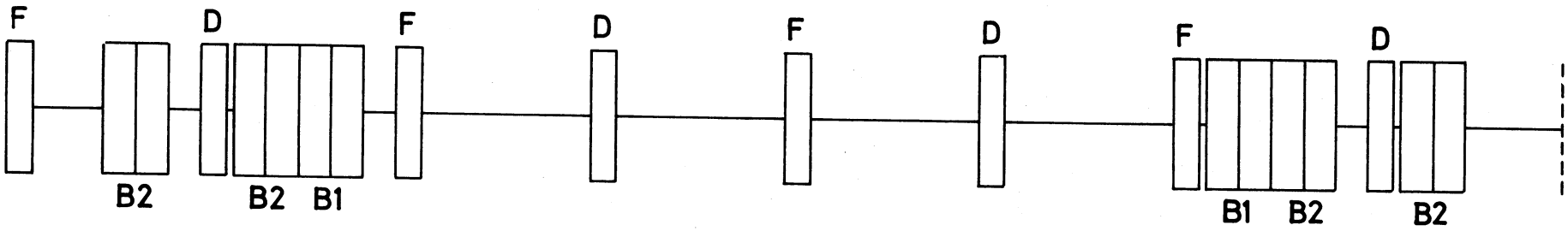

Fig. 2.3 b) The insertion (Stage C)

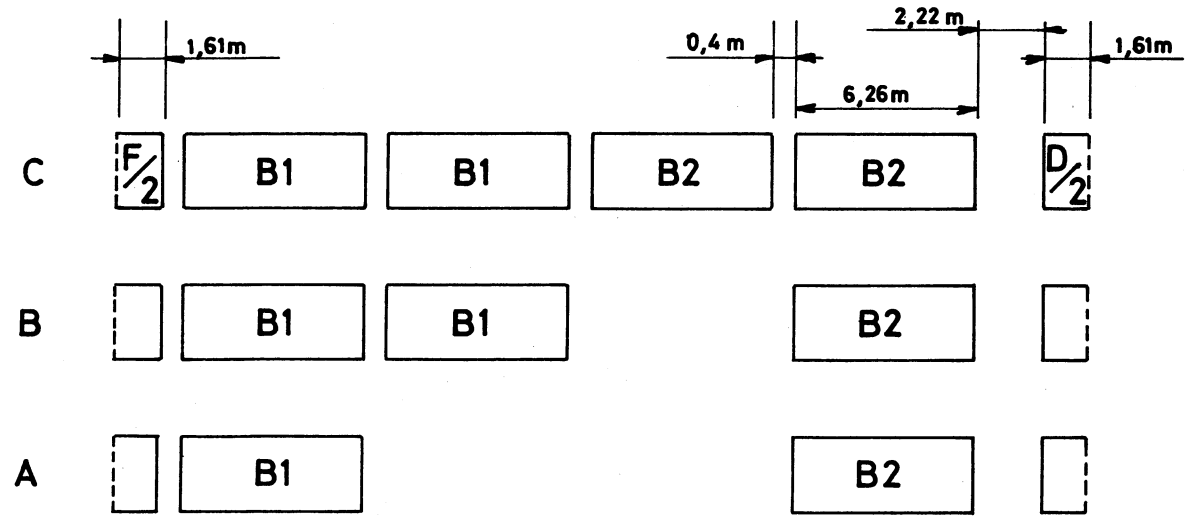

Fig. 2.4 a) Normal semi-period

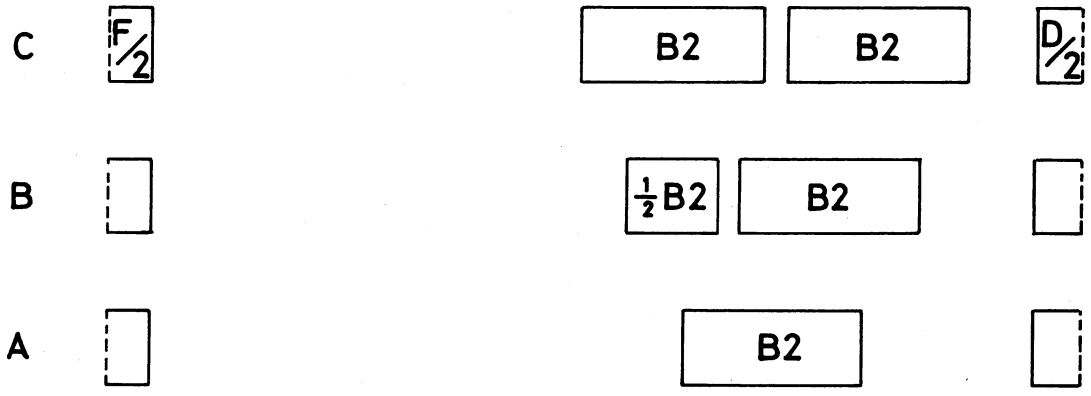

Fig. 2.4 b) Special insertion

In a later Section we shall see that the superperiodicity (S = 6) gives rise to a pattern of stop bands which determine the working point Q. A smaller number of insertions would cause this pattern to shrink and it would be hard to find a Q value sufficiently far from a stop band. The superperiodicity of six also places the injection and ejection paths in good alignment with the existing ejected beam from the CPS and with the West Area.

The sequence of special periods in the insertion is shown in Fig. 2.3b for the full (Stage C) machine. The pattern is mainly determined by the design of the extraction channel. In straight section 3, three of the empty semi-periods will be filled with the r.f. cavities of the accelerating system. In the two straight sections used for extraction the four empty semi-periods provide space for the septa of the extraction channel. The two semi-periods which contain only half the normal complement of magnets, the special semi-periods, leave room for fast ejection kickers and other elements of the extraction system.

Figure 2.4 shows the arrangement of magnets in these special semi-periods at the three stages. In order to maintain the 2/3/4 ratio in the development of the bending strength one B2 magnet and a half version of B2 will be used in Stage B.

There is no break in the regular focusing structure of the machine since enough space can be made for the extraction channel simply by omitting bending magnets. This has the advantage that only one type of quadrupole need be made and numerological relationships linking resonance lines with the sixfold symmetry in focusing are eliminated. Inevitably, as in any machine with a superperiodicity in the pattern of bending, the momentum compaction function, α_p, beats around the ring so that its peak excursion is almost twice as large as it would be in a homogeneous machine (Fig. 2.5). This, however, can be turned to our advantage. α_p is small in the neighbourhood of the insertion itself and the beam does not fill the horizontal aperture of the magnets. This provides valuable space for the injected and ejected beam paths. Another useful feature is that beam losses can be localised in a few regions where α_p is maximum and where special precautions may be taken against radiation damage.

2.5 Aperture Requirements

The beam size at injection and transition is calculated by adding the amplitude of betatron oscillations for a given emittance, the expected amplitude of closed-orbit distortion and, in the horizontal plane, the allowance for the momentum spread. The random errors which will cause closed-orbit distortions are listed in Table 2.3 together with their individual contributions to the uncorrected closed-orbit amplitude.

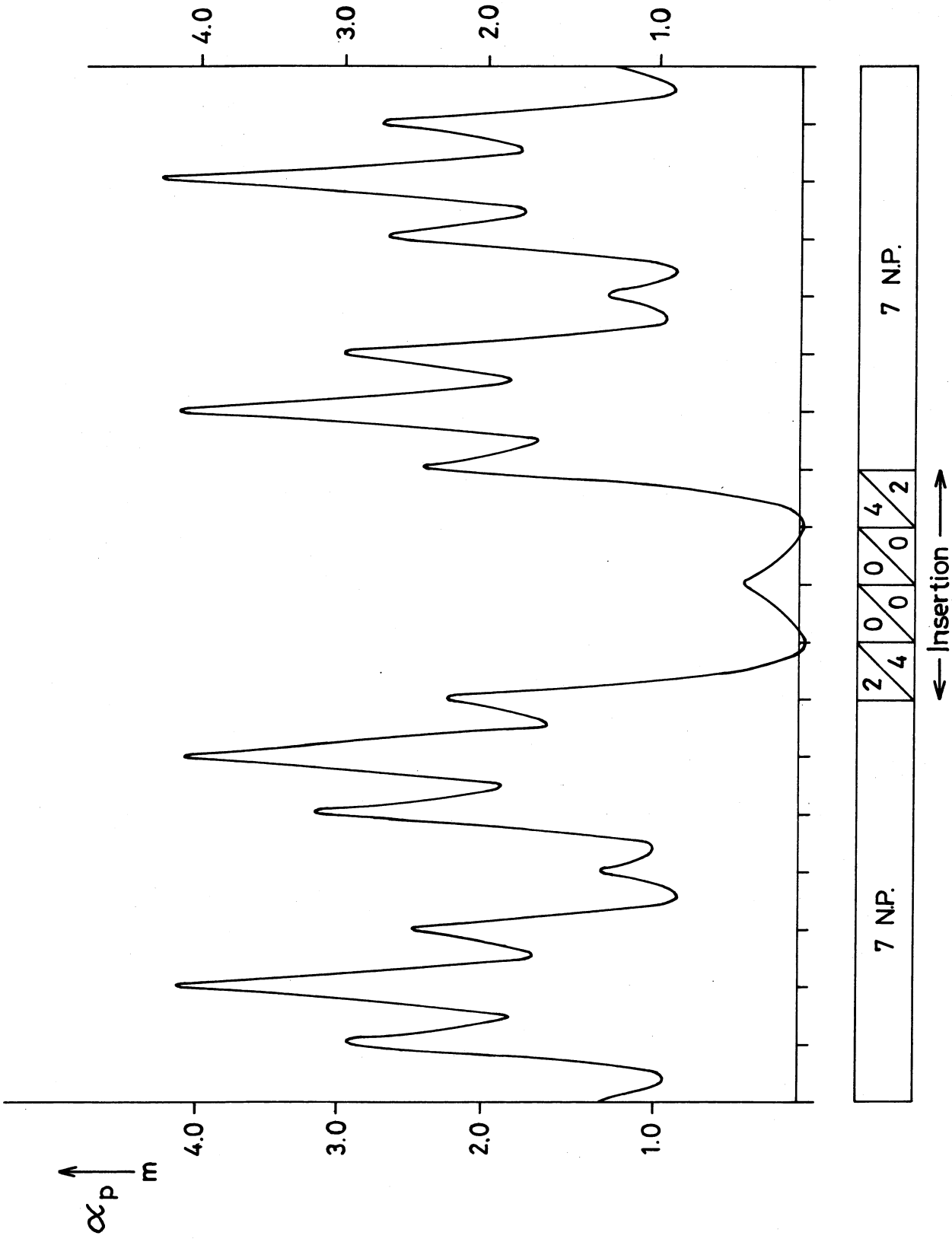

Fig. 2.5 Momentum compaction function in one super-period

Table 2.3

Random error	Tolerance (r.m.s.)	Distortion amplitude (mm) horizontal	vertical
Misalignment of quadrupoles	0.15 mm	14.4	14.6
Field errors ($\Delta B/B$)	5×10^{-4}	21.1	
Median plane tilt	0.2 mrad		8.6
Stray vertical field	0.28 G	20.8	
Stray horizontal field	0.11 G		8.3
r.m.s. sum of components		33.0	18.7

These contributions and their r.m.s. sum are computed at the 98% confidence level. There is only a 2% probability that they will be exceeded. This procedure for estimating the closed-orbit allowance is similar to that which was adopted in the 1964 Design Report following a detailed examination of measurements of closed-orbit amplitudes in the CPS. In the 1964 Design Report, however, apertures were calculated by combining the uncorrected closed-orbit allowance with the full design emittance of the injected beam. This resulted in apertures which we now consider to be too large. Since 1964 the correction of closed-orbit distortion by cybernetic techniques has been successfully applied to the CPS and other accelerators. It now seems reasonable to determine apertures by combining the design emittance, not with the uncorrected closed-orbit amplitude, but with the amplitude after correction has been applied. This saves a large fraction, about 30%, of the magnet aperture and reduces the cost of the magnets and their power supply considerably.

Figure 2.6 shows how we expect the correction of closed-orbit distortion to be progressively applied and acceptance to improve during the development of the machine. The "staircases" mark the boundary between the allowance for closed-orbit distortion and the allowance for betatron oscillations. The upper diagram shows the breakdown of apertures at injection at a point in the lattice where β_V is maximum, the centre of a D quadrupole.

In the first step we see the breakdown before systematic correction is applied. There is just room for a pencil beam to circulate. As correction is applied acceptance improves until, in the final step, the closed-orbit distortion amplitude assumed is close to the 5 mm residual amplitude we expect after full correction has been applied (Chapter 9). The vertical acceptance of the machine will then be 3.4 π mm mradians at injection ($E\beta\gamma$ = 36 π mm milliradians).

In the horizontal plane shown in the lower figure at a position where both β and α_p are maximum the picture is more complicated. The first step as before shows the space available for a pencil beam and the next two steps show how larger injected beam emittances are accepted as correction is applied. The second of these corresponds to the largest emittance

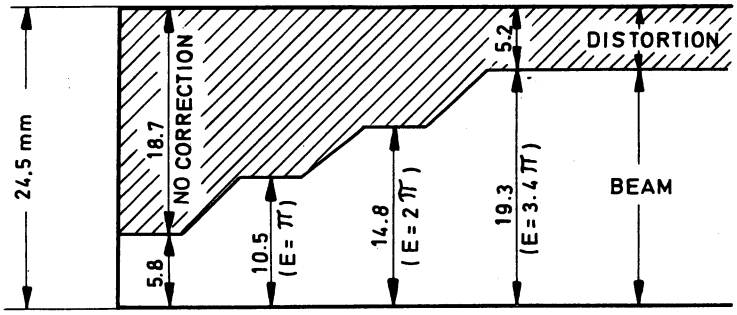

a) Vertical

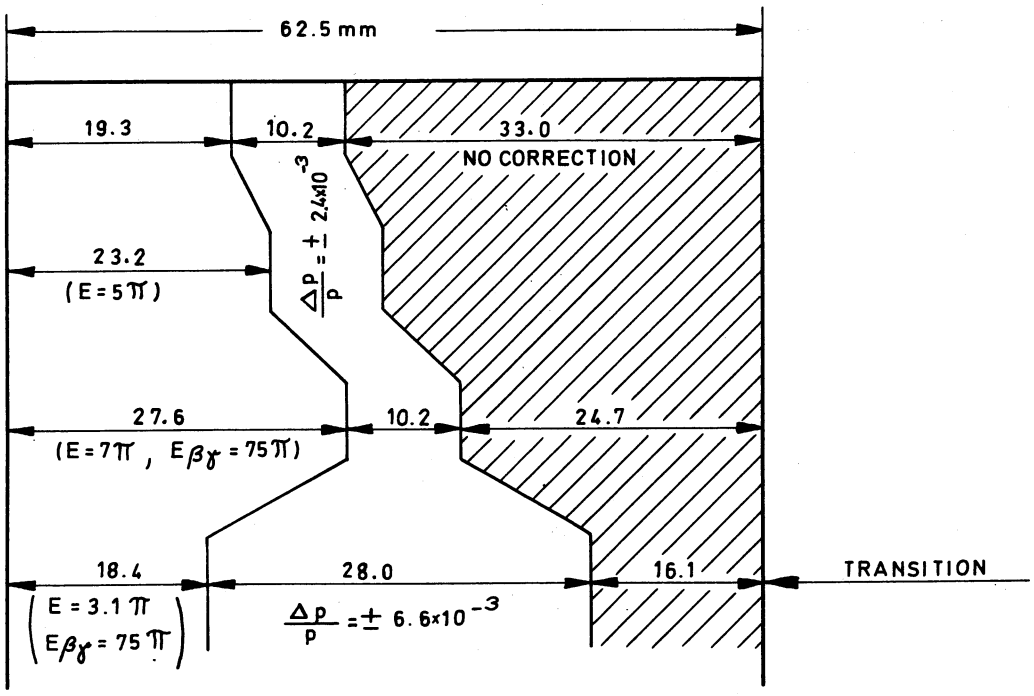

b) Horizontal

Fig. 2.6 Breakdown of semi-apertures for 10 GeV/c at β_{max} and $\alpha_{p,max}$

and momentum spread expected from the CPS. At transition the emittance shrinks adiabatically to 3.1 π ($E\beta\gamma$ = 75 π mm milliradians) and the momentum spread in the absence of special measures grows to $\pm$ 6.6 $\times$ 10^{-3}. This is shown in the last step. Clearly the spare aperture (shaded) is larger than the 10 mm residual closed orbit amplitude expected. Nevertheless, bearing in mind the need for a large horizontal aperture for extraction and the uncertainties in the estimates of momentum spread to be expected from the CPS it is not judged prudent to reduce $a_H/2$ below 62.5 mm.

In Fig. 2.2 the horizontal and vertical envelopes of the beam corresponding to the last step in each case are plotted through a complete period in which α_p is maximum. The semi-apertures required by the beam in each of the magnets (Table 2.4) are determined by this profile. In Fig. 2.7 a three dimensional picture of the beam envelope is shown together with the physical and magnetic boundaries.

Table 2.4

	Semi-apertures required by the beam (mm)	
	H	V
Q_F	62.5	10.1
Q_D	27.2	24.3
B1	60.9	16.5
B2	42.9	23.7

The apertures and other parameters of the machine are adequate should it be decided to add a fast cycling booster as part of some future intensity improvement programme.

The emittance and magnet apertures determine the intensity at which the space charge Q shift becomes serious. For a Q shift of about 0.25 at 10 GeV/c and assuming a bunch factor after injection from the CPS of 0.02, the incoherent space-charge limit is 5.6 $\times$ 10^{13} ppp and the coherent space-charge limit is 8.8 $\times$ 10^{13} ppp. Clearly these limits are comfortably above the design intensity of the machine.

2.6 Choice of Working Point

It can be shown that stop bands occur at Q values given by

$$kQ = nS \text{ or } nN$$

where: k, the order of the stop band is 1, 2, 3 or 4

n is any integer.

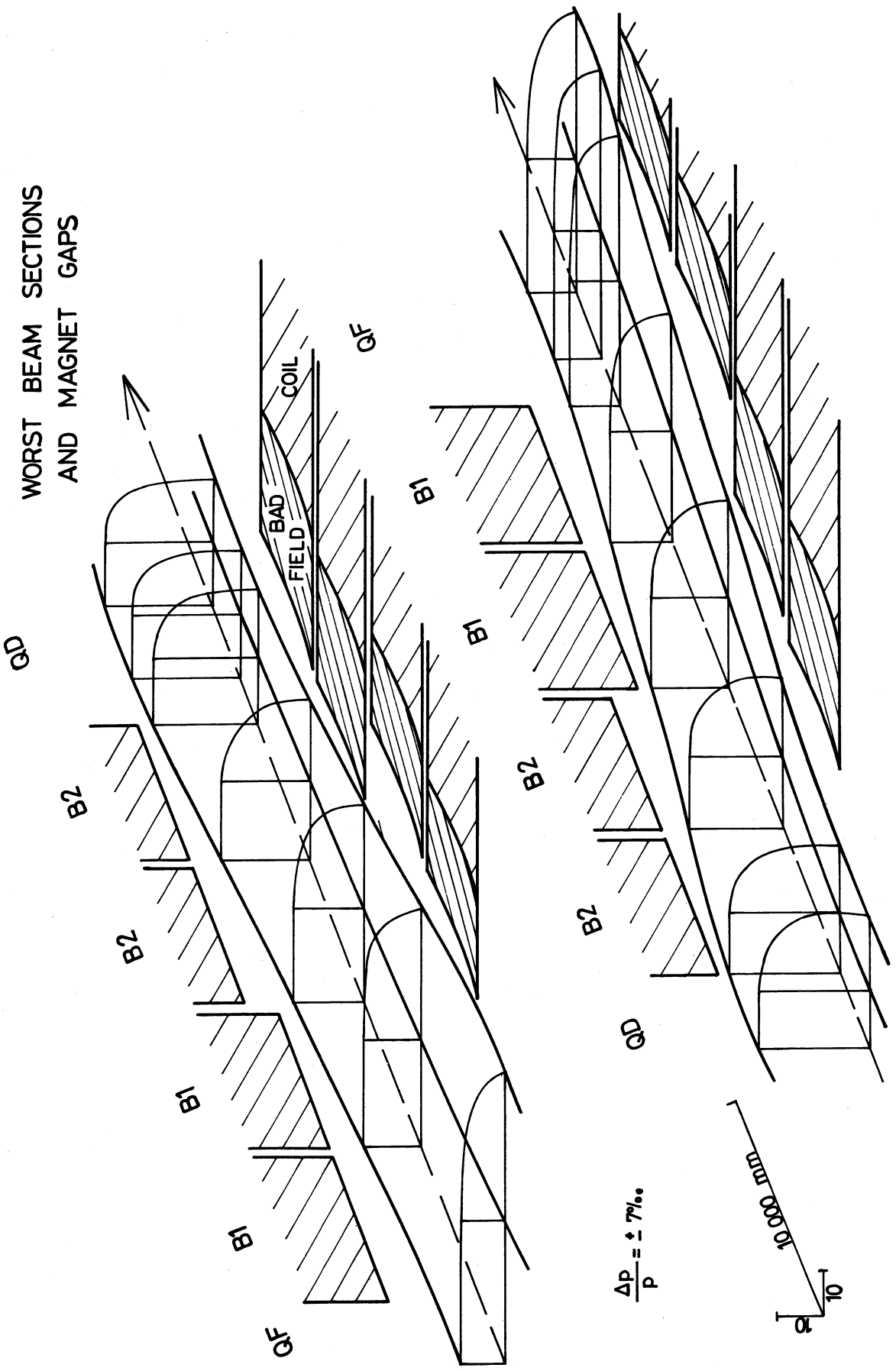

Fig. 2.7 Beam envelope

For a superperiodicity S = 6 this leads to the pattern of stop bands shown in Fig. 2 8. There is a strong tendency to choose a Q close to the centre of the diagram and remote from the k = 1 stop bands. This minimises $\hat{\alpha}_p$. At the same time it is wise to avoid the k = 2 stop band at Q = 27 and the higher order stop bands, k = 3 and k = 4, should not cut the integer square in which the working point is located. This leaves only 26.25 and 27.75 as desirable working points. Since Q is in general driven downwards by space charge we prefer 27.75 and have chosen this as the nominal working point.

The only stop band in the vicinity which is associated with the periodicity, N, is the fourth order stop band, 4Q = N at Q = 27.0. This can only be driven by systematic octupole errors in the field of the quadrupoles. Since the quadrupoles are symmetric such errors will be very small and we expect the stop band to be sufficiently weak and remote from the nominal working point.

It is clearly an advantage of the separated-function lattice that the nominal Q can be moved to an adjacent integer square by programming the quadrupole currents should experience with the machine suggest that this is desirable. An alternative working point is 28.75. The k = 4 stop band just below it, may well prove to be very weak indeed. It can only be driven by octupoles of superperiodicity six which, in our homogeneous lattice, do not exist to a first order. We therefore intend to ensure that the quadrupoles can drive Q to 28.75 even at the peak machine energy and in Table 2.1 quote parameters for both working points.

Finally, we should point out that the machine will, in practice, be tuned so that there is a small difference between Q_V and Q_H.

2.7 Element Reference Numbers

The standard numbering system for lattice elements referred to in later Chapters is as follows. Each period is divided into 20 sections corresponding to the quadrupoles, gaps, dipoles and short straight sections of a normal period of Stage C. Each of these locations in the superperiod is numbered in the order seen by the protons starting with an F quadrupole. Thus each element has a three-digit number from 1 to 360 which signifies its position in the superperiod. Division of these three digits by 20 gives the period number (dividend + 1) and the element position within the period (remainder). A fourth digit from 1 to 6 is added in front where it is necessary to identify in which superperiod the element is placed.

2.8 Conclusion

Several years of study have been devoted to the choice of the machine lattice to ensure that it represents the most economic configuration of machine components yet is sufficiently flexible to leave room for improvements stemming from operational experience. It is encouraging that frequent re-examinations of the design have not substantially changed this feature of the machine.

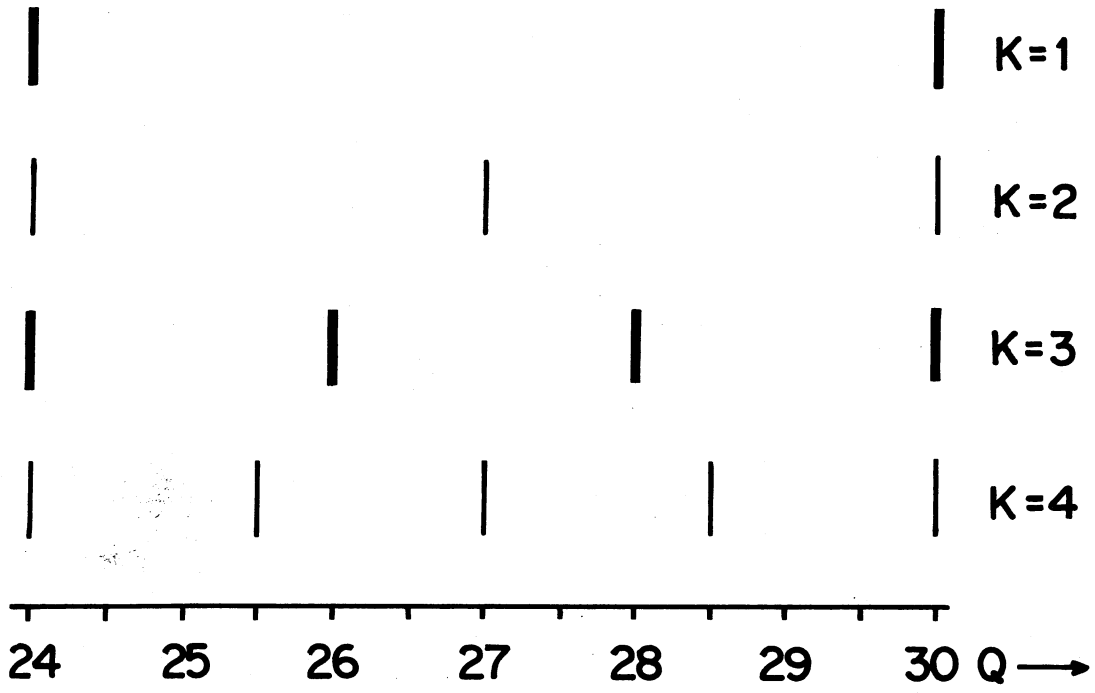

Fig. 2.8 Structure stopbands S = 6

Chapter 3

THE INJECTION SYSTEM

3.1 Introduction

The CERN Proton Synchrtoron (CPS) will be used as injector for the main ring. It is expected that the construction of the PS Booster and the CPS improvement programme, now underway, will raise the CPS intensity to 10^{13} protons per pulse. It is planned to inject one such pulse at 10 GeV/c into the SPS and accelerate it to full energy every 3 or 4 seconds. During the interval between these filling pulses the CPS has time to provide a normal 25 GeV pulse to its own experimental areas. In Stage C the SPS repetition time is long enough for two 25 GeV/c pulses to be accelerated. Clearly, other variations are possible [3.1,2].

The transfer momentum, 10 GeV/c, is chosen for a number of reasons. Clearly, a low transfer energy means that kicker magnets, septa and the beam line elements between the two machines can be cheaper and radiation damage caused by losses will be less severe. The duty cycle of the CPS for its own physics programme will also be least disturbed. There are, in addition, indications that the CPS beam does not in practice shrink in size above 10 GeV/c. But more important still is the condition that the injection energy be well away from the transition energy of the main ring if debunching and r.f. capture are to be successful. 10 GeV/c is as close as one dare approach transition energy.

In the bunch by bunch transfer scheme the aim is to kick the 20 CPS bunches into equidistant locations around the SPS circumference. The exact 11 : 1 radius ratio of the two rings is chosen with this requirement in mind. Several technical solutions to this problem are discussed in Section 3.3. It is expected that even at 10^{13} p/p a beam transferred with this technique would be acceptable for the main ring.

An even more attractive possibility is a continuous transfer based on a very thin electrostatic septum in the CPS. A detailed study has shown that this scheme is very promising and it will soon be tried out at the CPS. The septum will "peel off" the CPS beam during eleven revolutions. In this case the horizontal emittance is reduced. As there is no need with this scheme to leave gaps in the beam for kicker rise and fall times, the longitudinal transformation of the 10 MHz CPS bunches into 200 MHz bunches could in principle be made partly or fully in the CPS, resulting in a smaller longitudinal bunch area in the main ring. Initially, however, it is only foreseen to debunch the beam adiabatically in the CPS before transfer to the main ring, and the momentum spread will be decreased by a factor which depends on the degree of adiabaticity of this process.

Since the main ring parameters have been chosen to be compatible with all transfer schemes described here, no immediate need exists for the selection of one particular scheme. It is planned to explore their feasibility and relative merits during 1972 and to make a choice at the end of the year.

Further variations in which the SPS is filled by more than one CPS pulse can also be imagined though these may require a main ring r.f. holding system and other more minor modifications.

The first part of the existing CPS-ISR transfer line will be used for transfer to the main ring. The additional line has a total length of about 850 m.

3.2 General Transfer Parameters

3.2.1 CPS Output Beam - Expected Characteristics

Estimates of the phase space volume of the CPS beam after transfer are given in Table 3.1.

Table 3.1

Expected Main Ring Beam Emittances (in units of 10^{-6} rad m) and Main Ring Bunch Areas (in rad) at 10 GeV/c and 10^{13} p/p

Transfer scheme \ Quantity	$E_H\beta\gamma$	E_H	$E_V\beta\gamma$	E_V	A
Bunch by bunch	75π	7π	36π	3.4π	0.18
Bunch by bunch and main ring debuncher (3.5)	75π	7π	36π	3.4π	0.08
Continuous ejection	25π	2.3π	36π	3.4π	0.08

We arrive at these estimates as follows. The beam to be transferred from the PSB into the CPS (at 1.463 GeV/c) will have :

$$E_H\beta\gamma \approx 50\pi\ 10^{-6} \text{ rad m} \qquad E_V\beta\gamma \approx 20\pi\ 10^{-6} \text{ rad m}$$

Some blow-up will occur up to 10 GeV/c, as was measured recently [3.3] with 1.6×10^{12} p/p. Extrapolating the blow-up towards 10^{13} p/p is difficult [3.4]. The main ring vertical acceptance of $3.4\pi\ 10^{-6}$ rad m corresponds to $(E_V\beta\gamma)_{max} = 36\pi\ 10^{-6}$ rad m and is compatible with a blow-up of $\Delta E\beta\gamma \approx 10\pi\ 10^{-6}$ rad m in the CPS and an additional blow-up of twenty percent in the transfer from the CPS. Using similar blow-up assumptions for the horizontal plane leads to the emittance values given in Table 3.1 for bunch by bunch transfer. In case of continuous ejection, a reduction of E_H by a factor three is assumed (Section 3.4). If so desired, the H and V phase planes could be exchanged in the transfer line (Section 3.5.4).

In longitudinal phase space, we expect a bunch area of 0.01 rad at transfer from the PSB. A blow-up of 2 may occur when passing transition and another factor 2 may be found

due to the instabilities above transition. We thus assume a CPS bunch area of

$$A = \pi \, \Delta(\beta\gamma)\phi_{rf} = 0.04 \text{ rad}$$

at 10 GeV/c and 10^{13} p/p.

For bunch by bunch transfer with simple "debunching" in the main ring, the main ring bunch area is given by the energy spread of the CPS bunches (see Section 3.3). For schemes with debunching (and possibly prebunching at 200 MHz) in the CPS (Section 3.4), we assume a blow-up of two for the total debunching and rebunching process. When using a debuncher in the main ring [3.5] the coupling impedance of the 200 MHz r.f. structure must be lowered to preserve the self-bunching limit in spite of a lower $\Delta p/p$.

3.2.2 Debunching and trapping

As the two machines have different radii and the r.f. systems work at different frequencies, the beam has to be debunched and rebunched before acceleration can start in the main ring. During this process the beam will suffer a blow-up of the bunch area. However, the momentum spread of the transferred beam before trapping and hence the resulting bunch area in the main ring must not be too large because of three kinds of bottle-necks.

Firstly, the bunches must be smaller than the main ring buckets. The bucket area has two minima, one at $\gamma \doteq \sqrt{3}\,\gamma_{tr}$, and another near injection.

Secondly, the horizontal aperture will limit the permissible bunch area, as momentum oscillations contribute to the beam width. Two limitations are important: at transition, where the momentum oscillations have their maximum, and at injection, where the betatron oscillations are large.

Thirdly, the betatron oscillation frequency of each particle undergoes a tune shift which depends on its momentum deviation. At transition this might be large enough to cross the integral and half-integral resonances, even without considering nonlinear effects [3.6].

The momentum spread is related to the bunch area by the following formulae:

i) Debunched beam (at injection)

$$\left(\frac{\Delta p}{p}\right)_{db} = \pm \left\langle \left[\frac{A}{4\pi\beta\gamma} \right] \right\rangle_{db} \qquad (3.1)$$

ii) Bunched beam, full stationary buckets

$$\left(\frac{\Delta p}{p}\right)_{fsb} = \pm \left\langle \left\{ \frac{A}{8\,\beta\gamma} \right\} \right\rangle_{fsb} \qquad (3.2)$$

iii) Bunched beam, full moving buckets

$$\left(\frac{\Delta p}{p}\right)_{fmb} = \pm \left\{ \frac{A}{8\,\beta\gamma} \frac{\sqrt{(\pi/2 - \phi_s)\sin\phi_s - \cos\phi_s}}{\alpha(\phi_s)} \right\}_{fmb} \qquad (3.3)$$

iv) At transition [3.7]

$$\left(\frac{\Delta p}{p}\right)_{tr} = \pm \left\{ \sqrt{A}\,\frac{0.465}{\beta} \frac{\left[\frac{1}{f_{r.f.}}\,\frac{\dot{cp}}{E_o}\right]^{1/6}}{\left[\gamma \tan\phi_s\right]^{1/3}} \right\}_{tr} \qquad (3.4)$$

Where

- A = bunch area in $\left[(\Delta p/m_o c) \times \text{r.f radians}\right]$
- β = ratio of particle velocity to that of light
- γ = ratio of total energy of particle to its rest-energy
- ϕ_s = synchronous phase angle between beam and zero-crossing of r.f. voltage
- f_{rf} = accelerating frequency
- $\alpha(\phi_s)$ = moving bucket factor

In Table 3.2 all these limits are summarized and related to the maximum acceptable momentum spread of the transferred CPS beam, i.e. before trapping.

For calculating Table 3.2 the following assumptions were made :

A = 0.22 rad
$\alpha_p = \hat{\alpha}_p$ = 4.25 m
$\beta_H = \hat{\beta}_H$ = 109 m
$\gamma_{transition}$ = 24
available half aperture (HA) = 62.5 mm

$\phi_s = 45^o$
$\dot{p}$ = 166 $\frac{2}{3}$ GeV/c/s
f_{rf} = 200 MHz
$N = 10^{13}$ ppp

The aperture situation is given under the assumption of a normalized emittance of $E_H \beta\gamma = 75\pi\ 10^{-6}$ rad m.

Table 3.2

R.F. bucket size at injection	$\pm 1.64 \cdot 10^{-3}$
R.F. bucket size at $\gamma_{tr}\sqrt{3}$	$\pm 1.64 \cdot 10^{-3}$
Aperture at injection (24.9 mm for momentum oscillations)	$\pm 3.73 \cdot 10^{-3}$
Aperture at transition (34.5 mm for momentum oscillations)	$\pm 1.97 \cdot 10^{-3}$*
Coupling between betatron and synchrotron oscillation at transition under the assumption $\Delta Q/Q = -1.33\ \Delta p/p$.	$\pm 1.43 \cdot 10^{-3}$

* (can possibly be increased by phase switching, fast Q-jump or voltage ducking at transition).

During the debunching - rebunching process, interaction between the beam and the cavities or other coupling impedances may cause problems. Beam-induced voltages may prevent the beam from debunching, or may cause self-bunching at an unwanted frequency. Debunching in the presence of a coupling impedance resonating at a frequency much higher than the bunch frequency is an unsolved theoretical problem. We use a self-bunching criterion [3.8,9] which establishes the condition under which a coasting beam of circulating current I_o is stable against self-bunching. Experiments indicate [3.10] that the criterion gives reasonable results for a bunched beam, if I_o stands for the average current.

The debunching criterion can be rewritten in the following convenient form [3.11]:

$$A \geq \left[\frac{64\pi}{0.7}\ \frac{\beta\gamma}{|\eta|}\ \frac{|Z|/h^*}{Z_o}\ \frac{Nr_p}{R}\right]^{\frac{1}{2}} \qquad (3.5)$$

where h* is the undesired harmonic number, $|Z|$ and Z_o denote the impedance of the cavities and of free space, r_p the classical proton radius, R is the radius of the machine, N the number of particles and A is the bunch area after (ideal) trapping. $\eta = |1/\gamma_{tr}^2 - 1/\gamma^2|$.

3.3 Bunch-by-bunch transfer

The proposed bunch-by-bunch ejection scheme injects 20 × 1 CPS bunches, spaced equidistantly around the main ring. For this purpose pulse generators are required which permit repetitive pulsing of the CPS fast kickers. Three possible approaches have been proposed [3.12, 13] and are under study. All involve a 100 ns cable pulse forming network (PFN)

switched by a thyratron, but differ in the technique of fast recharging the PFN for which the following three proposals have been made :

i) a PFN producing a 4 ms pulse at high voltage which is discharged into the 100 ns PFN by a second thyratron [3.12,13],

ii) a number of small capacitors at high voltage, each switched into the 100 ns PFN by a small thyratron,

iii) a number of capacitors charged to about 7 kV from which the energy is transferred to the 100 ns PFN via a pulse transformer [3.14].

The latter proposal is being pursued most actively because it is the simplest and most reliable of the three. It is planned to have a complete model circuit operating early in 1972. No tests of this system in the CPS are planned at the moment since its behaviour is believed to be essentially predictable on the basis of experience with the existing fast ejection system.

The fastest conceivable transfer could take place in one main ring revolution and would require to kick every eleventh bunch, i.e. one pulse every μs (t_s). In order to adjust the interval between bunches to the time given by the recharging method, t_s may be multiplied by any integer which has no factor in common with 20. The many possibilities obtained in this way result from the choice of R_{MR} = 1100 m. T_s = 100 μs is about the permissible limit if one wants to preserve the option for a debunching system [3.5] in the main ring. Otherwise one could relax T_s to about 4 ms [3.13].

After transfer, the 20 CPS bunches must be smeared around the circumference of the SPS before the beam is captured in the 4620 buckets of the main ring r.f.

The simplest way to "debunch" the transferred beam is to let the beam drift until bunches overlap due to momentum spread. The debunching time is given by :

$$t = \frac{1}{n\, f_{rev} \left(\frac{\Delta p}{p}\right) |\eta|} \qquad (3.6)$$

where n is 20 for the 20 × 1 bunch mode. Here t is twice the time after which bunches just touch. $\Delta p/p$ is the momentum spread <u>before</u> capture as given in Table 3.2.

Table 3.3 shows the expected momentum spread of the improved CPS for bunch-by-bunch transfer. For A = 0.04 rad, the figure $\Delta p/p = \pm 1.3 \times 10^{-3}$ implies that one would lower the CPS r.f. voltage to reduce the momentum spread, leaving gaps 75 ns wide for kicker rise and fall times.

Table 3.3

Main ring beam properties for 10 GeV/c transfer momentum
and $N = 10^{13}$ p/p

Parameters used:

$f_{rev} = \beta c/2\pi R = 43.2$ kHz	$\beta\gamma = \gamma = 10.705$
$n = 20$ (20 × 1 bunch mode)	$h_{MR} = 4620$
$\eta = \lvert 1/\gamma_{tr}^2 - 1/\gamma^2 \rvert = 0.007$	$Z/h^* = 1$ kΩ

Values computed

Expected CPS momentum spread for bunch-by-bunch ejection	$\Delta p/p = \pm 1.3 \times 10^{-3}$
Momentum spread after trapping and full buckets	$\Delta p/p = \pm 2 \times 10^{-3}$
Momentum spread after trapping and full r.f. voltage	$\Delta p/p = \pm 2.4 \times 10^{-3}$
Momentum spread at transition without special measures	$\Delta p/p = \pm 6.6 \times 10^{-3}$
Minimum momentum spread required to avoid self-bunching	$\Delta p/p \geq \pm 0.9 \times 10^{-3}$
Corresponding bunch area	$A \geq 0.120$ rad
Debunching time for $\Delta p/p = \pm 1.3 \times 10^{-3}$	$t = 130$ ms

Table 3.3 was arrived at by assuming an ideal machine. If longitudinal or transverse blow-up occurs between injection and transition, the acceptable bunch area and therefore the momentum acceptance decrease and debunching times become longer.

The momentum spread could be further reduced below the estimate in Table 3.3 by a debuncher cavity in the main ring [3.5], which can be added at any stage.

3.4 Continuous Transfer

The continuous transfer system must yield a burst of approximately 23 μs (1 main ring revolution) duration and rather constant intensity during that time. The principle of this system is that the beam is progressively pushed across an electrostatic septum which acts as a "peeler" (cf. Figs. 3.1 and 3.2). By suitably adjusting the displacement of the beam with time, a relatively constant intensity can be ejected during 11 revolutions.

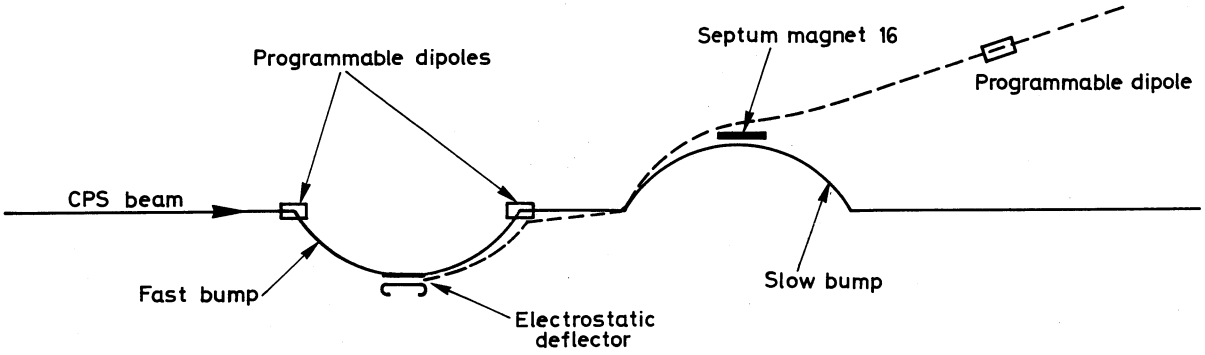

Fig. 3.1 Continuous ejection (schematic)

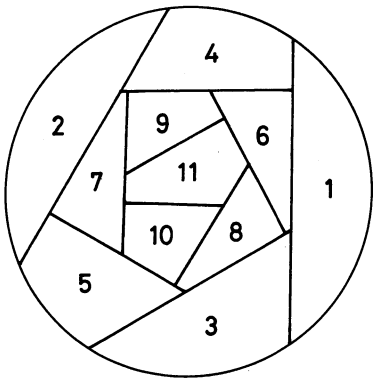

Fig. 3.2 Eleven-turn continuous ejection in the horizontal phase plane

The results of an extensive numerical analysis of the continuous transfer scheme are presented in Ref. 3.15. A typical dipole step function k(t) and the resulting intensity I(t) (for a longitudinally uniform CPS beam) are shown in Fig. 3.3, where realistic transverse CPS beam distributions and realistic rise times of the individual steps have been used. The analysis reveals a rather strong sensitivity of the system to variations of transverse beam distribution. The step functions, therefore,will have to be adjusted experimentally. The system is, on the other hand, rather insensitive to variations of other machine parameters.

The main factors which influence the current vs. time functions are listed in Table 3.4.

Table 3.4

	estimated peak variation
Spikes due to imperfect step function	+ 10%
Variations due to fluctuations of CPS parameters	± 10%
Modulation due to bunch population (at CPS rev.frequency)	± 5%
Modulation due to imperfect debunching (at CPS acceleration frequecy)	- 20%

The beam losses on the electrostatic septum are expected to be smaller than 5%. The horizontal emittance will be reduced by a factor 3 in the ejection process. It may then be advantageous to exchange the horizontal and vertical phase planes in the transfer channel. Its variation during the spill (due to the beam density profile) could be compensated by a programmed dipole in the transfer channel.

An experimental verification of this new proposal is essential. Therefore, experiments on the CPS are planned for 1972. A possible arrangement of the elements in the CPS has been found [3.16] which makes use of the septa of the slow ejection system. A design of the programmed pulse generators for the two dipoles has been worked out [3.17] which consists of a series of 11 cable pulse forming networks switched on successively by thyratrons. It is expected that ejection tests can start in May 1972.

The continuous ejection method can probably work with any debunching scheme. However, debunching in the CPS, which is much faster than debunching in the main ring, will give a small momentum spread and thereby ease continuous ejection.

One can foresee two debunching methods:

(i) adiabatic r.f. voltage reduction down to the value corresponding to a full stationary bucket. The $\Delta p/p$ obtainable at 10 GeV/c in the CPS is according to Eq. 3.2:

$$\frac{\Delta p}{p} = \pm\ 0.47 \times 10^{-3} \text{ for } A = 0.04 \text{ rad}$$

The method may suffer from the presence of coupling impedances in CPS [3.18.19],

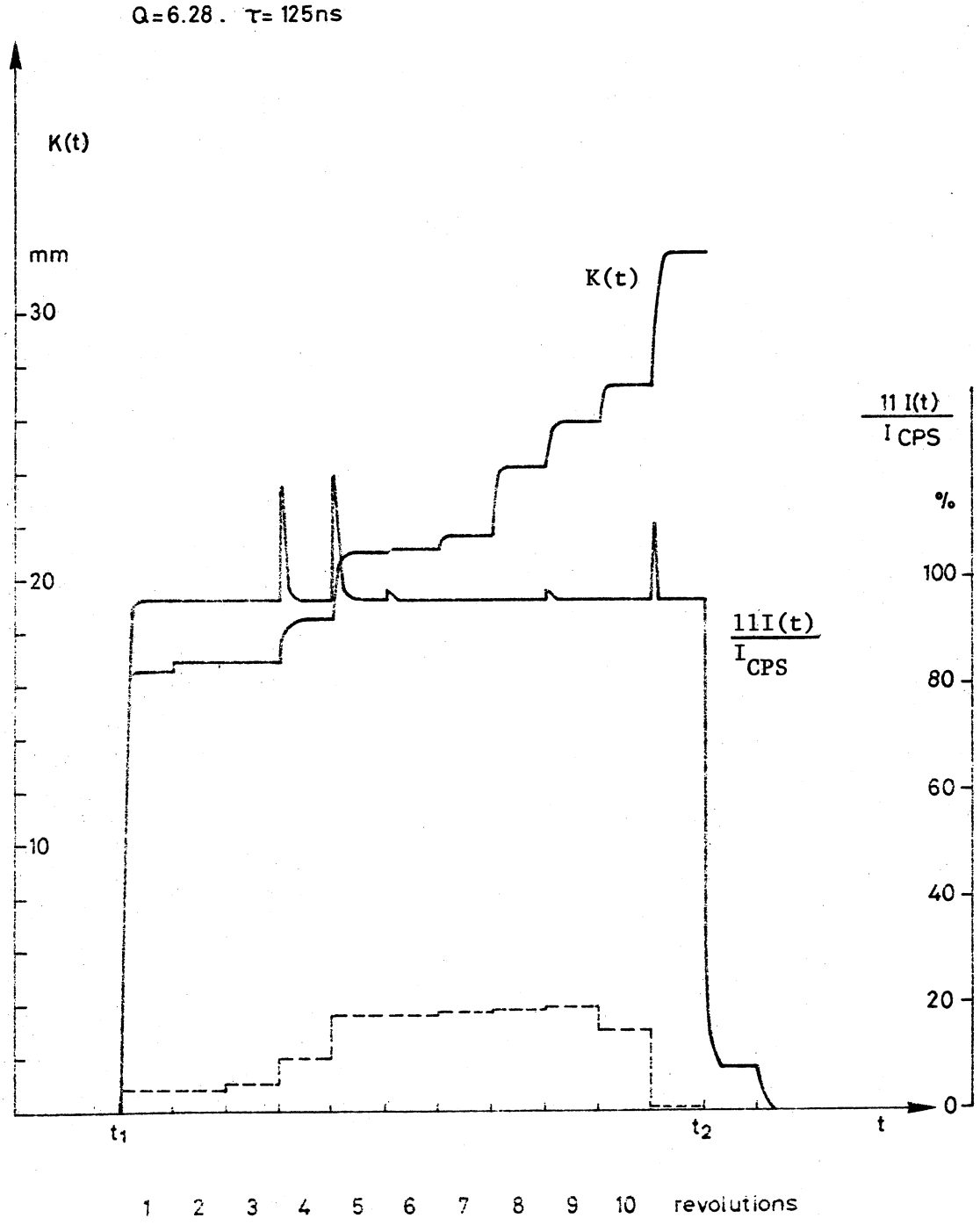

Fig. 3.3. Ejected intensity and kicker programmes for continuous injection The broken line indicates the strength for the programmed dipole in the transfer line for keeping a constant emittance through the whole ejection

(ii) debunching by r.f. gymnastics, e.g. phase jump to the unstabled fixed point followed by a bunch rotation. This method, similar to that used at present in the CPS can give momentum spreads comparable to method (i). The advantage is that the r.f. system can work at a relatively high voltage so that beam loading and coupling impedances are less critical.

The best procedure for debunching will result from a compromise between :

(i) final momentum spread (or beam blow-up)
(ii) self bunching and beam loading
(iii) residual r.f. structure
(iv) debunching times

Rebunching of the beam in the main ring at the high harmonic number can be started immediately after transfer, i.e. the self-bunching limit of the momentum spread can probably be lowered considerably. It seems possible, therefore, to transfer a beam with this scheme which only has about half the momentum spread as with the bunch-by-bunch scheme.

For special cases one may think of prebuching at 200 MHz already in the CPS. This would ease r.f. trapping, but it could create beam loading problems, since the amplitude of the main ring r.f. voltage must then be adjusted to the requirement of injecting the bunches into matched buckets.

The main ring voltage V_{MR} required for matching is related to the CPS voltage V_{CPS} by:

$$V_{MR} = \frac{|\eta|_{MR}}{|\eta|_{CPS}} \frac{R_{MR}}{R_{CPS}} V_{CPS} \approx 4.3\, V_{CPS} \qquad (3.7$$

This voltage turns out to be uncomfortably low. As an alternative, one could foresee to inject CPS bunches into unmatched buckets (higher r.f. voltage), perform a 90° rotation in phase space, and then match by a fast increase of the r.f. voltage [3.20].

3.5 Transfer Line

3.5.1 General description

After ejection from CPS ss 16, the beam travels along the existing CPS-ISR transfer line TT2 and branches off after 320 m (about 26 m downstream from the switch of TT2 and TT2a) towards the main ring. From this point onwards a new transfer line (TT10) has been designed. For injection into the main ring, the following characteristics of this line have been worked out:

Table 3.5

Some Characteristics of the Transfer Line

Total length up to downstream QD 1191	872 m
Horizontal angle between TT10 and TT2	- 196 mrad
Horizontal angle between TT10 and main ring long ss 1	+ 83.4 mrad
Difference in level of floor TT2 and main ring	32.0 m
Vertical bending angles	66.1 mrad
Crossing of St. Genis road	- 29 m

As shown in Fig. 3.4 the transfer line will, in addition to the first part of the existing TT2 line, consist of three sections with different functions.

1. The branching-off from TT2, including the total horizontal bend of 196 mrad and the matching to the main ring lattice (about 62 m).

2. The long distance transfer, including the vertical bends at both ends (about 800 m).

3. Injection into the main ring.

The geometry of the transfer line is such that protons of full CPS energy may be transported. This is merely to ensure that it presents no artificial bottleneck. Within the Programme sufficient magnetic strength will be installed to transfer the 10 GeV/c beam required by the SPS.

3.5.2 Branching-off from TT2

A pulsed bending magnet close behind QF 333 with a bending angle of 65 mrad will deflect the beam clear of the following quadrupole QD 334. Thereafter, two more d.c. bending magnets which are still placed in the existing TT2 transfer tunnel to the ISR will provide the remaining horizontal bending angle. No magnetic element of the existing TT2 beam needs to be displaced, but the beam stopper just upstream of QD 334 cannot be cleared and must be shifted to the next straight section between QD 334 and QF 335.

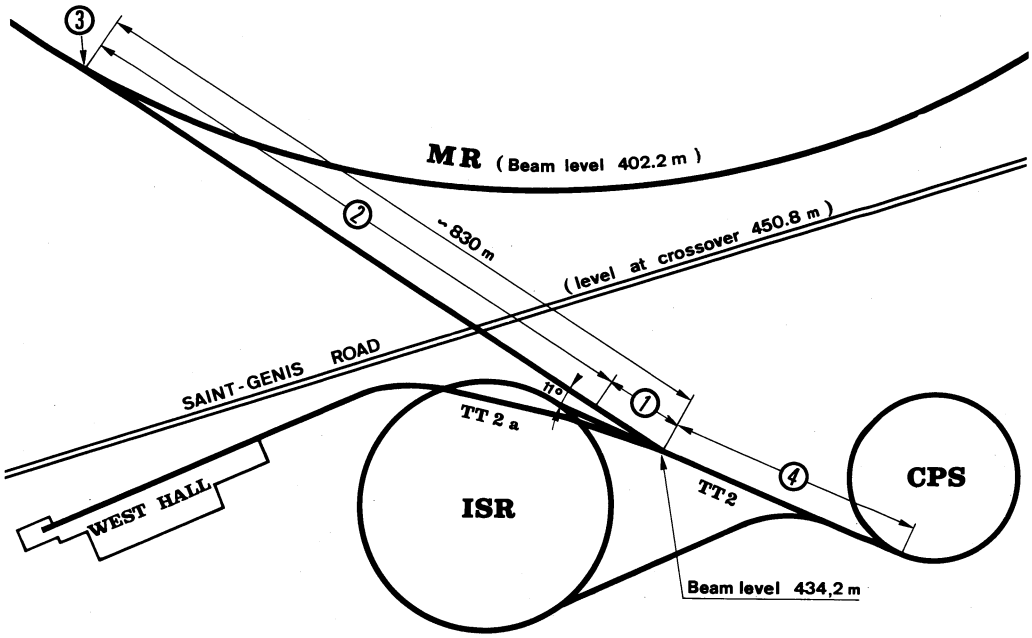

① Branching off section and matching section (~62 m)

② Long distance transfer section (~820 m) ③ Injection into MR in long SS1.

④ Part of the existing CPS-ISR transfer line TT 2.

Fig. 3.4 CPS-MR transfer line (schematic)

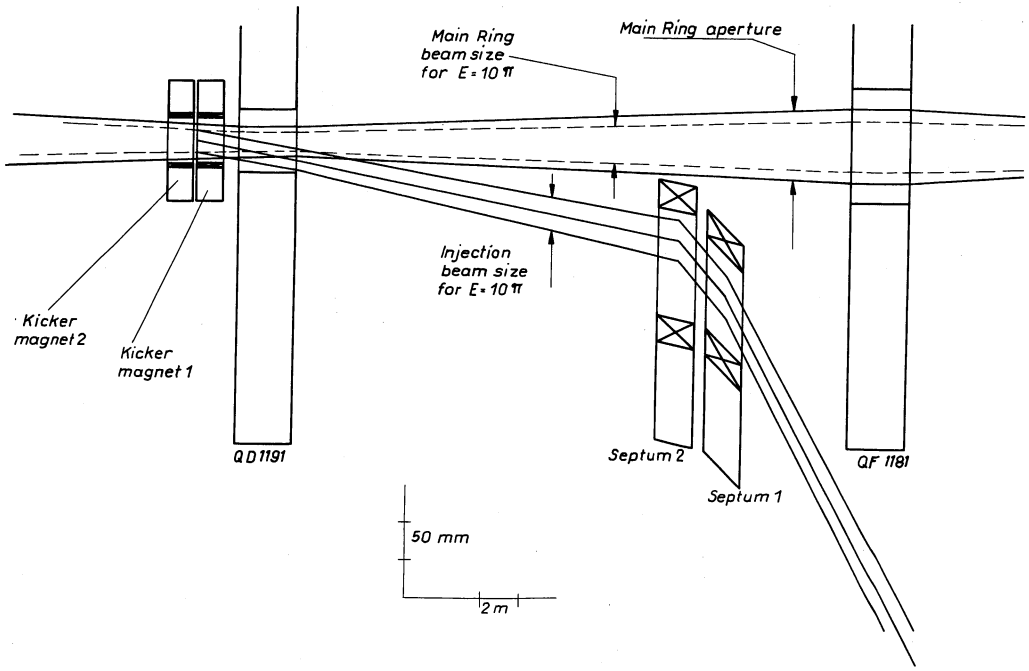

Fig. 3.5 Layout of injection system

3.5.3 Lattice for the long distance transfer

The lattice of the long distance transfer will be very similar to the FODO lattice of the main ring. This has the advantage that no special matching quadrupoles need to be inserted between the end of the long distance transfer and the point of entrance into the main ring. There are, however, small differences in period length and phase advance per period, determined by the fixed total length and the need to match both the horizontal and vertical dispersion of the transferred beam to that of the main ring at the point of injection, taking into account the various horizontal and vertical bends along the transfer line. This has led to a period length of 60.5 m and a phase advance per period of about 100° for the horizontal motion and about 90° for the vertical motion. Similarly, it is necessary to change the phase advance of the common part of the TT2 line for transfer to the main ring. For the normal lattice of the new long distance transfer line, a total of 26 quadrupoles (13D + 13F) is required. The F and D quadrupoles will be separately powered in series.

The vertical bends are inserted about two wavelengths apart near the beginning and end of this section. Their exact positions have been chosen such that the vertical dispersion is zero when the beam travels again horizontally, taking into account also the dispersion due to the small vertical bends in the transfer line before and after the passage of the CPS linac beam.

Betatron matching between the TT2 lattice and the main ring lattice will be done with the first 4 separately excited quadrupoles after the branch-off point.

3.5.4 Exchange of horizontal and vertical phase planes

It is expected that in case of continuous ejection the horizontal emittance of the ejected CPS beam will be reduced by a factor 3, as discussed in Section 3.4. It is therefore of interest to foresee the possibility of exchanging the horizontal and vertical phase planes in the transfer. This can be done by inserting a small number of skew quadrupoles at suitable positions into the transfer line. The best position for the installation of these skew quadrupoles is probably in TT2 where the horizontal and vertical dispersions are smallest, since this would minimize the difficulties with the matching of both dispersions of the transferred beam to the main ring.

3.5.5 Injection into the main ring

A horizontal injection scheme as shown in Figure 3.5 has been chosen. Its design is compatible with either bunch by bunch transfer or continuous transfer. The experimental data on the deionisation time of thyratrons indicates that bunch by bunch transfer may require a transfer time of up to 4 msec [3.13]. This time is too long for pulsed septum magnets excited by a capacitor discharge. It is therefore preferred to construct the septum magnets for d.c. current operation. This also avoids the wear of the septum insulation

due to pulsing and it reduces the voltage which the coils have to stand.

The long free ss length permits to design for a relatively large separation between the injected beam and the main ring aperture at the position of the septum magnets without making the inflector too difficult. This large separation makes it possible to use a multi-turn septum so that the d.c. current can be reduced to a convenient level. The lay-out shown in Fig. 3.5 permits the use of a 12 turn septum with a total thickness, including insulation, of 36 mm and which operates in air. The injected beam passes through a vacuum chamber in the gap of the septum magnets which links up downstream of these magnets with the vacuum chamber of the main ring.

Experience with the injection into the ISR has shown that the beam loss at the septum can be made negligible with nominal clearances of the beam on either side of the septum of about 10 mm. It is foreseen, therefore, to construct the septum coil in a conventional way, using glass mica tape and radiation resistant epoxy as insulation. Further details on the characteristics of the septum magnets are given in Table 3.6.

The layout of Fig. 3.5 has been calculated for a horizontal emittance of 10π mrad mm for the transferred beam from the CPS, in order to assure that the injection system will in no way limit the use of the main ring aperture. The nominal deflection of the inflector is 4.5 mrad. The maximum useful strength of the inflector at any given position downstream of the D quadrupole is limited by the beam excursion in the quadrupole aperture. The layout of Fig. 3.5 leaves a clearance of only 2.9 mm between the edge of the injection beam and the inner wall of a circular vacuum chamber in this quadrupole. It is forseen, therefore, to use a horizontally widened vacuum chamber in order to increase this clearance.

At the downstream end of the septum magnets the centre of the injection beam is at 126 mm from the central orbit. A pulsed bump at that position would therefore reduce the inflector strength by only 10%, which is not worthwhile in view of the operational complication which the bump would add.

It is proposed to make an inflector consisting of two full aperture ferrite magnets of the window frame type, each 1.4 m long. In the case of bunch by bunch ejection, the magnet will be excited by the same type of pulse generator as proposed for the CPS ejection discussed in section 3.3. For continuous transfer scheme, however, an excitation by means of a rectangular pulse of 23 μsec is required.

This pulse will be generated by discharging a lumped parameter delay line of 7.5Ω characteristic impedance through the magnet into its terminating resistor. The line will be charged to 31 kV for the injection of 10 GeV/c protons. This pulse must have a fall time of less than 1 μsec, a flat top which is constant within $\pm$ 2%, and no reflections with an amplitude above $\pm$ 2% beyond 1 μsec after the end of the flat top. Since the inflector is placed at a position where β_H = 22 m, an error of 2% in the deflection gives at β_{Hmax} = 109 m a coherent betatron oscillation of 4.4 mm amplitude. Tentative parameters for the inflector magnet are given in Table 3.6.

Table 3.6

Tentative Characteristics of the Main Ring Injection System for 10 GeV/c injection

a) Septum Magnets	
Number of magnets	2
Magnet length	2 m
aperture (H × V)	140 mm × 47 mm
inductance	1.35 mH
resistance	12 mΩ
Number of turns	12
Total septum thickness	36 mm
d.c. current	1.08 kA
d.c. voltage	37.8 V
magnetic field	0.35 T
b) Inflector Magnets	
Number of magnets	2
Magnet length	1.4 m
aperture (H × V)	50 mm × 48 mm
inductance	1.83 μH
Magnetic field	0.054 T
Characteristic impedance of pulse forming network	7.5 Ω
Voltage on pulse forming network	30.7 kV
Current	2.05 kA

3.6 Conclusions

The CPS fulfils the requirements for an injector for the main ring. Either bunch by bunch or continuous transfer can be used. The latter provides a safer alternative if, when rising the CPS intensity from 2×10^{12} to 10^{13} p/p, an unexpected beam blow-up occurs in the main ring between injection and transition. Both transfer schemes are being developed at the CPS and will be tried out before a choice between the two schemes is made.

The transfer momentum of 10 GeV/c is a compromise between the necessity to provide large enough r.f. buckets and the requirements to debunch the beam after injection into the main ring. A high transition energy is useful to improve the horizontal aperture limitation with large bunches and to provide large enough buckets at $\gamma_{tr} \sqrt{3}$. These requirements and the desire to have long enough straight sections for extraction at top energy led to the compromise $\gamma_{tr} \approx 24$.

The main ring acceptance looks just sufficient even for bunch by bunch transfer at 10^{13} p/p.

References

(3. 1) O. Barbalat, W. Hardt and K.H. Reich, The improved CPS injector for the 300 GeV synchrotron, CERN MPS-SI/DL/70-8.

(3. 2) D. Möhl, W. Schnell, A. Sørenssen and C. Zettler, the feasibility of using the PS as an injector for "Project B", RF problems, CERN/MPS-DL/70-6,

(3. 3) E. Brouzet, C. Johnson and P. Lefèvre, Mesures des dimensions verticales du faisceau du PS, MPS/DL -Note 70-21.

(3. 4) C. Bovet et al., Evolution of proton density between ion source and ISR, CERN/MPS-SI/Int-DL/70-7.

(3. 5) W. Hardt and D. Möhl, Debunching in "Project B", MC-34.

(3. 6) Y. Baconnier, K.H. Kissler and B. de Raad, Effect of field distortions in the 300 GeV main ring bending magnets, CERN II/300-BT/71-2.

(3. 7) A. Sørenssen, The effect of strong longitudinal space-charge forces at transition, MPS/Int. MU/EP 67-2.

(3. 8) A. Sessler and V. Vaccaro, Longitudinal instabilities of azimuthally uniform beams in circular vacuum chambers with walls of arbitrary electrical properties, CERN 67-2.

(3. 9) E. Keil and W. Schnell, Concerning longitudinal stability in the ISR, CERN/ISR-RF/69-48.

(3.10) Y. Baconnier et al., Debunching in the presence of high-frequency cavities, MPS/DL/Note 70-14 (MC/33).

(3.11) D. Möhl, A. Sørenssen and C. Zettler, How to inject into which lattice, MC-41.

(3.12) A. Brückner, A proposal for 20 × 1 or 10 × 2 bunch ejection from the CPS to the 300 GeV machine based on a new fast charging system, MPS-SI/Note 300/INJ/2.

(3.13) D. Grier, A fast charger pulse generator for 20 × 1 bunch ejection from the PS to the 300 machine, MPS/SR/Note 71-26.

(3.14) P. Pierce and D. Fiander, A proposal for a pulse generator for bunch by bunch transfer from the CPS to the SPS. MPS/SR/Note 71-37.

(3.15) C. Bovet, Continuous transfer from CPS to 300 GeV, a numerical analysis of fast-shaving ejection, 300-DI-PA/INS-2.

(3.16) F. Schäff, Arrangement of elements in the PS for continuous ejection tests, 300-DI-PA/71-7.

(3.17) D. Grier, Proposal for a "staircase" pulse generator for continuous transfer from the CPS to the SPS, MPS/SI/Note 71-36.

(3.18) H.G. Hereward, Effects of cavities on debunching, rough estimates for the CPS, CERN/MPS/DL 69-7.

(3.19) A. Sørenssen, What sort of coupling impedances are tolerable in the future CPS, MPS/70-1.

(3.20) See for example H.H. Umstätter, Data on longitudinal phase space matching for beam transfer from the booster into the PS at 800 MeV, MPS/SR/Note 69-20 Rev.

Chapter 4

THE MAGNET SYSTEM

4.1 General description

The main magnet system for the 300 GeV proton synchrotron is of the separated function type in which the proton beam is bent around on an approximately circular orbit by uniform-field dipole magnets while quadrupole focusing magnets are used to constrain the beam within the vacuum chamber.

The overall arrangement required consists of alternate horizontally and vertically focusing quadrupoles equally spaced around the machine to form 108 focusing periods. Between consecutive quadrupoles up to 4 bending magnets are located depending upon the energy range of the accelerator. In some focusing periods some or all of the bending magnets are omitted to leave space for beam injection, accelerating structures or beam extraction. The details of the overall configuration are covered in Chapter 2 together with the required apertures. In order to match the magnetic apertures to the varying beam cross section through the focusing period, there are two types of normal dipoles, B1 and B2, which have apertures matched to the requirements in the vicinity of the F and D quadrupoles respectively. As described in Chapter 2, a half-length version of the B2 magnet would be required only in stage B of the machine development. Although the quadrupoles are referred to as QF and QD, they are identical elements which have a circular aperture suitable both for the horizontally focusing position and the vertically focusing position (horizontally defocusing). The overall magnet parameters, together with the number of magnets of each type required at the various stages, are given in Table 4.1.

Table 4.1

Composition of the Main Magnet System

	Q	B1	B2	B2/2
Length (m)	3.22	6.26	6.26	3.13
Field (T)		1.8	1.8	1.8
Gradient (T/m)	20			
No. for stage A	216	180	192	-
No. for stage B	216	360	192	12
No. for stage C	216	360	384	-

4.2 Dipole design

The overall design of the main magnet system has been greatly influenced by several factors. One of the most important considerations came from more detailed studies of the extraction process[4.1], and its implications for the tolerances on magnetic field uniformity. These tolerances imply larger field volumes in all the magnetic elements that had been previously foreseen. It was found, as a result of these studies, that the maximum allowable deviations from field uniformity must be less than 3 parts in 10^4, at full excitation level. In addition to this requirement a detailed study of the free space required for the extraction system and other components, reduced the total space available for the bending magnets to such an extent that conventional H type dipole magnets with flat coils would have been required to run at 1.9 T in order to reach 400 GeV proton energy, due to the space occupied by the coil ends between magnet yokes. For this reason it was decided to use bending magnet coils with bent-up ends which allowed the peak energy of 400 GeV to be reached at a field level of 1.8 T. The need to have coils with bent-up ends implied a magnet yoke fabricated in two halves. This has the incidental advantage that the gap height and therefore the peak stored energy could be reduced considerably by reducing the space required between the poles for the vacuum chamber.

Following this, a careful comparative study was carried out in order to compare magnets with bent-up coil ends both with and without conductors between the pole pieces. In the case where an inner coil was included, a generous allowance of 3/4 of a gap width was allowed between the edge of the required good field region and the copper of the inner coil to avoid excessive field errors resulting from variations in the copper position. For the purposes of this study, both the total copper cross section and the fraction of ampere-turn in the iron circuit were maintained constant. Under these conditions, removing the inner coil resulted in an increase in the magnet stored energy of 18% and an increase in the steel weight of 25%. The cost of these increases was found to be $1\frac{1}{2}$ times the expected fabrication cost of an inner coil with normal tolerances, so that there would be considerable savings by introducing the inner coil. In this context it is worth noting that following discussions with industry and after studying the tolerances achieved on the ISR main magnet coils, it became clear that tolerances on the inner coil of ±0.5 mm vertically and ±1 mm radially could be readily achieved. Analytic[4.2] and computational[4.3] studies of the effect of inner coil positional errors indicated that with these tolerances the distance of the coil from the edge of the good field region could be reduced to a width equal to half of the magnet gap, thus further reducing the magnet stored energy. This specific comparison confirmed results which had been obtained in an earlier general study[4.4].

During the studies of magnets with and without inner coils, the comparisons were based only on cost considerations associated with magnet steel and power supplies. However, it should be noted that the higher stored energy of the magnet without an inner coil, besides increasing the cost of power supply would also increase the rise time of the accelerator due to the limitation on peak pulsed power required from the electricity network. This would have the effect of lengthening the machine cycle, particularly at the higher excitations so that even with the same copper cross section the rms power consumption would be also increased.

The choice of the number of types of dipoles was governed mainly by economic considerations, but also by the need to have very close tracking between the different types of magnets at all field levels from 0.045 T up to 1.8 T. A comparison was then made between the overall costs of one, two or three types of bending magnet with apertures matching the beam requirements as closely as possible but with the magnet gaps adjusted to be in ratios of small integers. The optimum integer ratios were found to be 3:4 for two types and 3:4:5 for three types. Under these conditions the 15% savings in stored energy between 2 and 3 types was estimated to be considerably less than the extra costs of design, tooling and coil fabrication. On the other hand, one type of magnet increased the stored energy by 35%. In this case the number of turns could not be reduced significantly both because of increased cable costs, and problems in coil fabrication and eddy currents associated with very large conductors. Consequently the greatly increased stored energy could not be offset by corresponding reductions in coil costs.

Having reduced the basic design of the two types of window-frame dipole magnets, the coil design proceded on the basis of minimizing the overall costs of the system for 50,000 hours of operation, within certain boundary conditions. The most important of these were a minimum insulation thickness to ground of 2 mm and a maximum cooling requirement of 40 MW. Other important considerations included good packing factor, coil costs, ease of fabrication, eddy current effects and cable costs. As a result of this, provisional designs were obtained with 16 turns in the B2 magnets, 12 turns in the B1 magnets and a total ring resistance of about 3 Ohms. The magnet cross sections (fig. 4.1) were then computed by means of the computer programmes MARE and MAGNET using the steel characteristics obtained for the ISR magnets. The computed field shapes are shown in Fig. 4.2, for low and high field levels.

The resulting magnet cross sections were found to be within a few millimetres of each other and so at this stage the outer dimensions were made identical and the coil cross sections adjusted very slightly until correct tracking was obtained between the two types of magnet. The resulting main characteristics of these dipoles are summarized in Table 4.2.

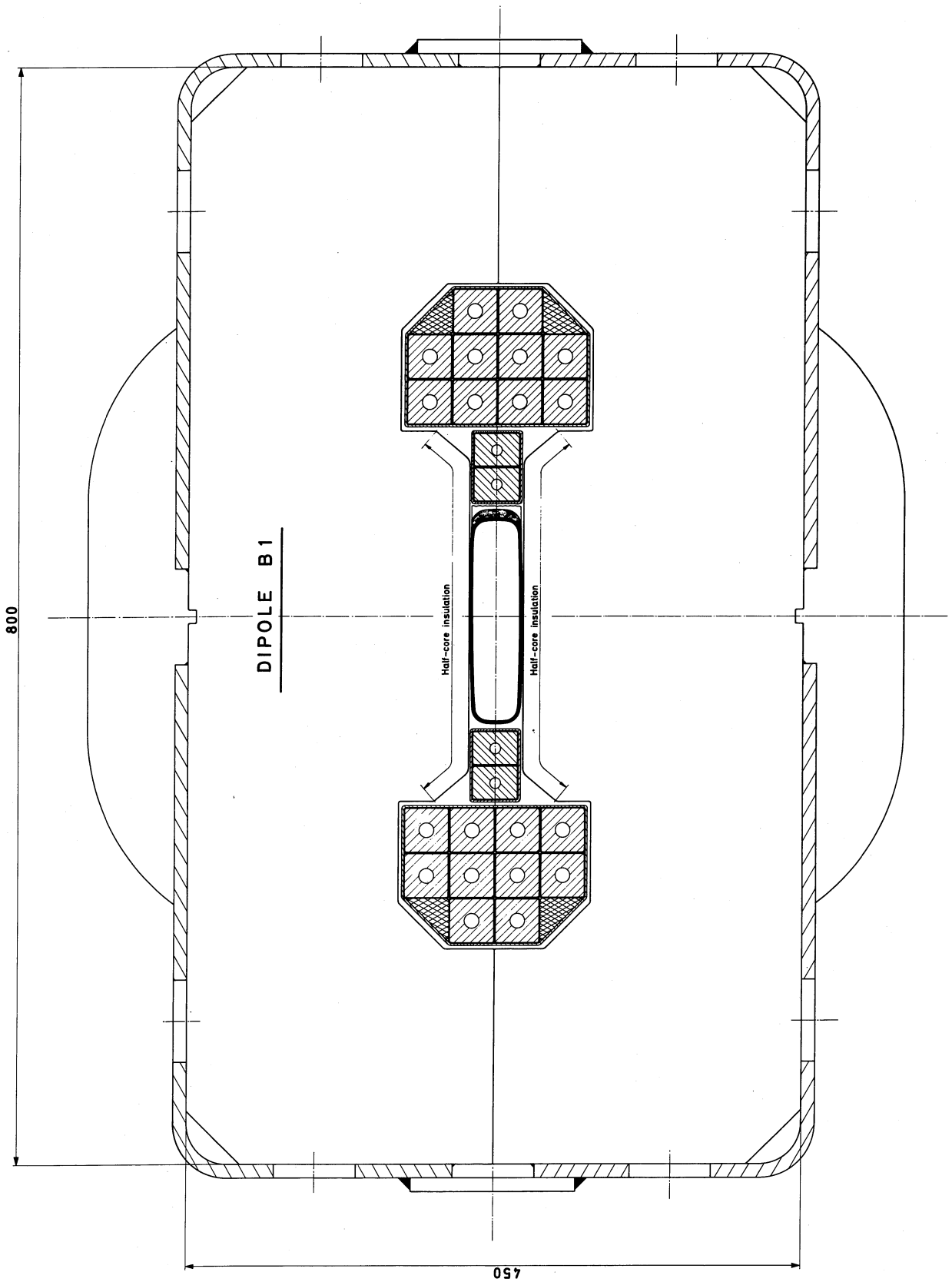

Fig. 4.1a Dipole cross-section B1

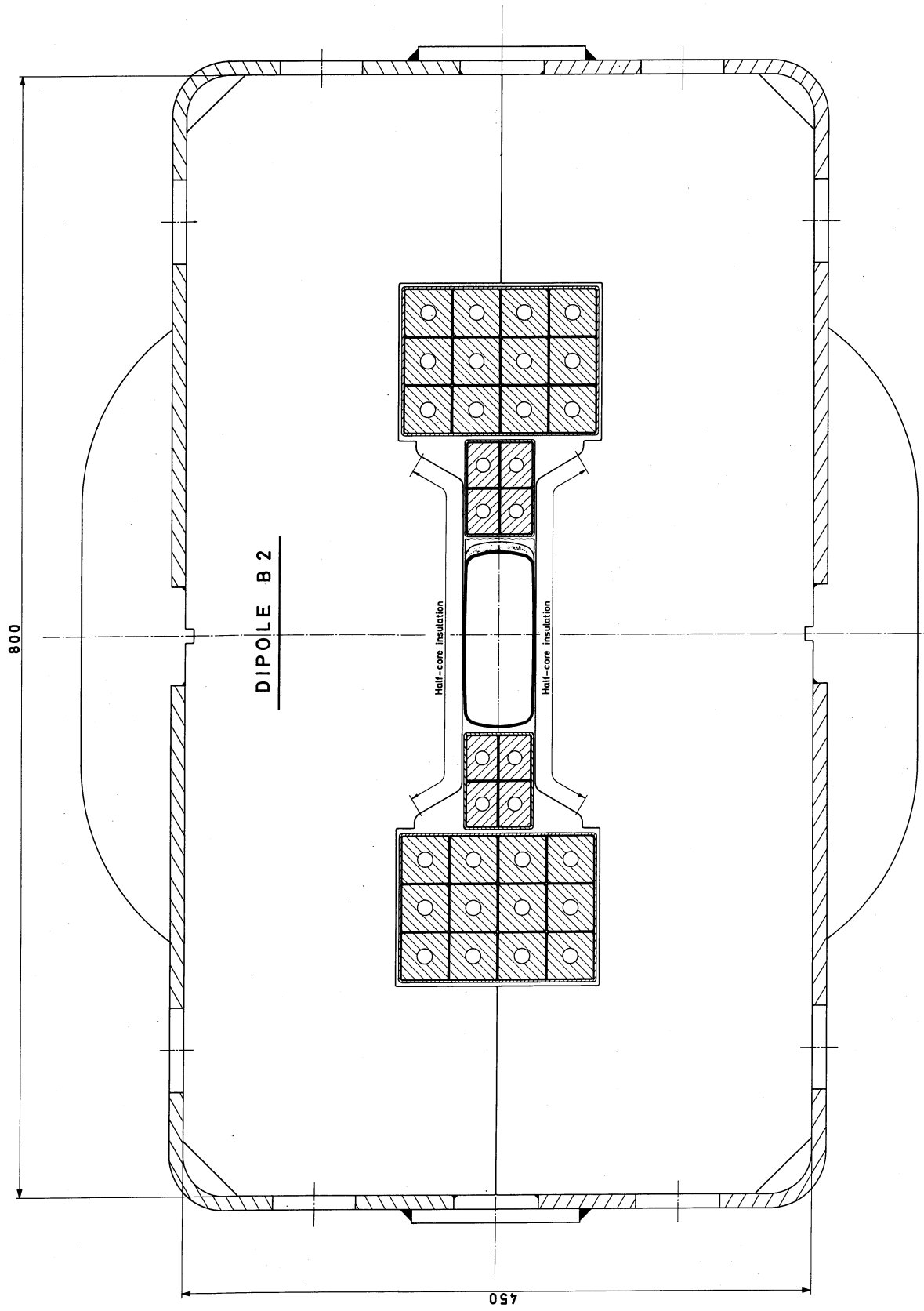

Fig. 4.1b Dipole cross-section B2

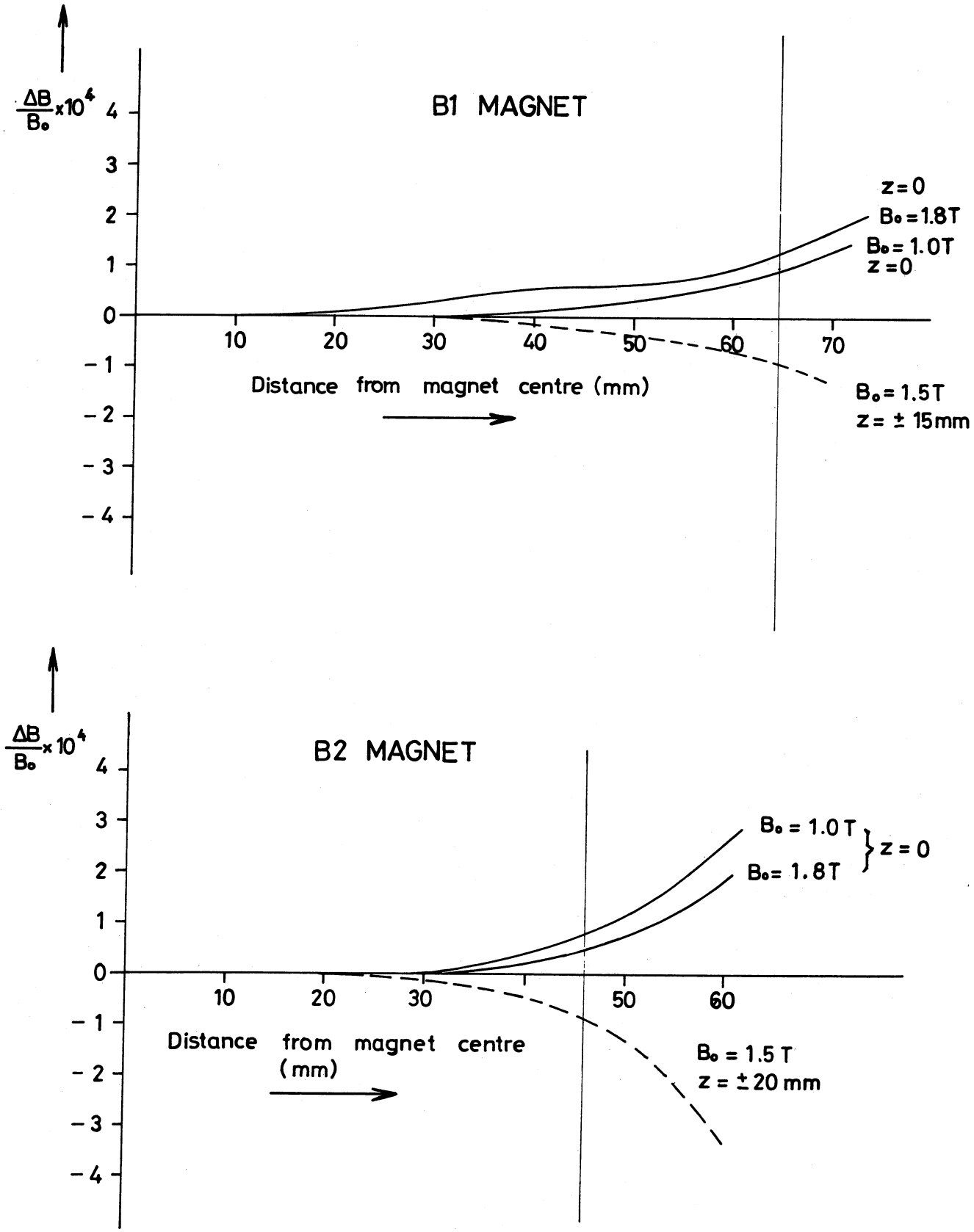

Fig. 4.2 Computed dipole fields

Table 4.2

Dipole characteristics

Magnet type		B1	B2	B2/2
Basic parameters				
Magnetic length	(m)	6.26	6.26	3.13
Maximum field	(T)	1.8	1.8	1.8
Aperture height	(mm)	39	52	52
Aperture width	(mm)	129	92	92
Core characteristics				
Length	(m)	6.220	6.200	3.07
Lamination height	(mm)	2x225	2x225	2x225
Lamination width	(mm)	800	800	800
Packing factor	(%)	96	96	96
Core weight	(ton)	16	15.5	7.7
Blank weight	(ton)	20	20	10
Coils characteristics				
Maximum length	(m)	6.507	6.476	3.346
Number of turns		2+10	4+12	4+12
Conductor inner coil	(mm^2)	24x33	32x22.5	32x22.5
Conductor outer coil	(mm^2)	32x32	33.5x33.5	33.5x33.5
Cooling hole inner coil	(mm)	6.5	10.2	10.2
Cooling hole outer coil	(mm)	10	11	11
Number of water circuits		3	3	3
Amount of cooling water	(m^3/h)	1.9	2.59	3.6
Temperature rise	(^oC)	14	14	6
Pressure drop	(kg/cm^2)	6	6	6
Copper weight	(ton)	1.38	1.88	1.05
Excitation				
Peak ampere-turns	(A)	58800	78400	78400
Peak current	(A)	4900	4900	4900
Rms current	(A)	3102	3102	3102
Average current density(rms)	(A/mm^2)	3.42	3.36	3.36
Resistance	(mΩ)	3.23	4.42	2.47
Inductance maximum	(mH)	7.73	9.9	5.0
Inductance at 1.8 T	(mH)	7.35	9.4	4.7
Losses	(kW)	31.1	42.3	23.6
Peak stored energy	(kJ)	88.2	113	57
Ampere-turns in iron (1.8 T)	(%)	5	5	5

4.3 Dipole fabrication

It is self evident that the main magnet for a large proton synchrotron is the most crucial and expensive single technical component. For this reason it is necessary to ensure that its construction employs well established industrial techniques. Fortunately there is now a wealth of experience available which allows for the design and construction of the system without the necessity for more than a minimum of models and prototypes.

The dipoles are laminated structures, assembled from precision punched, 1.5 mm thick steel laminations. In order to fabricate the magnets from preassembled half-cores to the required precision, it is proposed to utilize the mechanical and structural techniques which were employed at the NAL 200 GeV machine.

The steel to be used will be the same specification as that employed in the ISR magnet system[4.5], which has been successfully produced by several European steel manufacturers. The mechanical properties required for the steel are determined by the need for the precision punching of laminations and also for the fabrication of the half-cores to the required tolerances. Current experience of the mechanical properties of the steel indicates that the maximum thickness for achieving the required precision by punching is 1.5 mm. Due to the simple geometry of the laminations it is believed that the required tolerances will be achieved with a single punching operation.

The important magnetic properties of the steel are a low coercivity and high saturation induction. However, the absolute values are less important than the uniformity of magnetic characteristics over the whole steel delivery. With this type of magnet the spread of magnetic properties with present production techniques does not significantly influence the field distribution within the aperture of the individual magnet. However, in order to avoid excessive variations of the ejection field level between magnets, it will be necessary to mix the steel used in each magnet so as to reduce the effective spread in coercivity by a factor of 5. Based on the experience gained with the production of the steel for the ISR magnets, it is believed that adequate statistics for the classification of the steel will be available after 25% of the steel production.

In order to achieve the required uniformity in effective lengths from magnet to magnet, it is necessary to achieve a stacking factor which is constant to 0.1%. This can be achieved by weighing batches of laminations to this accuracy and compressing them to a fixed length. The nominal weight, and therefore the stacking factor is determined by applying the maximum available pressure to the first stacks and then fixing the weight at a value of 0.5% less than the maximum. This ensures that with variation in crown and insulation thickness, the nominal stacking factor can still be reached.

The basic dimensions of the magnet coils have been given in Table 4.2 and the overall magnet cross sections are shown in Fig. 4.1. The fabrication of the coils can be separated into two stages. The inner and outer coils would be fabricated separately as conventional

vacuum impregnated coils, each with their own ground wrap, after which the two would be assembled into an accurate fixture to locate the inner coil and the two subsequently glued together. This allows the very rigid outer coil to be used as a locating and supporting device for the more flexible and critical inner coil. This assembly can then be mounted in a magnet half-core and pressed inwards during assembly by means of rubber pads or metal springs. In this way the coil assembly can be accurately located radially, but allowed to move freely longitudinally, to allow for thermal cycling of the magnets.

The insulation system for the coils must be suitable for reliable operation in a high radiation environment. It is generally accepted that the most suitable insulation system consists of glass fibre tape which is fully vacuum impregnated with a conventional diglycidyl ether resin system. Although the use of an integrated mica glass tape increases the initial electric strength of the insulation, the loss of mechanical strength together with possible problems caused by gas evolution and irradiation have led to the elimination of mica from the proposed insulation system.

4.4 Quadrupole design

The overall design of the quadrupole system was influenced by very similar considerations to those for the dipoles. The most important of these was the tight tolerances on field gradient uniformity at high excitations. This indicated the need to avoid the appearance of an octupole component at high excitations. Thus the F quadrupole was designed with complete quadrupole symmetry. The inscribed circle radius is 44 mm and the good field width is ±62.5 mm. This results in a minimum gap between adjacent poles of 24 mm (Fig. 4.3).

Using this basic design two possibilities were examined, namely to fabricate the quadrupoles in two halves or from four quarters. In the first case the maximum coil height which can be introduced between the poles is 24 mm, corresponding to a copper height of 18 mm. In order to achieve an optimum copper cross section it was then necessary to use 2 coils per pole, leaving 24 mm between the coils of adjacent poles. This had the effect of producing a long pole and therefore high ampere-turns drop in the steel.

The alternative solution in which the whole coil window can be filled with coil, allows a single two-layer coil to be fitted to each pole. This has the advantage of lower optimized power consumption, improved field quality, reduced coil costs and considerably simplified connections. None of the magnet manufacturers so far consulted have raised objections to this method of fabrication.

The different aperture requirements for the D and F quadrupoles allows a smaller quadrupole to be used in the horizontally defocusing positions. In this case a convenient inscribed circle radius is 35.9 mm which corresponds to a 3:2 turns ratio between F and D quadrupoles, giving an overall saving of 15% of the quadrupole power consumption. However, in this case in order to obtain precise tracking between the two types it proved necessary to reduce

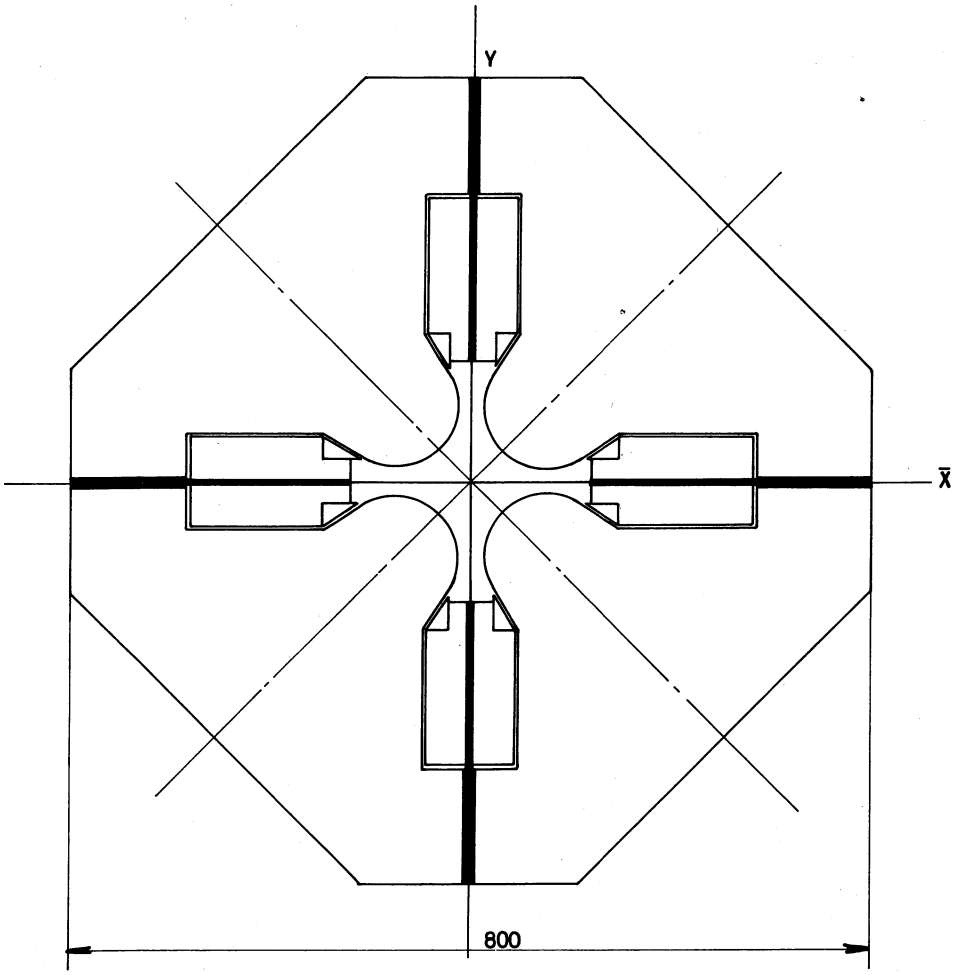

Fig. 4.3 Quadrupole cross-section

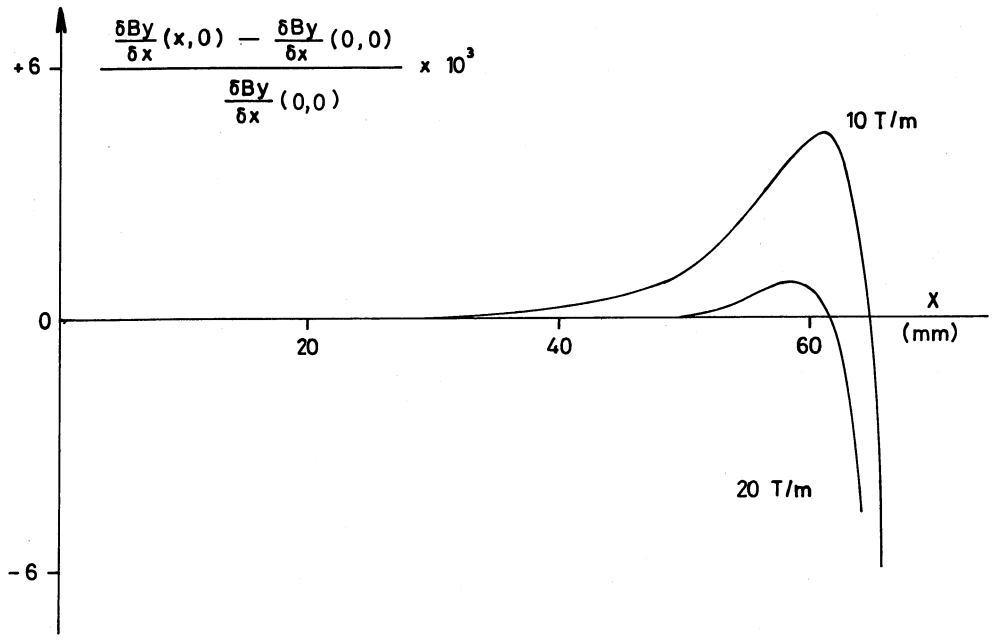

Fig. 4.4 Computed quadrupole gradient

the fraction of ampere-turns in the steel by increasing the overall length of the Q quadrupoles. Also, with the extraction systems proposed, it would be necessary to build two special D quadrupoles to allow the extracted beam orbit to pass through them. In order to maintain the superperiodicity of 6, this would imply a total requirement of 108 F quadrupoles, 96 D quadrupoles and 12 special D quadrupoles. This solution was estimated to be both more expensive, less flexible and give inferior field quality. Thus, the solution adopted is to use identical quadrupoles for the F and D positions. In this case the extracted beam orbit passes through the available aperture in both D positions and requires only a reduced coil height in one F quadrupole to have a beam path on the horizontal symmetry plane.

The coil design was based on the same insulation thickness as the dipoles and its cross section adjusted to minimize overall costs. Following this the outer dimensions were found to be within a few millimetres of the dipole width. Consequently it was decided to increase the coil window slightly to make the overall widths equal and take advantage of possible savings in handling and support systems. It should be noted that the very low current density used in this design is the result of the somewhat unusual constants of a limit to the maximum cooling available together with the maximum permitted peak power demand from the electricity network[4.6]. This has resulted in a current density which is almost a factor of two lower than would have resulted from a completely independently optimized quadrupole system.

4.5 Quadrupole characteristics

The pole profiles and field distributions have been computed using the computer programme MARE. This indicates a variation from low excitation to peak corresponding to a total variation of $4 \cdot 10^{-3}$ in gradient at the edge of the required radial aperture. Since corrections are more difficult to apply at high energies, the pole shape has been adjusted so as to give almost ideal conditions at 400 GeV excitation. The computed gradient curves for the quadrupole are given in Fig. 4.4 and the overall characteristics are listed below.

Table 4.3

Quadrupole characteristics

Basic parameters		
Magnetic length	(m)	3.22
Peak gradient	(T/m)	20
Half-beam height in D quadrupole	(mm)	24.3
Half-beam width in D quadrupole	(mm)	27.2
Half-beam height in F quadrupole	(mm)	10.1
Half-beam width in F quadrupole	(mm)	62.5
Radius of incribed circle	(mm)	44
Core characteristics		
Length	(m)	3.13
Packing factor	(%)	96
Lamination height	(mm)	800
Lamination width	(mm)	800
Core weight	(ton)	9.6
Blank weight	(ton)	12.6
Coil characteristics		
No. of turns per pole		11
Conductor dimensions	(mm^2)	26x20
Cooling hole diameter	(mm)	6.2
Copper weight	(kg)	1346
Pressure drop	(atm)	6
Temperature rise	(^oC)	15
Excitation (Stage C)		
Peak current	(A)	1500
Peak ampere-turns in iron	(%)	7
Average current density (rms)	(A/mm^2)	1.95
Resistance	(mΩ)	11.36
Losses	(kW)	10.24
Peak stored energy	(kJ)	30

4.6 Quadrupole fabrication

The quadrupoles will be constructed from the same type of steel used in the dipoles. This will be stacked to form four identical quarter cores. During the stacking process, the laminations will be 'flipped' at regular intervals to maintain complete symmetry. It is believed that this, together with the simple shape of the quarter lamination, will allow the tolerances to be achieved with a single punching operation.

Following the assembly of the coils into the quarter cores, these can be welded intermittently in pairs so as to equalize the stresses introduced at the four mating surface locations. It has been shown that by carefully controlled welding techniques this balance can be obtained and the surfaces mated to better than 0.02 mm. Although the detailed design of the quadrupoles is not yet complete, the only outstanding problem foreseen is in the fabrication of the end-plates to avoid splaying out of the pole tips at the ends. Several possible solutions are being considered.

Table 4.4

Overall characteristics of the main magnet system

Dipoles		Stage A	Stage B	Stage C
Number of B1 dipoles		180	360	360
Number of B2 dipoles		192	192	384
Number of B2/2 dipoles		-	12	-
Peak field	(T)	1.8	1.8	1.8
Gross steel weight	(ton)	7500	11200	15000
Copper bar weight	(ton)	610	883	1220
Resistance (without cables)	(Ω)	1.43	2.07	2.86
Resistance (including cables)	(Ω)	1.73	2.37	3.16
Maximum inductance	(H)	3.29	4.8	6.58
Peak current	(A)	4900	4900	4900
Stored energy	(MJ)	37.6	57.6	75.2
Dissipation	(MW)	16.65	22.8	30.4
Quadrupoles				
Number of elements			216	
Gradient at 400 GeV	(T/m)		20	
Gross steel weight	(ton)		3670	
Copper bar weight	(ton)		292	
Resistance (without cables)	(Ω)		2.46	
Maximum inductance	(H)		6.1	
Current at 400 GeV	(A)		1500	
Stored energy	(MJ)		6.9	
Dissipation	(MW)		2.2	

References

(4.1) Y. Baconnier, et al., 300-BT/71-2.

(4.2) R. Billinge, 300-MA/Int-71-4.

(4.3) M. Giesch and F. Schäff (private communication).

(4.4) W. Hardt et al., MC/22.

(4.5) L. Resegotti (private communication).

(4.6) S. Van der Meer, 300-PS/71-1.

Chapter 5

THE MAGNET POWER SUPPLIES

5.1 Acceleration cycles and choice of main parameters

The magnet power supplies differ from most previous installations in two important points. Firstly, they will be connected directly to the public supply, instead of using a motor alternator set as a buffer and secondly, the magnet load will have a smaller time constant. For example, compared with the CERN PS magnet, the stage C magnet will have a 5.8 times higher stored energy, but a 14 times higher mean dissipation.

Due to this second feature, the excitation voltage and power are determined to a large extent by the magnet resistance; at the end of the rise, it will absorb about 60% of the total voltage. The resulting peak power still permits direct connection to the public supply, although special measures will have to be taken to keep the power and voltage fluctuations within acceptable limits.

Figures 5.1 illustrates a typical stage C cycle. It will consist of the following parts :

(i) 200 ms debunching time, needed only with the bunch by bunch transfer scheme.

(ii) 190 ms front porch, required to keep about constant r.f. bucket area.

(iii) 1940 ms linear rise, needed in order to limit the r.f. phase angle to 45°.

(iv) 350 ms further rise, now limited in speed by the magnet voltage available. At the end of this interval the current rise is 27% faster than the field rise, due to saturation of the magnets.

(v) 60 ms round-off between rise and flat top, required by the public supply authority in order to improve the distribution of the power transient between generating stations.

(vi) 700 ms flat top

(vii) 120 ms round-off, as under (v)

(viii) 950 ms descent

(ix) 260 ms recovery time.

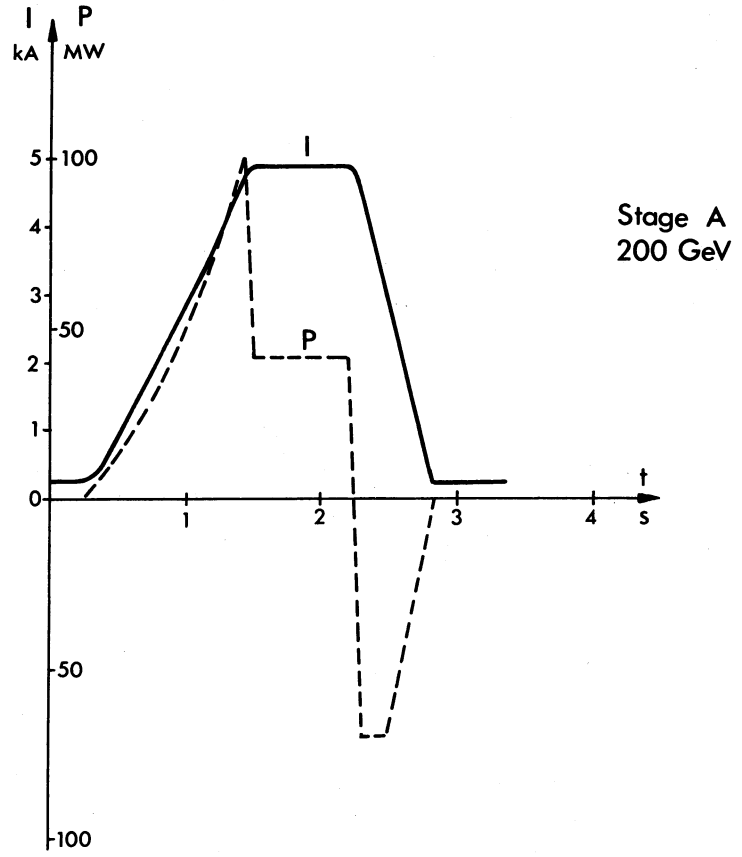

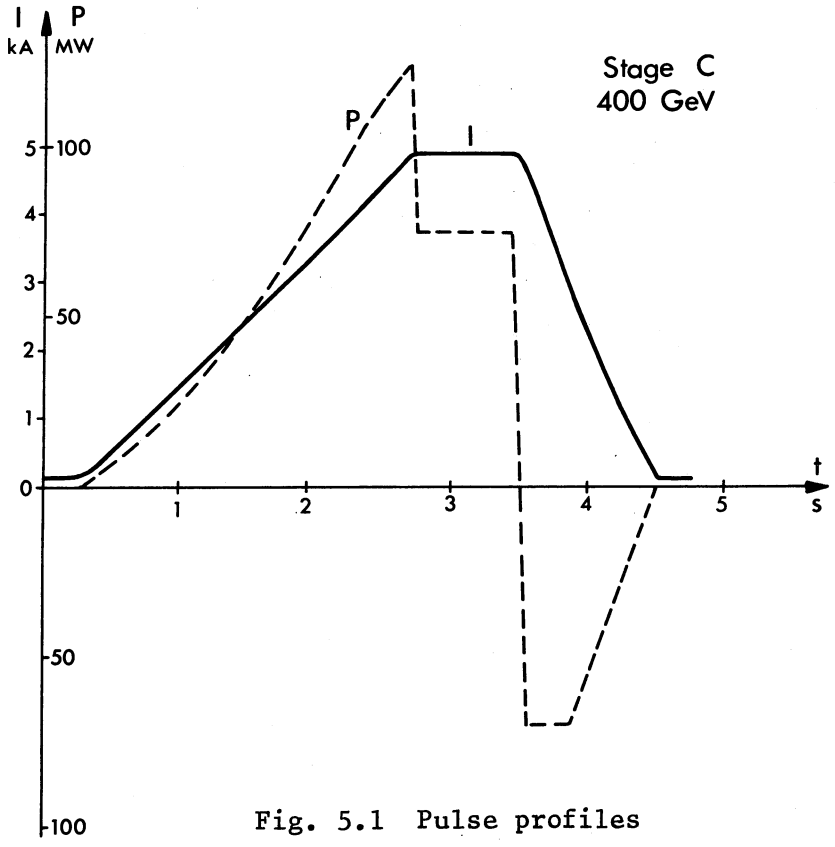

Fig. 5.1 Pulse profiles

The peak power supplied to the magnet was chosen to minimize the total cost of power supply and capitalised power consumption, taking into account the limit imposed by the electricity suppliers EdF*) on the difference between peak and minimum (i.e. negative) power consumption during the cycle.

Clearly, a higher peak power would shorten the rise time and therefore reduce the power loss but due to this limit it would be necessary to reduce the power fed back during descent and therefore again increase the loss during that period. With the parameters finally chosen, the peak power for bending magnets and quadrupoles together will be 135 MW, but during the first part of the descent the power fed back into the network will be limited to 76 MW by controlling the inverter voltage.

The mean power consumption of bending magnets and quadrupoles together will then be 33.5 MW. With the same mean power a cycle with 2s flat top and 8s total duration could also be made, if required. It should be said, however, that slow extraction over such a long flat top may not be possible.

In stages A and B the mean power consumption will, of course, be less than in Stage C, but in order not to exceed the maximum r.m.s. current a small increase of the dead time between cycles would be necessary. The full magnet voltage will not be used during the rise due to r.f. limitation. Total cycle times for each stage with 700 ms flat top will be:

Stage	Cycle Time (s)
A	3.36
B	4.09
C	4.77

More details are given in the parameter list at the end of this report.

5.2 Direct connection to the network

Experience has shown that the motor alternator sets used to buffer most large pulsed accelerators are a potential source of trouble due to the periodic torque reversals which these machines are not usually designed to withstand but which they experience in this application. Moreover, they represent an important fraction of total power supply cost, require complicated auxiliary equipment and a considerable amount of maintenance. It is for these reasons that the present supply will not contain alternator sets but will consist of rectifiers, connected directly to the supply network.

---

* Electricité de France

This is possible because CERN will be connected by a 380 kV line to a strong point of the French electricity grid at Génissiat, ∿30 km from the CERN site. Measurements with pulsed loads and calculations performed by EdF have shown that the power fluctuations caused by CERN will be acceptable, provided that :

(i) the cycle time will never be smaller than 3 s,

(ii) the round-offs mentioned in 5.1 are respected,

(iii) the reactive power variations during the cycle are compensated in order to keep the voltage fluctuations sufficiently low.

Two separate 380/18 kV transformers will be used at CERN, one to feed the pulsed power supplies and one for constant loads. The two 18 kV systems will be completely separated, mainly in order to reduce the phase swing on the constant load system. Under the worst conditions (maximum power cycle, minimum short-circuit capacity of network) the peak-to-peak voltage and phase angle fluctuations produced by the pulse will be :

	Voltage	Phase
at Génissiat (380 kV)	0.30 %	1.6 °
at CERN (normal system, 18 kV)	0.45 %	2.6 °
at CERN (pulsed system, 18 kV)	1 %	26 °

5.2.1 Reactive power compensation

In order to obtain voltage fluctuations as low as those quoted above, the reactive power compensation must be a function of the reactive and the active power consumption of the rectifiers. Taking into account the main magnet supplies as well as other pulsed supplies for r.f. and beam transfer magnets, it appears that the peak reactive power to be supplied during the cycle will be about 80 MVA. This peak will occur at the end of the rise.

The exact type of compensation has not yet been chosen. There are various possibilities such as :

(i) saturable reactors combined with a capacitor bank,

(ii) capacitors, switched on and off stepwise by thyristor switches,

(iii) chokes, switched by thyristors, combined with a capacitor bank ,

(iv) one large choke with current regulation by phase-controlled thyristors, combined with a capacitor bank,

(v) a rectifier working at short-circuit with 90° firing angle and variable current, combined with a capacitor bank.

The choice between these solutions will mainly depend on their respective cost and can only be made after competitive tendering.

Filter chokes will be connected in series with the capacitors used for reactive compensation in order to suppress the harmonic voltage distortion produced by the rectifiers.

5.3 Rectifier stations for the bending magnets

In order to reduce both magnet voltage to ground and delay line effects in the magnet circuit, the series connected magnet ring will be supplied at 12 points. The mid-point of one of the rectifier stations will be earthed.

The 12 stations each supplying a maximum of 2133 V and 4886 A, will be located in pairs in the 6 plant buildings (Fig. 5.2).

Each rectifier station will consist of four series connected rectifier bridges, forming two sequentially controlled 12 phase groups. In addition each station will contain a passive and dynamic filter to reduce the ripple per station to less than 1V. The low ripple is needed in order to limit the modulation of the slow-ejected proton beam.

It is not now intended to use by-pass rectifiers in parallel with each station or with each rectifier bridge because the reduction of reactive power that they permit will not be obtainable when it is most needed, i.e. at the end of the rise. Moreover, it appears that they cannot be used at low currents, where all stations will have to be voltage-controlled simultaneously in order to minimize closed orbit distortion due to delay-line effects in the magnet circuit. A sufficient precision will nevertheless be achieved at injection because in each station two groups will be inverting and two rectifying, so that a result very similar to the use of bypass rectifiers will be achieved.

At higher currents the reactive power consumption would become too high in this mode of operation, and the 12 rectifier stations will then be controlled sequentially in pairs.

5.4 Rectifiers for the quadrupoles

Two rectifier stations will feed the F and D quadrupoles independently. Since the current in both groups will be about equal, a considerable saving in cabling can be achieved by combining the return cables for both systems into one item, which can then be dimensioned for the maximum difference in current between F and D (Fig. 5.3). The requirement of zero current circulating around the ring circumference is still satisfied.

The small auxiliary supply shown in Fig. 5.3 will be needed for adjusting the horizontal betatron phase shift between ejection points 2 and 6 to an integral number of periods, while keeping Q_H and Q_V unchanged. This will be required for obtaining satisfactory sharing

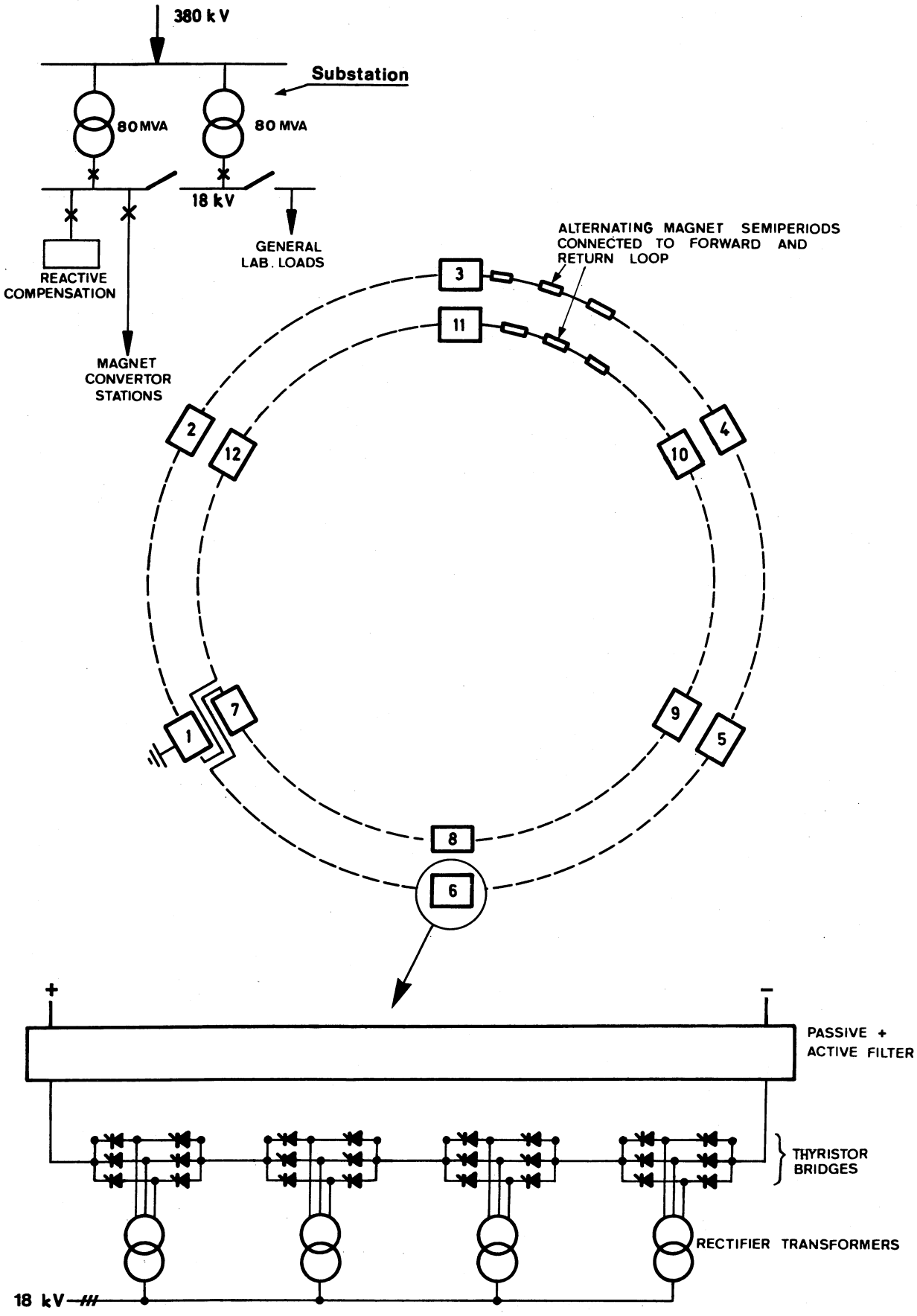

Fig. 5.2 Bending magnet power supply layout

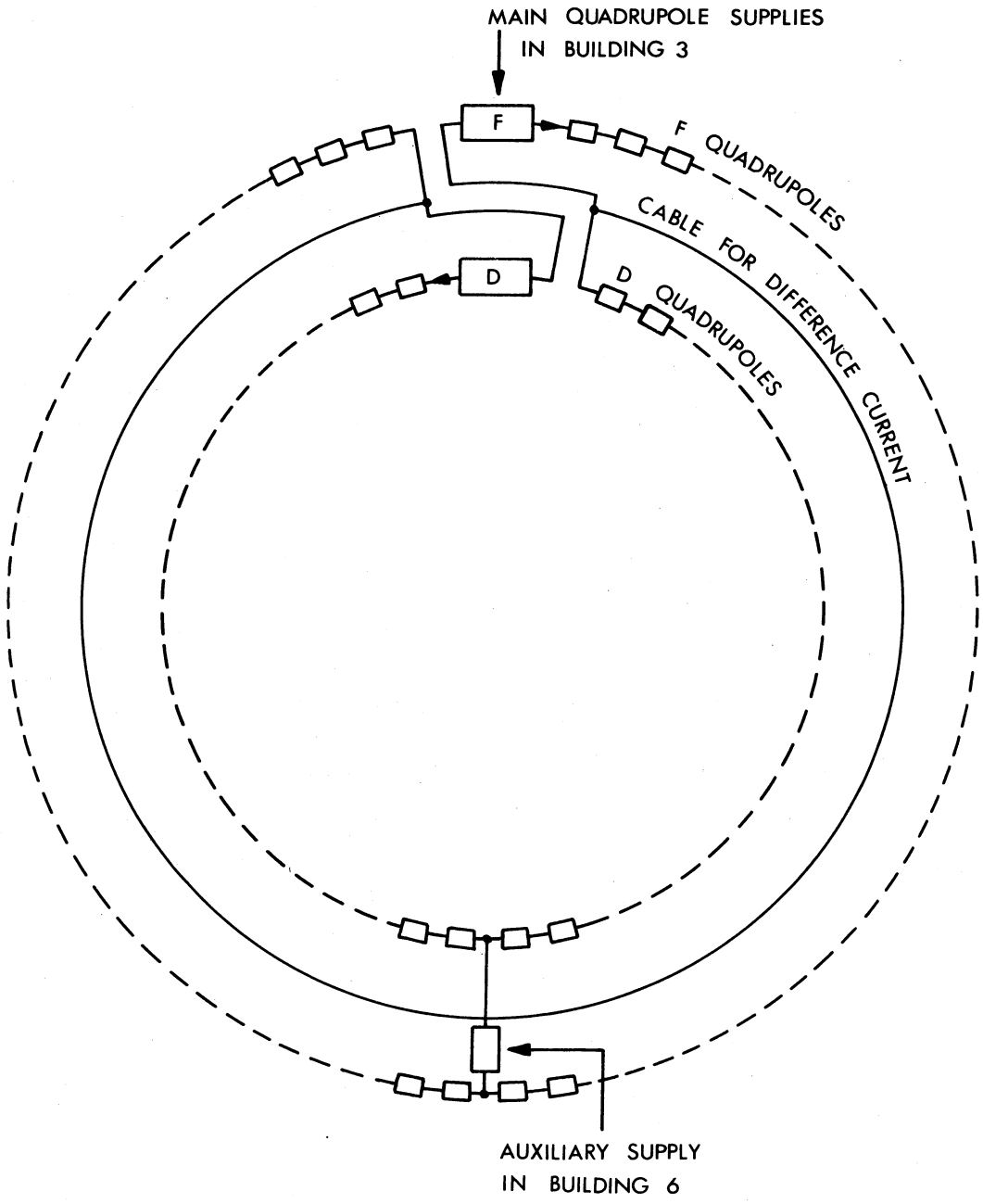

Fig. 5.3 Quadrupole power supply layout

between the two slow ejection systems. With the circuit as shown, the mutual coupling between the three supplies will be a minimum, and the auxiliary supply will not influence the Q values in first approximation.

The two main quadrupole rectifier stations will be similar to the 12 bending magnet rectifiers though their peak current and voltage will be different (1500A and 4090 V).

5.5 Regulation and controls

5.5.1 Bending magnet regulation

Because of the flexibility needed in generating many different types of magnet current cycles and the complication involved in the differing sequential voltage changes required at the 12 convertor stations it is intended to have 12 reference programmes generated by a computer equipped with digital to analogue convertors.

During most of the rise time the rectifier output voltage is the important parameter to be considered. However, during the injection and debunching platform as well as during flat-top, current is the controlled quantity. During decay the convertor voltage is controlled subject to considerations of invertor safety angle.

The computer will therefore generate 12 voltage reference waveforms. In addition, the magnet field or the output current will be monitored by the computer so that corrections can be applied to the various references during and between pulses in order to obtain the required voltage distribution between stations and output current waveshape. The latter would hardly be obtainable through current feedback alone because of the low loop gain available at the frequencies present in the current programme.

The necessary suppression of the effect of mains voltage fluctuations will be easily achieved with the required precision through the voltage regulation alone. The current regulation will mainly be required to reduce the influence of magnet resistance changes on injection and flat-top currents.

5.5.2 Quadrupole regulation

The regulation system of the quadrupole power supplies will be similar to that of the bending magnets. The bending magnet current will be used as a reference in order to improve the tracking precision. Corrections may, of course, have to be added for the different saturation characteristics of magnets, F lenses and D lenses. The use of field and gradient pick-up coils mounted in the reference magnets and lenses and giving signals proportional to the Q errors might also be considered.

5.5.3 Reactive power compensation control

If a "switched step" form of reactive power compensation is chosen, the control of the steps can be satisfactorily achieved by the same computer that generates the magnet programmes, since the required reactive component of the a.c. current is a sufficiently well defined function of the magnet current programme.

5.5.4 Other controls

Nearly all other controls and status signals will be transferred between the equipment buildings and the control centre by means of the multiplex system (See Chapter 9).

The only exception will be a few hard-wired interlock circuits needed for the main circuit breakers, short circuit switches etc.

CHAPTER 6

THE ACCELERATION SYSTEM

6.1 Introduction

The r.f. accelerating system has to provide for a minimum total peak accelerating voltage per turn, V, which is given by two conditions. Firstly, the bucket area (longitudinal phase space), at injection and throughout acceleration must be large enough to accommodate the energy spread of the injector. Secondly, sufficient energy gain of the particles per turn must be available to obtain a reasonably short accelerating time.

For both conditions the stable phase angle ϕ_s plays a very important role. The smaller the value of ϕ_s the larger the bucket area becomes, but the accelerating time increases also. This is illustrated by the following two equations.

Bucket area
$$A = \alpha(\phi_s) \left(eV \frac{\gamma}{|\eta|} \frac{128}{h \pi E_0} \right)^{\frac{1}{2}} \tag{6.1}$$

Accelerating rate
$$\dot{p} = \sin \phi_s \frac{eVc}{2\pi R} \tag{6.2}$$

where:

A = bucket area in units of $\Delta(\beta\gamma)\phi_{rf}$

ϕ_s = synchronous phase angle (measured from zero crossing of the accelerating wave)

$\alpha(\phi_s)$ = moving bucket factor

γ = energy to rest energy ratio

$\eta = \frac{1}{\gamma^2} - \frac{1}{\gamma_t^2}$; $\gamma_t = \gamma$ at transition

h = harmonic number

E_0 = rest energy

c = velocity of light

R = average machine radius .

At injection ϕ_s is zero ($\dot{p} = 0$) and, once transfer and transition energy are chosen, the free parameters which determine the bucket area are only the voltage and the harmonic number which in turn determine the frequency. In practice these two parameters are not completely free

since they also determine Q_s, the number of phase oscillations per turn, which must be kept small.

$$Q_s = \frac{\sqrt{\cos \phi_s}}{\beta} \sqrt{\frac{|\eta|}{\gamma} \frac{heV}{2\pi E_0}} \tag{6.3}$$

Q_s should be less than 0.2 and preferably even less than 0.1 if the accelerating gaps are not distributed symmetrically around the ring[6.1]. This certainly presents a strong argument for having a frequency as low as possible, a fact which will be taken into account in the next sections. For a given choice of harmonic number, Equations 6.1 and 6.3 give us the lower and upper limits for the accelerating voltage. These voltage boundaries change with ϕ_s as soon as acceleration starts and tend to diverge towards the end of the accelerating cycle. To keep within the boundaries, voltage as well as ϕ_s, can, or must, be programmed over certain parts of the cycle. ϕ_s must only be increased slowly after injection during the so-called front porch. This subject will be dealt with in detail in Section 6.8. Later on in the cycle ϕ_s can be increased to higher values, but for stable operation it should not exceed a certain maximum. It is felt that the safe limit of ϕ_s is 45°. Thus the boundary conditions of choice of voltage are determined throughout the cycle and the accelerating voltage can be chosen within them.

6.2 Choice of Frequency

The choice of frequency is influenced by a number of factors, some of which are technical and some of which are concerned with beam dynamics. We shall now give a survey of the most important of all the relevant arguments.

First of all, it can be said generally for all r.f. systems that have been proposed so far, that their shunt impedance per unit length tends to increase with increasing frequency, i.e. for an accelerating structure occupying a given length along the particle orbit, the r.f. power required to generate a given accelerating voltage tends to decrease with increasing frequency. Another advantage of a higher frequency is that, due to a smaller energy storage, filling and discharge times are reduced. This might be important for a more sophisticated phase jump scheme at transition and for various other phase correcting procedures.

Factors against the choice of a high frequency are the constraints on bucket area and on the number of phase oscillations per turn mentioned above. Also, physical aperture decreases with increasing frequency, losses are possibly higher in the cavities, and suitable hardware may be difficult to obtain.

One of the novel features of the SPS is the small frequency swing required between injection and full energy. This is only 0.44% for injection at 10 GeV/c. It is this small bandwidth that allows us to consider untuned wideband systems which we prefer over ferrite

or mechanically tuned alternatives. The reasons for this preference are set out in Section 6.4. The choice of a wideband cavity has been the deciding factor in our choice of frequency.

6.3 Acceleration Parameters

In Table 6.1 we list those machine parameters which are related to the r.f. accelerating system design:

Table 6.1

Injection momentum	10 GeV/c
$\gamma_{transition}$	24
Maximum bunch area, A_{max}	0.22 rad
Maximum synchronous phase angle, $\phi_{s\ max}$	45°
Average circulating beam current for 10^{13} p.p.p.	70 mA
Maximum bending field	1.8 T

There is, of course, some uncertainty in the maximum momentum spread which is to be expected in the beam transferred from the improved CPS, but it is estimated to be below $\pm 1.3 \cdot 10^{-3}$ for bunch-by-bunch transfer. Taking this value and allowing for an increase of 25% due to transfer and trapping, we obtain for the maximum bunch area, A_{max}, the value given above. A_{max} sets the lower limit for the size of the bucket area which is to be maintained by the r.f. accelerating voltage over the whole cycle. There are two "bottlenecks" which require special consideration: the problems near injection and a minimum in bucket area around $\sqrt{3}\ \gamma_{tr}$ for V = const.

The requirements to provide this bucket area and, at the same time, keep Q_s below 0.05, places an upper limit on h, the harmonic number. This is most restrictive at injection where Q_s is high and we can write, combining (6.1) and (6.3) to (6.4):

$$h \leq 16 \cdot \frac{Q_s}{A} \cdot \left\{ \frac{\beta\gamma}{|\eta|} \right\}_{injection} = 5500 \qquad (6.4)$$

$$\text{for } Q_s = 0.05 \quad \text{and} \quad A = 0.22 \text{ rad} \ .$$

We have chosen a harmonic number of 4620 which yields an r.f. frequency of 200 MHz. This happens to be a multiple of the CPS harmonic number and it also contains the ratio of the radii of both machines and the superperiodicity of six. This facilitates transfer and beam control to a certain extent. At the same time, there is already some experience in handling high r.f. power at about this frequency, as most of the big proton linear accelerators are using it.

For this harmonic number we get the following voltage boundaries, imposed by the need to provide sufficient bucket area without too high a value of Q_s:

Table 6.2

	Injection	$\sqrt{3}\,\gamma_{tr}$
V_{min} for A = 0.22	3.4 MV	5.4 MV (for $\phi_s = 45°$)
V_{max} for Q_s = 0.05	4.9 MV	-

For high accelerating rates modulation of V over the cycle will be necessary in order to reduce the r.f. voltage near injection to values below 5 MV.

6.4 Choice of Travelling-Wave Structure

Of all possible methods of r.f. acceleration we have adopted an untuned wide-band travelling-wave system. Compared with the conventional solution of servo-tuned resonant cavities - such as ferrite cavities - our system offers the following advantages:

(i) total absence of tuning equipment (ferrite saturation, ferrite cooling), with the associated cost and complexity;

(ii) absence of any equipment other than passive metal structures in the accelerator tunnel;

(iii) the possibility of concentrating the total r.f. power in a few large power sources located in a surface building, leading to economy and simplicity;

(iv) the feature that the accelerating structure and the power source are separated by a matched transmission line, making it possible to add or change power source at any time in order to cope with increasing beam intensity or repetition rate;

(v) the peculiar property of our structure to convert power loss into beam power at increasing beam intensities, leading to an increase of efficiency with increasing beam load.

Points (iv) and (v) are particularly valuable for an accelerator of expandable intensity and energy.

In such a travelling-wave system the accelerated particles are in nearly continuous interaction with an accelerating wave. A particle would experience a maximum energy gain if it rode on the crest of the accelerating wave all the time or, in other words, the velocity of the phase of the r.f. wave, v_p, should equal the velocity of the particles.

In a periodically loaded waveguide v_p and the propagation speed of energy, the so-called group velocity, v_g, are independent variables. v_p is chosen so as to equal one

particular particle velocity, whereas v_g determines the phase slip between particles and wave per unit guide length as a function of particle velocity variation. In linear approach we obtain the phase slip between beam and r.f. wave, τ, and the circuit impedance V^2/P:

$$\tau = \frac{L}{|v_g|} \omega_0 \left(\frac{\beta}{\beta_0} - 1 \right) \tag{6.5}$$

$$\frac{V^2}{P} = \frac{R}{Q} \frac{\omega}{v_g} L^2 \frac{\sin^2 \frac{\tau}{2}}{(\tau/2)^2} \tag{6.6}$$

L = interaction length

ω_0 = r.f. angular frequency for which $\tau = 0$

β_0 = particle velocity for which $\tau = 0$

τ = phase slip between beam and r.f. wave

$R/Q = 2 \times \frac{\text{characteristic impedance}}{\text{unit length}}$ of the structure

For a given r.f. power and a given frequency the energy gained by a particle is proportional to the interaction length along the beam, as long as the phase slip and both losses and beam load are small. On the other hand $|\tau|$ increases with length for a given β/β_0. This effect can be used to provide the modulation for the energy gain of the particles without modulating the r.f. power sources (see Table 6.2). For this reason β_0 should be close to unity so that the full energy gain is available during the steep rise of the magnetic field, whereas the downward modulation near injection is adjusted by proper choice of v_g and L.

It follows from Equation (6.6) that the accelerating structure should have as high a value of R/Q as possible if power input is to be economized. The first possible choice that comes to mind is, of course, the usual disc-loaded guide. A typical value of R/Q for this structure is about 270 Ω/m at 200 MHz. There are, however, several other structures which exhibit substantially higher R/Q values than the disc-loaded structure. The ones that seem to be most interesting for our purpose belong to a group of bar-loaded structures which have become known under names such as jungle-gym, wire-loaded, or cross-bar structures. These structures consist of circular or square guides which are periodically loaded with transverse bars. The bars may be single or double with or without drift tubes. Measurements of bar-loaded structures have been carried out at CERN[6.2] yielding R/Q-values up to 650 Ω/m by adding drift tubes. As the ratio of R/Q-values to the corresponding v_g-values is nearly constant with varying drift tube length, an appropriate choice can be made to match the modulation requirements at injection.

6.5 Beam Power Loading

The presence of beam loading modifies the spatial distribution of the electric field along the guide. The change of input power required to restore the average accelerating field to its desired value does not necessarily equal the beam power, in fact, it may even be negative under certain circumstances. At the frequency at which the phase velocity equals the particle velocity, the average beam-induced voltage in the guide ($\underline{V}_b$) is 180° out of phase with the beam and of purely decelerating nature. The angle is leading with a purely decelerating field when the frequency is below this centre value and lagging when the frequency is above. The total equivalent accelerating voltage of amplitude V_t and phase ϕ_t with respect to the beam is the sum of $\underline{V}_b$ and the r.f. driven voltage $\underline{V}_{rf}$. For symmetric bunches we may write $\phi_t = (\pi/2) - |\phi_s|$; ϕ_t is negative below transition and positive above, as the accelerating peak of the r.f. voltage has a lagging phase angle with respect to the beam below transition and vice versa. Fig. 6.1 shows the vector diagram for all these voltages with respect to the beam phase.

In order to compensate for the beam loading the r.f. input has to be adjusted so as to make $\underline{V}_t$ equal in amplitude and phase to the desired acceleration voltage. If we subtract $\underline{V}_b$ from $\underline{V}_t$ we will obtain the required r.f. voltage $\underline{V}_{rf}$

$$\underline{V}_{rf} = V_t \left[\left(\cos \phi_t + \frac{P_b}{P_t} \frac{1}{4 \cos \phi_t} \right) + j \left(\sin \phi_t + \frac{P_b}{P_t} \frac{1}{4 \cos \phi_t} \operatorname{tg} \phi_b \right) \right] \qquad (6.7)$$

with $\operatorname{tg} \phi_b = - \dfrac{\tau - \sin \tau}{1 - \cos \tau}$

and beam power $P_b = V_t J_{rf} \dfrac{\cos \phi_t}{2}$

P_t stands for the power which is necessary to obtain V_t without beam loading

$$P_t = \frac{V_t^2}{(V^2/P)} \quad \text{with} \quad (V^2/P) \quad \text{from (6.6)} \ .$$

The phase angle of the driven r.f. voltage is given by

$$\tan \phi_{rf} = \frac{2 \sin 2\phi_t - P_b/P_t \operatorname{tg} \phi_b}{2 \cos 2\phi_t + 2 + P_b/P_t} \qquad (6.8)$$

and with $\tau = 0$; $\phi_t = 45°$

$$\tan \phi_{rf} = \frac{1}{1 + 0.5 \, P_b P/_t} \qquad (6.8a)$$

The phase jump at transition does not cause any abrupt change of beam loading conditions if ϕ_b equals π, which is the case for a phase slip $\tau = 0$. Therefore β_0 in Equation (6.5) should

be made equal to β at transition, which leads to a negative τ for all frequencies below transition and positive above, without any difference whether a forward or a backward wave structure is chosen. One realizes easily by checking with Fig. 6.1 that beam loading has a flat maximum around $\tau \approx 0$. The required r.f. power for this region and for our maximum $|\phi_s| = \pi/4$ is:

$$P_{rf} = P_t \left\{ \left(\frac{P_b}{P_t} \right)^2 \frac{1}{8} + \frac{P_b}{P_t} \frac{1}{2} + 1 \right\} \quad . \tag{6.9}$$

Another interesting fact is that shortly after injection a phase difference of less than $\pi/2$ between $\underline{V}_b$ and $\underline{V}_t$ is possible and therefore a reduction rather than an increase in r.f. power is required for increasing beam load during this part of the cycle. The phase angle of the driven r.f. voltage is not equal to ϕ_t, but is a function of the beam loading as expressed by (6.8) and (6.8a). However, a probe right at the middle of the tank measures the phase of $\underline{V}_t$ which can be compared with the phase of the beam, thus allowing normal control of the r.f. wave.

6.6 Parasitic Beam Loading

The beam-induced voltage does not only affect the r.f. power balance, but it produces some other effects also. There is, for example, the problem of self-bunching of the beam at any of the harmonic numbers that fall within the passband. This effect is mentioned already in Chapter 3.

For a possible harmonic number h^*, the coupling impedance must be low to allow for high intensities. On the other hand a high cavity shunt impedance is needed, in order to obtain a reasonable ratio of P_b/P_t. The best way to get out of this dilemma may be to use a feedback system which can be switched on during the critical debunching time. Such a system could work in the following way: a signal is picked up from the beam, either by the cavity itself or by a pick-up electrode with the same band-width as the cavity. It is possible to delay this signal and invert it in phase until the same bunches which have induced the voltage come back. Since during one turn synchrotron oscillations can never be larger than 18° at injection and $\sim 3^\circ$ above transition, a certain counteraction on an unwanted bunch structure is possible even in the case of rotating bunches. Care must be taken to fulfill certain phase gain conditions in the feedback loop and a special small r.f. cavity may be required should such a system prove necessary. One hopes, however, that the conditions will, in any case, be met.

Parasitic resonances outside the passband or higher passbands might also make beam-cavity interaction possible. In fact, longitudinal cavity resonances of this sort were found in most cases to be responsible for the coherent longitudinal instabilities, as they provide the necessary coupling between the fields in the wake of the bunches and the subsequent bunches. These instabilities may lead to bunch blow-up at high intensity. There

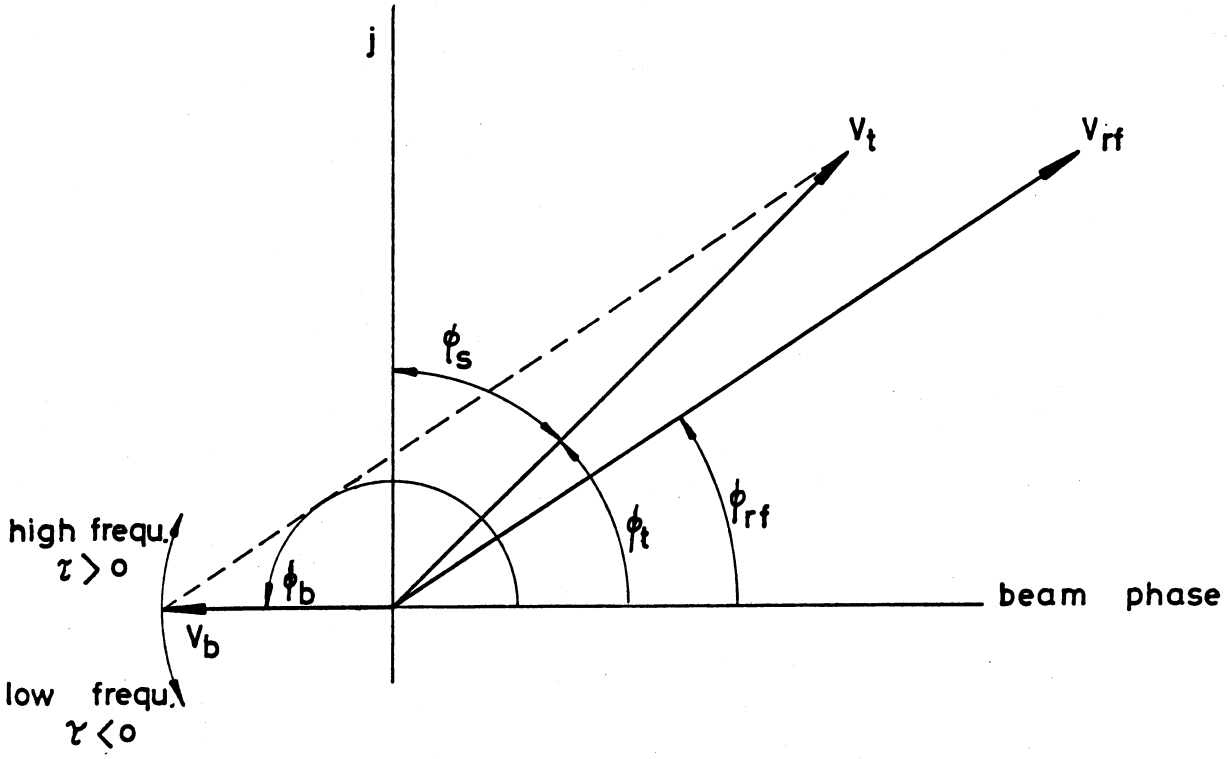

Fig. 6.1 Vector diagram just above transition (τ = 0)

exist also so-called deflecting modes such as those responsible for the wellknown beam break-up in electron linacs. Fortunately, it is an advantage of the proposed travelling-wave structure that no resonance or mode has been found which has the same phase velocity at its fundamental space harmonic as the beam. Interaction may be possible, however, at higher order space harmonics. All the modes of this particular type investigated until now have shown coupling impedances which are low enough not to affect the beam appreciably. Nevertheless, provision can be made to suppress the most important parasitic resonances by selective resistive loading, if need be. It is also possible to stagger detune the higher modes from cell to cell by tapering of the cell dimensions, without the fundamental being detuned.

6.7 Details of Construction

The proposed accelerating structure is of the backward wave type and consists of a circular guide loaded with double transverse bars and with drift tubes. All bars are in parallel position, which yields values of group velocities appropriate for our application.

By using pairs of bars instead of single stems together with properly designed drift tubes, it is possible to use uninterrupted pipes for the water cooling. This is important as it avoids complicated welds in the system. Fig. 6.2 gives an impression of this arrangement. The optimum tank length is about 20 m. On either end of each tank there is a coupler of coaxial construction for the transmission lines (rigid coaxial lines) going up to the equipment room at surface level; this is shown in Fig. 6.3. Only the accelerating guides themselves are placed in the machine tunnel. The power amplifiers and terminating loads are accessible when the machine is running. One long straight section accommodates three structures with couplers and flanges. The distance between power amplifiers and structures is at least 60 m and one has to take into account a power attenuation of 5% for coaxials of this length. More and/or bigger power amplifiers can be added later, without major difficulties, if higher accelerating rates and higher beam intensities are desired, as the structures represent matched loads, and cooling and sparking problems leave a wide margin. Fig. 6.4 shows the layout of the accelerating cavities. Table 6.3 lists the most important r.f. parameters for a proposed accelerating system, which is able to provide the necessary longitudinal phase space and a reasonable rate of acceleration under the given maximum beam loading. Should this prove in the light of experience with the improved CPS to be overgenerous, it may be possible to dispense with one of the three r.f. cavities.

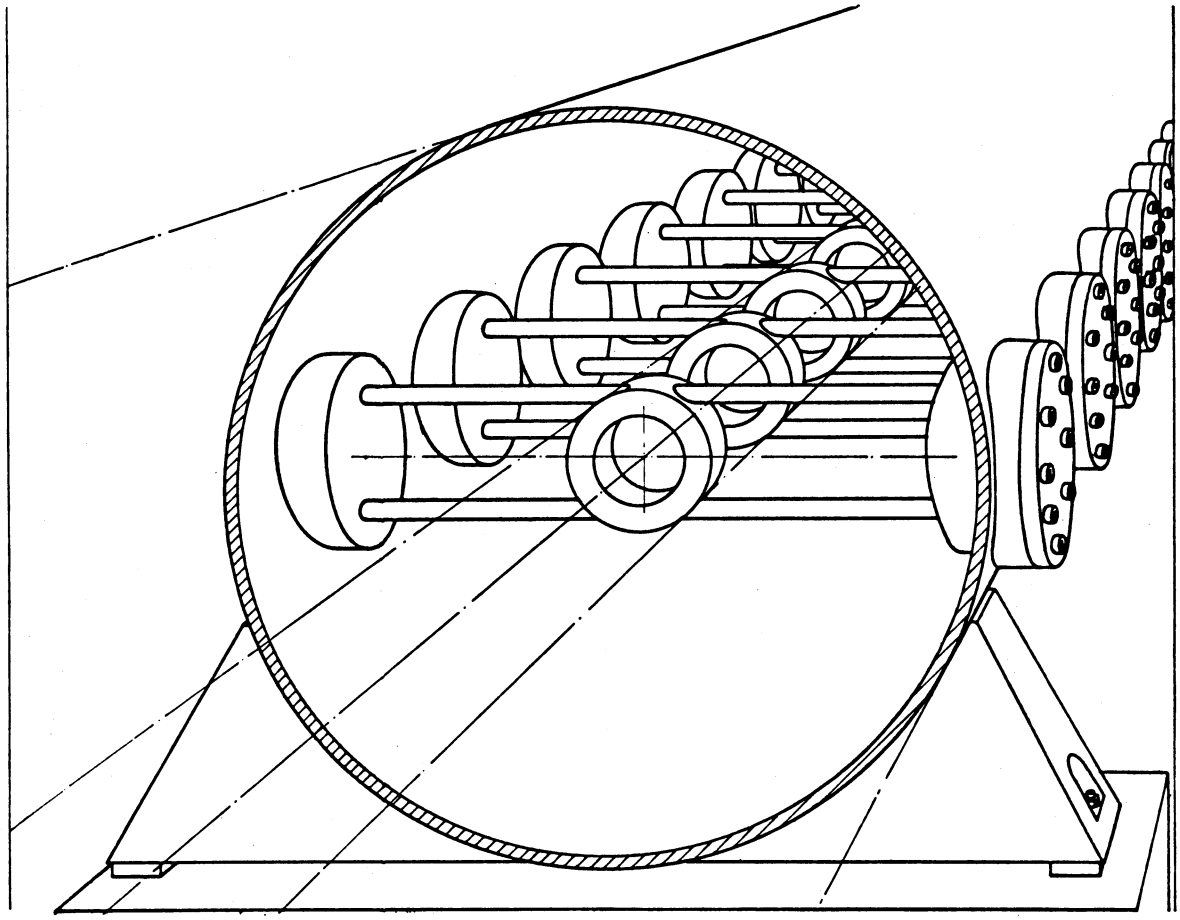

Fig. 6.2 Cut through the structure

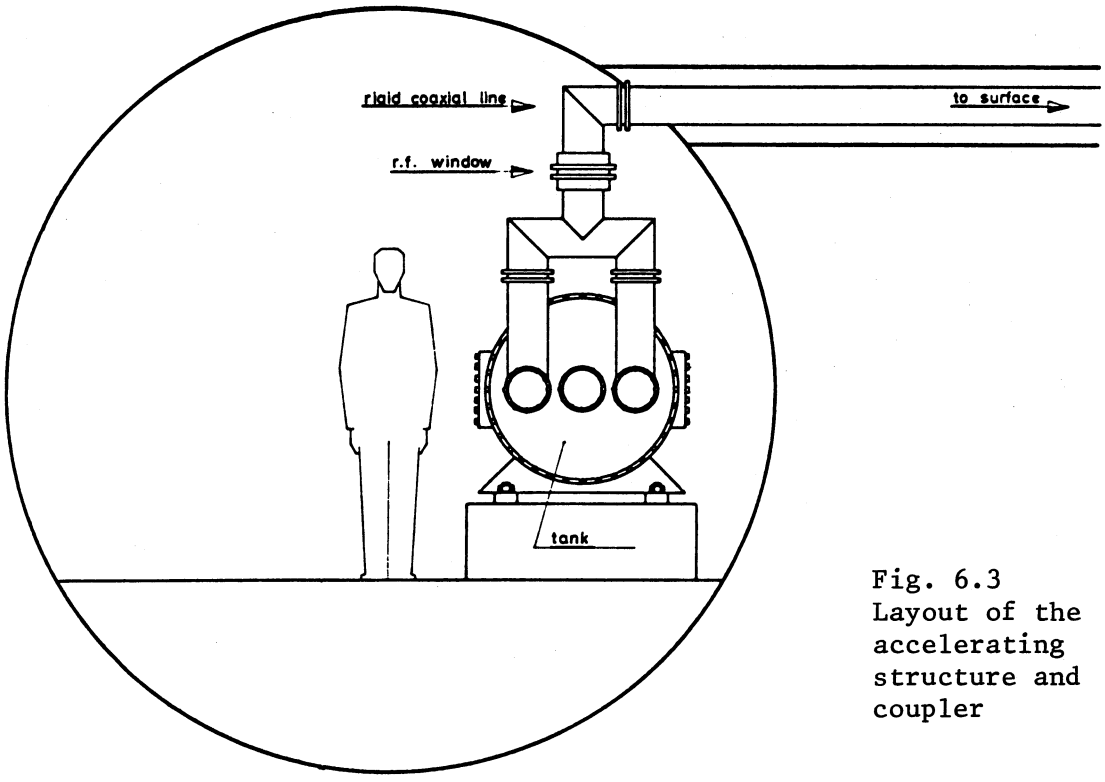

Fig. 6.3
Layout of the accelerating structure and coupler

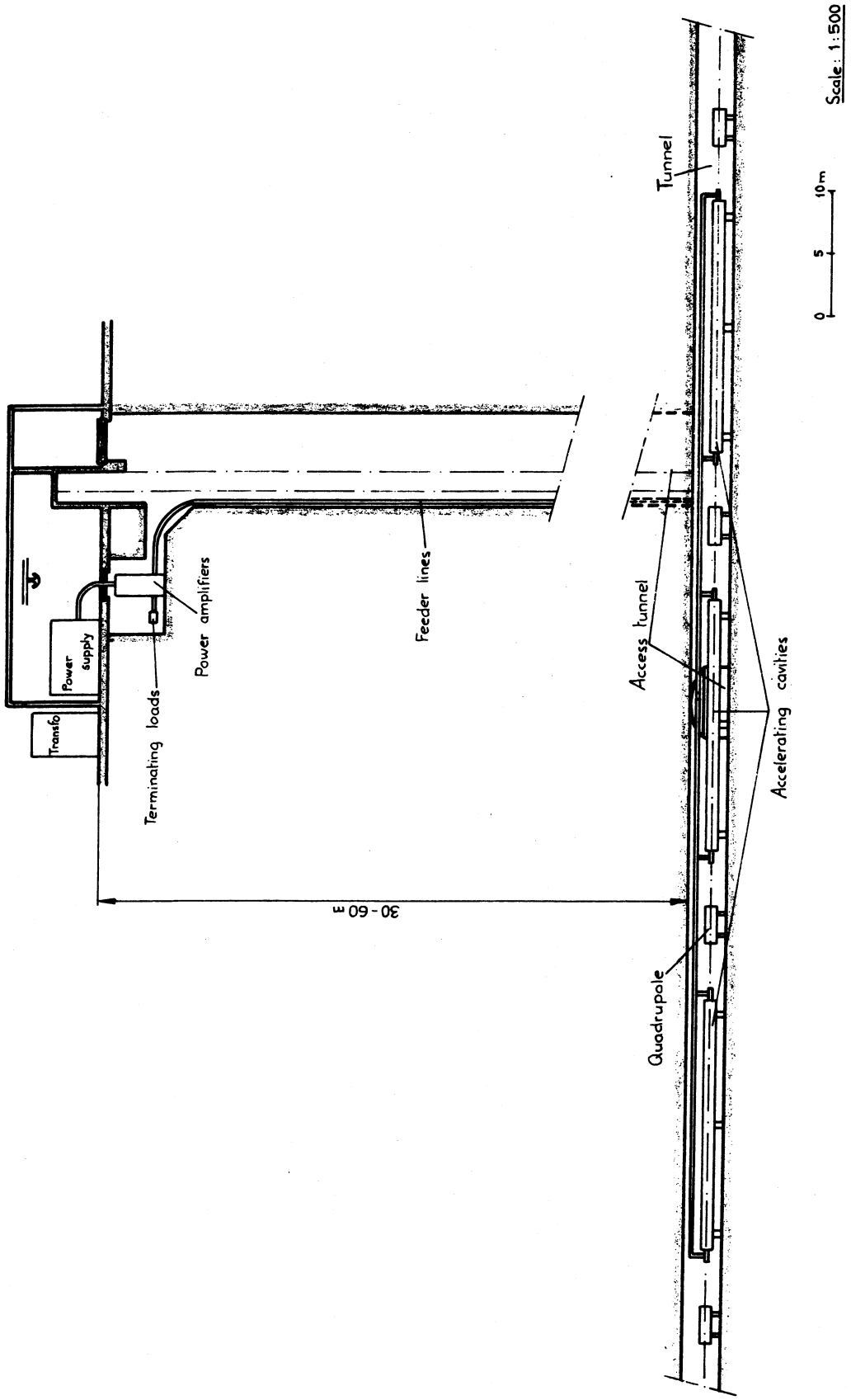

Fig. 6.4 Layout of cavities

Table 6.3

Number of RF cavities	3	
Total RF power per cavity	500	KW
Harmonic number	4620	
Frequency at transition	200. 225	MHz
Total frequency swing	0.44	%
Peak RF volts per turn (10^{13} p.p.p.)	5.4	MV
Peak RF volts per turn at injection*)	3.7/4	MV
Frequency of synchrotron oscillations at injection*)	1.9/2	kHz
Maximum of RF bucket area during front porch	0.22	rad
Maximum possible momentum spread in PS-beam	$\pm 1.64 \cdot 10^{-3}$	
Maximum momentum spread after trapping and full buckets	$\pm 2.6 \cdot 10^{-3}$	
Maximum rise of momentum	166.7	GeV/c/s
Maximum beam loading	270	kW
Maximum phase angle	45	Degr.
Phase angle at start of front porch	1	Degr.
Time for front porch	0.19	sec
Momentum at end of front porch	19.63	GeV/c
Interaction length of cavity	18.7	m
Diameter of cavity	0.8	m
Cells per cavity	50	
Phase advance per cell at transition	$\pi/2$	
R/Q	650	Ω/m
Maximum effective shunt impedance per cavity	11	MΩ
Group velocity over velocity of light	0.088	
Phase slip between beam and RF		
At injection	-180	Degr.
At end of front porch	- 14	Degr.
At $\beta = 1$	44	Degr.

*) Values for negligible beam loading and 10^{13} p.p.p.

6.8 Front Porch

It follows from all that has been said in the preceding sections that, for a given r.f. power, the ratio between the available accelerating voltage at injection and the voltage for a given beam load during maximum rise of the guiding field will be given by appropriate choice of the length of each accelerating structure and the group velocity. If full use is made of the available r.f. power, the voltage follows a certain function during the part of the magnet cycle which is called "front porch". Now, one must avoid

loss of particles due to spillout later on after capture. When acceleration starts, ϕ_s becomes finite and if additional voltage is not provided the bucket will shrink to a minimum size which must be maintained at least all over the cycle. This condition leaves the moving bucket factor $\alpha(\phi_s)$ as the only free parameter for Equation (6.1) during the front porch until the limit corresponding to a $\phi_s = \pi/4$ is reached. From there on the bucket area will grow, a fact which marks the end of the front porch. The parameter $\alpha(\phi_s)$ is adjusted by shaping the magnetic field rise as a function of γ.

$$\dot{B} \propto V \sin \phi_s \tag{6.10}$$

The required time for the front porch is obtained by

$$t_{f.p.} = \int_{B_{inj}}^{B(\gamma)} \frac{dB}{\dot{B}} \tag{6.11}$$

The proposed r.f. system, as listed in Table 6.3, provides a maximum bucket area of A = 0.23 at injection and for stationary buckets. If we allow a reduction to A = 0.22 (see Table 6.1) rather than increasing the r.f. power, we obtain a front porch length of 190 msec. This value is calculated for the worst conditions, i.e. negative beam loading is neglected but positive beam loading is taken into account. Fig. 6.5 shows the variation during the front porch of the magnetic field B, the magnetic field gradient $\dot{B}$ and the synchronous phase angle ϕ_s. It also shows the ratio of $\dot{B}/B$ which may present a limit due to eddy current effects in the vacuum chamber (see Chapter 8). The plotted curves in Fig. 6.5 only represent an upper limit for $\dot{B}$, and therefore also for B, as far as the r.f. power capacity is concerned, but the use of lower values for $\dot{B}$ in order to reduce these eddy current effects may be considered.

6.9 Low Level System

The r.f. system will be equipped with a phase-lock beam-control system which will be similar, in principle, to that of existing strong focusing machines. In such a system the frequency and phase of the accelerating voltage is derived from the bunched beam itself by means of an induction electrode.

The phase lock system must be supplemented by a radial control system in order to keep the beam at the desired orbit. In this system a voltage derived from two radial-displacement electrodes, displaced by half a betatron wave-length, controls the average energy gain per turn via the stable phase angle so as to maintain the particles at the correct radius.

The possible error due to the measurement being made at a single region of the machine circumference may be checked by a comparison with the average value of the closed orbit

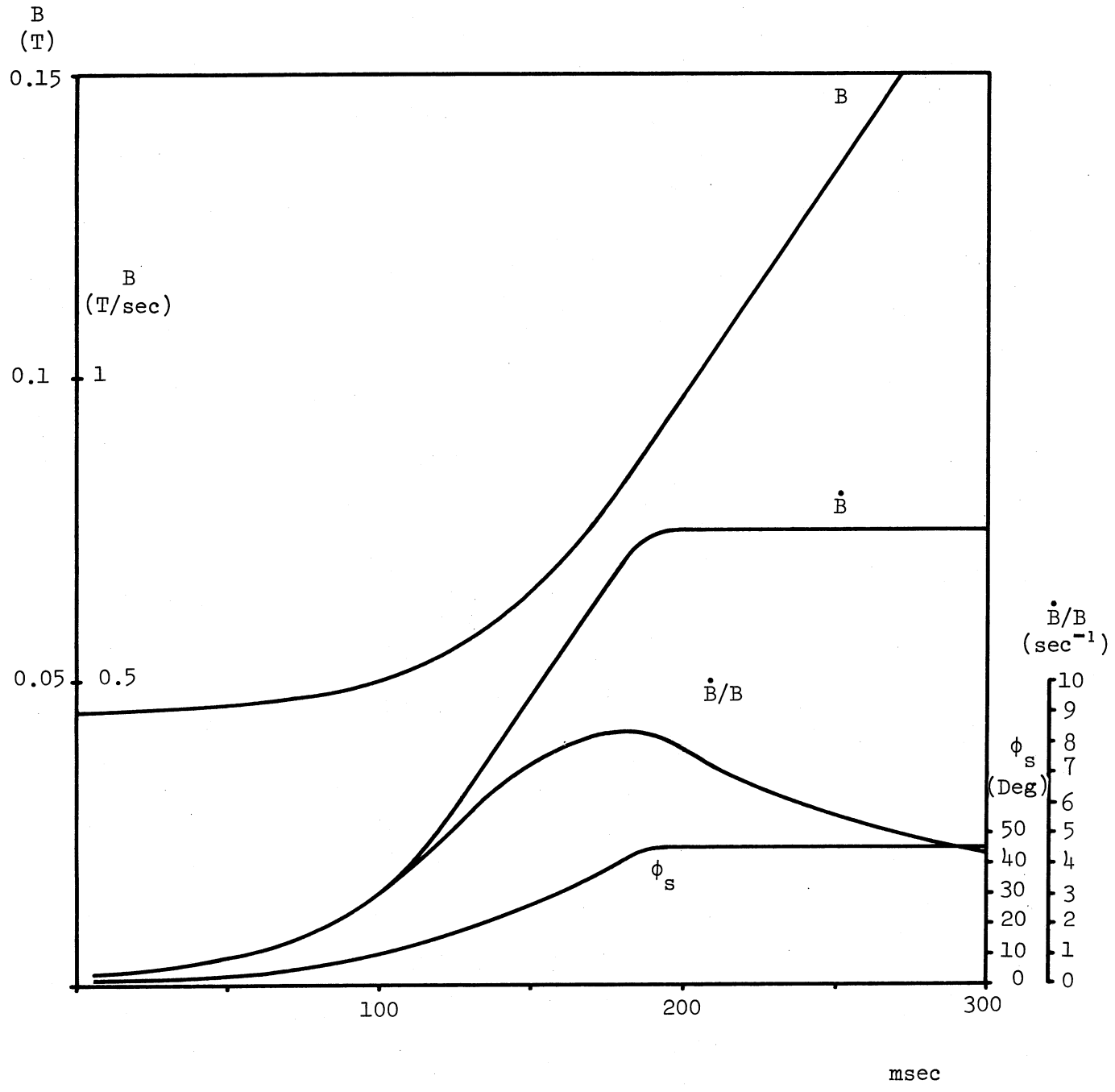

A = 0.22 rad; stage C (p_{max} = 400 GeV/c)

for stage A and B multiply B and $\dot{B}$ by 2 and 4/3 respectively.

Fig. 6.5 Front porch

(see Chapter 9) or by a simultaneous measurement of the magnetic field and the frequency. At full energy, i.e. on a flat top, an increased radial stability can be achieved by phase synchronisation of the frequency with a reference frequency.

The system will also include phase and voltage programs in order to allow a matched crossing of transition, servo-systems and intensity and energy-related pre-programs to correct variations of phase and amplitude due to beam loading and a device to damp bunch rotations.

The electronic circuitry for these systems tends to become rather simple because of the small frequency swing. It is possible to isolate the fundamental component of the bunch frequency from the signal induced in the beam induction electrode by means of a fixed-tuned filter. Furthermore, the absolute frequency variation of about 1 MHz is much smaller than in the CPS for example, in spite of the higher harmonic number, so that narrow-band amplifiers can be employed.

References

(6.1) K.R. Symon, J.D. Steben and L.J. Laslett, Proc. 5th Int. Conf. on High-Energy Accelerators, Frascati, 1965 (Comitato Nazionale per l'Energia Nucleare, Rome, 1966), Session VI, p. 296.

(6.2) W. Schnell, Proc. 5th Int. Conf. on High-Energy Accelerators, Frascati, 1965 (Comitato Nazionale Energie Nucleare, Rome, 1966), Session I, p.38.

Chapter 7

THE VACUUM SYSTEM

7.1 Introduction

This Chapter covers vacuum systems for the main ring, injection, ejection, transfer lines and accelerating structures.

The system is considered on a modular basis so that in the subsequent stages of the development of the machine each magnet can be added with its own vacuum system.

To minimize gas scattering effects, the pressure should be below 10^{-6} torr[7.1, 2]. However, since sputter-ion pumps are proposed, a working pressure of 10^{-7} torr is technically attractive (see Section 7.3) and should also allow sufficient margin for effects such as ion induced instabilities[7.3], which may appear later if higher intensities are accelerated.

7.2 Vacuum chambers

The vacuum chamber in the magnet sections will be quasi-rectangular and will be manufactured from low permeability (< 1.004) stainless steel. In order to reduce the eddy current effects (Section 7.2.2) Inconel or a similar alloy could be used in the B1 magnets instead of stainless steel. The chamber material must have good welding characteristics and a low outgassing rate. The chambers could be manufactured from sheets which are bent into round tubes and seam welded. The final shape would be obtained in a separate forming operation. Alternatively, the tubes could be manufactured from two pre-formed half shells which are welded together in the plane of the major axis of the chamber. A rigorous process of degreasing and detergent cleaning will be necessary. In a normal period, at least the two short straight sections will include an isolating section, probably combined with a demountable flange joint. Every magnet chamber will be insulated from the magnet by a layer of insulating material to prevent shorting of the magnet laminations.

In order to make efficient use of the aperture it is proposed to use vacuum chambers which are compressed in the bending magnet gap during assembly of the two magnet halves. This can be done as the bending magnets are of the window frame type. No further deflection will take place during pumping (see Section 7.2.1). Because of the radiation level, the mechanical forces and the difficult access, a very reliable insulation must be used between the chamber and the magnet. The chambers will be connected by welding or quick release vacuum couplings. Flexible bellows will be included in each magnet chamber for installation and alignment purposes. It will not be necessary to have bake-out facilities.

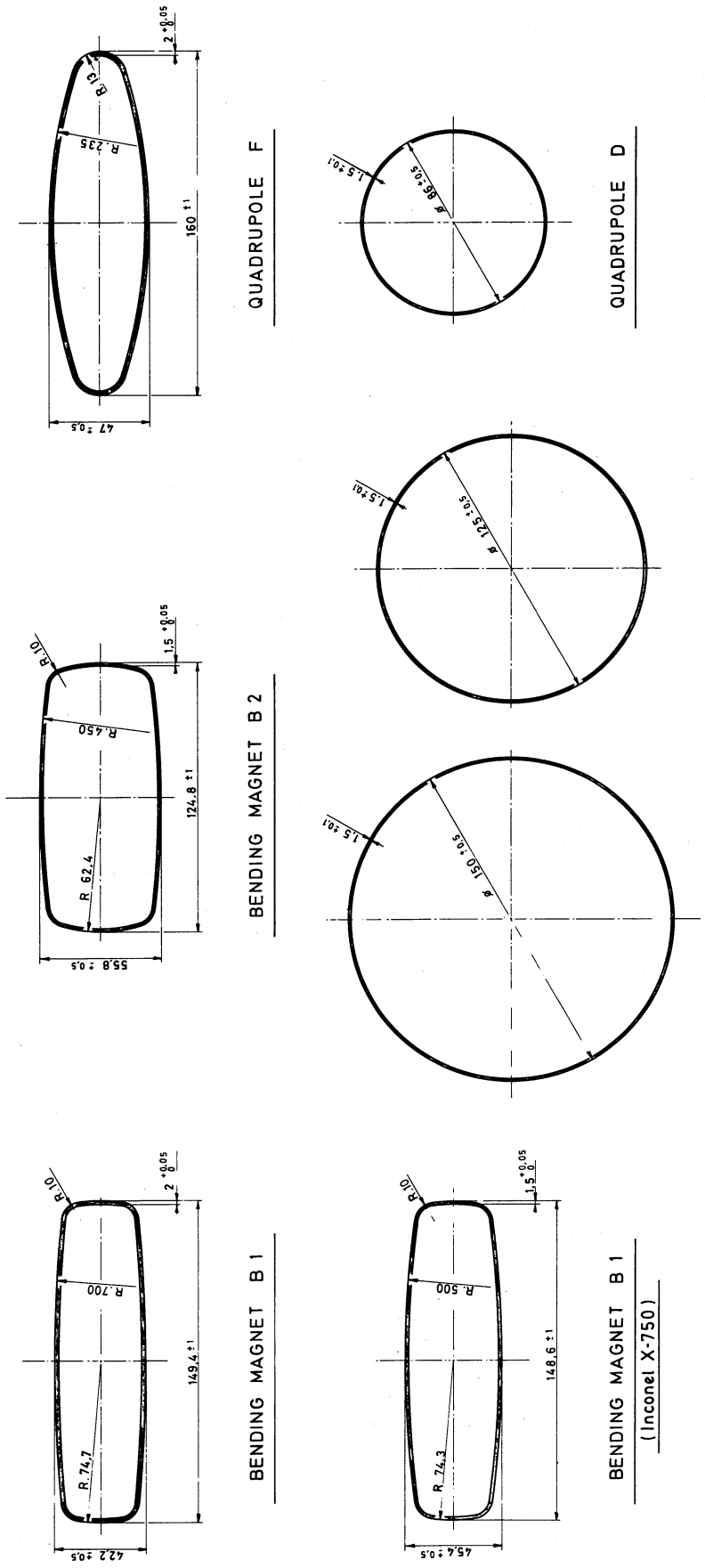

Fig. 7.1 Vacuum chamber cross-sections (tentative designs for bending magnets, focusing magnets and certain straight sections).

7.2.1 Aperture considerations

The shape of the vacuum chamber in the various magnet gaps is determined by the good field region required.

The magnet aperture must be sufficient to allow for the good field region and for the vacuum chamber thickness and tolerance.

To determine the thickness of the bending magnet vacuum chambers, the inside width of the chambers has been assumed to be the width of the beam plus an extra 11 mm clearance at 400 GeV in B1 chambers (4.4 mm at 200 GeV). In B2 chambers at 400 GeV the clearance is 18 mm. No allowance is needed for the sagitta if the chambers are curved in the magnets. The corresponding saving in chamber width permits a decrease in wall thickness which saves aperture and reduces the effect of eddy currents. Cold stretching or rolling of the chamber material will be required to maintain an adequate safety factor in the areas of maximum stress.

With the vacuum chamber pre-stressed in the magnet gap, the allowance for tolerance, as well as for deflection, can be reduced to almost zero in the bending magnets. There will be, in this way, a significant saving in ampereturns and stored energy. A tentative design of chamber dimensions is summarized in Fig. 7.1 for the different bending and focussing magnets as well as for the straight sections.

7.2.2 Eddy currents

The dipole component of the magnetic field distortion due to eddy currents cannot be compensated by a simple current adjustment because the two different type bending magnets are connected in series. In B1 magnets the distortion $\Delta B/B$ at transition is estimated at 6.3×10^{-3} and in B2 chambers at 2.9×10^{-3} if stainless steel is used for the vacuum chamber in both magnets. By using, for example, Inconel for the B1 chamber the field distortion could be made nearly the same in both magnets and compensation by current adjustment becomes possible. Compensation could also be achieved by properly adjusting the values for the damping resistors proposed to be mounted in parallel with all bending magnets.

The sextupole component of the field distortion for stainless steel chambers at transition, is estimated at 3.3×10^{-3} in B1 magnets (at $x = 64.4$ m) and 0.87×10^{-3} in B2 magnets (at $x = 45.4$ mm). With Inconel in the B1 chambers one gets 1.5×10^{-3}.

The eddy current heating requires careful study as the chambers are compressed in the gaps of the bending magnets. For example, an increase in temperature of 10°C would make a 6 m chamber expand by about 1 mm. The chamber should therefore be able to slide somewhat in the magnet without tearing the layer insulating it from the magnet laminations.

7.3 Vacuum pumps

The continuous pumping of the system will be by a large number of small sputter-ion pumps. This type of pump has been selected because it is simple, clean, has no access to

atmosphere and can act as a convenient pressure gauge. The pump could also be used for leak detection.

The conductance of the chambers limits the useful size and spacing of the pumps and as all pumps must be outside magnet units their size and spacing is governed by the magnet lattice, the gas desorption rate of the chamber and its cross-section. With the optimum arrangement, 4 ion pumps per lattice period each with a pumping speed of about 50 ℓ/s will be adequate to keep the pressure in the pumps near 10^{-7} torr. This assumes a gas desorption rate of 10^{-10} torr ℓ/s cm^2, which could be expected from well-cleaned, unbaked stainless steel after 100-200 hrs of pumping. With this outgassing rate the average pressure in the ring would be approximately 3×10^{-7} torr.

The estimated life of an ion pump is 40'000 hours at 10^{-6} torr and 400'000 hours at 10^{-7} torr. A working pressure of 10^{-7} torr will thus give extended life to the ion pumps and, with an all metal system, it is reasonably easy to achieve. However, starting and pump-down operations will reduce the expected life nearer to the 40'000 hour figure.

The initial pumping before starting the ion pumps could be achieved by a number of 2-stage mechanical rotary pumps: 1 per period, pumping through activated alumina traps, capable of reaching 10^{-4} torr and isolated by a remotely controlled valve when not required. These pumps will be sited so that they tend to be shielded from radiation by the magnet blocks and connected by quick release couplings, plugs and sockets to allow for remote servicing. Each pump with trap will have a pumping speed of about 40 m^3/h and be spaced approximately 64 m apart.

After prolonged exposure to humid air, it could take up to 24 hours of pumping to reach the lower 10^{-4} torr range everywhere in the system. After a rapid intervention and by using dry nitrogen to protect the chamber, the corresponding pumping time can be reduced to a few hours.

Extra turbomolecular pumps have been allowed for sections where opening of the vacuum system to air is frequent. Some mobile units could also be used for local reinforcement of the pumping speed, particularly in the pressure range 10^{-4} - 10^{-5} torr. Due to the high power dissipation and the associated outgassing in the sputter-ion pumps at these pressures, stable operation is sometimes difficult to obtain, especially after the pumps have been in use for a few years.

The time needed for the sputter-ion pumps to bring the pressure to a level at which the accelerator becomes operational, depends very much on the history of the vacuum system. After prolonged exposure to humid air the outgassing rate after 10 hours of pumping with the sputter-ion pumps is still likely to be about 10^{-9} torr ℓ/s cm^2. The average system pressure could then be 3×10^{-6} torr. A pressure below 10^{-6} torr could be expected after about 48 hours. The time needed to reach this pressure could be reduced to as little as a few hours if venting with dry nitrogen is used and provided only a small port was opened to the ambient air. It is recommended that the system should not remain open for a period exceeding 30 minutes and the chamber should be held under a slight over-pressure of dry nitrogen.

If alternate pumps failed in limited regions of the machine the pressure rise between pumps would still be acceptable, except during the early phases of the pumping cycle.

The total number of sputter-ion pumps for the main ring system is 432. For the rough pumping 108 mechanical pumps with alumina traps will be required. For local reinforcement of the rough pumping action it would be desirable to include 6 turbomolecular pump sets, each with a pumping speed of 75 ℓ/s. In these numbers are not included the pumps needed for the injection, acceleration, ejection and dump regions.

It will be necessary to ensure that the effects of the stray magnetic fields from the sputter-ion pumps are negligible at the orbit. For the 50 ℓ/s pumps this can be achieved by connecting the pump through a tee piece approximately 300 mm long.

7.4 R.F. cavities

The pressure in the R.F. cavities must be better than 10^{-7} torr. This pressure must be maintained also with the cavities excited. The cavities with their drift tubes are essentially 3 cylinders each 20 m long and with 0.8 m internal diameter. The suggested pumping system consists of eight 500 ℓ/s sputter-ion pumps connected below each cavity through 150 mm diameter ports. Each cavity would also be equipped with a 250 ℓ/s turbomolecular pump for rough pumping and with three 1000 ℓ/s titanium sublimation pumps to speed up the pump-down.

Pumps required for the R.F. system:

500 ℓ/s sputter-ion pumps	24
250 ℓ/s turbomolecular pumps	3
≃ 1000 ℓ/s sublimation pumps	9

Instead of 500 ℓ/s sputter-ion pumps one might consider fitting 1000 ℓ/s pumps as an economy measure. The sublimation pumps could later be replaced by sputter-ion pumps if the long term gas load should turn out to be excessive.

There will be isolation valves between the R.F. section and the rest of the main ring vacuum system and perhaps between successive cavities.

7.5 Injection system to the main ring

The transfer line length is 800 m including bends. The expected aperture is smaller than that of the main ring. Since the pressure requirement in the injection (and ejection) transfer line is not so stringent, 10^{-4} torr would be satisfactory. However, sputter-ion pumps again provide the best solution because of simplicity and reliability provided they are allowed to operate mainly in the 10^{-7} torr range. A 50 ℓ/s pump about every 30 m would probably be adequate. This gives 27 pumps for the line. Initial pump-down could be achieved by one trapped mechanical pump for each 100 m length. The whole line will be separated from the ring and the PS by isolation valves.

Pumps needed for the injection transfer line:

50 ℓ/s sputter-ion pumps	27
40 m^3/h mechanical roughing units	8

The following additional pumps will be required for the kicker magnets of the inflector:

500 ℓ/s sputter-ion pumps	2
250 ℓ/s turbomolecular pumps	1
≃ 1000 ℓ/s sublimation pumps	2

It would be useful to be able to isolate the section containing the inflector by two valves.

7.6 Extraction from the main ring

The initial extraction line to the West Hall will be 800 m long and eventually the line to the North Hall will be about 2'500 m long. The pumping requirements for these lines will be similar to that for the injection line.

Pumps needed for the West extraction transfer line:

50 ℓ/s sputter-ion pumps	27
40 m^3/h mechanical roughing units	8

Pumps needed for the North extraction transfer line:

50 ℓ/s sputter-ion pumps	85
40 m^3/h mechanical roughing units	25

Additional pumps will be required for the fast and slow extraction systems. These systems include 13 different tanks with a total length of 35 m. In the electrostatic septum a pressure of 10^{-8} torr is needed.

Large pumps required for the extraction systems:

500 ℓ/s sputter-ion pumps	31
250 ℓ/s turbomolecular pumps	9
≃ 1000 ℓ/s sublimation pumps	12

Here again the proper balance between sputter-ion pumps and sublimation pumps would be determined by tests. Some isolation valves will, of course, be provided.

7.7 Beam dump system

The beam dump kicker magnets are placed in two tanks each of about 2 m length. The following big pumps are needed:

500 ℓ/s sputter-ion pumps	2
250 ℓ/s turbomolecular pumps	2
≈ 1000 ℓ/s sublimation pumps	4

In addition, one 500 ℓ/s sputter-ion pump is needed in the area of the beam absorber block.

7.8 Components

Organic seals will be avoided to prevent radiation damage.

Depending on position, the flanges will either be of the weldable type[7.4] or of the demountable, quick-release type, the latter in areas were space is narrow and radiation level is high.

For convenience of maintenance it will be necessary to divide the ring into suitable sectors by valves. These should preferably be of the all-metal gate valve type, remotely controlled. The valves should be automatically operated in case of a large leak developing.

Each superperiod will have at least 3 valves, one isolating the long straight section, the other two dividing the 14 normal periods.

Some additional valves will be required, as already stated, for the R.F., injection, ejection and dumping systems. This brings the total to approximately 30.

7.9 Controls

The control and monitoring of pressure will take place primarily in the six auxiliary buildings which will house the sputter-ion pump power units. These units will provide pressure indication around the ring which will be computer monitored with display devices.

For interlock and safety, pressure gauges of the Pirani and Penning type will be used to operate pre-set level relays. These will be mounted near the roughing stations. In total about 125 gauges of each type will be needed.

A computer-controlled ion pump start-up is recommended for such a large number of pumps.

References

(7.1) Design Study of 300 GeV Proton Synchrotron, Vol. I, p. 137, Nov. 1964.

(7.2) W. Hardt, ISR-300/GS/68-11.

(7.3) H.G. Hereward, P.I. Morton and K.H. Schindl, MPS-SI/Int.DL/68-4.

(7.4) J.M. Voss, ISR-VAC/67-23.

Chapter 8

CORRECTION ELEMENTS

8.1 General

There will be a system of 216 dipole magnets, one at each machine quadrupole, which will be used to correct closed orbit distortion due to magnet imperfections and misalignments but apart from these we do not expect to have to power correcting magnets to secure the initial operation of the accelerator. For instance, no multipole magnets or poleface windings are foreseen to compensate inhomogeneities in the guide field. However, there are certain features of the accelerator, notably its large circumference and momentum spread, which make it prudent to install initially a set of sextupoles to adjust the chromaticity $P\partial Q/Q\partial P$, of the machine. Experience with other accelerators suggests that other correcting elements, octupoles and correcting quadrupoles for example, will prove useful later in the development of the machine. Space is reserved for these elements in the short straight sections but only a set of sextupoles and perhaps some skew quadrupoles will be ordered before the machine operates.

The design intensity of the machine, 10^{13} ppp, is well below the incoherent space charge limit of 5.6×10^{13} ppp and the coherent space charge limit of 8.8×10^{13} ppp which correspond to $\Delta Q \sim 0.2$. We do not expect, therefore, to have to correct stop bands or to programme Q when using the improved CPS as an injector. The longitudinal space charge forces are also weak and are not likely to manifest themselves at transition.

However, the momentum spread of the SPS beam, if simple bunch-by-bunch transfer is used, is large. At transition it could be as large as $\Delta p/p = \pm 7 \times 10^{-3}$. This, coupled with the natural chromaticity of the machine, the sextupole field inevitably present in the bending magnets and the even larger sextupole field due to eddy currents, leads to unacceptable Q spreads in the beam, comparable with $\Delta Q = 1$. If the momentum spread is as large as this it will be necessary to use sextupoles to control the chromatic properties of the machine at all field levels.

A review of space charge effects and instabilities has revealed a number of effects which must be treated with respect and in some cases may need to be corrected. These are mentioned below.

8.1.1 The effect of wall impedance on coherent longitudinal oscillations

The impedance presented to the beam by the vacuum chamber is typically a few ohms while cavity like objects can have higher impedances. The r.f. cavities themselves have an impedance $|Z/h|$, of about 1 kΩ. These impedances can lead, in the case of a coasting beam, to coherent longitudinal instabilities which might cause the beam to rebunch at an undesired mode number during debunching immediately after injection and during the flat top. This injection problem is discussed in Chapter 2. The momentum spread after bunch-by-bunch transfer is sufficient to stabilise the instability.

During flat top, where the beam may also be debunched, the critical impedance is $|Z/h| < 10$ kΩ with $\Delta p/p = \pm 10^{-3}$. This is safely above the cavity impedance.

8.1.2 The effect of wall impedance on coherent transverse oscillations

Coherent transverse oscillations may develop in an unbunched beam of this intensity. Such effects have been observed and corrected on the ISR. At injection when in both the bunch-by-bunch and continuous transfer schemes the beam is for a time coasting, the natural chromaticity of the machine, $\partial Q/Q = -1.3\ \partial p/p$, has the right sign and is strong enough to prevent this instability. The other coasting beam situation which could arise is during slow extraction of a debunched beam. Since this is above transition, the sign of $\partial Q/\partial p$ which stabilises the effect is positive and, in the event that slow extraction of an intense debunched beam is required, correcting sextupoles may have to be powered to reverse the natural chromatic properties of the machine.

8.1.3 Head tail effect

Empirical results on the ISR suggest that sextupoles may have to be powered to introduce a modest Q spread to damp this instability. This is confirmed by recent advances in the theory of this instability.

8.1.4 Ion instabilities

Provided the vacuum is kept to 10^{-7} Torr or below, ion instabilities should have acceptable growth times. There is a danger that electrons produced by ionisation of residual gas may cause some instability in a coasting beam. Such an effect has been observed in the ISR and, at the higher pressure of the SPS, may make it difficult to hold the coasting beam after bunch-by-bunch transfer. A gap in the circulating beam about 100 ns long could avoid this danger. Such a gap can easily be made during continuous transfer.

8.2 The Chromatic Properties of the Machine

The natural chromaticity of the machine is

$$\frac{\Delta Q}{Q} = -1.33\,\frac{\Delta p}{p}\,.$$

This is calculated assuming a pure dipole field in the bending magnets and a pure quadrupole focusing field. The sign and magnitude is the same for both horizontal and vertical dynamics.

In addition to the ideal chromaticity other effects, and in particular sextupole fields due either to magnet saturation or eddy currents in the vacuum chamber, modify the chromatic behaviour of the machine.

For example, there is a tolerance of $\pm\ 3 \times 10^{-4}$ placed on bending magnet field which defines the edge of the good field (x = a). If it were all sextupole distortion this would give

$$\left(\frac{\Delta B}{B}\right)_{x=a} = 3 \times 10^{-4} = \frac{B'' a^2}{2B}$$

The change in Q which results is then

$$\frac{\Delta Q}{Q} = \left[\frac{1}{4\pi Q B\rho} \int_0^c \beta(s)\alpha_p(s)B''(s)\ ds\right] \frac{\Delta p}{p}$$

The bracketed quantity may be evalued numerically, an approximate value is 0.4. This may be compared with 1.33 for the natural chromaticity.

Sextupole fields produced by eddy currents in the B1 vacuum chamber produce an effect which at peak $\dot{B}/B \simeq 8\ \text{sec}^{-1}$ (close to transition) is three times larger than that due to the magnetic field shape. The eddy current effects and the saturation of the bending magnet both reinforce the negative slope of dQ/dP in the horizontal plane but oppose it in the vertical plane.

We can use the above expression to evaluate the effect of, say, 36 sextupoles each preceding an F quadrupole and each with a strength of 150 Tesla/m^2 × 0.85 m. This gives

$$\frac{\Delta Q_H}{Q_H} = \pm\ 2.5\ \frac{\Delta p}{p} \text{ at } 400 \text{ GeV}$$

which is enough to reverse the sign of the chromaticity even when the bending magnet saturates. Should it also prove necessary to modify the chromaticity in the vertical plane a further set of 36 sextupoles preceding D quadrupoles will be needed. Because they are in a less favourable lattice location where α_p is smaller these give only

$$\frac{\Delta Q_V}{Q_V} = \pm\ 1.0\ \frac{\Delta p}{p} \text{ at } 400 \text{ GeV}$$

However, the beam is smaller in diameter at these positions and if additional strength is required this can be provided by a smaller aperture, and therefore stronger, sextupole design.

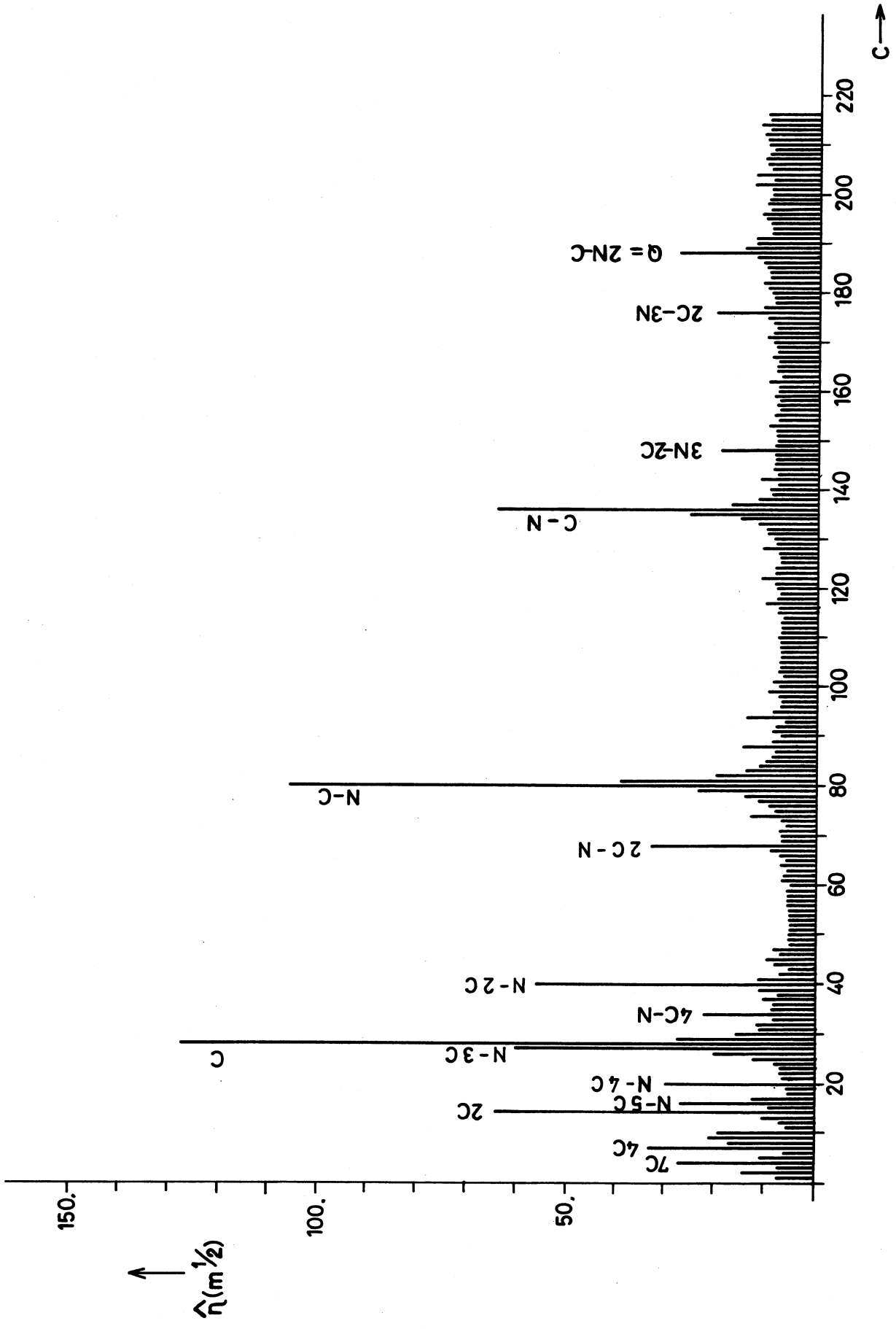

Fig. 8.1 Closed orbit spectrum

8.3 Dangerous Systematic Periodicities

Closed orbit distortions can be caused not only by random errors in the field or stray field of the machine but also by systematic errors having a defined superperiodicity C. If C is not simply related to N, the period number or Q, the working point, systematic errors associated with, say, steel reinforcement of the ring tunnel or temperature gradients in the magnets along a superperiod can still cause significant closed orbit errors if they are more than ten times the random error tolerance. However, a more severe danger is due to errors as small or smaller than the random tolerances but simply related to Q or N. In a machine without focusing superperiodicity the dangerous superperiodicities for closed orbits are

$$Q = |m\,N \pm \ell\,C|$$

where $\ell = 1, 2, 3, 4 \ldots$

$m = 0, 1, 2, 3 \ldots$

If the machine had a significant focusing superperiodicity of 6 all these dangerous superperiodicities would have side bands ± 6. Figure 8.1 shows the relative sensitivity of the closed orbit amplitude to a spectrum of superperiodicities of error. It is assumed that the error distribution consists of C equally spaced delta functions and that for each

$$\int_0^{2\pi R/C} \frac{\Delta B}{B\rho}\,ds = 1$$

$\hat{\eta}$ is the peak closed orbit distortion normalised:

$$\hat{\eta} = \hat{y}/\sqrt{\beta}$$

$\hat{\eta}$ has been maximised in each case by choosing the worst azimuthal phase relation between errors and lattice. Clearly the peaks should be avoided and where possible all objects in the ring building (including even fire extinguishers) distributed with a safe periodicity, e.g. 216, 160, 108, 54, 22, 12, 6, 3.

8.4 Symmetry Constraints

The basic pattern of the correcting elements with respect to the main focusing and defocusing quadrupoles is shown in Fig. 8.2 for one superperiod. Others are identical. In the figure S indicates a sextupole and O an octupole, skew quadrupole or some other correcting element. Dipole magnets and other elements have been omitted for simplicity. The basic pattern of the S and O elements in the figure is contained in three periods and is repeated without interruptions 36 times around the ring. In determining the azimuthal orientation of this pattern two consecutive straights empty of correcting elements are made

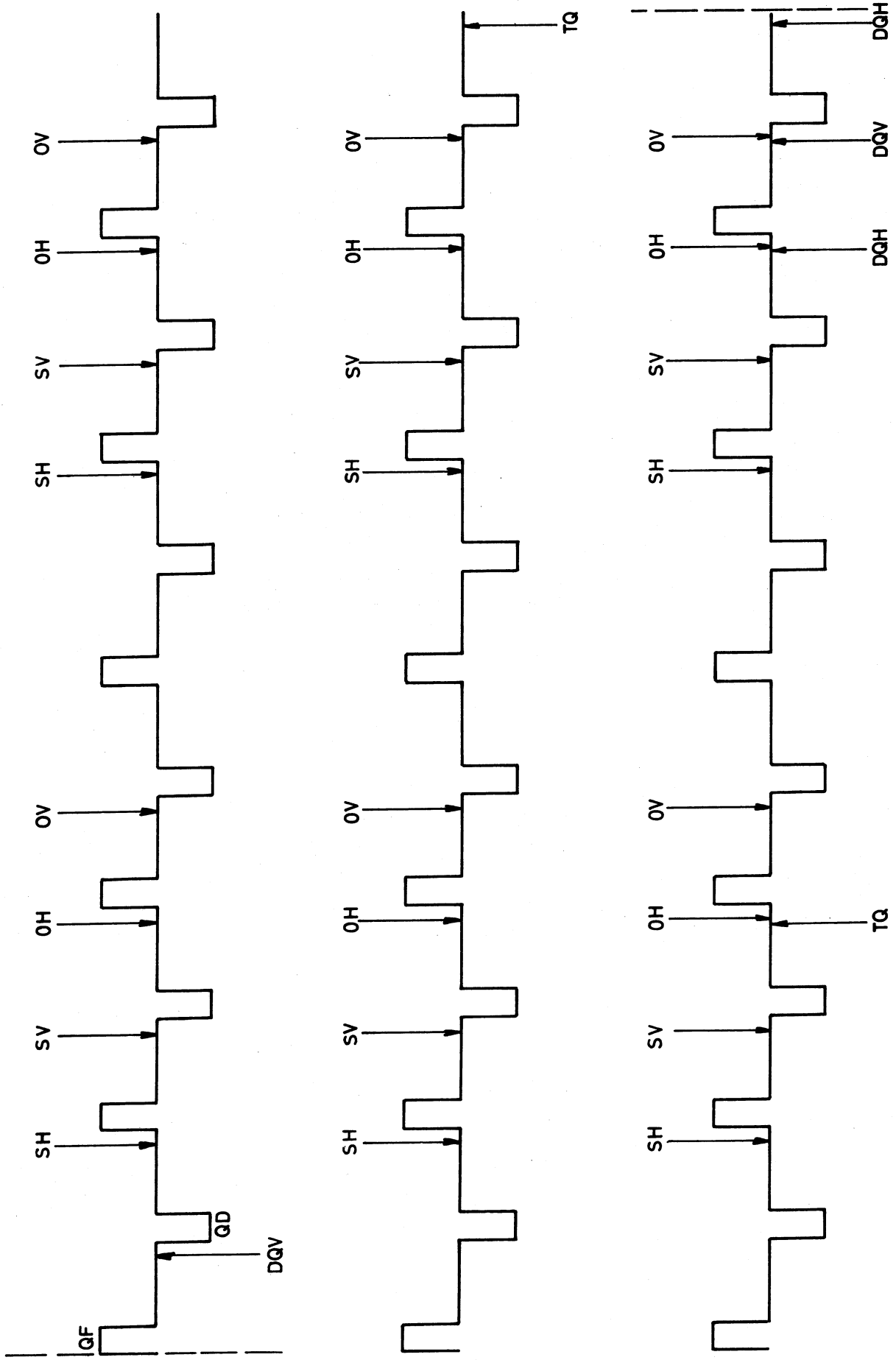

Fig. 8.2 Pattern of correcting elements in a super-period

to coincide with the points in the extraction straight section where the extracted beam is just outside the normal beam. This anchors the rest of the pattern. Empty short straight sections also then occur in the neighbourhood of the injection system and beam dump. The high superperiodicity of the basic pattern also ensures that correcting elements are not themselves likely to cause dangerous stop bands. It is envisaged that sextupoles and other elements like octupoles or skew quadrupoles will be used to impose a zero harmonic correction, at least until more sophisticated corrections suggest themselves. Sets of these elements will therefore be series powered.

At first only one third of the sextupoles, i.e. 12 in F straights and 12 in D will be installed and all other elements, except perhaps skew quadrupoles, will be specified only after the machine has operated.

The main quadrupoles will themselves be used to manipulate the working point of the machine and no special quadrupoles will be provided for tuning. But if machine intensity is raised as part of a future improvement programme a set of gamma transition jump quadrupoles can be installed. The two quadrupoles in each superperiod (TQ in Fig. 8.2) lie in F straight sections half a betatron wavelength apart where $\alpha_p/\sqrt{\beta}$ has maximum slope. In this location they affect γ_{tr} with minimum disturbance to Q. Space is reserved for a further set of four correcting quadrupoles (DQH and DQV) in each superperiod. These could be used to correct neighbouring half integer stop bands. All these quadrupoles would be low energy correcting devices and could be very short, 10 to 30 cm.

8.5 Design of Correcting Elements

Experience with the construction of sextupole magnets for the ISR suggests that 150 T/m^2 is a possible strength for a magnet of 13 cm aperture diameter. It is envisaged that the overall length of each sextupole will be less than 1 m and their effective length 0.85 m. Their detailed design will be considerably influenced by the need to bring very long current leads from power supplies located outside the ring tunnel.

In reserving space for octupoles and correcting quadrupoles nominal lengths of 0.7 and 0.3 m, respectively, have been assumed. It must be admitted that a machine with as much octupole correction as this would be very difficult to operate given the momentum spread which we anticipate. These nominal lengths are for the moment only upper limits and detailed design and specification of these elements can safely be left until later.

Chapter 9

THE CONTROL SYSTEM

9.1 Introduction

The control system for an accelerator of this size has to be more than just a collection of controls transferred from the various subsections to a main control room. It is desirable that the whole accelerator should be operated from a single point by a small operating crew. For this to be possible, means must be found to analyse the vast amount of data available, and present it to the crew in a suitable form for easy assimilation, and to carry out routine settings and measurements. Both these functions can be provided by a suitable computer-based control system.

If computers are considered as integral parts of the control system from the start, rather than something added to a conventional control system, as has usually happened in the past, many additional benefits can be obtained. The additional benefits come mainly from the flexibility of such a system, and the ability to process the data and present it in a form most convenient for the operator, or to initiate control functions without the intervention of the operator. In order to achieve this, it is essential that all subsystems should be designed to make the maximum use of the control system.

The reliability of computers today minimizes the risk taken in relying on their use for the operation of the accelerator. However, provision will be made for the operation of most of the subsystem with the control computer out of action, although it will not be possible to operate the complete accelerator under these conditions. In addition, it will also be possible to operate individual items, using plug-in control boxes for commissioning and test, even when the satellite computers and controllers are out of action.

To provide separate cables for each control and indication function, as in a conventional system, would be very expensive, due to the large size of the ring and the wide distribution of the component parts, and so extensive use of multiplexing must be made.

As the CPS will be used for physics up to 28 GeV in the existing experimental halls in the foreseeable future, as well as supplying the ISR, the CPS will continue to be run from its own control room. As a result, it does not seem necessary to transfer any machine controls from the CPS to the new control centre, although some beam line controls and status information will be required.

9.2 Overall system layout

At first sight, it would seem that the best way to achieve the stand-alone operation of the various subsystems is to have a satellite computer for each subsystem, under the overall control of a main computer associated with the control centre. This can be satisfactory for subsystems which are well defined and geographically discrete, but some of the subsystems have elements distributed widely around the ring tunnel, and for these such a system would lead to wasteful multiplication of equipment. A combination of separate satellite computers for some subsystems, together with a geographical distribution of other satellite computers which have multiple duties, has been chosen as a good compromise, and a schematic diagram of the system is shown in Fig. 9.1, which differs slightly from the layout proposed previously. A tree branch structure would seem likely to require an unnecessary amount of data transfer from one computer to another. Instead all the satellite computers are connected by data links to an interface computer. This will act as a message switching device allowing the updating of the data bank, which will hold the most recent values of all relevant parameters, and allow the transfer of data from satellite to satellite, without involving the main computer. The latter will then be able to carry out programmes called for by the operator without being constantly interrupted to carry out routine operations. This fits in with the philosophy that, as far as possible, the operations required to take place at a time linked to the machine cycle will be carried out at the satellite level, while those required to take place at a time determined by the operator should be carried by the central computer.

9.3 Control computers

The main computer associated with the control centre will be of medium size, and will be equipped with a full range of peripheral apparatus, including graphics terminals. Some of the satellite will be miniature computers of the process control type, with stored programmes and a minimum of permanent peripherals. They will be able to control the data acquisition process and carry out simple operations, such as checking values against limits. Others, controlling discrete parts of the accelerator, will have greater capability and more peripheral equipment. This system, which provides considerable local computing capability, means that it is only necessary to pass information higher up the tree when significant changes occur. This, together with the ability to schedule parts of the machine cycle for data transfer, can simplify the interrupt system, and allow the use of simple modular software systems.

In the past, a shortage of good real-time executive software has involved many users in a large amount of computer system analysis before work could start on applications programmes. Fully adequate executives are now available from several computer manufacturers. It is intended to provide a simple interpretive language to simplify the writing of user programmes.

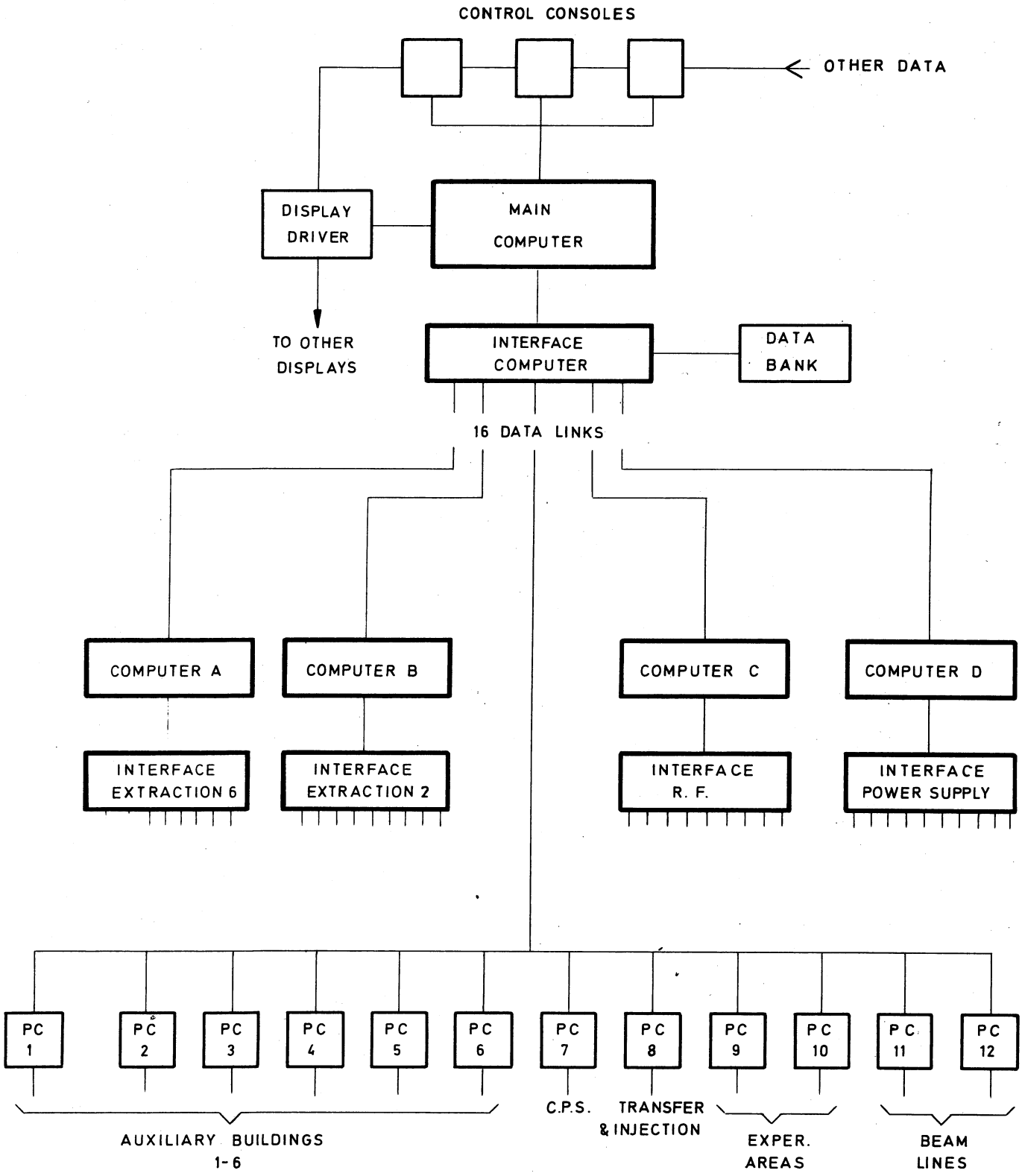

Fig. 9.1 Control System Schematic

Computers A to D are small computers with disc-based system.

Process controllers 1 to 12 are mini computers with simple configuration.

9.4 Data links

Serial data links, similar to those already in use over comparable distances at CERN, should have adequate capacity for this application. The possibility of using a common data highway calling in at each point has been investigated but it seems that the resultant complication of the organization of the data transfer would outweight the cost of the extra data links.

9.5 Interface

In the past, many of the difficulties in applying computers to control applications have been due to the lack of a simple but versatile method of connecting the various data and control points, through multiplexers and converters where necessary, into the computer. The standard system known as CAMAC, first evolved for data acquisition for High Energy Physics experiments, will probably be used as the basis for the interface system.

A standard format will be laid down for signals to and from equipment to be connected to the system, and local controls for equipment should be designed to conform with the standard, and to make the maximum use of the control system.

9.6 Multiplex

A multiplex system, for data acquisition and control round the ring tunnel, will be divided into six sectors, with a controller in each of the auxiliary buildings. One possible scheme would use a multiway twisted-pair cable round the sector to provide an address and data highway, connected to each of the multiplex terminals. A controller would interrogate the terminals in sequence and pass the information gathered to the local satellite computer. Commands flowing the opposite way could fit into programmed gaps in the interrogation sequence. The cycle time, and time constants of most of the apparatus, are sufficiently long to allow this method of operation, which reduces the need for sophisticated programming of the controllers.

A number of coaxial cables will run round the ring tunnel system, calling in at the auxiliary buildings, and terminating at the control centre. These will be used for the transmission of analogue waveform signals, up to about 100 kHz, and the multiplex system can be used to connect signals to these highways as required by the operator.

9.7 Beam monitors

Beam intensity and position monitors are required for the transfer path, the main ring, and the extracted proton beam lines. In the transfer path, the problems are similar to those for the ISR, and similar monitors can be used. Two types are required for the main ring, relatively narrow band monitors for the closed orbit control, and wide band monitors for commissioning and diagnostic purposes. The monitors for closed orbit control may be similar to the electrostatic position monitors developed for the PCS and ISR, and their use is described in the section on closed orbit control. The wide band monitors are required

to study detailed beam behaviour, and a band width of up to one gigaherz is required. While this can easily be achieved for the pick-up unit itself, the connection of a long length of cable would seriously degrade the performance. Therefore these monitors will be located close to the shaft leading up to the auxiliary building housing the control centre, so that they can be linked by short lengths of high grade coaxial line to oscilloscopes for observation.

Beam profile monitors will be required in the main ring, to observe beam envelope oscillations, and in the transfer path and the extracted beam paths, for emittance measurements. Interception monitors of the luminescent screen and secondary emission types and non-interception monitors of the ionization beam scanner type have been developed for the PS and ISR and modifications of these shall be suitable.

9.8 Closed orbit control

It has been shown, in Chapter 2, that the closed orbit distortion amplitude resulting from the tolerances assumed could be over 32 mm in the horizontal direction and nearly 20 mm in the vertical. In order to reduce the magnet aperture required, it is assumed that this distortion amplitude is reduced to a maximum of 10 mm in the horizontal plane and 5 mm in the vertical. It is expected that the beam size will be a maximum in the vertical direction at injection and in the horizontal direction either at injection or at transition, and so the closed orbit correction will be most critical at these times.

To assist alignment, the beam position monitors will be fitted to one side of each quadrupole, in an extension to the quadrupole vacuum chamber. The signals from the units will be integrated over several turns, to reduce the effects of coherent betatron oscillations. The relatively slow signals can then be transmitted by a multiplex system, but since the information from all 108 monitors in one plane will be required for the same point in the time cycle, in such case it will be necessary to store the information at the monitor point until interrogated.

The closed orbit will be corrected at injection by means of small dipoles in the short straight sections. The dipoles will have individual power units, controlled through the computer system. After measurement of the position of the closed orbit, the corrections will be computed and the dipole current adjusted to the corrected values. The excitation of the dipoles will be only sufficient to correct the closed orbit at injection and transition and their effect at high energy will be small. Correction at high energy will be by movement of the main quadrupoles, so that when the high energy closed orbit has been determined, the corrections to the quadrupole positions will be computed, the machine shut down and the positions of the quadrupoles adjusted. Since the stability of the tunnel in the molasse rock is expected to be very good, it should not be necessary to make this adjustment very often.

The closed orbit amplitude after correction depends on the number and location of beam position monitors and correcting elements and the accuracy of measurement and correction. Simulation studies have shown that if at least four sensors and corrections are provided per

betatron wavelength, the most dangerous harmonics of the closed orbit distortion can be made small, although zero reading on the sensors does not mean that the amplitude disappears everywhere. The correctors and sensors should be located close to each other, and maximum sensitivity is achieved if they are positioned close to the point where the amplitude function is a maximum. Thus the monitors and correctors for the horizontal plane will be placed near a horizontally focusing quadrupole and those for the vertical plane near a horizontally defocusing quadrupole. The requirement for about 4 units per betatron wavelength results in a unit at every quadrupole, giving a total of 216 monitors and 216 correcting dipoles.

Several procedures can lead to the reduction of the closed orbit amplitude, and simulation studies for two of these were made as part of the earlier ECFA Study. In one case, all measurements were made and the best possible correction that could be made by the use of a single corrector element was computed by a least square fit. This procedure has to be repeated a large number of times to reduce the distortion to an acceptable level. The influence of observational errors in the correction are very small, but the amount of computation for each correction is rather large. In the other case, corrections to the closed orbit are made locally, using three adjacent corrections to form a 'half wave' beam bump, adjusted to reduce the error signal at the centre point to zero. This method requires a trivial amount of computation, but the result is strongly dependent on errors in observation and correction. It was shown in the ECFA study that for the tolerances given in Table 9.1, the beam bump method would enable the closed orbit distortion to be kept within the required 10 mm in the horizontal plane, but the tighter tolerance in the vertical plane would require the beam bump correction to be followed by a few iterations to the first method. Further work has shown that these positional and instrumental tolerances may have to be tightened.

In addition to these simulation studies, practical applications of close orbit control on the CPS, ISR and at DESY and NINA, have shown that there should be no insuperable difficulty in achieving the required control.

Table 9.1

Beam Position Indicators	
Length of pick-up plates	200 mm
Tolerance of centre line position	1.0 mm rms
Observation error	0.5 mm
Dipole Magnets	
Horizontal correctors:	
Length	250 mm
Beam size	125 mm × 25 mm
Maximum field	0.17 T
Vertical correctors:	
Length	250 mm
Beam size	50 mm × 50 mm
Maximum field	0.07 T

9.9 Timing system

Since the CPS will be supplying beams to experimental targets as well as acting as injector for the main ring, many modes of operation must be catered for. As the time cycles will not synchronize exactly, in some modes the CPS will have to wait until the main ring is ready to accept a pulse, and in others the main ring will have to wait until the CPS is ready. In either case, the CPS ejection prepulse will be used to start the main ring time cycle.

Timing signals to be distributed round the machine and supplied to experimental areas are expected to include a series of pulses at equal flux increments (the B-train), a series of pulses generated at the beam orbital frequency, a sequence of trigger pulses generated at significant points in the machine cycle, and real time clock pulses.

9.10 Radiation monitoring

Radiation monitoring requirements are divided into two categories, (a) recording of levels round the machine and experimental areas under normal operation, and (b) alarms or prevention of operation of the machine under abnormal conditions, when dose rates may become excessive in some areas.

For both categories it will be advantageous to use the control data acquisition system, in areas where it is available, to avoid an excessive number of additional cables. However, to connect monitors which are far away from the normal communication lines into the control data acquisition system would be very costly, and it should be adequate to use battery-operated monitors fitted with recorders for this purpose. It is then only necessary to collect the records periodically.

Radiation monitors will be placed at danger points to give alarm or to switch off the beam if dose rates become excessive. Similar monitors will also be placed in positions where mis-steering of the beam could cause damage to machine components.

Simple beam loss monitors will be distributed at frequent intervals round the tunnel system, so that the pattern of beam loss can be observed and recorded for analysis.

9.11 Communications

Because of the great length of the tunnel system it would be expensive to provide permanently-installed telephones at frequent intervals, and the main method of communication round the runnel will be by the P.A. system. This will be arranged, as in the ISR, to allow headsets to be plugged in at frequent intervals.

Mobile radio telephones will be used for communication round the Site, particularly for the service vehicles which will be needed for transport between the access points.

Television equipment will be provided for surveillance of the personnel access system, and for beam monitor viewing. In addition, each maintenance vehicle may be fitted with a camera which can be plugged into a trunk line running round the tunnels to allow personnel at the control centre to inspect the progress of the work.

9.12 Personnel protection

The tunnel will be divided into nine areas, six sectors and three beam tunnels, so that the search can be carried out in each independently and breaking the interlocks in one section does not require the whole tunnel system to be searched again. To give the maximum security, two independent 'hard wire' circuits will be completed by door interlocks at the access points connected in series, so that opening either circuit will prevent injection from the CPS, except under special test conditions. Additional contacts will transmit the information on the locations of the open circuit to the control centre. The access procedure, which will allow identified personnel into the ring without requiring a search after they have left, can also be monitored by the data acquisition system. Consideration is being given to a system which would require the use of the radiation film badge, fitted with a coded insert, to obtain access to the ring, so that this identification would enable the computer system to keep track of personnel entering the ring under these conditions. A selective system of emergency stop buttons will be included in the Personnel Protection System.

9.13 Diagnostic apparatus

Apart from the beam monitors, other diagnostic equipment will be required. This will include apparatus for measuring the vertical and radial Q during the cycle. Apparatus developed for the ISR, using a short pulse to excite coherent betatron oscillations and a pick-up electrode system with filters, could be used for this purpose. Other diagnostic apparatus is likely to be required to investigate effects resulting from the high beam intensity that may be possible eventually, but this cannot be specified at present.

9.14 The control centre

With the involvement of the computer in the control system it is possible to make all controls and indications available to a single operator. This may well be suitable for the final stage when the accelerator is working routinely, but it is likely to lead to congestion and frustration during commissioning and in the development phase. The best solution seems to be to have a small group of control areas, specializing in particular aspects of the machine operation, one of these dealing with the system as a whole. It is expected that, as experience is gained, it will be possible to concentrate the whole of the control at this one position, where one or two oscilloscopes, a graphics display terminal, one or two storage display units for alarms, etc. and one or two keyboards will be all the equipment required.

A room of visitors will be provided adjacent to but separated by windows from the main control room, to allow observation without disturbing the operation of the accelerator. This room will also be equipped with models, display units and demonstration equipment.

9.15 Displays

The control system is required to provide information not only to the operators, but to any position round the site where it may be of interest or importance, and particularly to the experimental areas. To provide this wide coverage at minimum cost, the main display system will most likely be of the type that uses a translator to change coordinate alpha-numeric and vector data from the computer system into TV raster form, and stores this information on a fixed-head disc. In the case of one system now available, the disc can store about 16 separate displays. At each rotation of the disc, a frame waveform is produced at each pick-up head, and after amplification this can be transmitted to any number of standard TV monitors for display. Displays in colour can be produced by using more than one channel.

As it is foreseen, several channels would be reserved for control room presentation, but several other channels would be used for presenting information at the local control stations and elsewhere round the site. The choise of display on a distant standard TV receiver could then be made by the channel selector. Channel 1 could be reserved for status information on the machine, such as peak energy, beam current, extraction and targetting conditions when running, and reasons for stoppage or other fault, with estimated delay for the return to normal conditions. It could also have a list of the displays available on the other channels. It is thought that this could be particularly useful to give information to the experimental areas. If anything unexpected happens, the experimenters could always turn to channel 1 to obtain the latest status information.

9.16 Cable administration

Although the extensive use of multiplexing will reduce the number of cables required, it still adds up to an impressive total. Computer-aided design, involving the listing of requirements, choice of route, and the production of cable schedules has been successfully used for the ISR, and it is planned to use a similar system for this project.

Chapter 10

THE SURVEY SYSTEM

10.1 Introduction

Altogether, the 800 MeV booster, the 28 GeV PS, the transfer tunnels and the two rings of the ISR comprise about 4 km of tunnelling in which some two thousand components have been positioned in relation to each other with an accuracy of a 10th of a millimetre. We shall in this Chapter relate our proposals to this experience, because the rock in which the SPS will be bored is the same as the rock of that complex, and many of the instruments developed to achieve the accuracy needed for the positioning of the PS and ISR will be used for the survey of the SPS.

From the survey point of view, the 300 GeV accelerator represents a two-fold increase in scale compared with the above complex, but the tolerances necessary for correct accelerator operation remain the same as for the ISR.

The evolution of survey techniques,and the constant improvement in the instruments developed at CERN specifically to meet the particular requirements involved in the construction of large machines, will provide a potential solution to the metrological problems to be encountered with the new accelerator.

10.2 Siting the tunnel - Connection to the 28 GeV synchrotron and West Hall

Like the ISR, the 300 GeV accelerator will be an extension to an already existing machine. The precise location of the new accelerator is determined by the actual position of the 28 GeV PS in the latter's system of reference coordinates.

The survey measurements for the siting of the tunnel will be made in two stages.

The first will be an external trilateration (Fig. 10.1), based on the survey network of CERN I, using electromagnetic distance-measurement instruments, e.g. Geodimeter, tellurometer, distomat and CERN mekometer. This will be a general-purpose trilateration but will at the same time be designed specifically to fix the coordinates of the survey points at the shafts. The self-consistency of these points will be to within ± 5 mm in relation to each other and to the survey network of CERN Lab. I.

The second will be an underground traverse, the bearing being obtained by a Wild GAK 1 gyroscopic theodolite (bearing accuracy: 60 centesimal seconds). According to Foucault's law the axis of a gyroscope tends to become parallel to the rotation axis of its support. The axis of a gyroscope located on the surface of the earth will therefore become parallel to the earth's rotation axis, i.e. the pole axis. The lengths will be measured with an MA 100 tellurometer (accuracy over these distances: ±1.5 mm). The boring machine will be

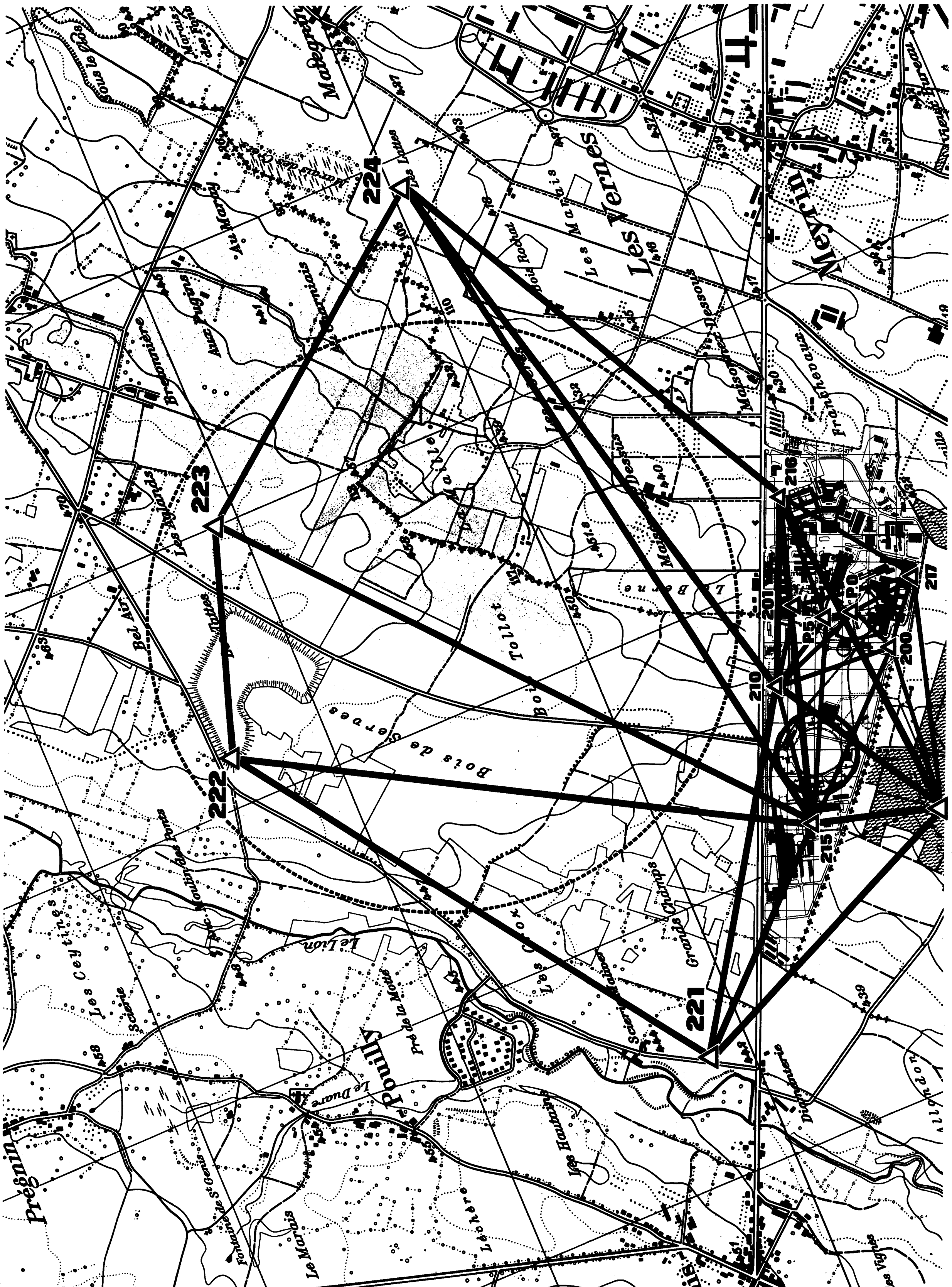

Fig. 10.1 Site trilateration

guided by a normal theodolite and a special target system. Constant control of the alignment is provided by a TV camera.

As the shafts will be located close to the long insertions which separate the superperiods, the survey system will have to be matched to this periodicity. These six shafts will, in fact, be the only possible means of connecting the trilateration on the surface with the underground traverse before the injection and ejection tunnels are bored; the traverse will extend from the civil engineering shaft in the injection tunnel to shaft No.1. It is an absolute pre-requisite of the survey system that shaft No. 1 be already dug, to enable the traverse to be closed on a reference point, the coordinates of which have been determined from the surface trilateration and transferred down to the bottom of the shaft, thus a check can be made on the bearing and location of the synchrotron after only 200 m of traverse. The traverse will then continue from shaft No. 1 to shaft No. 2. Once this position has been reached, a double check can be made using shaft No. 2 and the north ejection gallery, both of which will have been already completed. The tranverse deviation of 1/6th of the circumference can be ascertained and adjusted to avoid any cumulative errors over the following sections. The precision which can be attained on one sector is given by the standard deviation of a gyroscopic traverse:

$$\frac{L \cdot d\alpha \cdot \sin 1''}{\sqrt{n}} = 36 \text{ mm}$$

where:

L : length of the traverse between two shafts = 1152 m
$d\alpha$: standard deviation on a bearing in one station = 60 centesimal seconds
n : chosen number of stations = 9
sin 1" : 1/636,619.772

The probable transverse error (50% chance of not being exceeded, 2/3 of the standard deviation) is likely to be 24 mm, and the maximum transverse error (99% chance of not being exceeded, 2.5 standard deviations), 90 mm.

Levelling will be carried out by means of an automatic level; the accuracy achieved will be ±2 mm per km.

The reference marks of the traverse have to be materialized, either on the floor or on the roof of the tunnel, to enable positioning of the brackets on the wall for accelerator metrology, and the provisional location of the machine components on the floor. This marking will be sufficiently close to the final positioning to enable it to be used for the installation of the components.

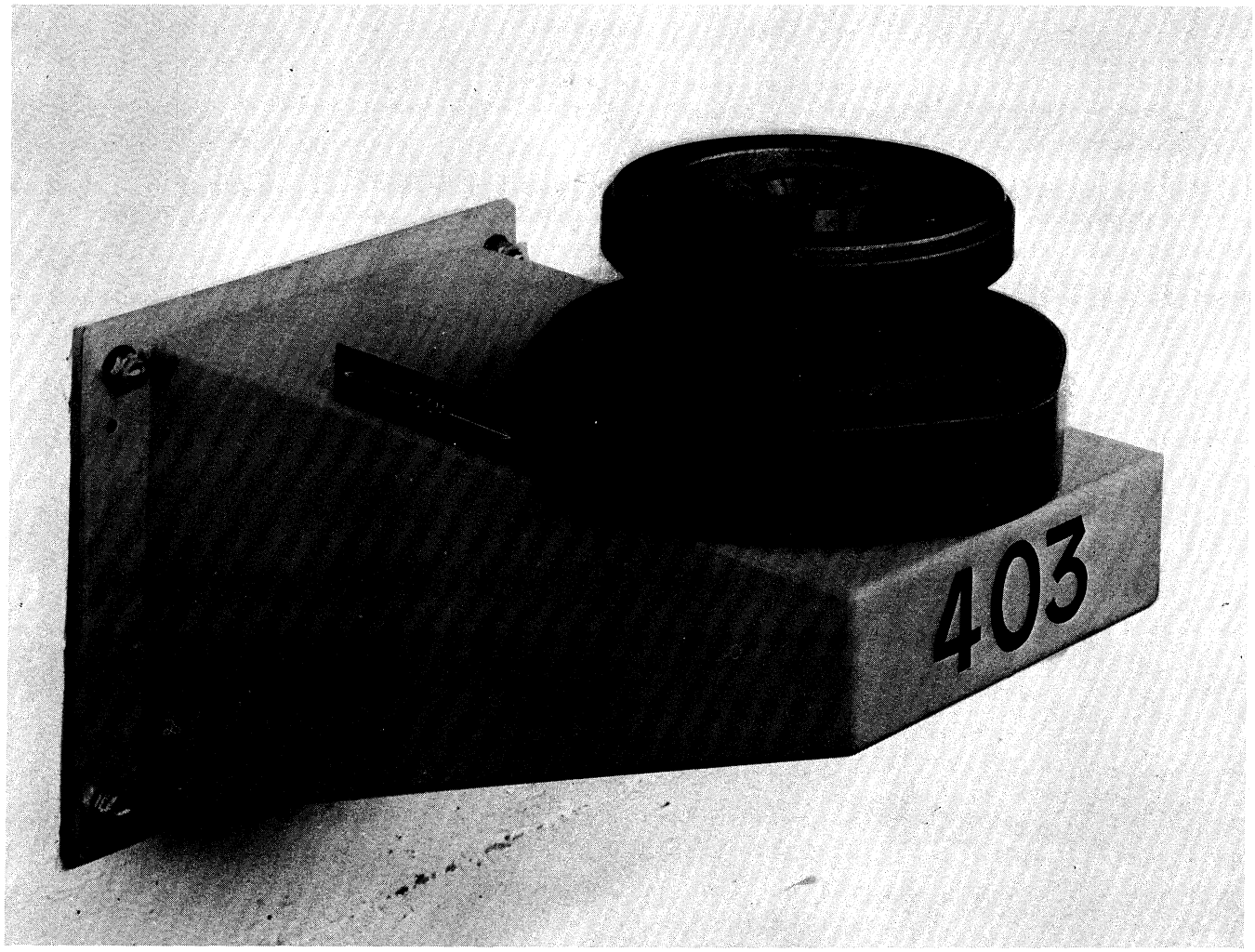

Fig. 10.2 Bracket or Cantilever fixed to the tunnel wall with adjustable socket carrying the precision hole

10.3 300 GeV accelerator metrology

The 'missing-magnet' concept affords a very considerable degree of flexibility for the construction of a synchrotron in which the energy is increased in successive stages. A complete metrological scheme must therefore be devised that enables the magnets to be correctly repositioned as each energy stage is reached, since the orbit will be different in each case.

This concept calls for much more than a geometrical survey for the purpose of making measurements to determine a closed orbit; it requires a permanent geometrical structure so that the accelerator components can be repositioned prior to reaching the next energy stage.

The reference marks of this structure will be located on wall brackets opposite the quadrupoles and must remain fully accessible at all times (Fig. 10.2). Moreover, as the synchrotron tunnel will be bored on the average 40 m below ground level, and, at the most unfavourable point, will be at least 11 m below the surface of the molasse, we may, on the basis of past experience with the ISR transfer tunnel, be confident of the stability of the brackets. The advantage of this system is that further surveys around the full circle of the accelerator will be needed only at the start of each new stage, prior to the installation of new magnets and re-alignment of those already installed. In the meantime, local alignments will be made by reference to the nearby brackets.

The 300 GeV lattice is of separated-function type and FODO configuration (Fig. 10.3). The over-all circumference will be divided into six sectors, each composed of fourteen normal periods with a radius of 847.2 m, and a long insertion which is a combination of straight sections and curves with the same radius, 947.2 m.

Section 8.3 explains how systematic errors are least dangerous if they have the same frequency as the quadrupoles of the machine. It is important therefore that the metrological system should follow this pattern (Fig. 10.4). Thus, there will be two brackets respectively, on the inner and the outer wall of the tunnel opposite each quadrupole. Therefore the reference figure will be a chain of braced quadrilaterals measured with invar wires. Additional links will be made using offset measurements with nylon wire. In the general adjustment this process will minimize the effects of the unfavourable ratio of the distance between two brackets (3.4 m) and the length of the quadrilateral (32.0 m). All the distances will be measured with invar wire standardized on CERN's calibration bench (standard deviation: 0.02 mm for a distance of 64 m) and the deviation of the middle point from the alignment will be measured against a nylon wire stretched between the two outer sockets (standard deviation: 0.03 mm).

In the long straight sections, the shape of the braced quadrilaterals will be matched to the size of the tunnel, especially at the start of the normal curved periods.

There will be 432 sockets, 216 on the inner wall, 216 on the outer wall, opposite the quadrupoles. Consequently there will be 216 braced quadrilaterals. In the general adjustment, there will be 864 unknowns, 1080 (5 × 216) equations due to length measurements, and 648 (3 × 216) equations due to offset measurements.

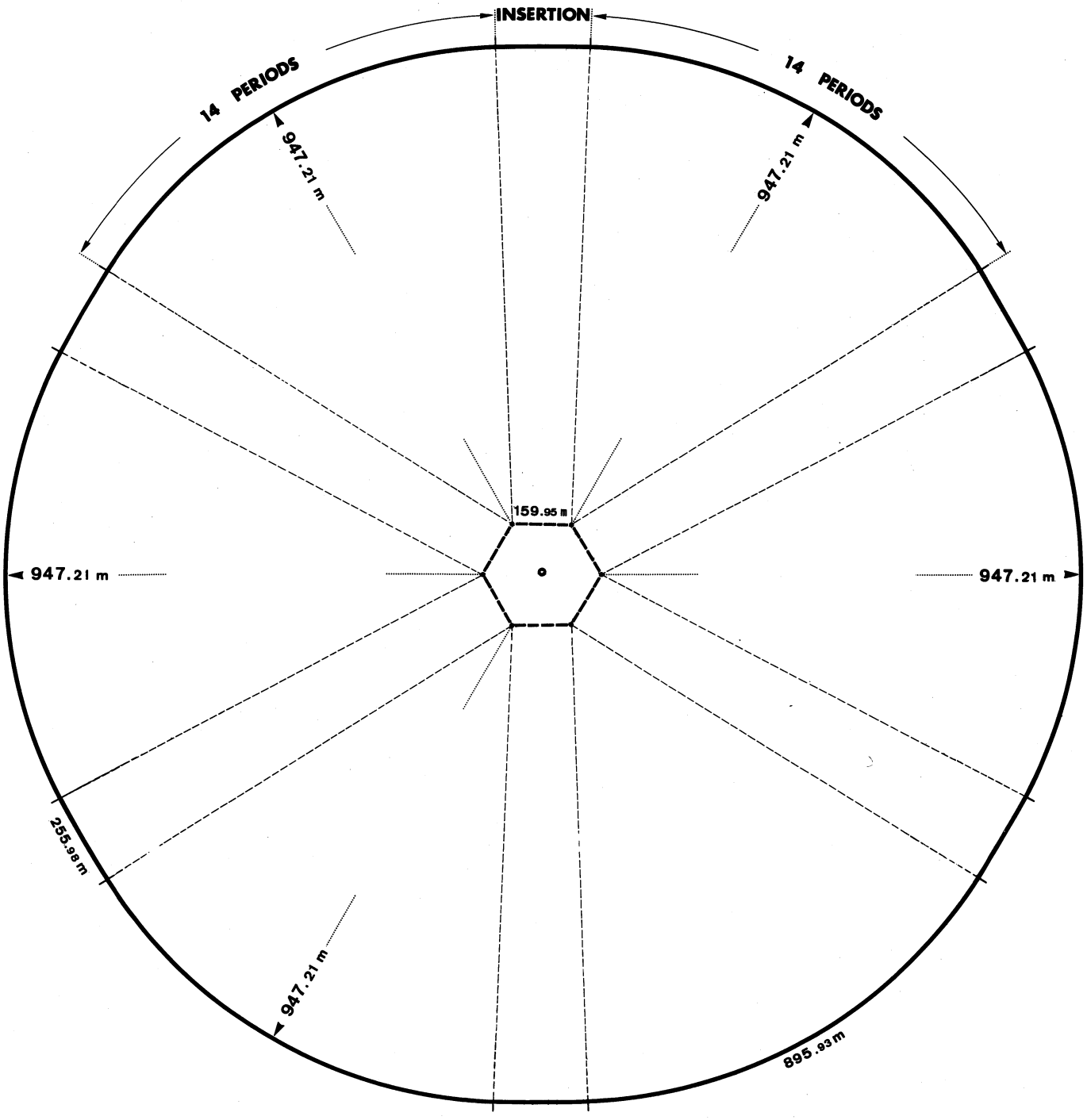
INSERTION
14 PERIODS
14 PERIODS
947.21 m
947.21 m
159.95 m
947.21 m
947.21 m
255.98 m
947.21 m
895.93 m

Fig. 10.3

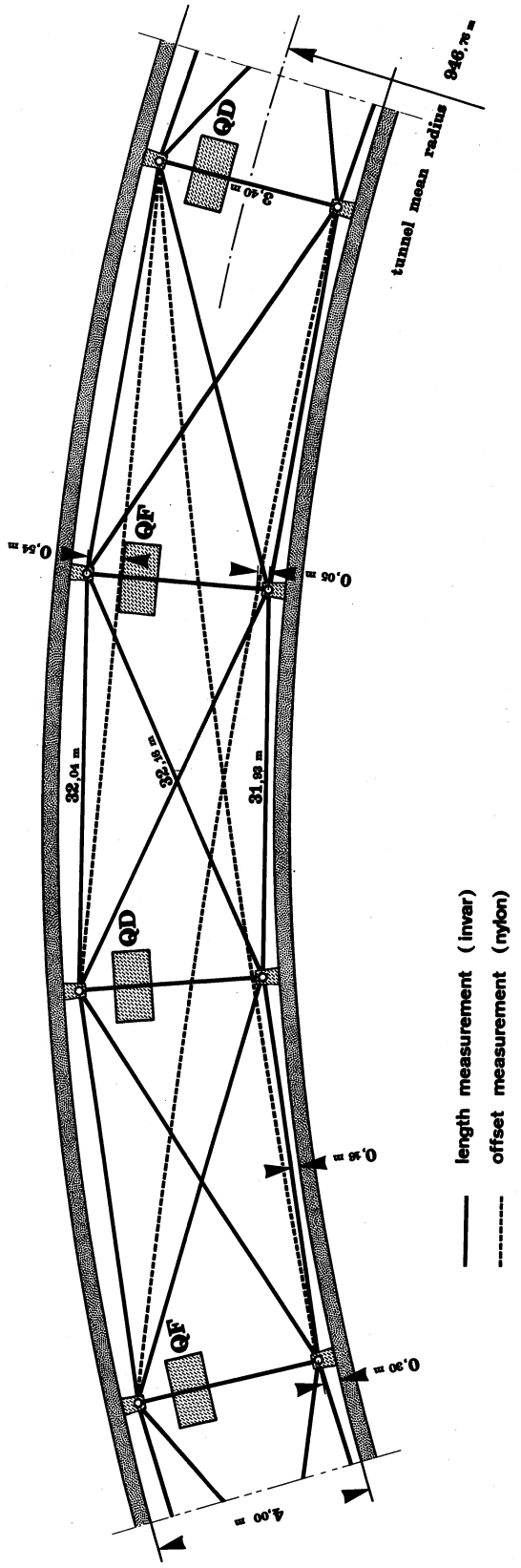

Fig. 10.4 Basic metrological scheme for the 300 GeV PS.

The geodetic adjustment methods, as developed for the ISR reference figure, provided a great degree of flexibility in meeting a schedule which was not particularly favourable for the survey. In the least squares method of adjustment using the coordinate variation method, the contribution made by the Metrology Group was to adopt, as the coordinate for the approximate positions, the theoretical positions computed from the machine's parameters. The result of the adjustment gives directly the deviations for which the sockets must be corrected to bring them into their theoretical position, thus enabling the 'theoretical figure' to be constructed. The least squares solution is obtained by making

$$\sum_{1}^{1080} \left[d\ell_{1\ 2} - \left[dx_2 - dx_1 \right) \sin G_{(1.2)} + (dy_2 - dy_1) \cos G_{(1.2)} \right] \Bigg]^2$$

$$+ \sum_{1}^{648} \Bigg[da_2 - \left[dx_1 - dx_2 + (dx_3 - dx_1)k \right] \cos G_{(1.3)}$$

$$- \left[dy_1 - dy_2 + (dy_3 - dy_1)k \right] \sin G_{(1.3)} \Bigg]^2$$

minimum, where:

$k = \ell_{1.2}/\ell_{1.3}$

$\ell_{1.2}$ = length between 1 and 2

$d\ell_{1.2}$ = measured length minus theoretical length between 1 and 2

$G_{1\cdot 2}$ = theoretical bearing between 1 and 2

da_2 = alignment offset of point 2 in relation to the straight line 1.3

dx_1, dy_1 = unknowns.

By using the theoretical network as an approximate network, any reference figure can be positioned before the entire circumference of the 216 braced quadrilaterals has been measured. This figural adjustment, based on points originating from the external trilateration, enables each sixth sector to be given its precise shape, but its position is within the accuracy of the trilateration points, transferred down into the tunnel.

As soon as one of the sixth sectors has been built, the reference sockets can be positioned on the brackets and each magnet can be aligned as it arrives in the tunnel. Once the injection and ejection tunnels have been completed, thus providing a link with the 28 GeV PS, a complete measurement of the 216 braced quadrilateral figure and of the transfer tunnels will enable the six mutually-independent sectors to be converted into the geometrical structure, the position of which is dictated by the 28 GeV PS and the West Hall. Inside each quadrilateral, the dipoles and quadrupoles will be located in their theoretical position.

In the ISR, the theoretical network was used as the approximate one for the adjustment; this meant that the magnets could be installed in octants which were independently positioned

in relation to each other. When the final adjustment was made from the results of the last adjustment, the magnets did not need to be moved more than 8 mm.

To quote an example, the accuracy with which the sockets of the ISR reference figure were positioned was ±13 μ for the measurements on 13 May and 25 September, and ±24 μ for those on 30 September 1970. These results are to a large extent due to the favourable shape of the reference figure. Moreover, before any adjustment, the distance measurements were checked by solving, for each braced quadrilateral, the condition equation for obtaining a geometrical structure: the mean closure values obtained for the three sets of measurements quoted above were 23 μ, 37 μ and 25 μ respectively.

Measurements of the radial deviation, dr, namely the deviation perpendicular to the orbit between the measured position and the calculated theoretical position, were completed in April 1971 for the 264 magnets in both rings of the ISR. The dr measurement accuracy fluctuated between ±0.02 mm for the magnets close to a pair of monuments and ± 0.06 mm for the magnets in the centre of the reference figure.

Inside a quadrilateral of the 300 GeV PS, the accelerator components will be positioned as follows. The distance between each component will be measured with an invar wire and the radial position will be determined by measuring the offset between the reference sockets on each magnet and a straight line provided by a nylon wire stretched between the two reference marks of the quadrupoles.

Attempts have been made to check the reliability of a closed-circuit hydrostatic level; the results, whilst sufficiently encouraging to justify the continuation of research in this direction, did not warrant its use for the ISR. Spirit-levellings, starting from a PS bench mark, were carried out through transfer tunnels TT1 and TT2. The results of these levellings indicated the stability of pillars 22 and 77 located at the junctions between the tunnels and the ISR. The sockets on these pillars were used as the reference bench marks for the spirit-levelling of the complete ring. The mean levelling closure error is ±0.5 mm for the 1 km circumference. The heights of the sockets on the pillars deduced from the least square adjustment of the circuit closing errors are used for levelling each individual magnet. The standard deviation of the dz was 0.07 mm.

For the 300 GeV PS, it is expected that, over the 1,152 m of superperiod, the same accuracy will be achieved in determining the height of the reference sockets. Inside a quadrilateral, the dz accuracy will be the same as for the ISR magnets.

The mean dt value - radial tilt of the magnets - will probably be less than ±0.02 mm, as achieved in the ISR.

10.4 Conclusion

Ground movements, consequent displacement of the sockets of the reference figure, magnet misalignments and inhomogeneities in the magnetic field, all have practically the same effect on the orbit of the accelerated protons.

The rate at which measurements were completed on the ISR represented an improvement on that previously achieved on the 28 GeV PS. The way in which the computations were carried out, and the large number of redundant observations make it possible to define the accuracy with which the accelerator components had been positioned. A comparison of successive sets of measurements will, therefore, enable slight movements of the sockets to be distinguished from position errors due to measurement uncertainties which cannot be overcome with the methods used.

In spite of the fact that the shapes of the reference figures in the 300 GeV PS are much less amenable than in the case of the ISR, it is possible to achieve the required accuracy, either by conventional methods such as invar wires with CERN distinvars or new ones such as nylon fishing-lines for alignments over distances greater than 100 m. If new instruments based on electromagnetic distance measurement achieve an accuracy equal to or better than that of the invar they would naturally be tested, built and used for metrological work on the 300 GeV PS.

The ISR calibration bench, whose microscope and 4-metre standard rule have already served for the survey of the 28 GeV PS, can be used for all tests on the new equipment as well as for calibration of lengths shorter than 64 metres.

Chapter 11

THE RADIATION PROTECTION SYSTEM

11.1 Introduction

11.1.1 Basic problems

We are concerned with the radiation protection of the public living in the neighbourhood of the Site, the personnel that are operating, maintaining and using the facilities and with the protection of the machine components and associated equipment against radiation damage.

In this Chapter we discuss how these problems affect the design of the main synchrotron ring and the experimental areas. Our conclusions are that there is sufficient natural shielding above the ring to allow the countryside over the accelerator to be used as at present, without disturbance, and that it is perfectly reasonable to design and operate the accelerator, the North and the West Areas with the loss rates envisaged whilst keeping radiation damage and dose-rates within acceptable limits. The theoretical and experimental justifications for the conclusions of this Chapter are not given here since they have been extensively described in a recent publication (CERN 71-21).

11.1.2 Protection of the personnel and the public

CERN has currently adopted the Swiss interpretation of the recommendations of the International Commission for Radiological Protection (ICRP) for limiting the exposure of the general public; these imply that the dose-rates in an unsurveyed area outside the perimeter fences of the laboratory should not exceed 5 rem/30 year (170 mrem/y or 30 μrem/h). Thus in the design of the accelerator it is assumed that everywhere outside the Laboratory site the radiation levels should be below this limit. Further following the French and Swiss regulations and the CERN internal rules the following requirements must be met:

Table 11.1

		Acceptable limits of exposure	Area	Dose-rate limits in area
1)	External exposure:			
	Members of the public	5 rem/30 years	outside fences	170 mrem/y 30 µrem/h (4500 h/y)
	Radiation workers	5 rem/y	controlled areas	2.5 mrem/h (2000 h/y)
		3 rem/13 weeks	restricted areas	6 rem/h
2)	Internal exposure			maximum permissible concentrations (of isotopes produced in air and water) $(MPC)_{air}$ $(MPC)_{water}$
	Members of the public	2 rem/30 years	outside fences	10^{-8} µCi/cm^3 10^{-6} µCi/cm^3
	Radiation workers	0.5 rem/year	controlled areas	10^{-7} µCi/cm^3 10^{-5} µCi/cm^3

Access to radiation areas will be regulated so that undue exposure is avoided. In areas where dose-rates are above 6 rem/h, work should be performed by remote manipulation. Experience has shown that around high-energy accelerators the risk from external exposure for radiation workers is much higher than from internal radiation. It is reasonable to assume that only 10% of the dose should be allowed to come from internal radiation. The ICRP gives, for the population, guide lines for the apportionment of the contribution to the dose and suggests that about 2 rem/30 years may be due to internal exposure.

11.1.3 Other radiation restrictions

Since the dose limits required to guarantee a useful life for components of the accelerator are liable to change in the course of technical development, it is not possible to define them quantitatively in a manner similar to the biological dose limits. Table 11.2 summarizes the present situation regarding the dose limits above which significant changes in the characteristics of the quoted materials have been observed*).

*) To estimate the corresponding flux densities, the following conversion factor might be applied in a radiation field with a predominant number of high-energy particles and high-energy gammas: 10^7 particles/cm^2 corresponds to 1 rad.

Table 11.2

Dose limits for various materials

Epoxy resins (magnet coil insulations, laminations)	$1\text{-}5 \times 10^9$ rad
Elastomers (rubber hoses, O-rings)	$5 \times 10^7\text{-}10^9$ rad
Glass (camera lenses, windows)	$10^4\text{-}10^6$ rad
Transistors (electronic components)	$10^4\text{-}10^6$ rad

Experimental requirements often call for more restrictions on background radiation than do the occupational dose limits. For large bubble chambers, the acceptable particle background must be about 100 times lower than that required from the average dose-rate limits for radiation workers.

11.2 The Interaction of Primary Protons and the Nuclear and Electromagnetic Cascade

11.2.1 Primary proton interactions

The interaction of protons in machine components is the starting point of all radiation problems. In routine machine operation practically the total beam will interact in external targets and beam dumps. In ejection septa or beam scrapers in the main ring not more than 3% of the total beam is expected to interact at a single point. In quiet regions of the main ring, no single magnet will receive more than 0.05% of all accelerated protons. Special beam dumps will be provided in the ring for an average of 1-10% of the total beam. The following table gives estimates of the number of interacting protons at some typical locations.

Table 11.3

Beam losses

Elements		Proton momentum GeV/c	Number of interaction protons per pulse
External targets	North Area	400	3×10^{12}
	West Area	200	10^{12}
Beam dumps	North Area	400	10^{13}
	West Area	200	10^{13}
	Internal	200-400	10^{12}
Ejection region		200-400	5×10^{11}
Beam scraper		200-400	2×10^{11}
Random loss point in main ring		200-400	5×10^8 average 5×10^9 maximum
Injection in main ring		10	3×10^{12}

In the estimation of shielding requirements for the main ring an intensity of 10^{13} protons per second at an energy of 1000 GeV is assumed: for all other radiation problems we consider a maximum intensity of 10^{13} p/pulse at 400 GeV with $4 \cdot 10^6$ pulses/year. A pulse repetition frequency of one per 4 seconds is assumed for dose-rate calculations.

In addition to the protons interacting at or near full energy one expects losses of 10 GeV/c protons at injection in the main ring; this represents a radiation problem similar to the operation of an internal target at the CERN Proton Synchrotron (PS).

11.2.2 The nuclear and electromagnetic cascades

The propagation and spatial distribution of the proton-induced cascade in shielding materials and in accelerator components is determined by the hadron component with energies above 100 MeV. In the transverse direction shield requirements are determined by the hadronic cascade alone, but in the forward direction the shielding is determined by penetrating muons from the decay of charged π- and K-mesons. The dominant mechanism of energy deposition at the envisaged energies is, however, the electromagnetic cascade induced by the decay of π^0-mesons into gammas.

Monte Carlo cascade calculations, which provide estimates of hadron fluence, star density and energy deposition, have been performed for a variety of geometrical arrangements which resemble closely the situations around an accelerator, for example:

(i) a massive cylinder which represents either an end-stop or a target,

(ii) a target in front of or inside a hollow cylinder, representing a target in front of a magnet unit or a target or beam stopper inside an empty tunnel,

(iii) a line source, representing the target, vacuum tube and some magnet units inside a cylindrical tunnel.

In Fig. 11.1 we give as an example of such calculations, the star density and dose per proton interacting in a target as a function of radius in an iron cylinder 20 m downstream.

11.3 Shielding

11.3.1 General method of shielding estimation

(i) Shielding against strongly interacting particles

Estimates of the attenuation of hadron flux densities are based on experience at 25 GeV extrapolated to 300 GeV and on Monte Carlo cascade calculations. Flux densities obtained outside the shield, and consequently the attenuation requirements, are expected to be correct within a factor of three. The stray flux

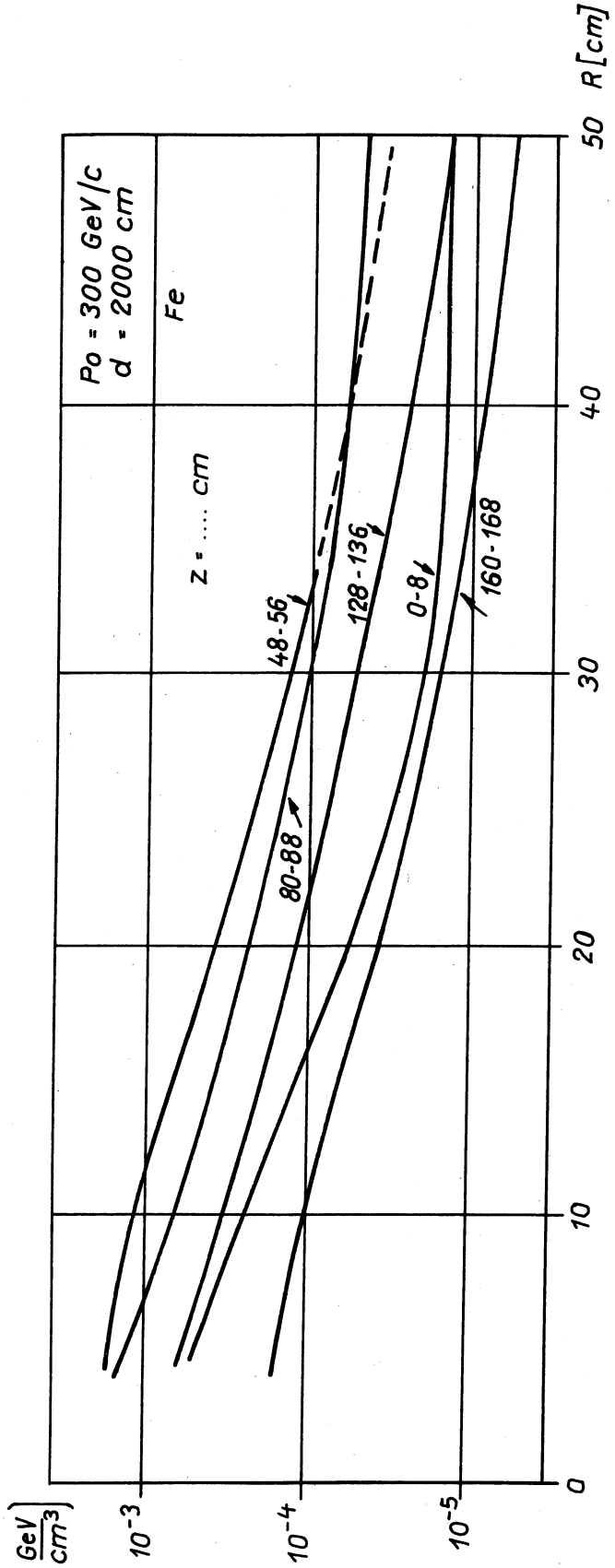

Fig. 11.1 a) Energy deposition per interacting proton

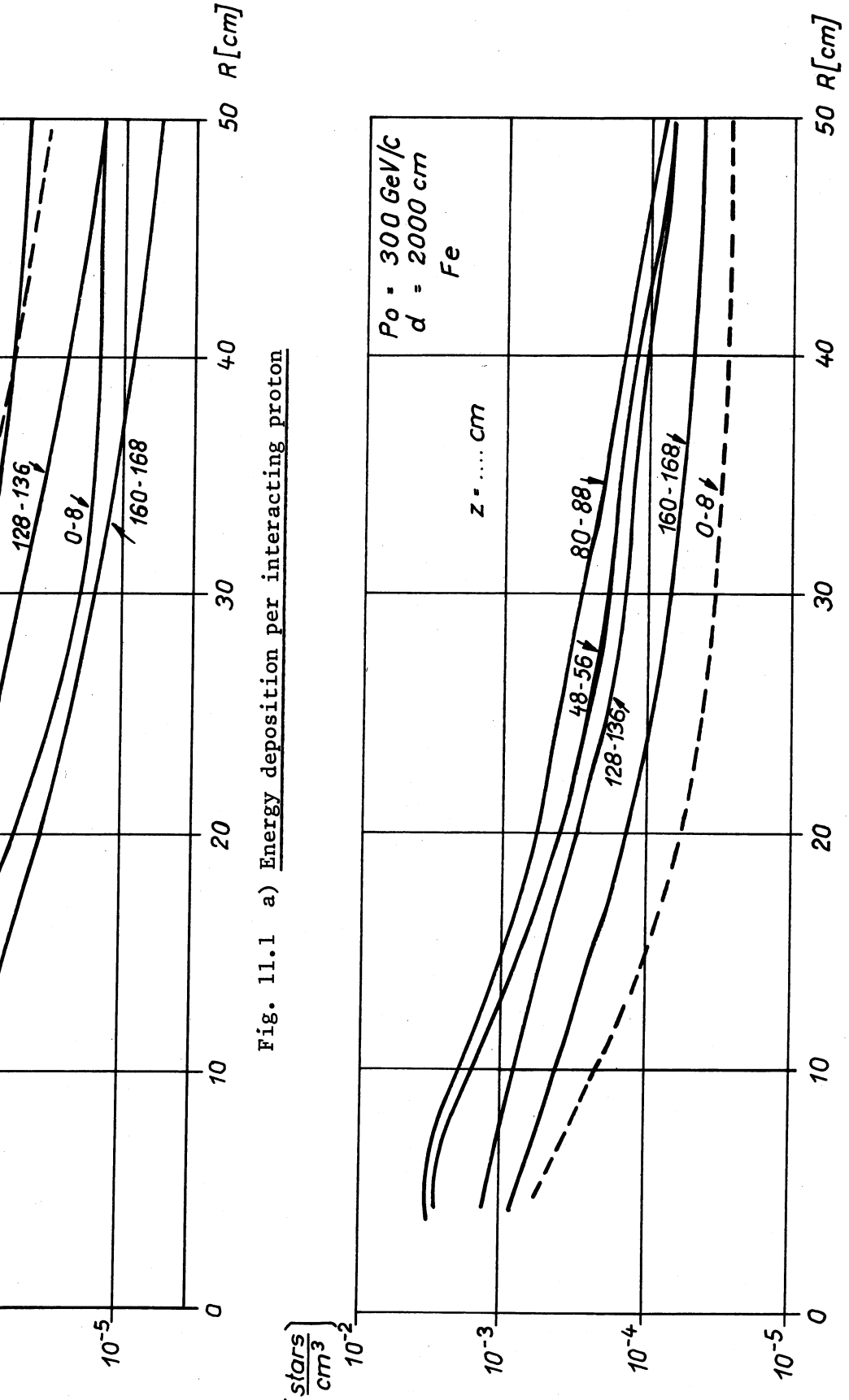

Fig. 11.1 b) Star density per interacting proton

outside the shield is assumed to scale with energy as $E^{0.7}$, and for calculating the attenuation in earth or rock at places where the radiation is in equilibrium we use an attenuation length of 115 g/cm^2. For an equilibrium spectrum it is assumed that 3 hadrons/(cm^2. s) having an energy $\geq$ 20 MeV or 1 hadron/(cm^2. s) having an energy $\geq$ 100 MeV corresponds to 1 mrem/h.

(ii) Shielding against muons

The muon shielding estimates are derived from the calculations described in CERN 71-21. In addition to the angular distribution of pion production, the deviation of pions and of muons by magnetic fields and the effects of collimators are also considered. At the energies considered, 10 muons/(cm^2. s) are assumed equivalent to 1 mrem/h.

11.3.2 Shielding of the main ring

It is assumed here that 5% of the beam intensity is lost at any single point in the main ring. The transverse shielding required to give dose-rates < 5 µrem/h on the shielding surface due to hadron is given in Table 11.4.

Table 11.4

Main ring shielding

GeV	p/sec	g/cm^2	ρ = 1.8 m	ρ = 2.2 m
300	$3 \cdot 10^{11}$	2400	13.5	11
300	$3 \cdot 10^{12}$	2650	15.0	12
1000	10^{13}	2900	16.0	13

From this table it is apparent that to obtain sufficient attenuation for the given conditions we need 16 m of earth (ρ = 1.8) or 13 m of rock (ρ = 2.2). Estimates show that the dose-rate from muons is lower than from hadrons at the surface. The lowest surface level on top of the main ring periphery occurs near Access Shaft 5 (about 422 m above sea-level); at this point the top layer of the molasse rock occurs at 415 m above sea-level. In order to provide a total of about 2900 g/cm^2, about 8 m of molasse rock shielding (1700 g/cm^2) would be needed in addition to the 7 m of earth and gravel (1250 g/cm^2). With the ring tunnel bored at 400 m above sea-level (lowest point of the circular tunnel) a comfortable safety margin is provided allowing even a full beam loss.

Of the 6 access shafts, two are at the ejection straight sections and one at the injection region. The shafts are between 20 and 60 m long, and are connected to the ring by horizontal access tunnels (see Chapter 15). The neutron attenuation in these tunnels has

been estimated in several ways; (i) with the three-dimensional mono-energetic Monte Carlo program ZEUS of the Saclay Group, (ii) with the ORNL AMC program - a three-dimensional multigroup Monte Carlo code, and (iii) by direct extrapolation from existing experimental data. All methods give essentially the same results.

The attenuation factor in the first leg of 3×4 m^2 cross-section (20 m length) is $\sim$50, and in the second leg of 6.5×6.7 m^2 cross-section (22 m length) is $\sim$100. The effect of an extension trap at the end of the horizontal tunnel is estimated to introduce an additional attenuation as does the dilution due to differences of the cross-sectional area between the first and the second leg. A total attenuation factor of $\sim 3 \times 10^4$ is thus obtained.

In order to estimate the actual dose-rate from radiation leaking through these shafts, a maximum beam loss of 1% is assumed to occur, spread over a ring sector of 30 m which includes the tunnel entrance. At the exit of the shortest shaft (22 m long) the dose-rate would be $\sim$30 mrem/h. A concrete cover($\sim$1 m thick) will reduce this to a level of 0.2 mrem/h, ensuring that at the perimeter fence around the top of these shafts the dose-rate will always be within the limits specified for the general population.

11.3.3 Shielding of experimental areas

Beam transfer tunnels to experimental areas will pass underneath places where the dose-rates will have to be less than 30 µrem/h, e.g. at Route Nationale 84. Estimates of the transverse hadron shielding requirements for these tunnels and external targets are shown in Table 11.5. Shielding estimates for the external targets are given for dose-rates of 30 µrem/h at the nearest point accessible to the general public and for dose-rates of 3 mrem/h in controlled radiation areas.

Table 11.5

Shielding requirements for external beams 200 GeV

Position	Loss condition interacting protons/pulse	Dose-rate at outer shield surface	Transverse shielding g/cm^2 (earth/concrete)
Transfer tunnels	10^{10}/100 m	30 µrem/h 3 mrem/h	1500 1000
Beam switchyards	10^{12}	30 µrem/h	2000
EPB target area	$3 \cdot 10^{12}$	100 µrem/h 3 mrem/h	2000 1600
Backstop	10^{13}	100 µrem/h 3 mrem/h	2700 2300

The transverse hadron shielding will provide an effective muon shield in the transfer tunnel and external target situation. In the forward direction at 200 GeV a muon backstop of $80 \times 3.6 \times 3.6$ m^3 will be required (neglecting the effects of any deflections due to magnetic fields). The alternative solution of a downward sloping EPB implies significant saving in the muon shielding required (see Chapter 13).

For 400 GeV operation, transverse hadron shields will need an extra 100 g/cm^2 of material and the length of the muon stop will almost double.

In the North Area the EPB and secondary beam lines will normally be below ground level; all targets could be installed at the extracted beam level, underground at $\sim$444 m above sea-level. With such a layout, advantage can be taken of the rising site around the experimental strip for muon shielding. The muons from one experimental area will not affect the background of the next one downstream, since the areas can be separated sufficiently in angle and/or distance. The underground EPB and the natural muon shielding imply important savings in shielding materials.

11.4 Induced Radioactivity

11.4.1. General method for estimating dose-rates due to remanent induced activity

Hadronic cascade star densities, obtained by Monte Carlo calculations in different idealized geometries are used to estimate the induced activities and gamma dose-rates from the radioactive isotopes produced in magnets and other components of the accelerator. The calculations of remanent dose-rate are standardized for a 30-day irradiation period and a 1-day cool down time.

11.4.2 Radioactivity in the accelerator

(i) Radioactivity in the accelerator structure

This is mainly confined to regions of large beam losses close to septa, beam dumps and scrapers. Some typical values, estimated for the 300 GeV operation of the accelerator, are given in the following table:

Table 11.6

Contact dose-rates 24 hours after the end of a 30-day irradiation

Septum tank	10-50 rem/h
Downstream septum quadrupoles (unshielded)	30-100 rem/h
Beam scraper	20 rem/h
Magnet surface average loss point in ring	30-100 mrem/h

(ii) Radioactivity in the tunnel walls

The remanent dose-rate due to induced activity in the tunnel walls depends mainly on thermal neutron capture by the sodium in the concrete. Near the wall the contributions to the dose-rate from the magnets and the wall (1% Na) are approximately equal. In quiet areas of the machine this dose-rate will be $\leqslant$ 1 mrem/h, but in the regions of the ring containing septa and scrapers the dose-rate from activity in the concrete near the tunnel walls will be $\leqslant$ 100 mrem/h.

11.4.3 Radioactivity in the transfer tunnel

With an assumed loss of 10^{10} ppp due to ejection in the transfer tunnel from the PS ring to the West Experimental Area, dose-rates at the most exposed surface of beam transport elements will be $\sim$2 rem/h; the dose-rate near the tunnel wall will be $\sim$10 mrem/h. These figures are based on a loss occurring at a single point: the average dose-rates in this region will be at least a factor of 10 lower.

Dumps for 1-10% of the beam are to be installed at the upstream end of the transfer tunnel, and in these regions the dose-rates will be high. At the entrance face of a 40 cm diameter steel dump $\sim 10^3$ rem/h can be expected locally; at the outer surface of the dump the contact dose-rate could be $\sim$10 rem/h. Losses of $\sim$5% in the splitting magnets will produce dose-rates from these components $\sim 10^2$-10^3 rem/h.

11.4.4 Radioactivity in target stations

The radioactivity induced in external targets and in downstream beam transport elements as well as in the shielding around the target is, together with the activity induced in the dumps, the most important radiation hazard when the accelerator is shut down. The following table gives estimated dose-rates for the most active components in a typical target station.

Table 11.7

Dose-rates in target stations
(10^{13} p/p)

Steel walls close to target	30 rem/h
First quadrupole magnet downstream	
pole face - front	800 rem/h
front-face - general	300 rem/h

To a first approximation, dose-rates due to the first quadrupole magnet are independent of downstream distances in the range 5-20 m. Dose-rates on the outer surface of the 1 m local steel shielding around a target station will be $\lesssim$ 100 mrem/h.

11.4.5 Radioactivity in cooling water

Cooling water for the r.f. cavities, magnets and quadrupoles of the main ring will be contained in a closed circuit. The majority of the long-lived activity in demineralized water will accumulate in an ionexchange column. Water from such cooling circuits will not be discharged directly into the normal drainage system. Pipes from the ring and primary beam lines carrying radioactive water will not pass through occupied areas or unshielded areas outside the fences where the required dose-rate levels are low. The highly radioactive cooling water from target stations must be kept separate from the other circuits. Most of the induced radioactivity in water has a short half-life and so decays quickly when the accelerator is off.

11.4.6 Radioactivity in ground water

Surface water will not be able to penetrate the dry molasse rock through which the accelerator ring tunnel is bored apart from a small amount of seepage down the vertical shafts drilled into the molasse. Measurements of ground water activity at the CERN-PS indicate that the activity in this seepage water is not expected to be significant. Water draining past the ejection tunnels and North Area target stations will be collected and only released into the normal drainage system after checking its activity.

11.4.7 Radioactivity in air

(i) Ring tunnel

The saturation concentration of gaseous activity produced in the air of the ring at machine stop will be about $3 \cdot 10^{-5}$ $\mu Ci/cm^3$ assuming a loss of $6 \cdot 10^{11}$ p/pulse. After 15 minutes the activity of the isotope mixture will have decayed to less than 1/10th of its initial value or to about the same order of magnitude as the maximum permissible concentrations. Therefore, access to the ring tunnel will not be restricted by air activation. A moderate ventilation rate of the ring implies that the radioactive air from the tunnel will arrive at the shaft's exit after a delay sufficient to ensure that the radioactivity will not exceed permissible limits for radiation workers. The predominant meteorological conditions in the valley (only two-wind direction and frequent inversions) are conducive to the deposition of any airborne activity in localized regions. Thus a means for suitable dilution of gaseous activity and filters to trap suspended activities (e.g. ^7Be) will have to be installed to ensure that levels are below those permissible for the general public.

(ii) Target stations

We expect that the specific air activity in the target station of the West Hall will be $2 \cdot 10^{-2}$ $\mu Ci/cm^3$. In the North Hall the concentration could be as high

as 10^{-1} μCi/cm^3. It follows that air from target stations must not be released directly to experimental areas, but must be filtered and scrubbed before recycling or exhausting.

11.5 Radiation Damage and Radiation Heating

11.5.1 General aspects

In the construction of particle accelerators and auxiliary equipment materials and components are used which are subject to radiation damage and hence, have a limited life (see Table 11.2).

The following table gives estimates of the dose levels to be expected in the accelerator. They have been obtained from the cascade calculations and by extrapolation from previous experience.

Table 11.8

Yearly dose-rates to components in rad
($4 \cdot 10^6$ pulses/year)

Components	Loss point in ring	Ejection region (unshielded quadrupole)	Target stations*) maximum values) 10^{13} p/p
Magnet coil	$2 \cdot 10^7$	$5 \cdot 10^9$	$5 \cdot 10^{10}$
Magnet steel	$4 \cdot 10^7$	10^{10}	$3 \cdot 10^{11}$
Control boxes floor level electronic components	$4 \cdot 10^4$	10^7	

*) Calculated on the assumption that one target station takes all available protons.

11.5.2 Control of radiation damage by selection of materials

Semi-conductors are the most radiation sensitive electronic components. Changes have been observed in some components at doses of 10^4 rad equivalent. If, therefore, they must be used in radiation environments, they should be carefully selected and installed as far as possible away from the radiation source. Radiation sensitive organics must be avoided in other components like capacities.

A careful selection of plastic materials and components will provide a group of materials which are capable of withstanding radiation doses of 10^9 to 2.10^{10} rad. An

important class of organic materials is the epoxy group, which are used for fabricating the magnet coil insulation. The radiation resistance*) of unfilled and unreinforced epoxy resin systems currently available for use as impregnation materials in the coil-making industry in Europe is limited to 5.10^9 rad. However, various epoxy resin pre-impregnated glass mica tapes used as insulation for magnet windings are available which will withstand up to 1.10^{10} rad. The radiation resistance of elastomeric components is limited to $2 . 10^9$ rad. A number of oils and greases tested to levels of 2.10^9 rad are available.

Concrete and ceramics withstand irradiation much better than organic materials, therefore these inorganics are to be considered for use in magnet construction and cable insulation in the target station.

Although permeability changes in magnetic materials can be expected at the highest dose levels quoted in Table 11.8 no problems are expected.

Although corrosion of metals in aqueous media has been observed to increase under radiation, it is estimated that this problem can be kept in hand by taking adequate precautions, i.e. water purification, resistivity and pH control, use of appropriate inhibitors, etc.

Aggressive chemicals produced by the irradiation of moist air in the tunnel consists of ozone and a mixture of nitrogen oxides. With the proposed rate of air exchange the concentration of these noxious gases is also acceptable. All critical materials used in the construction of the accelerator will be subjected to rigorous damage studies.

11.5.3 Radiation heating

Cascade calculations of the energy deposition in targets are in good agreement with experiments at 12 and 24 GeV/c. The calculations at 300 GeV/c are expected to have errors of up to 30% due to the somewhat arbitrary assumptions on π^0 production in inelastic events. The following table gives instantaneous temperature rises during one short burst, without considering heat dissipation.

---

*) Radiation dose (rad) to reduce the mechanical properties (flexural, tensile or shear strength to 50% of its initial value.

Table 11.9

Radiation heating (short burst)
300 GeV/c, 10^{13} incident protons

	ΔT (°C)
Cu target 2 × 2 mm^2	1000
Al target 2 × 2 mm^2	350
W target 2 × 2 mm^2	3700
Fe beam dump, beam 2 mm Ø maximum	1000

At intensities of about 10^{13} protons it is proposed to use rotating thin discs as targets; for long bursts this reduces the heat density by a factor 50 to 100. The construction of collimators and beam dumps must allow the dissipation of up to 200 kW of power. Solutions similar to the ones applied at the ISR are envisaged. Radiation heating ∿10 cal/(g. burst) is expected for the foil of the first septum magnet.

11.6 Control of Exposure to Radiation

11.6.1 Control of stray radiation

Beam losses inside the ring and the injection and ejection tunnels will be controlled to comply with the conditions for which the shielding has been specified and which give tolerable levels for induced activity and dose to accelerator components.

Radiation monitors are needed in areas outside the shielding, where high dose-rates could be expected or where the dose-rates have to be controlled within close limits (e.g. access shafts, beam transfer tunnels); the acceleration or ejection system will be interlocked with signals from these monitors. A site monitoring system will be installed to measure the influence of the operation of the accelerator on the natural environmental radiation and radioactivity.

11.6.2 Control of induced activity

Induced activity can best be reduced by controlling the beam losses in the tunnels. A beam loss monitor system with monitors in each lattice period will provide the beam loss data. This information can be used as guidance for the machine operation and for estimation of the induced activity levels.

The production of induced activity may be minimized to a limited extent by selecting material in which the primary protons interact. For example cobalt and nickel steel should be used as little as possible. In compact beam dumps light elements would be preferred

from the stand-point of low-induced activity but are not efficient at stopping beams. The use of depleted uranium in beam dumps and collimators should be limited because of the high levels of induced radioactivity produced. Lining the interior surface of a steel target station with 25 cm of marble, limestone or selected mortar can reduce the dose-rate from the walls by a factor of 10. Concrete should be made from aggregates which contain little sodium and manganese. It is proposed to use a similar aggregate to that used for the PS ring tunnel (0.3% Na). No special measures will then be needed to reduce the remanent dose-rate from concrete activation.

11.6.3 Control of exposure from induced activity

Dose accumulated by working in a radioactive area will be reduced by local shielding, remote handling, and by waiting for the decay of activity.

After a few hours of cooling time the average gamma energy of activation products is around 1 MeV; thus temporary local shielding using $\sim$5 cm of lead (attenuation factor $\sim$20) will allow access to many hot regions.

The exhaust gases from target stations where large amounts of active air and aerosols are produced can only be rejected after suitable filtration and suitable dilution. When working in active areas inhalation of dust can be avoided by suitable filtration of the air, by the painting of exposed surfaces as well as by keeping the most exposed machine parts clean.

11.6.4 Quick-connects

Shortening the time needed for a given job can be achieved by using standard quick-connections for services such as water and electricity. The main ring, transfer tunnels, target stations and experimental areas should all be designed on this philosophy.

11.6.5 Remote handling

As a general rule it is advisable to design remote handling devices for all those areas where the dose-rate at the working distance (40 cm) is estimated to be greater than 1 rem/h; remote handling is essential at dose-rates above 6 rem/h. Personal occupancy of such areas will have to be strongly restricted; 30 minutes occupancy of such an area would mean the accumulation of the maximum allowable dose for a three-month period. Small, highly active components, e.g. targets, should always be handled remotely.

For the accelerator ring tunnel a ground vehicle transport system for magnet handling will be the most effective. In the ejection areas where high dose-rates are anticipated, the same vehicles will be used in conjunction with manipulators and local shielding to reduce the dose to personnel. Remote handling facilities will be required for septa and

quadrupoles in the ejection regions and for beam scrapers and dumps.

Specialized remote handling devices are essential for the installation and removal of all components near targets. Access to the target station will be through the roof shielding. Removal and installation of components will be performed using a crane, the operator working in a shielded cabin.

A central storage facility including an active handling workshop in which highly active equipment can be allowed to cool down and being repaired is foreseen.

11.6.6 Personnel monitoring and access control

Exposure from prompt leakage radiation and from remanent activity will be controlled by personnel and area monitoring. Personal dosimeters will be necessary in those areas where the dose-rate cannot be controlled to levels below 1.5 rem/y. All dosimeters and area monitors will need to be sensitive to neutrons, charged particles and photons.

Access to radiation restricted areas (ring, ejection and EPB tunnels) will be remotely controlled and interlocked from the Main Control Centre via intercom, TV and perhaps magnetic cards.

Chapter 12

THE EXTRACTION SYSTEM

12.1 Introduction

This Chapter describes the extraction system for the 300 GeV accelerator [12.1]. It was found possible to place all the extraction elements in the lattice without introducing a special insertion. The extraction channel layout permits extraction up to the highest energy envisaged for the machine, including superconducting versions. There will be two extraction systems at straight sections 6 and 2, for the West and North Area respectively.

The same extraction channel will be used for both fast and slow extraction. Slow extraction is described in some detail and the required magnetic field and ripple tolerances for slow extraction are given. Beam sharing between the two different channels is described.

Fast extraction by beam shaving and beam dumping are discussed.

12.2 Expected Beam Properties

In the CPS one finds already at an intensity of 10^{12} p/p a considerable blow-up of the transverse and longitudinal emittances. The beam does indeed become smaller as it is accelerated but not as rapidly as single particle theory would suggest. Since the non-linear stop-bands in the 300 GeV machine are wider than in the CPS a similar blow-up is likely to take place in the 300 GeV.

The underlying mechanism of these phenomena is still obscure and it would not be realistic to attempt any sort of scaling of the PS data to another machine. Nevertheless, it is essential to allow for this type of beam blow-up in the design of the extraction system of a high intensity machine. We have therefore taken a somewhat arbitrary blow-up factor of 2 which we apply to the normalized emittance between injection and utilization energy. It is assumed that suitable compensation methods would be developed if a larger blow-up did occur and was found intolerable.

This leads to the following set of expected circulating beam parameters at extraction (a = maximum betatron amplitude).

Table 12.1

Circulating beam parameters at extraction

	200 GeV/c	300 GeV/c	400 GeV/c
E_H (π 10^{-6} rad m)	0.69	0.46	0.35
a_H (mm) at $\hat{\beta}_H$ = 109 m	8.7	7.2	6.2
E_V (π 10^{-6} rad m)	0.34	0.23	0.17
a_V (mm) at $\hat{\beta}_V$ = 109 m	6.1	5.0	4.3
$\frac{\Delta p}{p}$ from synchrotron oscillations	$\pm$ 5.10^{-4}	$\pm$ $3.7\ 10^{-4}$	$\pm$ 3.10^{-4}
ΔR(mm) at $\hat{\alpha}_p$ = 4.25 m	$\pm$ 2.2	$\pm$ 1.6	$\pm$ 1.3

As will be shown in the following, the beam size has a strong influence on the extraction efficiency. In fact, below 200 GeV/c we may have to decrease the beam emittance either by scraping off the halo, or by reducing the intensity of the accelerated beam.

A reduction in momentum spread could in principle be obtained by adiabatic debunching. However, it is necessary to have in the coasting beam a certain momentum spread to ensure its stability against rebunching induced by beam-equipment interactions and an even larger minimum of the acceptable momentum spread is given by the fact that the modulation of the extracted beam intensity by magnet ripple is inversely proportional to its momentum spread (see subsection 12.9.1). For this reason there will be a tendency to increase the momentum spread of the circulating beam above the value given in Table 12.1.

12.3 The lattice from the extraction point of view

The separated function lattice gives a large degree of freedom in the design of the extraction system. The layout of the extraction channel is shown in Fig. 12.1. It consists of an electrostatic septum (ES), a thin magnetic septum (TS) and a thick septum extractor magnet (EM). The distance from ES to EM is about one quarter betatron wavelength and in this region the extracted beam gradually moves out of the machine aperture.

The more important constraint on the lattice due to extraction is the requirement that there must be a sufficiently long free drift space downstream of the EM to allow the deflection of the beam away from the machine.

In principle the maximum available free space is determined by the distance in between successive quadrupoles. However, it is possible to modify the first quadrupole downstream

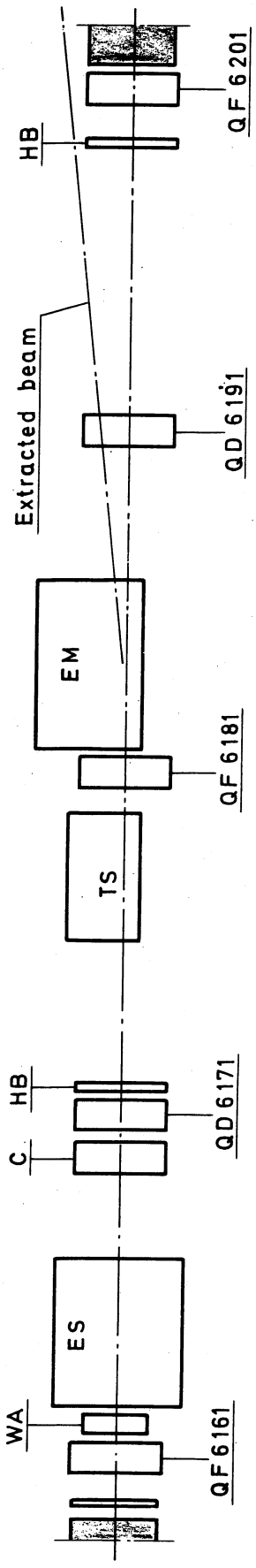

WA Wire Array
ES Electrostatic Septum
C Collimator
HB Horizontal Bumper
TS Thin Septum
EM Extractor Magnet

Fig. 12.1 Layout of the extraction channel

of EM so that it does not obstruct the extracted beam. By leaving out the bending magnets over a full period downstream of the EM an effective free straight section of about 60 m can be obtained. This procedure permits one to choose the number of periods and Q-value large enough to obtain suitable values for other machine parameters such as α_p, γ_{tr}, bending magnet length etc.

In the long straight sections where bending magnets are suppressed, the momentum compaction function α_p tends to be small. In the lattice which has been chosen, the value of α_p near any septum is only 0.4 m compared to a maximum of 4.25 m in the regular lattice. This allows the first septum to be pushed about 11 mm into the normal machine aperture and to be left there throughout the cycle.

12.4 The extraction channel

12.4.1 Layout of the extraction channel

The design of the extraction channel is based on the following principles:

(i) The same channel is used for slow and fast extraction.

(ii) All elements stay in a fixed position during the accelerating cycle.

(iii) The elements are designed for 400 GeV/c but the channel could be extended to higher momenta.

(iv) The radial position of the three elements is set near the beam envelope at injection. Because of the small value of α_p in the extraction region, the beam size there is roughly equal to twice the betatron amplitude.

Figures 12.1 and 12.2 show the layout of the extraction channel. The numbering of the machine components refers to extraction to the West Area at straight section 6. For extractions to the North Area at straight section 2, the first digit of the number must be changed accordingly. (See Chapter 2 for explanation of the numbering system).

The first elements of the extraction channel is the electrostatic septum ES, which is placed just after QF 6161. With this arrangement β_H is close to its maximum ($\sim$ 100 m) at the entrance of ES which minimizes the proton losses on the septum. To leave sufficient room for ES, the two B1 magnets after QF 6161 must be left out. The aperture of the following two B2 magnets would be just sufficient to accommodate the extracted beam, but since these magnets would be heavily irradiated by secondaries produced in ES, they are also left out. The aperture of QD 6171 is large enough to accommodate the extracted beam but its normally circular vacuum chamber must be enlarged. Its coils are sufficiently far from the aperture for them to be protected by a heavy collimator in front of QD 6171. The two B2 magnets downstream of QD 6171 are left out since their aperture would be too small for the extracted beam.

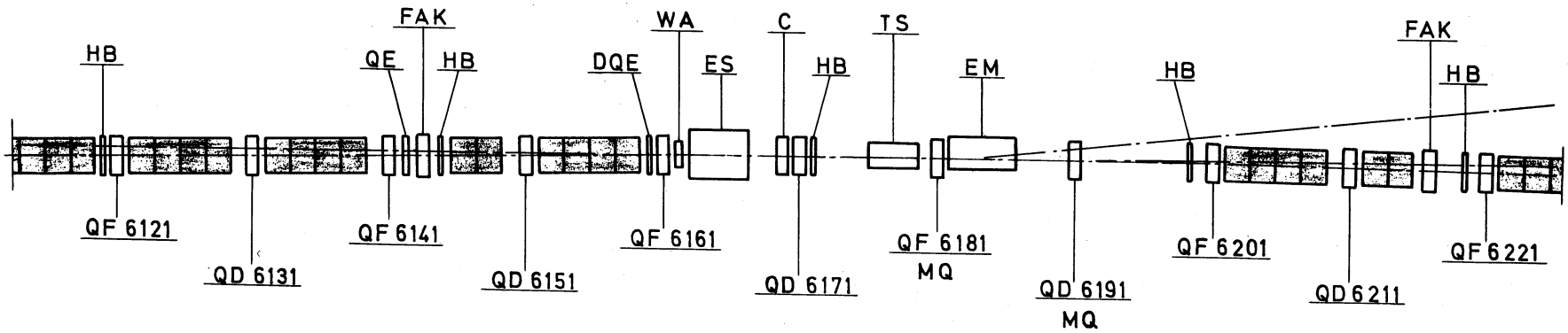

QE	Extraction Quadrupole
FAK	Full Aperture Kickers
HB	Horizontal Bumper
DQE	Extraction Correcting Quadrupole
WA	Wire Array
ES	Electrostatic Septum
C	Collimator
TS	Thin Septum
EM	Extractor Magnet
MQ	Modified Quadrupole

Fig. 12.2 Position of the extraction elements in the lattice

The TS should preferably be placed close to one quarter betatron wavelength after the ES in order to obtain a maximum hole (space between circulating beam and extracted beam deflected by ES) for a given deflection in ES. For the same reason it should be at a place where β_H is large. Both requirements are satisfied by placing TS at the location of the two missing Bl magnets upstream of QF 6181. The aperture of QF 6181 is too small for the extracted beam so that QF 6181 will be a special, longer quadrupole with enlarged aperture.

The EM is placed just after QF 6181. The main problem is then, to get the extracted beam past QD 6191. Since the latter has a symmetrical shape, the required bending angle would not be reduced by choosing for EM a vertically deflecting steel septum magnet. On the other hand, such a layout is very unfavourable for the design of the enlarged tunnel sections at the extraction points. For these reasons a horizontally deflecting current septum magnet was adopted for EM.

At QD 6191 the extracted beam is at about 240 mm from the machine centre line. This quadrupole will have a standard core but its coil will be made of smaller conductors. This leaves a slot in between its coils of about 50 mm for the vacuum chamber of the extracted beam. At QF 6201 the extracted beam is at 460 mm from the machine centre line and thus clears this quadrupole entirely.

The main parameters for the components of a 400 GeV/c extraction channel are listed in the following table.

Table 12.2

Extraction Channel Parameters at 400 GeV/c

	ES	TS	EM
Position in lattice (Fig. 12.)	6163 6165	6177 6179	6183 6185
Effective septum thickness (mm)	0.15	4	15
Effective length (m)	9	8	10
Field Strength	100 kV/cm	0.23 T	1.0 T
Vertical aperture (mm)	25	20	20
Horizontal aperture (mm)	20	50	50
Deflection (mrad)	0.225	1.4	7.5

12.4.2 The electrostatic septum ES

The 9 m long electrostatic deflector ES will provide electric fields up to 100 kV/cm to achieve a deflection angle θ = 0.225 mrad at the nominal momentum p = 400 GeV/c.

Its gap will be adjustable but would normally be set to about 20 mm to accommodate the jump for the slow extraction. The total voltage applied to the cathode in then -200 kV.

The anode will be at ground potential and will constitute the septum of ES and hence it must be as thin as possible and yet meet stringent geometrical and electrical requirements. Our present design assumes the use of a metal foil of thickness $\leq$ 0.1 mm. This should give an apparent septum thickness, including non-straightness, of about 0.15 mm over the total length of ES. It is possible that an array of wires could be made thinner than a foil septum but it is not yet clear that it could stand 100 kV/cm. The ES will be housed in 3 tanks with a combined total length of about 12 m.

In order to reduce the proton losses on ES an array of thin wires will be placed upstream of ES and aligned with its septum to Coulomb scatter some of the protons away from ES.

The size of the hole created by ES at the entrance of TS is proportional to the deflection in ES minus the angular divergence of the beam at ES. The latter is about 0.06 mrad and 0.125 mrad for slow and fast extraction respectively. The contribution of $d\alpha_p/ds$ to the divergence is very small. In this way one finds a hole size at TS of 12 mm and 7 mm for slow and fast extraction respectively.

12.4.3 The thin magnetic septum TS

The thin septum will be housed in 4 tanks with two magnets of 1 m length in each tank. It will produce a 1.4 mrad deflection and will have a gap height of 20 mm for a septum thickness of 4 mm. The septum will have 5 holes of 2.5 mm diameter for water cooling. The current density in the copper is 60 A/mm^2 for a field in the gap of 0.23T. This septum will increase the hole which is made by ES at the extractor magnet EM by an extra 15 mm to a total of 27 mm or 22 mm for slow and fast extraction respectively.

12.4.4 The Extractor Magnet EM

The extractor magnet will be housed in 5 tanks with two magnet units of 1 m length in each tank. It will produce a deflection of about 7.5 mrad and will have a gap height of 20 mm with a septum thickness of 15 mm. The current density in the copper will be 70 A/mm^2 for a field in the gap of 1 T.

TS and EM will be pulsed with rise times of a few tenths of a second.

12.4.5 Horizontal and Vertical Dipoles

Since the septa are located outside the aperture required for injection, the closed orbit extraction must be brought close to the septa with horizontal dipoles. Furthermore, the closed orbit position and direction at each septum must be accurately controlled to ensure that each septum falls just inside the hole created by the previous septum. For this

a total of 5 horizontal dipoles is required. Their positions are indicated in Fig. 12.2 which shows the layout of all extraction elements for straight section 6. To avoid vertical beam loss on the top and bottom poles of the septum magnets the vertical closed orbit will be corrected in the extraction region. For this purpose 2 pairs of vertical bumpers respectively upstream and downstream of the extraction region have been foreseen.

12.5 The various methods of extraction

The principle of slow extraction is to bring the Q-value of the machine close to a resonant value and to install at the same time a non-linear perturbation (e.g. with suitably distributed sextupoles) in such a way that particles with betatron amplitudes below a certain limit are stable but those above that limit are unstable. The most sensitive of the different parameters which determine if a particle is stable or unstable is, for integer extraction, the position of its closed orbit at the extraction quadrupole and for third integer extraction the parameter $\Delta Q = Q - 27\frac{2}{3}$. The spillout is usually controlled by a slow variation of these most sensitive parameters. Once a particle becomes unstable, the phase of the resonant oscillation becomes locked to that of the imposed perturbation and its amplitude increases faster than exponential on successive turns. Most particles will then jump across a thin septum (the ES) which is placed at a suitable azimuth. In a typical case the amplitude growth in between successive passages near the ES would be about 15 mm and the amplitude in the last turn, just before extraction, would be about 50 mm. For a 0.15 mm thick septum, taking into account the radial amplitude distribution and beam divergence at the ES one finds a theoretical efficiency of about 98%.

A systematic field distortion in the main ring bending magnets or quadrupoles, leads to an increase in the emittance of the slow extracted beam and a reduction in jump size or even complete stabilization of the resonance. For this reason tight tolerances must be imposed on systematic field distortions in the main ring (see section 12.8).

Ripple on the magnetic field causes a modulation of the rate of change of machine parameters and this results in a corresponding modulation of the instantaneous extracted beam intensity. The need to aim at a constant extracted beam current for counter experiments imposes severe tolerances on the permissible field ripple.

Resonant extraction of the integer ($Q = 28$) and the third integer ($Q = 27\frac{2}{3}$) type will be installed in the machine and both schemes are described below.

Integer extraction should be less sensitive to non-linearities in the main magnet since the particles before being extracted, spend less time oscillating at large amplitude in the integer extraction than in the third integer extraction. However, integer extraction might be more difficult to adjust, especially if the circulating beam has a larger emittance and momentum spread than expected. On the other hand, the third integer extraction efficiency may suffer from the survival of particles which cross the narrow stop band too fast.

The integer extraction imposes more severe ripple tolerances for bending magnets than the third integer. However, the feedback loop which could reduce the ripple induced modulation is more difficult for third integer extraction.

It may be desirable to perform slow extraction at 200 GeV to the West Hall during an intermediate flat top and to accelerate thereafter to a higher energy. In such a case there is a strong interest in keeping the beam bunched with the r.f. system in order to avoid the beam losses associated with rebunching at the end of the flat top. For experiments it seems to be acceptable if the extracted beam is bunched with a 200 MHz frequency since the spacing of the bunches is comparable to the resolution time of the electronics. However, it is not yet clear, without further study, that extraction with r.f. on is practicable.

An alternative slow extraction method uses a target to increase the betatron amplitudes of the particles by Coulomb scattering. The average amplitude growth on successive turns through a high Z target can be made a few mm. Therefore the theoretical losses in this type of extraction are 3 to 4 times larger than with resonant extractions[12.2]. The vertical emittance of the extracted beam is also somewhat increased by the scattering target. The main advantage of target scattering is that this extraction method puts much lower requirements on the field quality of the main ring magnets. The 300 GeV machine is designed for resonant extraction because of its much better efficiency. However, it is easy to install a scattering target if required.

12.6 Layout of quadrupoles and sextupoles for slow extraction

12.6.1 Integer Extraction

Suitable resonance conditions for extraction at $Q_H = 28.0$ can be established with an extraction quadrupole QE and a number of sextupoles. In principle one could leave the tune of the unperturbed machine at Q = 27.75 and bring the Q-value close to Q = 28 with a rather strong QE. Computations have shown, however, that the jump size of the particles at the ES becomes more uniform if the machine is tuned in the range $27.8 < Q_H < 27.9$ before extraction starts. This also leads to some reduction in the required strength of QE.

Since almost all the oscillation growth per turn comes from the quadrupole, this element should be as close to the extraction channel as possible. We have therefore decided to place it just one period upstream of ES. The sextupoles which introduce the required non-linearity into the scheme should be situated near places where the forced oscillation induced by QE is maximum. It happens that the sextupoles foreseen in positions 5300 and 6060 for third-integer extraction (see 12.6.2) fulfil this requirement sufficiently well.

When a proton becomes unstable, the phase of its resonant oscillation at a given azimuth remains approximately constant. This means that in a phase space diagram the proton makes increasingly large jumps along the so-called separatrix, which starts from the unstable

fixed point. Figure 12.3 shows the shape of the separatrices for different emittances using normalized coordinates [12.3] with the amplitude normalized to $\beta_H(max) = 109$ m and for an unperturbed $Q_H = 27.9$. When QE alone is excited, the angle of the separatrix with respect to the positive x - axis is about 40^o; (curves a). This is acceptable but the extraction efficiency can be improved if this phase angle is decreased with a correction quadrupole DQE just upstream of ES (curves b).

The position and strength of the elements used for the integer extraction are summarized in Table 12.3.

Table 12.3

Positions and strengths of extraction elements

Element	Function	Position	Core length [m]	nominal strength at 400 GeV/c
QE	Integer resonance quadrupole	6143	1.5	18 T/m
DQE	Integer resonance correction quadrupole	6160	0.5	18 T/m
S1'	Sextupole, third-integer	5180	1.2	150 T/m^2
S2'	Sextupole, third-integer	5219	1.2	150 T/m^2
S1	Sextupole, integer and third-integer	5300	1.2	150 T/m^2
S2	Sextupole, integer and third-integer	6060	1.2	150 T/m^2

12.6.2 Third integer resonant extraction

The resonance is excited by tuning to $Q_H = 27\frac{2}{3}$ and exciting four sextupoles which are arranged in two pairs. The two sextupoles of each pair have opposite polarity. This has the convenient result that the effect of the extraction sextupoles on dQ/dp of the machine is kept small.

A particle which just grazes the ES will make three more revolutions before returning with the same phase at the ES and being extracted. By a suitable choice of the phase advances and by selecting the most favourable of the three separatrices we have designed a layout where the pair of sextupoles S_1 and S_2 in positions 5300 and 6060 gives a separatrix (see Fig. 12.4) at ES which has about the right phase, the correct curvature (curved towards the x-axis, which gives the smallest angular divergence of the extracted beam at ES).

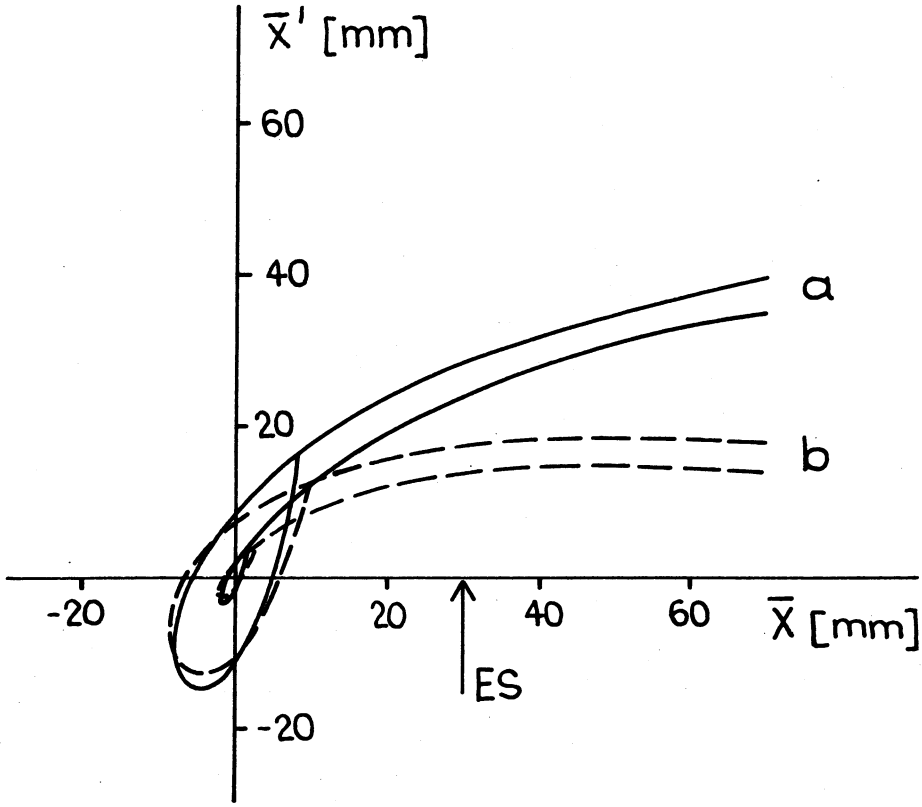

Separatrices at the entrance of ES for integer extraction

Curves a : QE excited only

Curves b : strength of DQE/strength of QE ≈ 1/3

Fig. 12.3

This scheme also provides a favourable jump sequence concentrating the resonance growth in the last traversals of the sextupole field.

The phase of the separatrix at the ES is quite critical. If it is more than 40° the extraction efficiency becomes too low. If it is smaller than 25° the second separatrix starts to fill the hole at the EM. For this reason a second pair of sextupoles S_1' and S_2' in positions 5180 and 5219 has been foreseen. Some examples of the phase shift they provide are given in Fig. 12.4.

In Fig. 12.4 it has been assumed for convenience that the emittance of the circulating beam was very small. Figure 12.5 shows the phase space diagrams for an emittance of 0.7π mm × mrad in the cases that the resonance is approached from below (from smaller Q-values, curve a) and from above (curve b). In the latter case the distance from the unstable fixed point to the ES is much smaller and the losses are correspondingly larger. This means that before the extraction process starts the Q-value of the machine must be lowered so that the beam is placed between $Q_H = 27\frac{1}{2}$ and $27\frac{2}{3}$. It may be necessary to compensate with small correcting sextupoles the stopband at $Q_H = 27\frac{2}{3}$ when it is being crossed. Alternatively the working points 26.25 and 28.25 which lie below third integer stop bands may be used.

Positions and strengths of the two pairs of sextupoles used for extraction at $Q_H = 27\frac{2}{3}$ are listed in Table 12.3.

12.6.3 Sharing between West Area and North Area

Simultaneous slow extraction to the West and North Area can be achieved by taking full advantage of the flexibility offered by a separate function machine. For sharing the phase advances in the machine are changed such, that the number of radial betatron oscillations from West to North is exactly 9.0. This is achieved by using an active bypass which shunts half of the machine quadrupoles and thus allows for different advance in the two halves of the machine. In one half of the machine, from point 6 to point 3 (position of the main power supply), the betatron wave number is adjusted to 13.5. In the other half, from point 3 to point 6, it will be adjusted to 14.166 or 14.5 for extraction at $Q_H = 27\frac{2}{3}$ or $Q_H = 28.0$ respectively. In that case, providing an adequate orientation of the separatrix at the first (West Area) ES automatically ensures the correct orientation at the second one. Only the quadrupoles and/or sextupoles foreseen for West Area extraction have to be powered.

12.7 Efficiency of slow extraction

The efficiency of a resonant extraction is closely related to the machine aperture available for the amplitude growth of the unstable particles. This relation was investigated in some detail for the case of third-integer resonant extraction. The procedure was as follows:

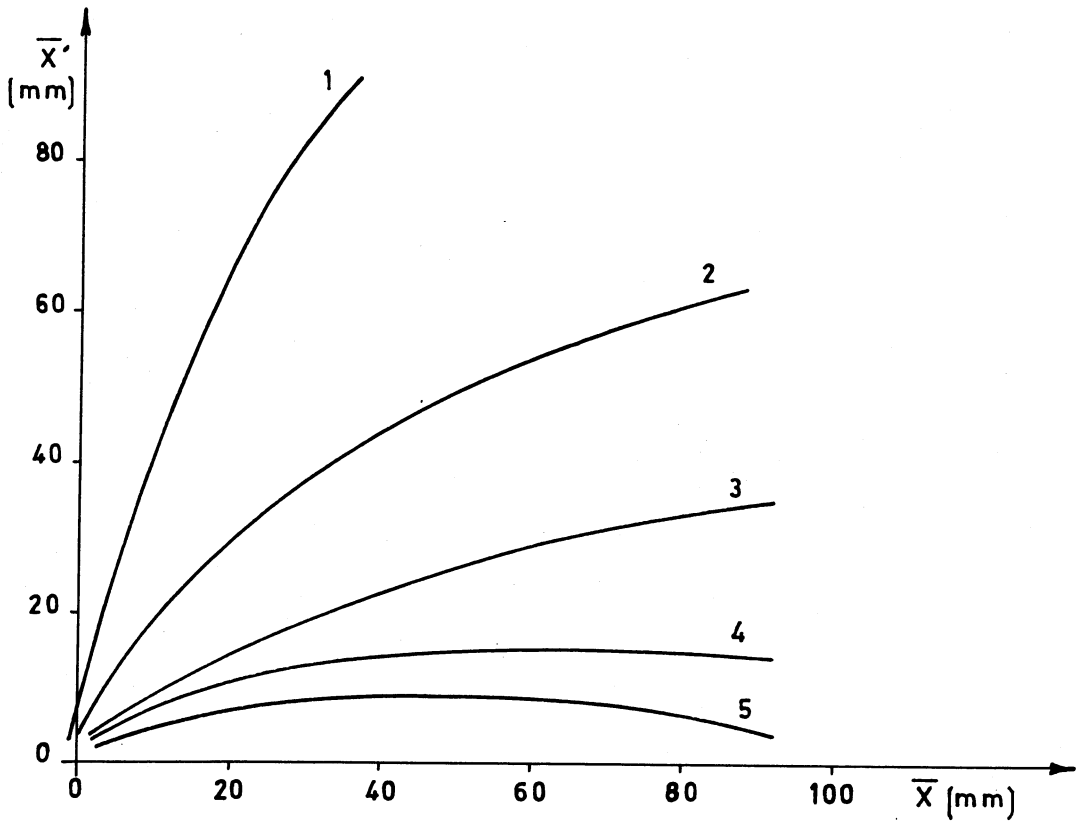

Outward-going separatrices at the entrance of ES for third integer extraction

The orientation can be adjusted within a large range by varying the relative excitations of the sextupole pairs.

Curve No	Polarity of the sextupoles S_1	S_2	S'_1	S'_2	Ratio of strength of the two pairs $\frlvert\bar{K}_s\frrvert / \frlvert\bar{K}_{s'}\frrvert$
1	-	+	-	+	1/2
2	-	+	-	+	1
3	-	+	not excited		÷
4	-	+	+	-	1
5	not excited		+	-	÷

Fig. 12.4

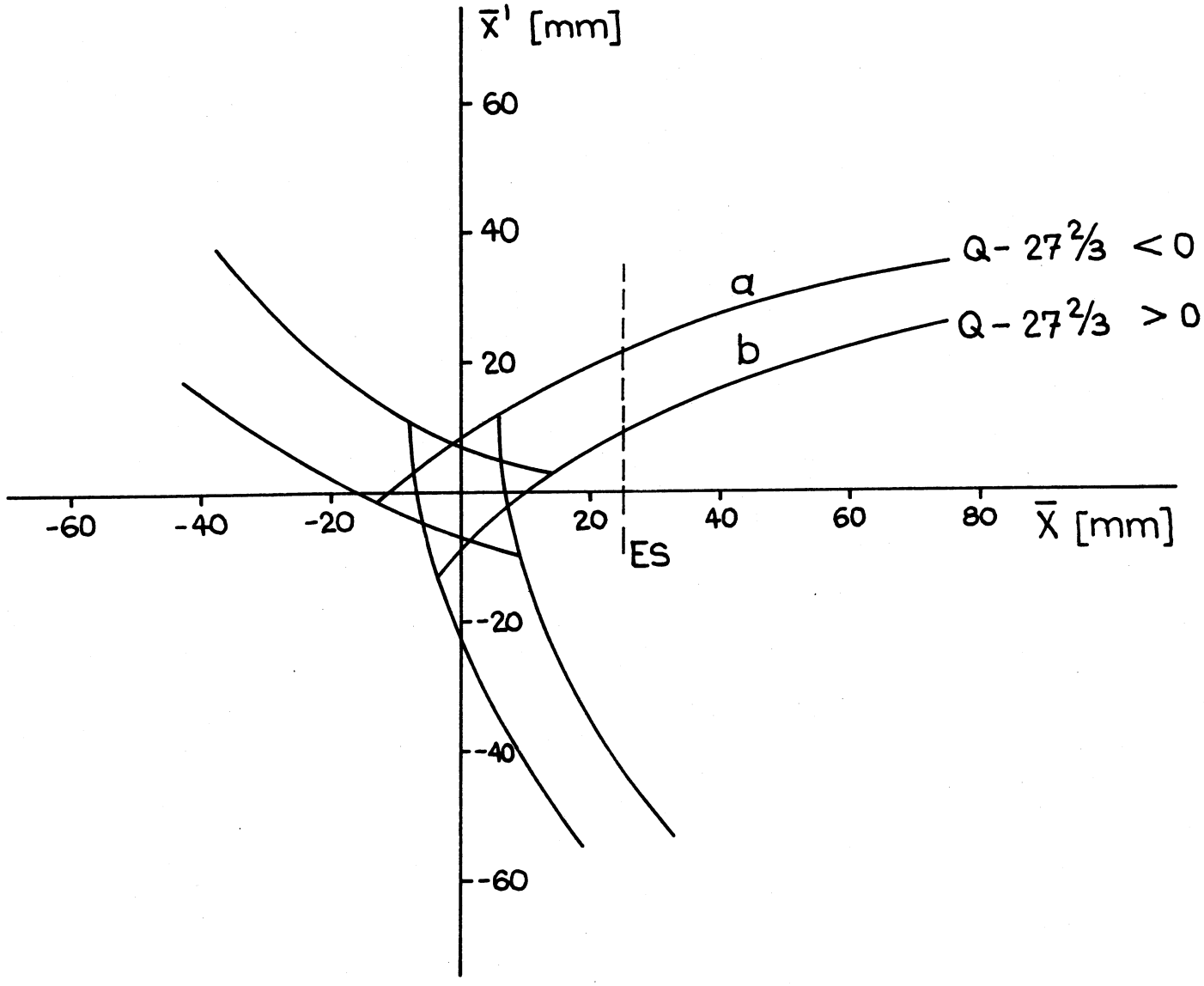

Separatrices at the entrance of ES when approaching the third-integer resonance from below (a) or from above (b).

Fig. 12.5

The resonance was excited by sextupoles S_1 and S_2 as described in Chapter 12.6.2, and the density $\rho(x)$ of spilt particles at the upstream end of ES was calculated as a function of the horizontal position. For a given maximum permissible betatron amplitude $\bar{r}$, the corresponding radial position of ES was calculated and the density $\rho(x)$ at this specific position was looked up. By varying the normalized strength $\bar{K}_s$ of the sextupoles the curves of Fig. 12.6 were obtained. They give the particle density as a function of the sextupole strength for different values of $\bar{r}$ and for different circulating beam emittances. For small emittances, $\rho(ES)$ can be decreased by increasing the sextupole strength. For larger emittances the curves go through a minimum. For an emittance $E_H = 0.7\pi$ mm × mrad, which corresponds to extraction at 200 GeV, this minimum occurs at $\bar{K}_s \approx 0.016$ mm^{-1} rather independent of $\bar{r}$. However, in order to save on sextupole strength one will in general tend to work with a somewhat lower value of $\bar{K}_s$. Figure 12.7 shows how $\rho(ES)$ depends on $\bar{r}$ for $\bar{K}_s = 0.012$ mm^{-1}.

The maximum permissible betatron amplitude $\bar{r}$ is calculated by subtracting from the nominal machine aperture the amplitude of the closed orbit distortion plus a distance corresponding to the momentum bite of the extracted beam : $\bar{r} = 62.5 - 10.0 - 2.5 = 50$ mm. The resulting particle density at ES is about 9 % per mm. Taking an effective geometrical septum thickness of .15 mm and considering the finite divergence of the spilt beam one calculates a loss of about 1.5 % on the septum.

To these 1.5% theoretical losses we have to add losses due to imperfect tuning of the machine in operation and losses occurring during setting-up sessions. Using the experience available at the CPS it seems reasonable to foresee that the operational efficiency will not be higher than 97% (3% losses) and that setting up losses might increase this average figure to 4 or 5% overall losses.

It is expected that the losses can be decreased by placing scattering wires in front of the ES. Insufficient work has been done to predict how much improvement can be reached in this way.

12.8 Magnetic tolerances for slow extraction

There is a large number of field errors, both systematic and random,which can perturb the resonant process. In general the effect of these field errors is up to an order of magnitude worse for the SPS than for the CPS, because of its larger circumference and Q-value. In Table 12.4 we have summarized tolerances for those field distortions which seem to be most important.

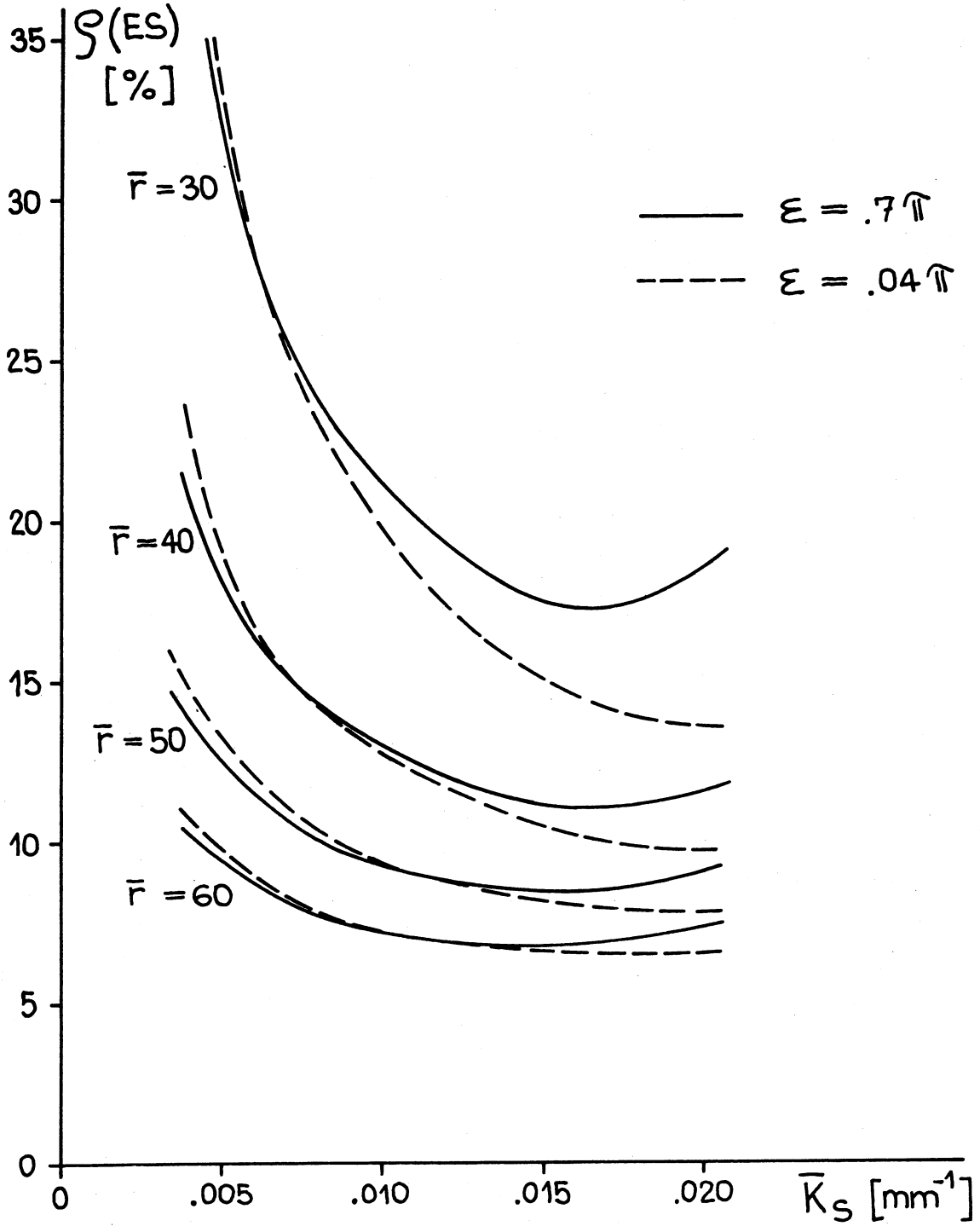

ρ(ES) as a function of $\bar{K}_s$ for different values of $\bar{r}$ and ε.

ρ(ES) = particle density at ES in % per mm

$\bar{K}_s$ = normalized strength per sextupole in mm^{-1}

$\bar{r}$ = maximum permissible betatron amplitude in mm

ε = circulating beam emittance in mm mrad

Fig. 12.6

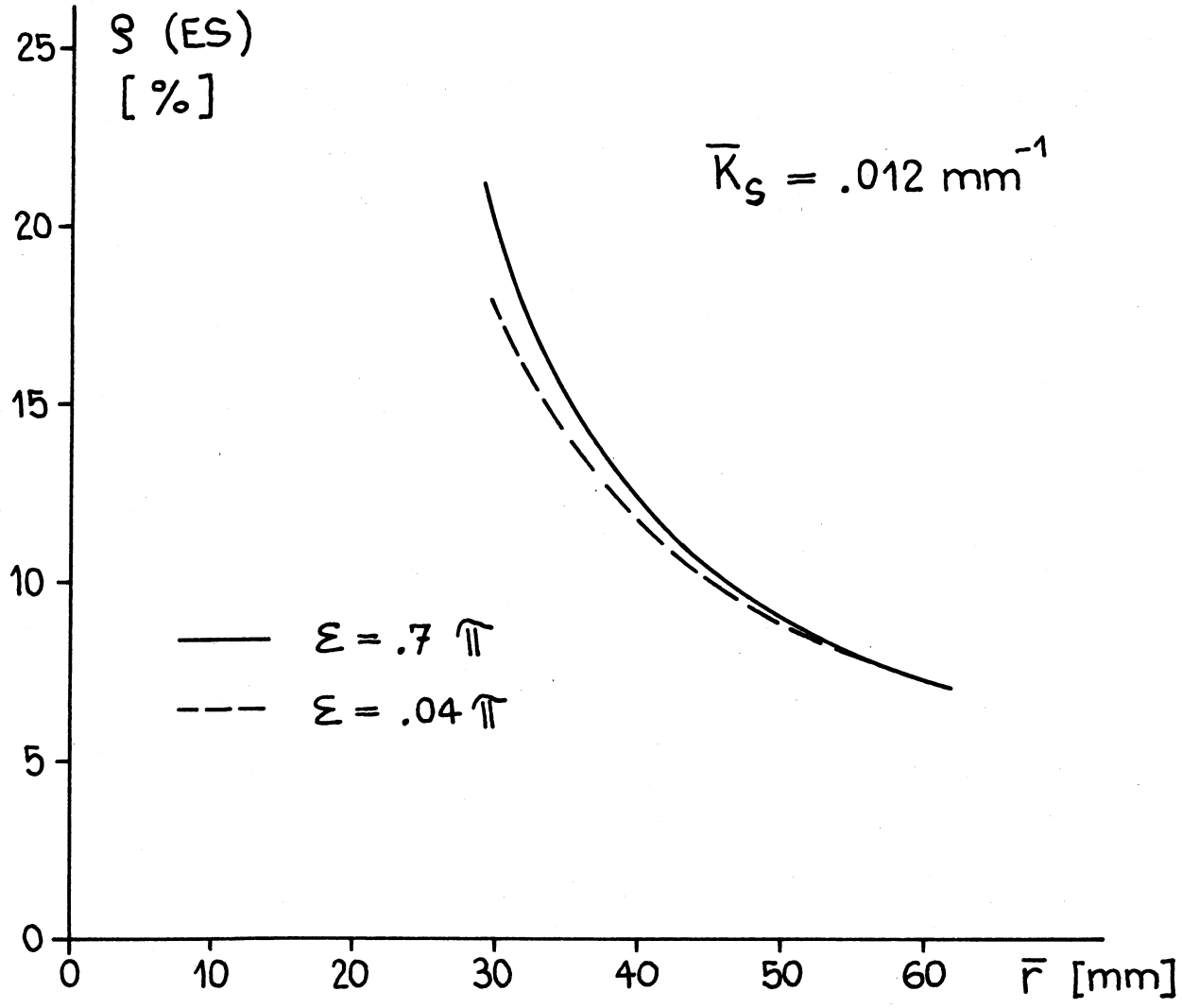

$\rho(ES)$ as a function of $\bar{r}$ for $\bar{K}_s = .012\ mm^{-1}$
and for different values of ε.

Fig. 12.7

Table 12.4

Magnetic tolerances for slow extraction

Type of error	Permissible distortion at the edge of the good field region
Systematic field errors in the main bending magnets (12.4)	
- sextupole component	$\Delta B/B \leq \pm 1 \times 10^{-3}$
- decapole component	$\Delta B/B \leq \pm 3 \times 10^{-4}$
Systematic gradient errors in the machine quadrupoles	
- duodecapole component	$\Delta G/G \leq \pm 2 \times 10^{-3}$
- higher poles such that	$\left[\Delta G/G\right]_{\text{total}} \leq \pm 3 \times 10^{-3}$

12.9 Power supply tolerances for slow extraction

To minimize the effect of systematic field distortions discussed in section 12.8, it is necessary to adjust the field of the bending magnets during the spillout in such a way that the closed orbit of each particle is close to the central orbit when it becomes unstable. Therefore the bending magnet current should track the quadrupole field with a precision of one part in 10^4.

The main problems for the power supply, however, are not so much related to the tracking but concern the permissible ripple as discussed in the following section.

12.9.1 Ripple tolerances

The extraction process can be described in a first approximation by neglecting the effect of the betatron oscillations and assuming that successive momenta are gradually pushed into the resonance by the slow variation of a suitable parameter. For a constant extracted beam current and a total spill time T momentum spread must be scanned with a variable speed, which has a minimum value

$$\frac{\dot{p}}{p} = \frac{s}{T} \frac{\Delta p}{p}$$

where s is the ratio of average to maximum particle density in the momentum distribution and $\Delta p/p$ the momentum spread of the beam.

Ripple on magnetic fields modulates the scanning speed and therefore the extracted beam current. Ripple tolerances for 100 % modulation are summarized in Table 12.5 assuming a $\frac{\dot{p}}{p}$ of 1.5×10^{-4} sec which corresponds to s = 0.5, T = 2 sec, $\frac{\Delta p}{p} = 6 \times 10^{-4}$.

Table 12.5

Ripple tolerances for slow extractions

Extraction	Parameter	Time derivative for 100% modulation
integer	Position of c.o. at the extraction quadrupole	$\dot{e} = 0.33$ mm sec^{-1}
	Zeroth harmonic of the current distribution in the quadrupoles	$\frac{\dot{I}}{I} = 1.5 \times 10^{-4}$ sec^{-1}
	Current in the extraction quadrupoles	$\frac{\dot{I}_Q}{I_Q} = 0.06$ sec^{-1}
	Current in the extraction sextupoles	$\frac{\dot{I}_s}{I_s} = 0.07$ sec^{-1}
third-integer	Antisymmetrical position error in the sextupoles	$\Delta\dot{x} = 3.8$ mm sec^{-1}
	Zeroth harmonic of the current distribution in the quadrupoles	$\frac{\dot{I}}{I} = 1.5 \times 10^{-4}$ sec^{-1}
	Current in the extraction sextupoles	$\frac{\dot{I}_s}{I_s} = 1.2$ sec^{-1}

12.9.2 Extraction with r.f. on

We shall now disregard the reservations made in 12.5 and assume that extraction with r.f. on is feasible. In that case the beam control loops will try to hold the beam at a well defined radial position. The result is, that any bending field ripple of a frequency equal or lower than the synchrotron frequency (about 200 Hz) will induce an energy modulation of the beam and is therefore equivalent to a quadrupole ripple.

In this frequency range the zeroth harmonic ripple on bending magnets and quadrupoles and ripple on the circulating beam energy are coupled and have the same tolerance

$$\frac{\dot{E}}{E} = \frac{\dot{B}}{B} = \frac{\dot{K}_Q}{K_Q} = \frac{1}{t} = 1.5 \times 10^{-4}$$

If the magnetic fields had no ripple, there could still occur a modulation of the r.f. frequency, for instance caused by 50 Hz pick-up in the electronics. The corresponding change in proton momentum is magnified by a factor R/α_p. The tolerance on the frequency modulation of the r.f. system, for a 100% modulation of the extracted beam then becomes

$$\frac{\dot{f}}{f} = \frac{\alpha_p}{R} \times \frac{1}{t} = 2 \times 10^{-3} \times \frac{1}{t} = 3 \times 10^{-7}\ s^{-1}$$

12.9.3 Servo control

In principle, one can make a feedback loop by measuring the instantaneous extracted current and using this signal to act on a suitable machine parameter to reduce the intensity modulation of the extracted beam.

The main limitation of such systems lies in the fact that after a particle has become unstable, it still makes a fairly large number of revolutions before it is extracted. This effect introduces a constant delay in the feedback loop and severely limits its frequency range.

12.9.4 Concluding remarks about ripple

We consider that magnet ripple is a major problem in resonant extraction. We are therefore studying methods of reducing the power supply ripple, modifications of the slow extraction system which make it less sensitive to ripple and more sophisticated servo loops with less time delay.

12.10 Fast extraction by beam shaving

Fast extraction in existing accelerators has up to now been done with a fast kicker magnet whose rise time is a small fraction of the revolution time or fits in the gap in between bunches. The latter arrangement is obviously impossible with a 200 MHz r.f. system. Even if a rise time of a few tenths of a microsecond is accepted, the resulting fast kicker for a 400 GeV machine is an expensive device.

It seems preferable therefore to use the so-called beam-shaving system. In this case a fast closed orbit deformation is made with two identical full aperture fast bumper magnets respectively 1/4 λ before and 3/4 λ after ES. The beam shaving kickers will be placed downstream of QF 6141 and upstream of QF 6221 respectively.

The rise and fall times are of the order of a few microseconds. The fraction of the circulating beam which is extracted is a function of the amplitude and pulse length in the fast bumpers. The beam loss on the ES is of the order of the septum thickness divided by the beam width and this corresponds again to a few %. The advantages of beam shaving extraction are

(i) The fast kicker magnets are simplified due to the larger rise time.

(ii) If only a few % of the beam must be fast extracted this can nevertheless be done during a full revolution, whereas fast extraction with one single fast kicker would make a short azimuthal hole in the beam. Such a hole would strongly modulate the intensity of a subsequent slowly extracted beam and could also cause longitudinal instabilities of the remaining circulating beam.

It is clear that in order to take full advantage of the beam shaving system the rise time of the fast kickers should be made as long as possible. However, the maximum permissible fast kicker risetime is limited by the pulse length of the r.f. separator which will be used to make a high energy separated beam of π's or K's or antiprotons in the West Hall.

12.11 Beam Dumping

During the setting-up of extraction, the external beam will be dumped onto an absorber block which will be installed at the beginning of the beam transfer line. One could also imagine using this system during some of the machine development runs, but this procedure is only feasible if the beam position is sufficiently stable and the beam size is not too large. In all other cases, an internal beam dumping system is required to dispose of the accelerated beam in a controlled way.

The kinetic energy of a beam of 10^{13} protons at 400 GeV/c amounts to 640 kJ. The repeated loss of beam pulses at the same point of the main ring therefore means a continuous local dissipation of about 100 kW. Severe thermal damage of main ring equipment would result if no internal beam dumping system would be available to prevent such an uncontrolled beam loss.

The other reason for an internal beam dumping system is, of course, the need to reduce as much as possible both the radiation damage of machine components and the induced radioactivity which results from uncontrolled beam loss.

The internal beam dumping system will consist of a pulsed magnet system which deflects the beam vertically onto an absorber block. The latter will be made of steel and will have a diameter of 1 m and a length of 4 m, with a rectangular hole in its centre for the circulating beam. The length is determined by the required stopping power for 400 GeV/c protons and the diameter by the required self-shielding against the induced radioactivity in the centre. Thermal shock and cooling problems will have to be studied carefully when designing the absorber block. In order to stop secondaries which are scattered through the aperture in the dump block a second, much simpler, absorber block will be placed half a period downstream of the dump.

The dumping magnets can be either a system of fast bumpers which create a fast rising vertical closed orbit bump or a straightforward fast kicker. A detailed comparison of price and performance, including the dumping efficiency, has still to be carried out before making a choice between the two schemes.

12.12 Extraction Losses and Scrapers

12.12.1 Absorption and Coulomb scattering of protons in septa and scattering targets

The interaction of primary protons with the extraction elements is inevitable. The most important of these elements are: the electrostatic septum, which is used for slow and fast extraction, subsequent magnetic septa, if the orbits are not properly adjusted, and scattering targets for slow ejection or scrapers for halo removal.

The fraction of primary protons interacting inelastically in these devices and the fraction scattered out can be calculated with Monte Carlo techniques [12.5], taking into account for a variety of situations the phase space distribution of the circulating beam and the geometry of the interacting elements, including reasonable misalignments of the elements.

Less than 20% of the protons intercepted by a wire septum are absorbed. In a corresponding foil system, absorption amounts to more than 60%.

12.12.2 The beam loss distributed in the main ring

There are two contributions to the loss distribution in the main ring,

(i) secondary particles created by protons interacting in extraction elements

(ii) a large fraction of Coulomb scattered protons.

The two types of loss distribution can be calculated with the Monte Carlo method and agree with loss distributions measured at the CPS.

Secondary particles from interactions in ES will hit the vacuum chamber usually in the first 25 m downstream of ES. Some of the scattered protons could be absorbed in a scraper which is placed very close to the beam edge. Suitable scraper positions are $(0.4 + k)\ \lambda$ after the ES, with $k = 0; 1$ etc. The position of $k = 0$ is not possible since it interferes with the extraction channel and the position $k = 1$ is already 360 m downstream of ES where about one third of the protons scattered in the ES are left over. A scattered proton which has travelled 360 m downstream of the ES has a good chance of remaining much longer inside the machine aperture. Consequently, if scrapers to remove this halo are considered desirable they can probably be placed at any convenient position around the machine and might be combined with the halo scraper discussed below.

12.12.3 Halo scraper

Halo trimming may be necessary before extraction. This is best done in the region of the dump to localize the radiation problem. Halo protons are Coulomb scattered in horizontal and vertical scattering targets located at suitable positions upstream of the dump. If the beam is held close to the edge of the dump with slowly pulsed dipoles, most of the scattered protons will be absorbed by the dump.

References

Reference 12.1 represents a more elaborate version of the above Chapter.

A large number of references concerning the work of the extraction study group can be found in the report CERN Int/MPS/DL-70-11, and in the White Book MC/60. We have benefitted from most of these publications. The publications to which we specifically refer in the test are mentioned below :

(12.1) Y. Baconnier, K.H. Kissler, A. Knezovic, W.C. Middelkoop and B. de Raad, The Extraction from the 300 GeV machine, CERN-LAB II/BT/71-4.

(12.2) Ch. Steinbach, Slow extraction by target scattering, CERN MPS-CO/70-7, EJ/27.

(12.3) P. Strolin, Resonant extraction from the CERN Intersecting Storage Rings, CERN 69-6.

(12.4) Y. Baconnier, K.H. Kissler and B. de Raad, Effect of field distortions in the 300 GeV main ring bending magnets, CERN-300-BT/71-2.

(12.5) K. Goebel ed., Radiation problems encountered in the design of multi-GeV research facilities, CERN 71-21.

Chapter 13

THE EXPERIMENTAL AREAS

13.1 Introduction

The exploitation of the 300 GeV accelerator will be based on the use of two experimental areas. The first is the West Hall, a facility already existing on the CERN site, which will be the first area to be available for physics experiments. The second is the North Area which will become available for extended experimental use only at the completion of the 8-year construction programme.

The incorporation of the West Hall into the 300 GeV machine programme is based on two factors. The first is the possibility to start experimental physics in the high-energy range at the earliest possible date. The second is the opportunity to profit from the considerable capital investment contained in the West Hall and the possibility to have available for use from the start of the accelerator two sophisticated pieces of experimental equipment, the Omega magnet and spark chamber system and the large hydrogen bubble chamber (BEBC).

In this Chapter details will be presented on a possible utilization of the West Hall as an area fed by 200 GeV protons, starting during the sixth year of the programme. It appears possible, although rather difficult, to consider a limited use of the Hall at an energy higher than 200 GeV. The further complications and the increased shielding problems will have to be carefully balanced against a timely development of the North Area and the best overall solution found. It should be stressed that the beam designs and layout in this report, especially for the Hall itself, are not intended as a definite plan for utilization, but more as an exercise to see where the problems lie and to get some reasonable feeling for a possible exploitation. One will clearly pay close attention to the experience to be obtained at the NAL accelerator before fixing the final layout, which will no doubt differ from that proposed below.

Regarding the use of the North Area, one will have even more time to benefit, particularly from the early operational experience of the NAL accelerator, but also of the West Hall utilization at 200 GeV in making the final decisions on the best layout. Thus only very preliminary ideas, certain basic alternatives and some considerations on the configuration of the ground are presented here.

13.2 Characteristics of the External Proton Beams

A summary of data of interest to users, some of which is discussed already in other Chapters of this report is given here for the sake of completeness. There will be two extracted beam lines, one towards the West and one towards the North Area. Their detailed layout and possible target stations are described in other sections.

Table 13.1

Characteristics of the External Proton Beams

Machine Intensity	Stage A 10^{13}	Stage B 10^{13}	Stage C 10^{13}	ppp
Typical cycle time				
0.7 s flat top	3.4	4.1	4.8	s
25% duty cycle	6.6	7.3	8.0	s
Fast extraction				
Extraction efficiency	∿ 98	∿ 98	∿ 98	%
Intensity range*	1-100	1-100	1-100	%
Pulse duration				
for 1% beam	∿ 5	∿ 5	∿ 5	μs
for 100% beam	∿ 40	∿ 40	∿ 40	μs
$\frac{\Delta p}{p}$ (minimum)	± 0.5	± 0.4	± 0.3	°/oo
Horizontal emittance**	0.7	0.5	0.4	π μrad×m
Vertical emittance**	0.35	0.25	0.2	π μrad×m
Minimum time separation between successive extractions	0.35	0.5	0.7	s
Slow extraction				
Extraction efficiency	∿ 97	∿ 97	∿ 97	%
Intensity range	5-100	5-100	5-100	%
Maximum pulse duration***	∿ 2	∿ 2	∿ 2	s
Approximate $\frac{\Delta p}{p}$ (total)	± 2	± 2	± 2	°/oo
Horizontal emittance**	$\leq$ 0.4	$\leq$ 0.3	$\leq$ 0.3	π μrad×m
Vertical emittance**	$\leq$ 0.4	$\leq$ 0.3	$\leq$ 0.2	π μrad×m

* Sharing unequal amounts of beam between slow and fast extraction is more stable if the extraction operation which removes the smallest number of protons is performed first.

** The values listed correspond to the maximum energies at stages A, B and C.

*** The effective pulse duration may be reduced by magnet ripple.

13.3 West Area

13.3.1 Existing experimental facilities

The West Experimental Area will contain two major items of experimental equipment which will have already been in use during the period 1972-1975, using the 25 GeV/c proton beams available from the CPS. These are the large European bubble chamber (BEBC) and the Omega magnet and spark chamber system which can be thought of as an electronic equivalent of a large bubble chamber. In addition, the West Hall will contain the beam transport, shielding, water and power necessary to operate the West Hall at the 25 GeV/c level for these two instruments. Thus the task of the Laboratory II construction team is basically the provision of high energy protons to the entrance of the West Hall. The equipping of the latter with secondary beams and experimental facilities is rather more a transformation from the 25 GeV level up to the 200 GeV level, and will be carried out by Laboratory I.

13.3.2 Beam layout

A possible layout of beams in the West Area to cover a wide range of secondary particles and momenta and making full use of BEBC, Omega and the available length of the area is shown in Fig. 13.1. The slow ejected proton beam (EPB) enters the complex via the Transfer Tunnel TT4 and makes an angle of 60 mrad with respect to the north wall. The beam is shared between three target stations in the hall, namely T_1, T_2 and T_3, by means of a beam split which enables the three targets to be fed with independently variable fractions of the incident protons. Details of possible beams which could be constructed from these targets are given in Section 13.3.7.

In addition, Fig. 13.1 shows the last half of the trajectory of the long r.f. separated beam which can provide separated beams of hadrons for the bubble chamber (BEBC) located at the end of the West Area. This beam originates in a special target located in the transfer tunnel between the accelerator and the West Area, thus allowing a long distance between the r.f. cavities which is needed for separation at high energies. From the target to the West Area, this beam is transported by bending magnets and quadrupoles positioned inside the transfer tunnel alongside the EPB. The vertical bend needed to follow the inclined tunnel is also used for the momentum analysis of the desired particles. This beam is discussed in detail in Section 13.3.5.

The beam line for the r.f. separated beam can also be used to transport protons to a possible neutrino target located inside the West Area, if it is desired to construct a medium energy neutrino facility which could be optimized to the possibilities of BEBC. In this way the slow ejected proton beam for counter physics and the fast ejected proton beam needed for a bubble chamber neutrino experiment can be kept physically separated. This not only facilitates installation, but leaves open the possibility to operate both beams simultaneously. This possibility for a medium energy neutrino beam is compared with an underground beam in Section 13.3.4.

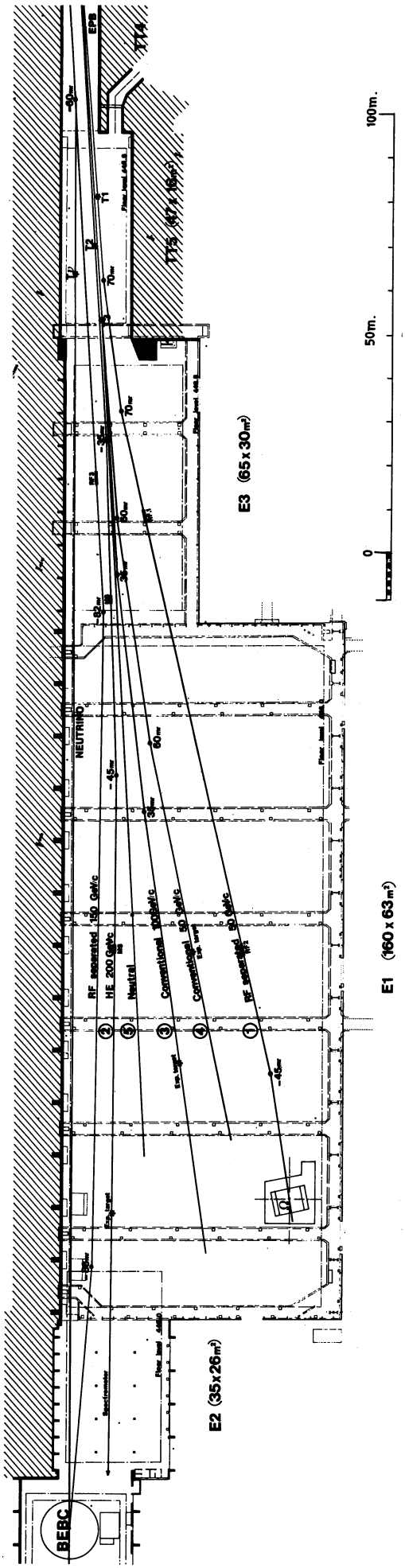

Fig. 13.1 Preliminary layout of beams in the West Hall

The principal changes in the proposed beam layout compared with the ideas presented in the Design Report MC/60 are :

(i) A beam transport from the accelerator to the West Area, which follows almost a straight line (in the horizontal plane), thus reducing the total amount of bending required.

(ii) A longer r.f. separated beam for BEBC which will enable particle separation to be achieved to higher energies.

(iii) The emphasis on independent targets for some of the secondary beams for counter physics in order to improve the efficiency of the beams, and simplify the magnet systems close to the targets.

(iv) The location of the three targets T_1, T_2, T_3 within the shielded tunnel TT5 in order to reduce shielding costs.

(v) The option of using an inclined EPB before the targets to reduce the cost of the back stop by directing the muons into the ground.

13.3.3 Beam transport to West Hall and underground beam switch

The layout of the transfer line between the main ring and the West Experimental Area is determined mainly by :

(i) The position and orientation of the main ring.

(ii) The junction of the transfer tunnel with the existing buildings.

(iii) The underground targets for a long r.f. separated beam and a possible neutrino beam.

The orientation of the main ring was defined by positioning the EPB line to the North Experimental Area approximately in the middle of the available strip of land, while the centre was prescribed within rather narrow limits by the geological and geographical features of the site. Entering the West Hall at an angle to its axis allows a better layout for secondary beams and reduces the total horizontal deflection in the transfer line. An upper limit to the angle of entrance is given by the shielding requirements for the public road (RN 84 see Section 13.3.9). The larger the angle is, the closer the beam will pass under that road. The angle chosen is 60 mrad.

The r.f. separated beam has also influenced the layout since it is not convenient to have any horizontal deflection between its target and the last cavity in the West Hall.

The layout of the transfer line in the horizontal and vertical planes is given in Fig. 13.2. The beam is extracted horizontally. Immediately after the transfer tunnel has branched off from the main tunnel the beam is deflected vertically (φ_1) to have the correct slope for aiming at BEBC. After a subsequent horizontal deflection (α_1), a switch follows to deflect the fast EPB to the target for the r.f. separated beam. Fig. 13.3 shows in more

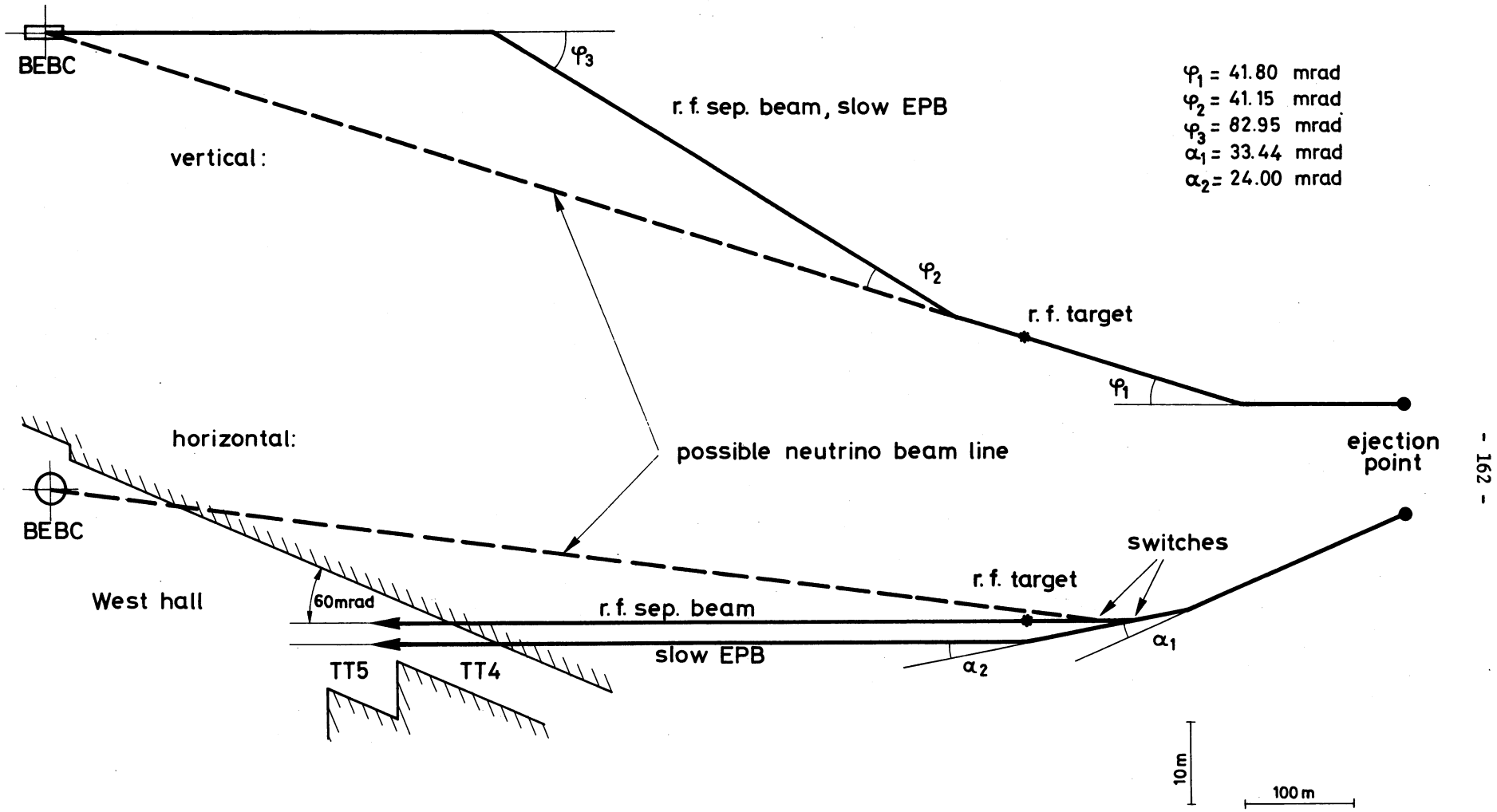

Fig. 13.2 Geometry of the transfer line to the West Area

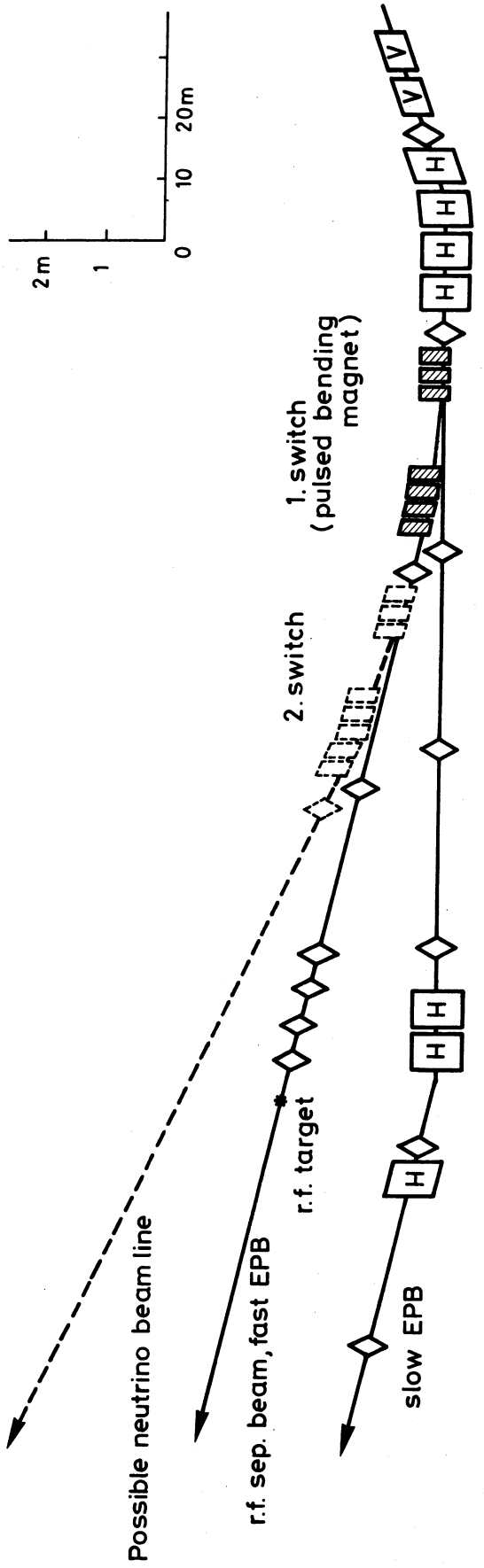

Fig. 13.3 Layout of the underground switch for the West Area

detail the layout of the underground switch, including a second branch of the fast EPB for a neutrino target. The other horizontal and vertical deflections shown in Fig. 13.2 are required to bring the beams to the chosen entry position in the West Hall.

The lattice of the main EPB line is very similar to that of the main ring. An external beam dump could be installed immediately before the first vertical bend, thus leaving enough length for the emittance measurements further upstream.

The maximum beam energy in the first common part of the transfer line and for the switches can be 400 GeV. This part of the line will be pulsed to follow the magnetic field of the main ring, so that protons of different momenta can be sent to counter and neutrino targets during the same machine cycle. The slow EPB line downstream the switch and the fast EPB up to the r.f. target can be designed for 300 GeV as maximum energy. At stage A of the programme some of the magnets could be omitted. The r.f. separated beam line, if used for the fast EPB, is for maximum proton energies of 150 GeV.

The bending magnets will have the same cores as the main ring B2 magnets, with (possibly) a different coil to reduce the current required.

The pulsed bending magnets required by the switches will be powered by a capacitor discharge, with a half sine wave of about 20 ms.

13.3.4 Neutrino beams

Neutrino experiments may well be among the most interesting experiments to be performed at the 300 GeV accelerator at CERN. Neutrino beams from the present CERN accelerator yield a spectrum where the flux of neutrinos is greatest in the region of 1 GeV. Because of the weak interaction of the neutrino and the consequent difficulties of its detection, the properties of the neutrino interaction in the region of energies greater than about 2 GeV are still largely unexplored. This region will be opened up by the new accelerator.

Neutrino beams used so far have all been of the so-called "wide-band" variety. In this type of beam, the π and K mesons of a given charge produced in a target are focused into a parallel beam by an achromatic focusing device called a neutrino horn. After a suitable driftspace to allow some of the π and K mesons to decay, a muon shield is required which stops the muons from entering the detector.

At the high energies available at the new accelerator, the thickness of this muon shield becomes large, making it costly and bulky. In the West Area building complex, the space limitation is such that the maximum energy of protons which one could use for a wide-band neutrino beam is in the range 100-150 GeV, depending on the detailed design of the beam. A high density material, such as steel, is needed for the muon shield.

An indication of how such a facility might be incorporated into the West Area beam complex is shown in Fig. 13.1. A fast ejected proton beam of momentum < 150 GeV/c is transported into the West Area by the r.f. beam transport system. Once inside the area, the protons are deflected by a suitable magnet so that they travel parallel to the north wall of the hall E_1 and are pointing at the bubble chamber (BEBC). These protons are then focused onto the target shown. For simplicity's sake the decay path and the final shield are not shown in the figure.

Another alternative neutrino beam could be constructed using a target and decay tunnel located underground between the accelerator and the West Area. The beam transport to the West Area has been designed so that, with some additional elements, the underground beam switch can be used to deflect some of the ejected proton beam into a tunnel which would branch off from the main beam transfer tunnel at the end of the beam switch section. These protons would then be pointing towards BEBC. The proposed underground tunnel would house the neutrino target and focusing system and serve as the decay region.

The main advantage of this solution would be to use the natural rock and earth between the end of the decay tunnel ($\sim$ 400 m length) and BEBC to stop 200 GeV muons. However the corresponding saving would be counterbalanced, at least partially, by the cost of the civil engineering for the underground facility (enlarged EPB tunnel section, decay tunnel and access pit). A much more detailed analysis is needed to assess this cost in a reliable way. Another claimed advantage is that such an underground neutrino facility could be operated later on at 400 GeV if part of the molasse at the end of the decay tunnel is replaced by steel. Apart from the practical difficulty and the additional civil engineering cost of such an operation, this implies the extension of the ejection system in LSS6 to 400 GeV only for the neutrino experiment. Obviously a detailed comparison should be made with a neutrino beam in the North Area, where longer distances are available.

Further possibilities are offered by considering the so-called "dichromatic" neutrino beams which are produced by focusing and selecting only a narrow momentum band of π or K mesons which are then allowed to decay. The neutrino spectrum thus obtained contains two peaks corresponding to the K- and π-decay neutrinos. By suitable design, it will be possible with such a beam to determine the energy of the neutrino which has interacted. Intermediate possibilities also exist which can be accommodated in either the underground solution or the solution in which the neutrino target is inside the West Area.

The many options for the first phase of neutrino physics with the new accelerator have not yet been fully evaluated and so no definite choice can yet be made.

13.3.5 r.f. separated beam for BEBC

It is proposed to build an r.f. separated beam (Fig. 13.2), using a target located in the EPB tunnel at the maximum possible distance from BEBC (904 metres). It will have a

maximum unseparated momentum of 150 GeV/c.

The vertical bend φ2 will be used to give momentum definition of the beam with a minimum $\Delta p/p$ of ± 0.2%. Mass separation is obtained in the horizontal plane by the use of three r.f. cavities, spaced by 192 and 312 m.

The maximum intercavity distance of 504 metres will permit the separation of $K^{\pm}$ to about 51 GeV/c (S-band) or 73 GeV/c (C-band) with complete rejection of π and p, and the separation of K^{-} to about 75 GeV/c (S-band) or about 100 GeV/c (C-band) with rejection of π^{-} only.

This large intercavity distance implies the necessity of mounting the first two cavities in the EPB tunnel with their associated controls and power supplies. As past experience has shown the cavities to be very reliable, it is not expected that lack of easy access will raise any major problem, however floor space in the form of alcoves in the EPB tunnel should be provided for the power supplies and the removal of the cavities from the beam line.

The maximum flux of primary protons to be used onto the r.f. target is expected to be a few 10^{10} ppp.

It has been suggested that the r.f. beam should be used to provide the primary proton transport for any neutrino facility installed in the West Area. The design of the beam is compatible with this use and could allow a neutrino target to be placed in the TT 5 area as shown in Fig. 13.1.

13.3.6 Beam split and target stations in the West Hall

It is suggested to use three target stations in parallel to feed secondary beams for counter experiments. One is for the Ω-facility (T_1), one for "conventional" and neutral beams (T_3) and one for a high energy high momentum resolution beam (T_2). The system can be built up in stages, - e.g. in the beginning only two targets and later on three.

A possible splitter and target focusing scheme has been studied. The length is restricted to about 80 m, which corresponds to the distance of the last vertical bending magnet of the transfer line to the middle of tunnel TT5. Targets much further downstream should be avoided for reasons of shielding and length for the secondary beams. The scheme has been studied for a maximum proton energy of 200 GeV.

It would seem that the best way to fit a three-way splitter into the available length would be to use horizontally deflecting steel septum magnets, with the beam strongly blown up to reduce losses.

Fig. 13.4 shows a module of a first splitter magnet which bends the central part of the beam horizontally, while the outer parts are not deflected. In a subsequent second splitter magnet, a module of which is also shown in Fig. 13.4, one of the two outer parts of the beam is also deflected horizontally. The beam losses occur mainly at the septum of the first splitter. Losses are estimated to be $\sim$ 1.5% when the beam is perfectly adjusted. The relative intensity of the three parts of the beam can be varied by changing the vertical beam size, by moving the beam centre or by replacing the first splitter by another one with a different gap height.

The addition of an electrostatic septum upstream of the splitter could probably reduce the total amount of losses. But this septum is difficult to install in the narrow rising transfer tunnel T60.

A possible layout of the splitter and target focusing area is shown in Fig. 13.5.

A problem connected with the restricted length results from the necessity of blowing up the beam some distance before the end of the vertical bend of the transfer line. The consequence is that bending occurs for a beam of very large β (the ellipse in phase space is very flat) so that the dispersion has the strongest effect. The strength of the vertical bending magnets must then follow the change of momentum during the spill of the slow extraction.

13.3.7 Secondary beams for electronic experiments

Fig. 13.1 shows a possible layout of secondary beams for electronic experiments. This layout contains two principal beams namely an r.f. separated beam for the Omega Magnetic Spectrometer, and a maximum momentum beam ($p_{max} \leq 200$ GeV/c), both produced at 0^{o} from their own targets (T_1 and T_2) fed by two branches of the EPB. The third branch of the EPB feeds a third target T_3 which is the source of three other beams. All the charged secondary beams remain in the plane of the EPB branches up to their momentum slits. This plane could be inclined to the horizontal by 13.5 mrad in order to reduce the μ back stop. After the momentum slits the beams should be bent back to the horizontal plane (or close to it). As a consequence the levels of the various beams and experiments will be different.

The three targets considered are all in tunnel TT5 which is provided with an external shielding (earth) and is serviced by a crane.

The important parameters of the secondary beams are listed in Table 13.2, and brief description of them is given hereafter.

(i) Beam 1. This beam, designed to supply particles to the Omega Spectrometer, may be provided with two r.f. superconducting cavities to produce enrichment of the requested particles. The intercavity distance is about 100 metres. The beam has

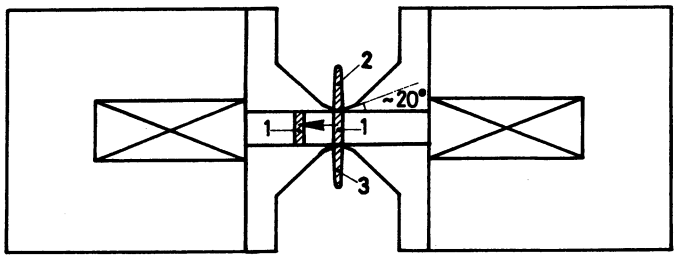

Splitter magnet 1 (scale 1:5)

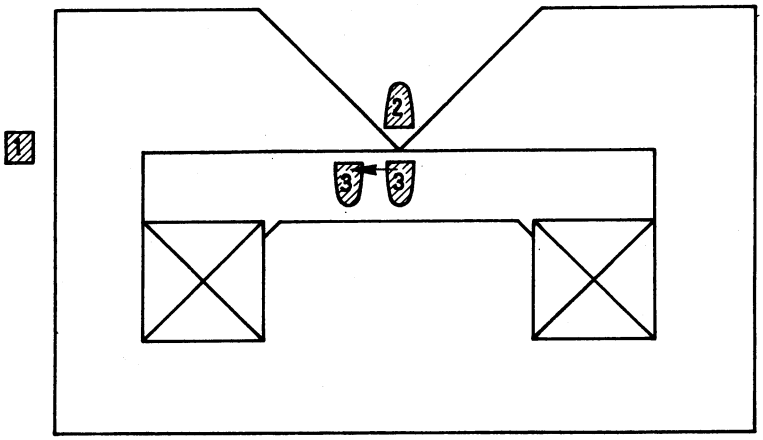

Splitter magnet 2 (scale 1:5)

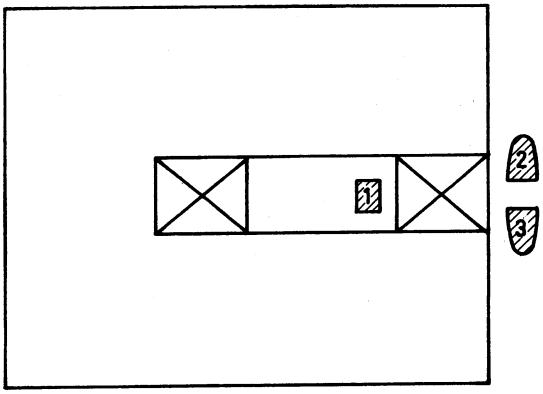

Window frame C-type magnet (scale 1:5)

Fig. 13.4 Magnets for the beam split

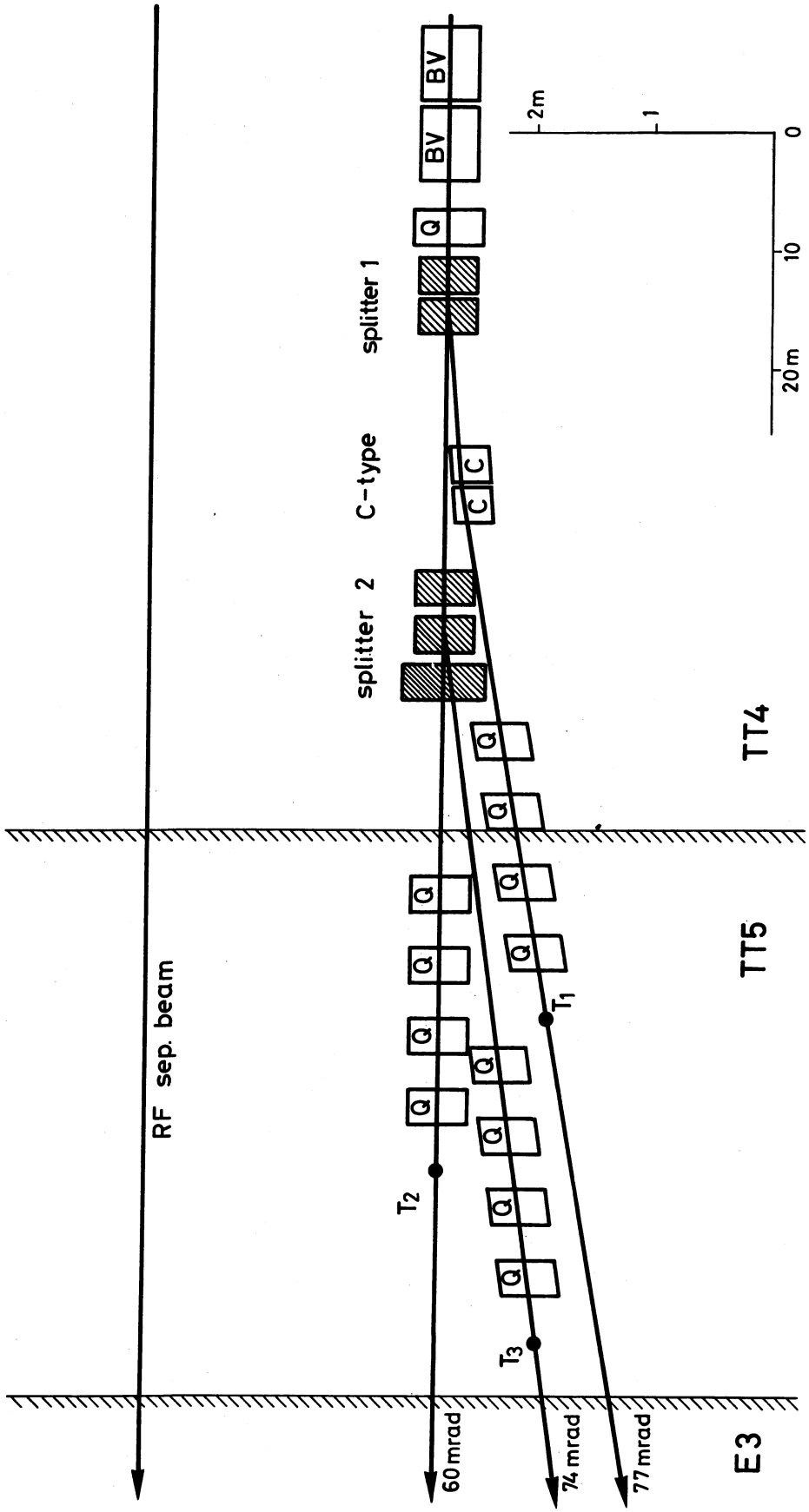

Fig. 13.5 Layout of beam split and target stations in the West Area

the usual structure of this type of beams: momentum selection stage, momentum recombination and matching to the first cavity, matching to the second cavity, and finally stopping of unwanted particles and matching to the experimental target. The frequency will be most probably in the S-band ($\sim$ 3000 MHz) at the beginning of the exploitation and eventually in the C-band ($\sim$ 6000 MHz), with of course smaller aperture cavities, afterwards. Enrichment will be possible, with a realistic field of 4 MV/m, up to about 23 GeV/c for K^+, 28 GeV for K^-, 44 GeV/c for $\bar{p}$ and π^+ with the S-band, and up to about 32 GeV/c for K^+, 36 GeV for K^-, 50 GeV/c for $\bar{p}$ and π^+ with the C-band. The angular acceptance of this beam is 30 μsterad, but it might be increased up to 120 μsterad for energy below 20 GeV. The production angle is 0° for both polarities. This minimizes the apparent target sizes and maximizes the achievable intensity. However this condition is not very stringent and it would be also conceivable to increase the production angle up to 10 - 12 mrad in order to allow for the installation of another beam from the same target.

(ii) Beam 2. This beam produced from T_2 should provide particles up to the maximum available momentum (200 GeV/c). The total length available for the beam and the experiment is $\sim$ 265 m. The beam shown in the figure has three stages: momentum recombination and measurement (with resolution of a pion mass up to the maximum energy), mass determination and matching to the target of the experiment. The first two stages need a length of about 80 m each. The third one needs about 60 m and has a parallel section ($\sim$ 10 m long) for a Disc Cerenkov counter. When operated for positive secondaries at energies above 40 - 50% of the primary energy, it will be necessary to change the production angle from 0° to about 3 - 4 mrad in order to reduce the proton background.

(iii) Beams 3 and 4. These two beams, both generated from target T_3, are conventional two stage beams and are designed for general purposes. Their maximum momentum is 100 GeV/c and 50 GeV/s respectively. Their production angle is about 3 mrad. The experimental space at the end of these beams is very large (70 and 90 m length respectively).

(iv) Beam 5. This is a neutral beam, suitable for instance for K_L^o experiments which might be produced between about 8 and 13.5 mrad angle. If the option of an inclined EPB is retained, the larger production angle would correspond to a horizontal beam line.

(v) Other beams. Many special beams can be considered as modifications or alternatives to the beams listed above. For example, the insertion of an electron separator (e.g. "chicane") in any of the charged beams could provide a clean electron beam.

Another possibility would be to replace beam 5 by a proton beam of moderate intensity, which could be used to produce a K_S^o or a hyperon beam. On the other hand it is important to point out that a high intensity muon beam is difficult to realize in the West Area because of space limitations.

Table 13.2

Parameters of Secondary Beams in the West Area

User	Target	Beam	p_{max} (GeV/c)	Prod. Angle (mrad)	Angle Accept. (μster)	Total length (m)	π^- yield*	K^- yield*
BEBC	T_{rf}	r.f.	150	0	4	904	-	-
BEBC	T_ν	ν (wide-band)	-	0	-	300 (surface sol.)	($10^8\nu/m^2$ at BEBC)	-
OMEGA	T_1	1) r.f.	50	0	30	230	$\sim 10^8$(50 GeV/c)	$\sim 3\times10^6$(50 GeV/c unseparated)
COUNTERS	T_2	2) H.E.	200	0 neg. 5 pos.	8	220	$\sim 1.6\times10^6$(150 GeV/c) $\sim 6\times10^4$(180 GeV/c)	$\sim 2\times10^5$(100 GeV/c) $\sim 8.3\times10^3$(150 GeV/c)
COUNTERS	T_3	3) Conv.	100	-3	3	160	$\sim 10^7$(50 GeV/c) $\sim 4\times10^6$(100 GeV/c)	$\sim 3.6\times10^5$(50 GeV/c) $\sim 5.8\times10^4$(100 GeV/c)
COUNTERS	T_3	4) Conv.	50	+3	4	140	$\sim 0.9\times10^7$(20 GeV/c) $\sim 1.3\times10^7$(50 GeV/c)	$\sim 3.8\times10^5$(20 GeV/c) $\sim 5\times10^5$(50 GeV/c)
COUNTERS	T_3	5) Neutral	-	8-13.5	-	> 100	-	-

13.3.8 Beam elements

While it is uneconomical and very difficult to arrive at a complete standardization of beam elements (e.g. only one type of bending magnet, and one type of quadrupole), it is important to minimize the number of new types of elements to be built and to use in the best way what already exists.

A tentative list of the most common requirements is given in Table 13.2 for classical elements with iron.

Magnetic field and current densities chosen correspond to the minimum of expenditure for investment and running cost over a $3 \cdot 10^4$ hours period. An economical way of producing bending magnets, excluding the target areas, would be to use the same laminated iron core as for the machine magnets with a different coil configuration.

The beam equipment which will become available for the 200 GeV physics when the 25 GeV physics will stop in the West Area, consists of the beam elements transporting the primary protons to the West Hall (tunnels TT2a, TT3, TT4, TT5) and the PS standard equipment for the secondary beams.

---

* Calculated for 10^{12} interacting protons at 200 GeV/c and $\frac{\Delta p}{p}$ = 1% (secondary) according to "Particle Spectra" by Grote-Hagedorn-Ranft CERN 1970

The characteristics of these elements are listed in Table 13.4 and, it is useful to compare them to the requirements of Table 13.3. The ISR type beam elements are rather well suited for use in other areas than the target zones. The PS standard elements are less attractive because of their high power consumption. However, they could be useful for low energy secondary beams (25 GeV/c) and where a large acceptance is needed (e.g. large acceptance spectrometer magnets).

A large number of power supplies, listed in Table 13.5, will also become available. Most of them can be used with the existing beam elements, and it seems a not too difficult problem to match the electrical requirements of the new beam elements to the PS standard rectifiers (R1B or R2B).

No specific studies for an extensive use of superconducting elements have been made yet. Present indications are that they are not yet an economical solution in the general case where no specific constraints exist. However for special applications (need of a short beam, possible improvement of performance, severe longitudinal space limitations) they may be essential.

In any case the evolution of the technique and of the cost is such that an extended study of their possible general application is needed at least for the North Area. The West Area could profit from such a study and it is possible that some pilot installations could be considered for it.

Table 13.3

	Bending Magnets		Quadrupoles	
	Target Areas	Other Areas	Target Areas	Other Areas
Nominal field (T) or gradient (Tm^{-1})	≥ 1.5	≤ 1.5	≤ 20	20
Range of length considered* (m)	2 - 6	2 - 6	1 - 5	1 - 5
Useful gap or diameter (m)	0.05 - 0.07	0.05 - 0.07	0.09 - 0.10	0.09 - 0.10
Type	C	H (C)	Slim	Normal
External dimensions (horizontal) (m)	< 0.30 (between beam axis and coils edge)	No constraints	< 0.30	No constraints
Current density ($A \times mm^{-2}$)	< 6 (if possible)	< 6	> 10	< 6
Minimum radiation resistance (rad)	$10^9 - 10^{10}$	$10^8 - 10^9$	$10^9 - 10^{10}$	$10^8 - 10^9$

* Suitable standard length of elements still to be established.

Table 13.4

Existing Beam Elements

Designation	Type	Gap or diameter (m)	Iron length (m)	Nominal field (T) or gradient (Tm^{-1})	Nominal current (A)	Power consumption at In (kW)	Quantity
HB 1	ISR	0.08	2.50	1.2	1 200	23	39
HB 2	ISR	0.08	2.50	1.2	400	30	14
QDS	ISR	0.091	0.82	20	500	15.5	34
QFS	ISR	0.10	0.80	20	500	16	37
QFL	ISR	0.10	1.20	20	500	25.5	5
M200	PS	0.11 - 0.20	2.00	1.8	830	140	11
Q200	PS	0.20	2.00	10	750	115	29
Q100	PS	0.20	1.00	10	625	80	7

Table 13.5

Existing Power Supplies

Designation	Type	Max current (A)	Max voltage (V)	Quantity
R2B	PS	1 000	230	30
R1B	PS	600	130	15
T1B	PS	250	32	15
D*	PS	1 000	150	10
Filter	PS	1 000	-	5
Series regulator	PS	1 000	-	5
"A great variety of rectifiers in limited numbers (1 to 3 units)"	ISR	165 to 1 550	40 to 510	17 (total)

* D = voltage boost to be used in conjunction with R2B

13.3.9 Radiation problems in the West Experimental Area

The West Experimental Area is situated close to the Route Nationale 84. The radiation field outside CERN must not produce a dose-rate higher than 170 mrem/y (=average dose-rate of ∿30 μrem/h with 6000 h of operation per annum). These low dose-rate levels at the fences determine the shielding requirements in most places of the West Area rather that the limits for unrestricted radiation areas inside the hall (< 2.5 mrem/h).

(i) Target stations in TT5 - transverse shielding. With 10^{12} ppp interacting in each of the three targets, transverse shielding thicknesses required for hadron attenuation around the targets themselves are typically 1900 g/cm^2 and 1500 g/cm^2 along the EPB. These figures are given for earth or concrete and are 25% higher for steel. The amount of hadron shielding needed will not depend much on the final energy chosen. Raising the energy from 200 GeV to 300 GeV requires about 50 g/cm^2 more transverse shielding thickness. Longitudinally the hadron shielding requires a total thickness of 5000 g/cm^2 concrete equivalent. In most practical cases the longitudinal hadron shield will be the first part of the muon stopper.

(ii) Muon shielding. The design of the shielding downstream of the production target must take into account the flux of muons resulting from the decay of pions and kaons between the production target and the beginning of the shielding. In particular, the average muon flux behind the West Area (∿ 500 m from the production targets) must be kept below the value of 1 μ/cm^2 × s, which corresponds to a radiation level of ∿ 0.1 mrem/h.

Considering first the case of a horizontal EPB, it is proposed to use a sufficiently wide steel beam dump (3 - 5 m), the length of which is a nearly linear function of the primary proton energy. For 200 GeV, 75 m are proposed in addition to the longitudinal hadron shield mentioned above. Along the side of this muon dump the dose-rate due to multiple scattered and deflected muons is estimated to be below 10 mrem/h. An external earth shielding of 1500 g/cm^2 around the transfer tunnel TT4, 1300 g/cm^2 at transfer tunnel TT5 and 1300 g/cm^2 on the north side of halls E3 and E1, can be provided.

Doubling the total number of muons produced (e.g. by doubling the average rate of interacting protons), would require increasing the shielding by ∿ 8 m of iron to keep the muon flux to the above-mentioned maximum level.

This solution for the shielding problem may turn out to be unrealistic, because of the very high cost involved for the total amout of iron needed. A different solution has therefore been proposed in which the primary proton beam is bent downwards hitting the targets at an angle of 12 - 14 mrad.The secondary beams are bent up again after the first MS, and therefore most of the muons produced between the target and the hadron stop, will continue downwards and enter the ground in the hall E1. Due to the sloping down of the ground between the West Area and the CERN boundary, 1 - 2 m of earth will have to be added outside E1 and in line with the EPB in order to keep the muons safely underground.

Although more detailed comparisons between this and the parallel solution have not yet been attempted, it looks promising and will perhaps be the only possible arrangement.

Finally, it may turn out to be necessary to use magnetized iron blocks as beam dumps for all the secondary beams exceeding an average intensity of 10^6 part/s, to bend the muons produced in the decay of the beam particles down into the ground.

13.3.10 Tasks of Laboratory II

According to the definition of the 300 GeV Programme (CERN/958/Rev.) and its description (CERN/963), the parts of the above tentative layout to be provided by Lab. II are the primary beam lines between the accelerator and the West Area and their supplies.

In the document MC/60 Volume 1, this is further specified as the primary beam transport system from the ejection system in LSS6 to a target for counter beams (T_1) and to a target for neutrino experiments (T_ν), inclusive of the switch section and of the shielding around the targets themselves.

The beam layout described above is rather different from the one in MC/60 and is a result of intensive discussions among the European physicists, especially during the ECFA Study Week on the 300 GeV Accelerator, held in Tirrenia (Italy) in September.

The implications on cost are still under active evaluation at the moment. It is important to note that the layout presented here, although preliminary, is a fairly complete one and corresponds to a full exploitation of the Area. Which part of it will be finally realized and when will be decided upon in due course.

In addition a final subdivision of expenditure between the two laboratories has also to be agreed upon.

Tentatively, the cost estimate for Laboratory II in Chapter 16 includes:

(i) The civil engineering work (tunnel, underground switch-yard, junction to West Hall in TT3 - TT4).
(ii) The external proton beam.
(iii) The switch to the r.f. target.
(iv) The split section and counter targets in TT5.

It is intended to complete the analysis and reach a final decision in 1972.

13.4 North Experimental Area (300 - 400 GeV/c)

The North Experimental Area (Fig. 13.6) will be designed with the aim of providing beams up to the highest energies available from the new accelerator. The size of its installations will make it prohibitive (from the economical point of view) to adopt the solution of housing in the same large Hall the secondary beam and the experiments at its end, as it is done usually in the present Halls. Almost inevitably, the secondary beams will have to be installed in tunnels and become rather fixed, at least in length and basic layout. The experiments will be housed in experimental zones at the end of the secondary beam tunnels.

These characteristics and the existence of the West Area (to be exploited first), suggest a rather natural subdivision of scope for the two areas. "Low" energy beams and beams to be kept flexible could be concentrated in the West Area, with a primary proton energy normally not exceeding 200 GeV/c. "High" energy and special long beams could be built in the North Area with primary proton energy up to the maximum delivered by the accelerator. In this connection, the possibility of a superconducting machine in the future will be taken into account.

As indicated in the Introduction, only preliminary ideas and certain basic alternatives will be presented at this stage.

13.4.1 Shielding at high energy

As can be clearly seen from Section 13.3.9, shielding becomes a major problem at higher energy, and the economy of using earth shielding is very attractive.

A possible way to achieve this situation is to keep the primary targets in the EPB or its branches below the surface level all the time. In this way the muon problem disappears since these are just stopped in the earth. Because one must derive secondary beams from targets in the EPB or its branches, a level not too deep below the surface should be preferred (about 8 m).

13.4.2 Beam transport and distribution of protons

The design of the system to transport the extracted beam from the accelerator to a point close to the surface should not present any particular problem. It will contain essentially two vertical bending magnet sections (bending angle approximately 100 mrad each), for transferring the beam from the level of the accelerator to a horizontal line close to the surface, the appropriate repetitive arrangement of quadrupoles, and at least one matching section before the target. A beam split section may be present or not depending on the choice of "parallel" or "series" targets (see below). The tunnel will be designed for 400 GeV but beam elements provided according to the maximum machine energy.

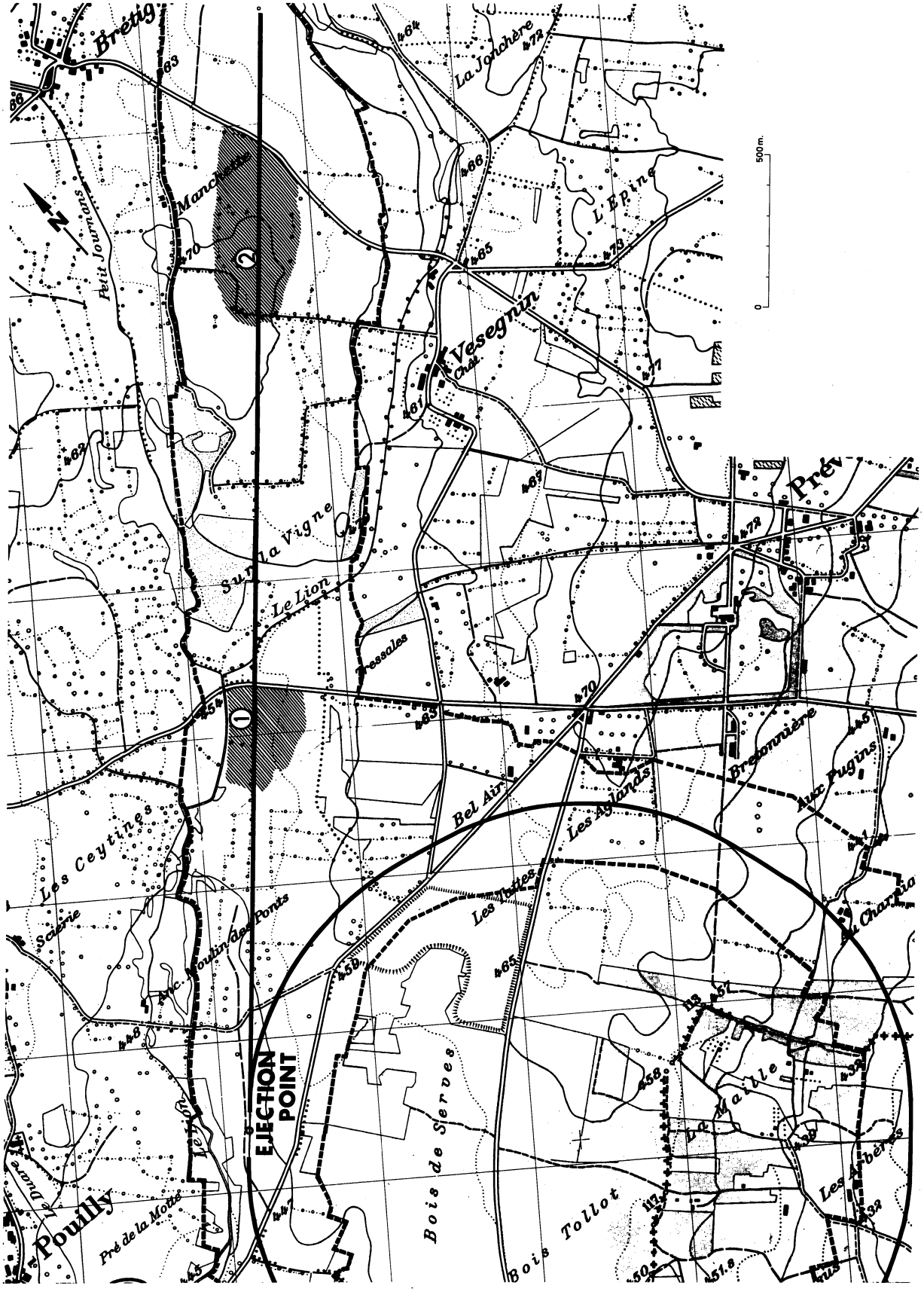

Fig. 13.6 North Experimental Area
1) and 2) possible locations of experimental zones

There are two possibilities of distributing protons to primary targets. The first is to split the EPB into branches, by means of suitable arrangements of septum magnets and let the targets be fed in "parallel". The second is to extend the EPB essentially through the area and let it strike targets in "series" as described in MC/60 (see Fig. 13.7). A well founded choice between these two solutions requires many more detailed studies. For the moment, it is sufficient to point out their relative advantages and disadvantages and the problems to be considered in more detail.

(i) Targets in "parallel"

Advantages:

- Greater freedom for the first part of secondary beams
- Possibility of varying easily the fraction of the total proton current on a particular target
- Less longitudinal space used for target focusing sections
- Reduction of the beam emittance in the plane of splitting.

Disadvantages:

- Additional cost of the splitting section
- Beam losses in splitting section, which may give rise to additional radiation problems.

(ii) Targets in "series"

In addition to the complementary remarks with respect to the above, one can mention:

Advantage:

- Better utilization of protons (since a target is always necessarily rather transparent).

Disadvantages:

- Additional cost of one wobbling section per target
- Increase of the EPB emittance after each target because of multiple scattering.

It is likely that the best arrangement could be a suitable combination of the two solutions, e.g. with a split of the EPB in, say, two branches with "series" targets in each of them.

The EPB line(s) and any primary target should be well below the surface at a depth of at least 8 m. The exact horizontal position of the proton line(s) will have to be chosen after a thorough study of the possibilities and limitations related to the ground configuration (see Section 13.4.4).

Finally, it is very important for such high energies to select production angles as small as possible. Both target solutions mentioned above allow the choice of 0° angles. However, while negative secondary beams can be extracted from the target without limitation

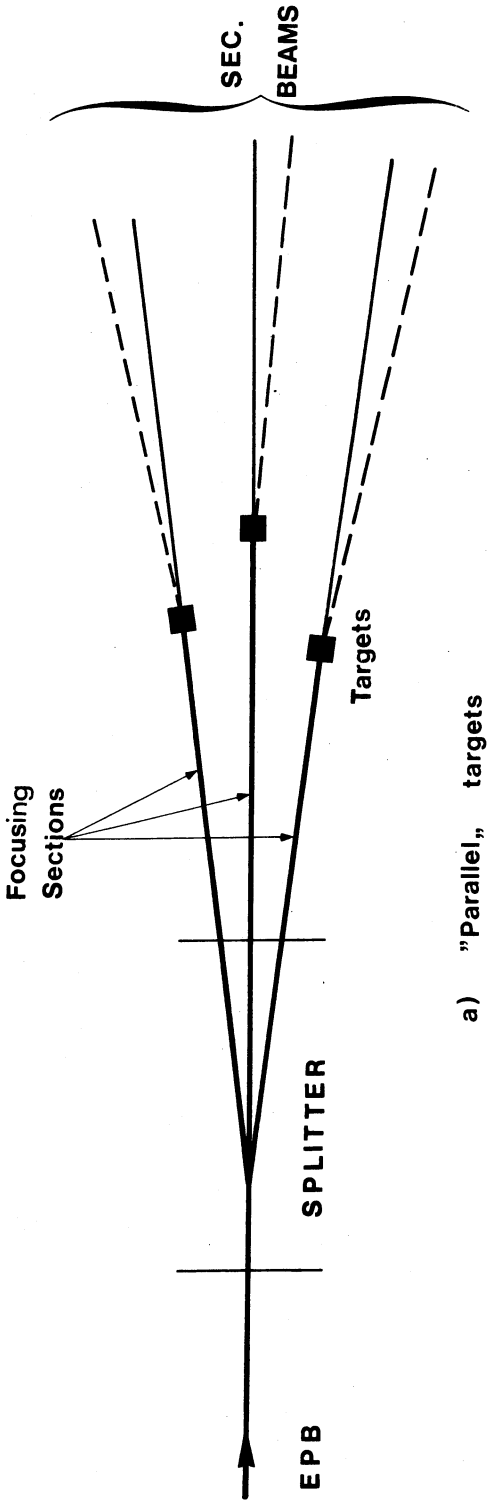

a) "Parallel„ targets

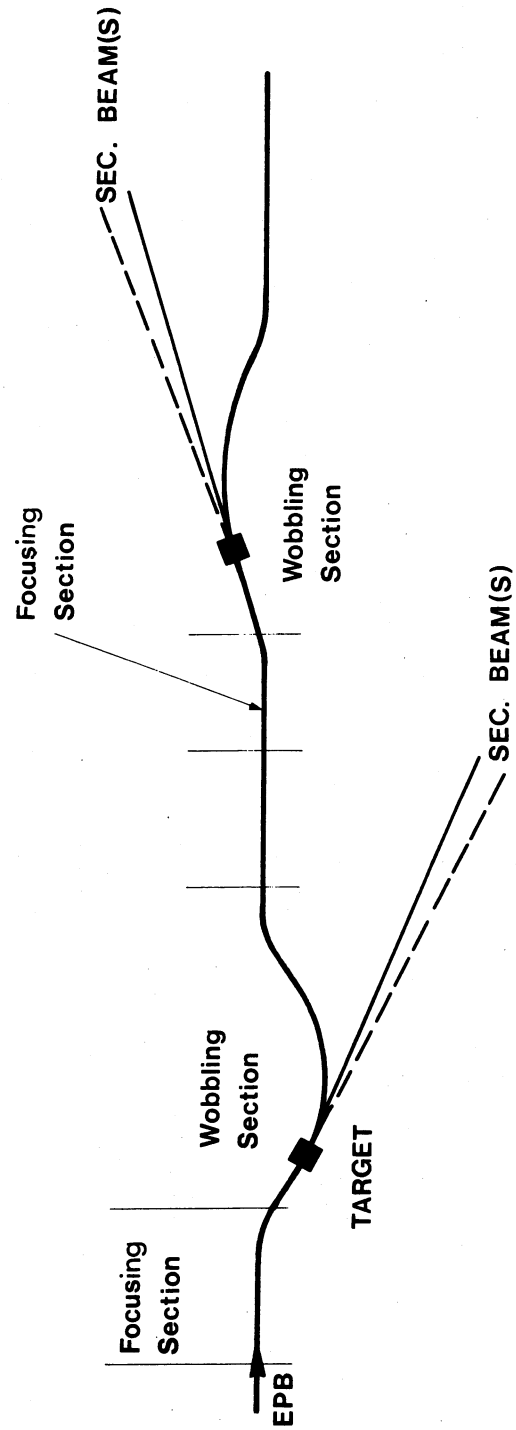

b) "Series„ targets

Fig. 13.7 Principles of target arrangements

in the momentum, positive secondary beams cannot go up to the primary momentum (because of the high contamination with protons). Finite production angles will have to be adopted in this case.

13.4.3 Secondary beams

As already mentioned, secondary beams will be derived from targets placed at a sufficient depth under the surface to be shielded completely by the earth.

The secondary beams could be installed in appropriate tunnels, which could be constructed with the cut-and-fill method, and remain generally well below the surface until they emerge into the experimental zones.

A typical length required by a normal high resolution, 400 GeV/c, secondary beam is of the order of 400 m (from production target to experimental target). The transverse dimensions of the tunnel should be kept as small as possible and it is believed that the best solution, both economically and technically, could be a tunnel of uniform cross-section all along. Such a solution retains a certain flexibility for the arrangement of quadrupoles and beam monitoring but of course practically none for the position of bends for the analysis. However the latter point is intrinsic in any layout of high energy beams for which large tunnels and halls are economically prohibitive.

The detailed planning of the area is not sufficiently advanced to allow the presentation of a meaningful layout.

The current thinking takes into account two to three primary targets and four to six secondary beams, for the initial phase of the utilization of the area; i.e. to be available in 1979.

Concerning special beams, the length available in the North Area could be of great advantage if one wishes to build a high energy neutrino and muon facility. The possibilities for such a combination are under serious study, but no details can be given at the present time.

13.4.4 Experimental zones

The experimental zones could be constituted by an apron, e.g. $\sim$ 30 m wide and $\sim$ 250 m long, resting on the moraine at a depth of several metres below the natural ground level. In this way it would not be necessary to install much additional shielding, in the form of expensive blocks, heavy walls and roofs.

If the areas were to be covered by roofs of light construction easy to slide open, gantry crane(s) installed in the apron could serve for handling the experimental apparatus through the roof. One could even consider to use building elements of modular construction

not too difficult to move and rearrange, so that only the part of the apron actually used for a particular experimental arrangement would be covered at any given time.

Alternatively, all the apron could be covered in a permanent way by a building of metallic structure incorporating an indoor crane.

The choice between these two solutions will be governed essentially by economical considerations.

As it is apparent from Fig. 13.6 important limitations in the utilization of the area are

(i) The road cutting across it at a distance of $\sim$ 1.5 km from the ejection point.
(ii) The stream "Le Lion" placed also transversely at an average distance of $\sim$ 1.7 km from the ejection point.

It is considered very convenient, in particular because of the ground configuration and of the proximity of the laboratories, to construct the first experimental zone, or zones, south of the road. This would make it important to design the EPB in such a way that the end of the second vertical bending magnet section (where the EPB is "horizontal" again) is at a distance of no more than 680 m from the ejection point. Taking into account (possibly) splitting sections and the necessary focusing sections onto targets, this would leave approximately 650 - 700 m for the secondary beams and experimental zones.

The EPB, or one of its branches, could continue at an approximate depth of 8 - 10 m under the road and "Le Lion" and eventually be directed onto other targets at a distance of approximately 2,000 - 2,200 m from the ejection point. Since the area extends for 3,800 m from the same point, this would leave 1,600 - 1,800 m for a second set of secondary beams and experimental zones.

One has to take into account however, that also this second part is traversed by a road at $\sim$ 3,250 m from the ejection point and therefore at about 1,000 - 1,200 m from the targets.

Finally, it is important to note that, in an area of total length approaching 4,000 m, the distribution of power and cooling water, the transmission of data, the provision of counting facilities, etc., will require extensive studies because of the financial implications and the far-reaching technical consequences.

In particular one will have to strike a balance between two contradicting requirements, namely to leave adequate space between experimental zones for extensions and modifications on the one hand,and to group them, in order to reduce the cost of various distributions and to facilitate communication among people, on the other hand.

13.5 Conclusions

This Chapter summarizes the results of about eight months of intensive studies following the approval of the Programme on 19th February 1971, which aroused considerable interest among the European community of high energy physicists. The use of the accelerator and the planning of the experimental areas gave rise to many discussions and studies, which culminated in a "Study Week on the 300 GeV Accelerator" organized by ECFA at Tirrenia (Italy) and attended by about 140 physicists from all over Europe.

The necessity of taking certain decisions concerning the civil engineering work and the different time-scale for the two Areas tended to focus most of the attention on the West Area. By now the basic layout of the accelerator and of the transfer tunnel is fixed and is compatible with the following changes with respect to MC/60:

(i) The beam transport from the accelerator to the West Area follows an almost straight line in the horizontal plane, thus reducing considerably the total amount of bending required.

(ii) The proposed r.f. separated beam for BEBC is considerably longer, enabling particle separation up to higher energies.

(iii) The targets for important secondary beams for electronic experiments can be made independent in order to improve the efficiency of the beams and simplify the magnet systems close to the targets.

(iv) The location of up to three targets within the shielded tunnel TT5 probably fed by inclined EPB branches, in order to reduce shielding costs.

(v) The possibility of constructing an underground neutrino facility which is now included in the civil engineering plans.

The layout which is proposed is still tentative since detailed installation plans have to be made in order to assess the compatibility of beams and start to design the shielding. Moreover it corresponds to a maximum programme, so that which part of it will be realized and when, will have to be decided in due course.

For the North Area only very preliminary ideas are given, together with certain basic alternatives and some considerations on the configuration of the ground. It will be imperative for such a long area to work out economical solutions for the civil engineering and the distribution of power, coolants etc., still retaining the essential features of the facilities which make the very best experiments possible. It is intended to devote a considerable effort to these problems during 1972.

Chapter 14

THE SITE

14.1 Introduction

The stability requirements for the foundation rock underlying particle accelerators first became critical with the advent of alternating gradient proton synchrotrons.

Non-specialists have difficulty in understanding these requirements because there are three basically different types of phenomena which influence the beam guidance field around the machine's circumference. These are:

(i) Slight movements of the foundation rock which, through more or less complicated structures, supports the magnets,
(ii) Errors in magnet alignment,
(iii) Errors in the beam guidance field itself.

The first of the above-mentioned causes of imperfection is virtually independent of technical considerations but is essentially the result of natural phenomena and the geological and geotechnical behaviour of the foundation rock.

The studies and measurements which have been carried out on CERN Lab.I site since 1954 in the area occupied by the 28 GeV synchrotron, and later in that of the ISR, have shown that the properties of the Chattian molasse of the Geneva basin, in which the tunnel is being bored, are sufficient to ensure the correct operation of the 300 GeV accelerator and proper operation of the experimental areas.

Whilst the molasse of the basin limited by the Jura and Salève is heterogeneous when examined in the form of samples, it constitutes a homogeneous geotechnical block. This is confirmed by the even statistical distribution of the moduli of deformability throughout the volume of the molasse. The absence of any water-table in the molasse complex, which is insulated by an impermeable overburden containing scattered and discontinuous small water-tables, has again been confirmed by the 36 borings made on the SPS site during the period July 1970 to June 1971.

The construction of the ISR added still better information on the quality of the molasse to that which was already known as a result of the construction of the 28 GeV proton synchrotron. It was ascertained that:

(i) The statistical value of the modulus of deformability, measured by jack tests at 162 points over 1 km of the ring, proved to be 12.3 kbar,

(ii) The almost total absence of water flow in the excavations for the rings and in the 600 m of transfer tunnels between the 28 GeV proton synchrotron and the ISR showed that this molasse was impermeable,

(iii) Repeated measurements made since the beginning of 1970 on the geodetic structure of the transfer tunnels demonstrated the stability of the reference markers embedded in the ground and walls of the tunnels. Over a period of one year, the system of monuments and brackets showed a stability of ±0.1 mm, both horizontally and vertically, over distances of about 100 m.

The dimensions and shape of the molasse structure are shown to be suitable for the construction of an accelerator with a diameter of 2.2 km.

As the experimental areas (the existing West Area, and future North Area) are located at a sizeable distance from the synchrotron, any movement in the ground due to changes in the loading, as a result of the subsequent use of the experimental areas, will have no effect on the natural stability of the 300 GeV tunnel.

14.2 Geology and structure of the Geneva basin

The Geneva basin is essentially a synclinorium which extends from the first chain of the Jura to the Salève anticline; it is occupied by the southern extremity of the perialpine molasse basin. Its structure is gently folded and part of it is isoclinal. This structure is revealed by three alignments of molasse hills running from SW to NE. The first alignment passes through the villages of Challex, Dardagny, Peissy, Choully, Bourdigny, Prévessin, Moëns, Ornex and Bossy; CERN I is situated on this alignment and so is the Laboratory II. The second starts at the Fort-Sainte-Catherine hill (to the East of Viry) and passes through the villages of Bernex, Pregny and Chambésy; the third can be seen only in the hill at Cologny. Some twenty million years elapsed between the formation of the oligocene molasse and the Ice-Age pleistocene deposits without leaving any trace in this basin.

The molasse in the area is normally of two types: a variegated molasse at the bottom, resting on Mesozoic formations, in particular on a Cretaceous foundation (Barrémian) and, at the top, a gypsum molasse. The latter formation is not encountered on the site of the SPS.

Traces of only two glaciations, the Riss and the Würm, are found on these molasse areas. The Würmian moraine is generally a clay of a yellowish colour at the surface, changing to blue-grey and steel-grey at depth; it may contain striated pebbles of alpine material and also change into a sandy or gravel moraine. This moraine, which is evenly spread over the whole basin, overlies the 'ancient' alluvium in those regions where it had been deposited; elsewhere, the moraine lies directly on the molasse.

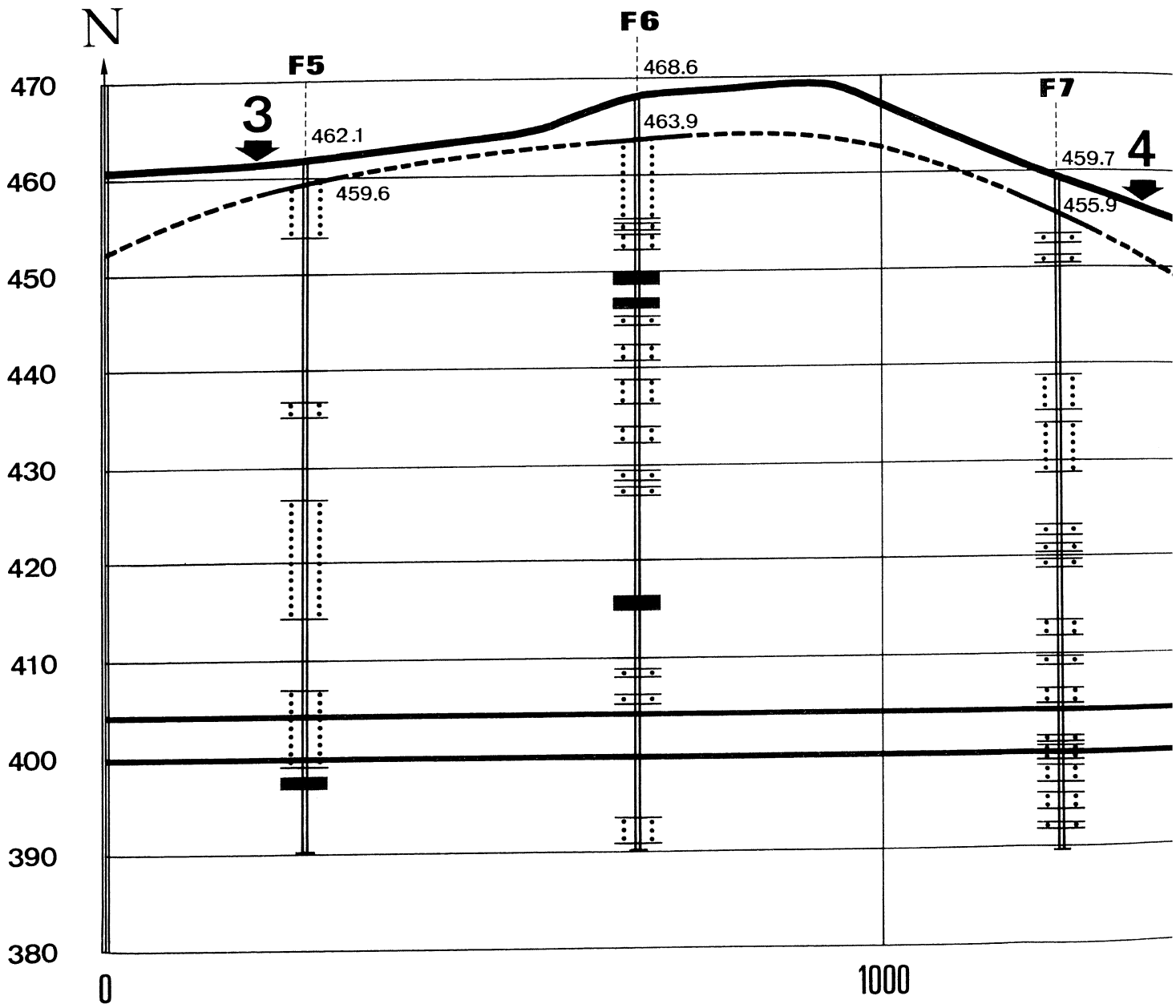
N
F5
F6
F7
468.6
462.1
463.9
459.7
459.6
455.9
3
4
470
460
450
440
430
420
410
400
390
380
0
1000

COUPE

---- Toit de la mola

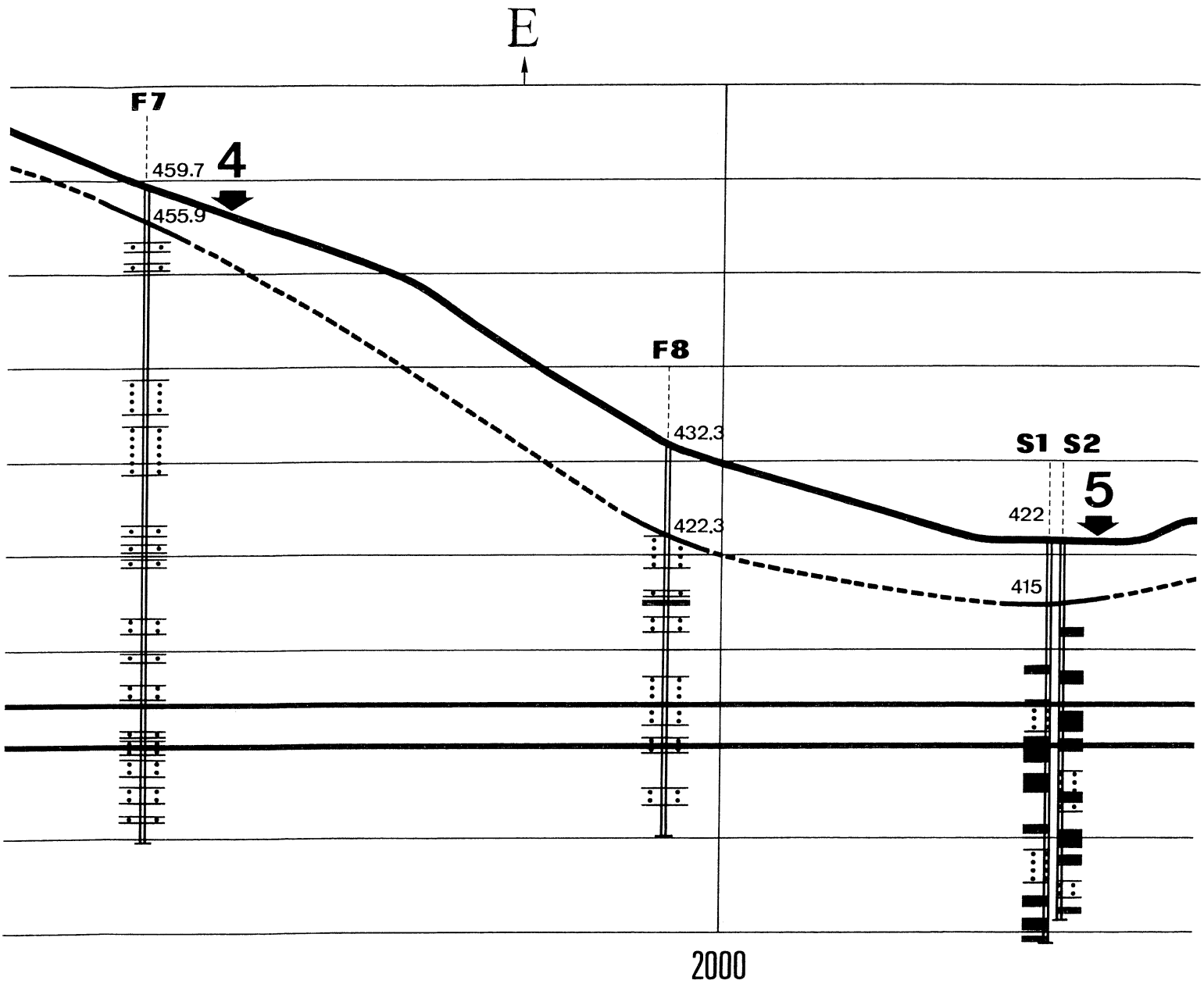

COUPE DEVELOPPEE

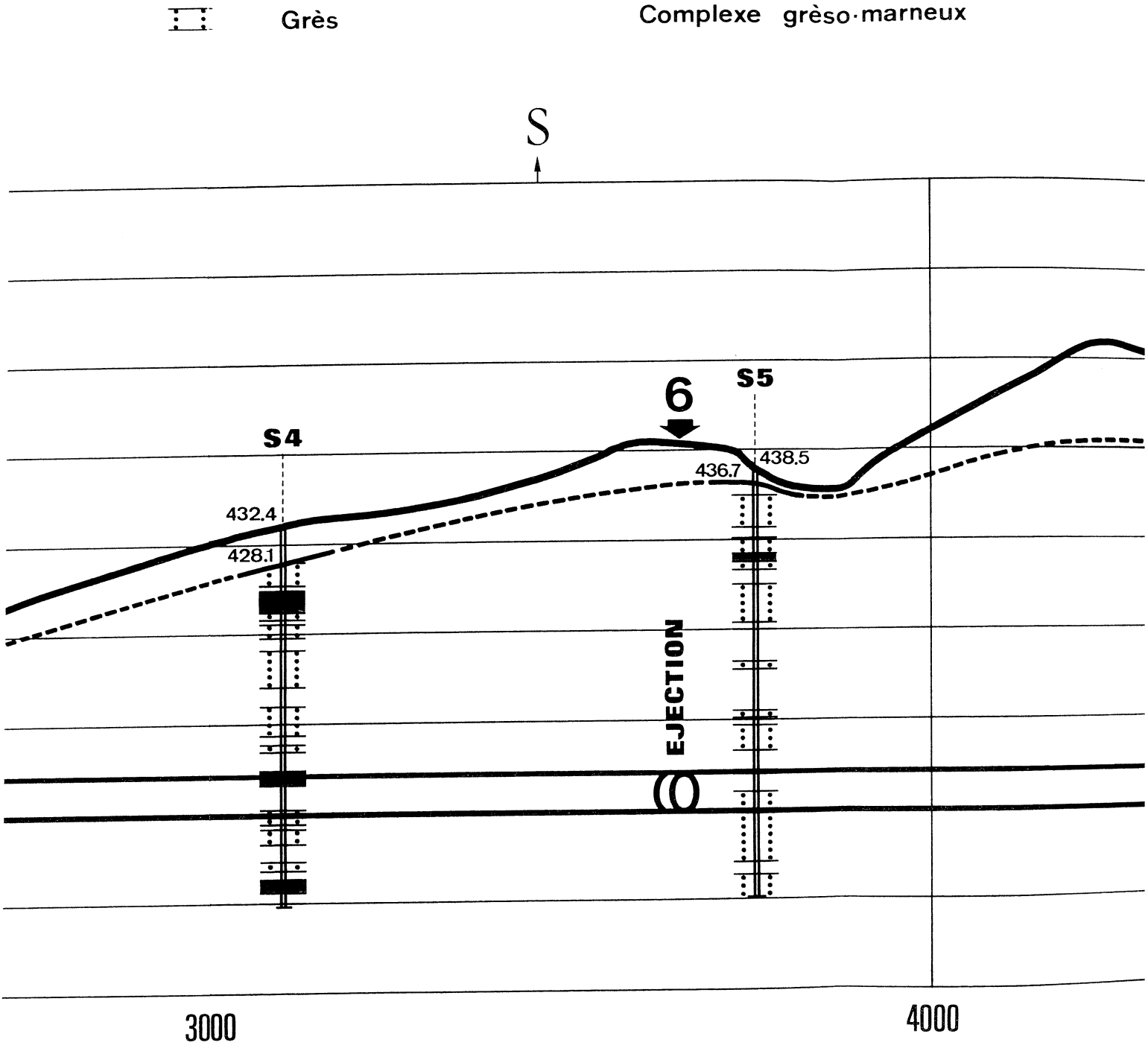
Grès
Complexe grèso-marneux
S
S4
S5
6
438.5
436.7
432.4
428.1
EJECTION
3000
4000

LE LONG

ux

Marnes bariolées

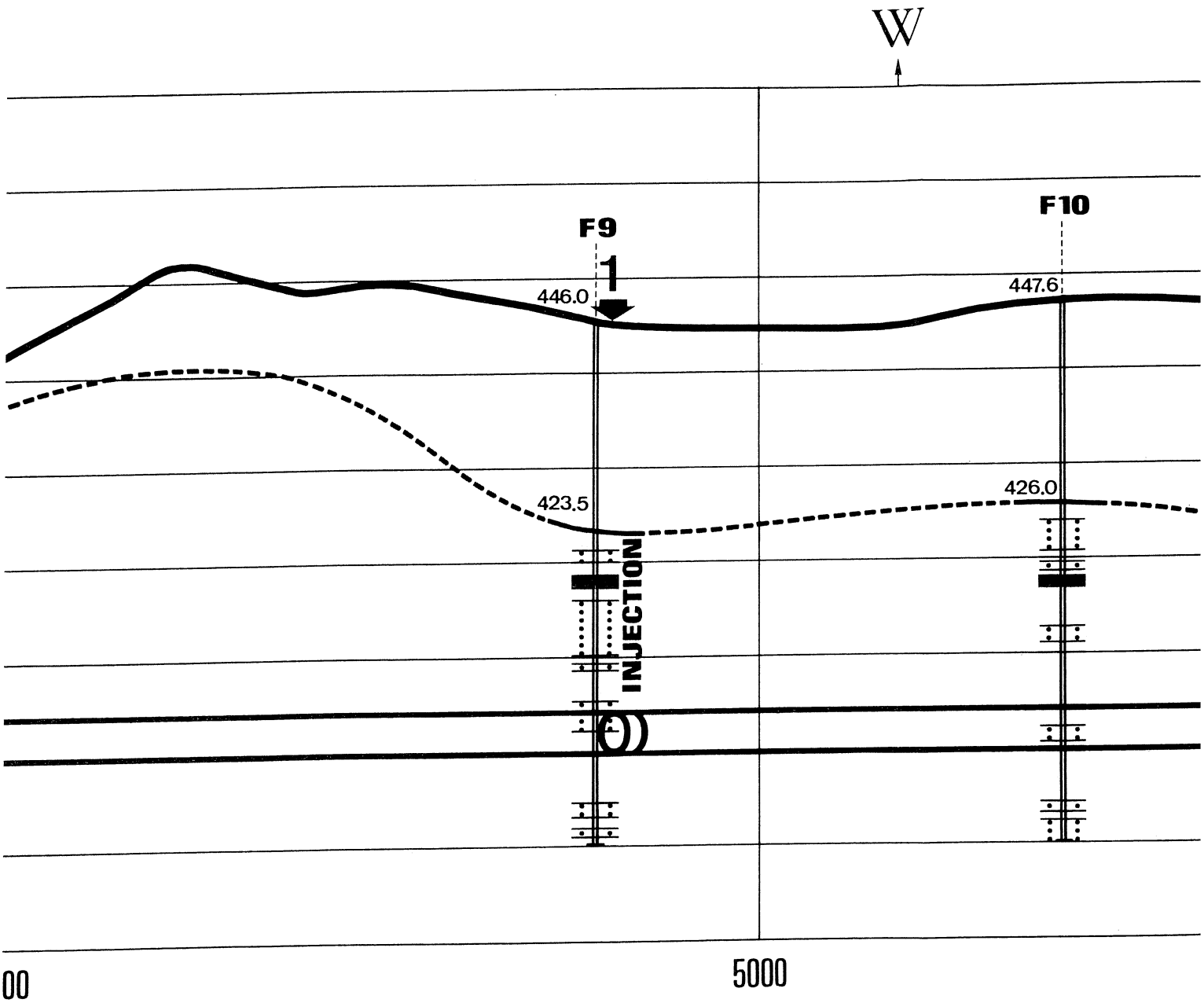

DE

L'ANI

Fig. 1

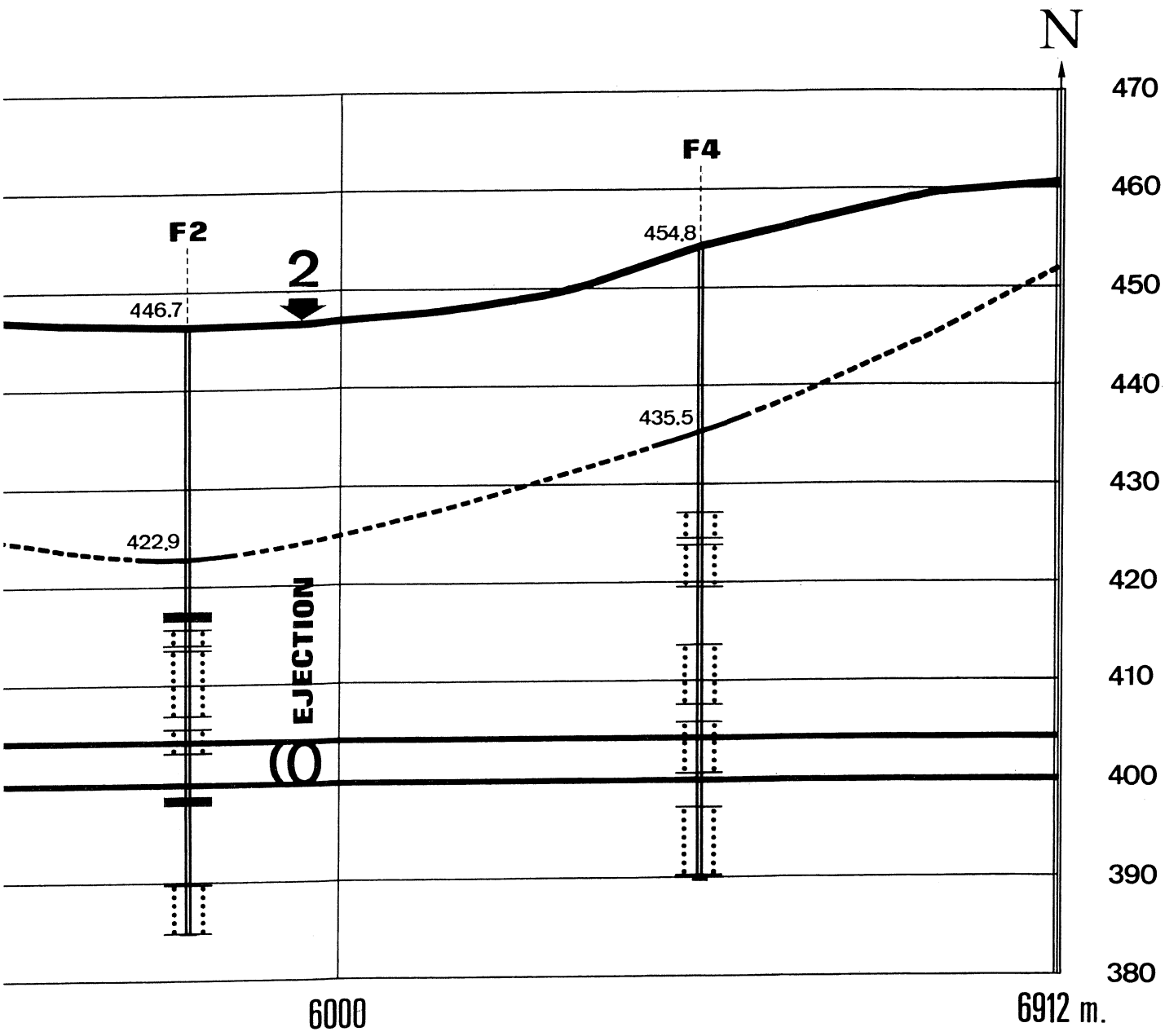
N
470
460
450
440
430
420
410
400
390
380
F2
F4
2
446.7
454.8
435.5
422.9
EJECTION
6000
6912 m.

NEAU

4.2

The accelerator tunnel, situated 22 metres below the lowest point in the topography, will be bored solely in the molasse of the Choully-Moëns-Ornex isoclinal structure. In no case will the moraine deposits overlying the molasse be used as a foundation for the machine.

The molasse of this structure belongs to the 'Upper Stampian' or 'Chattian' (O_3. Geological Atlas of Switzerland, sheet 12). The dating is confirmed by several Caseolus (Helicomela) ramondi (Brongniart) found in the boring samples.

The thickness of this molasse was determined at the SW end of the Choully-Prévessin-Ornex structure, by means of a borehole drilled near the village of Peissy in 1944 and 1945. The first calcareous horizon at the bottom of the molasse was not encountered until the boring had penetrated to a depth of 293 metres.

14.3 Location of the 300 GeV accelerator on the molasse structure of Choully, Prévessin and Moëns

As the accelerator will be housed in a circular tunnel bored in the molasse, practically all harmful effects on vegetation will be avoided. Even in the most unfavourable conditions, the intensity of radiation at ground-level will be well below permitted levels. As the accelerator will, on the average, be at a depth of about 40 m below the surface, the transfer tunnels for the injected and ejected beams will also be bored in the molasse. Consequently, major changes in the loading of the ground, due to the installation of the experimental apparatus and shielding in both the West and North areas, will in no way affect the operation of the synchrotron, since its physical stability will depend solely on the natural stability of the molasse hill in which the tunnel will be bored.

Borings F1, F2 and F3, and S1, S2 and S3 (see Fig. 14.1) served to determine the width of the molasse hill in a direction perpendicular to its axis running through Choully, Moëns and Ornex, since the centre of the synchrotron is located exactly on this alignment. From the results of these borings the radius of the accelerator has been defined as 1.100 metres.

A detailed examination of the core drillings obtained confirmed that the underlying molasse was quite suitable. The sandstones and sandstone marls offer an overall homogeneity and compactness which increase with depth. Located beneath the normal Ice-Age overburden, the molasse in the area where the accelerator will be sited is composed mainly of compact and homogeneous marls, for the most part sandy and micaceous, alternating with very homogeneous sandstones generally of fine or medium coarseness, of uniform size, marly with a marlaceous or marly calcareous cement. Occasional layers or variegated marls, soft and brittle are intermingled with these formations.

At the level where the ring will be located, i.e. between 400 and 405 metres, the formations found were shown to be sandy marls and sandstones, with small layers of variegated soft marls, generally much less than a metre thick (Fig. 14.2). As for fractures, only a few very small quasi-vertical or oblique fissures were found in the core drillings.

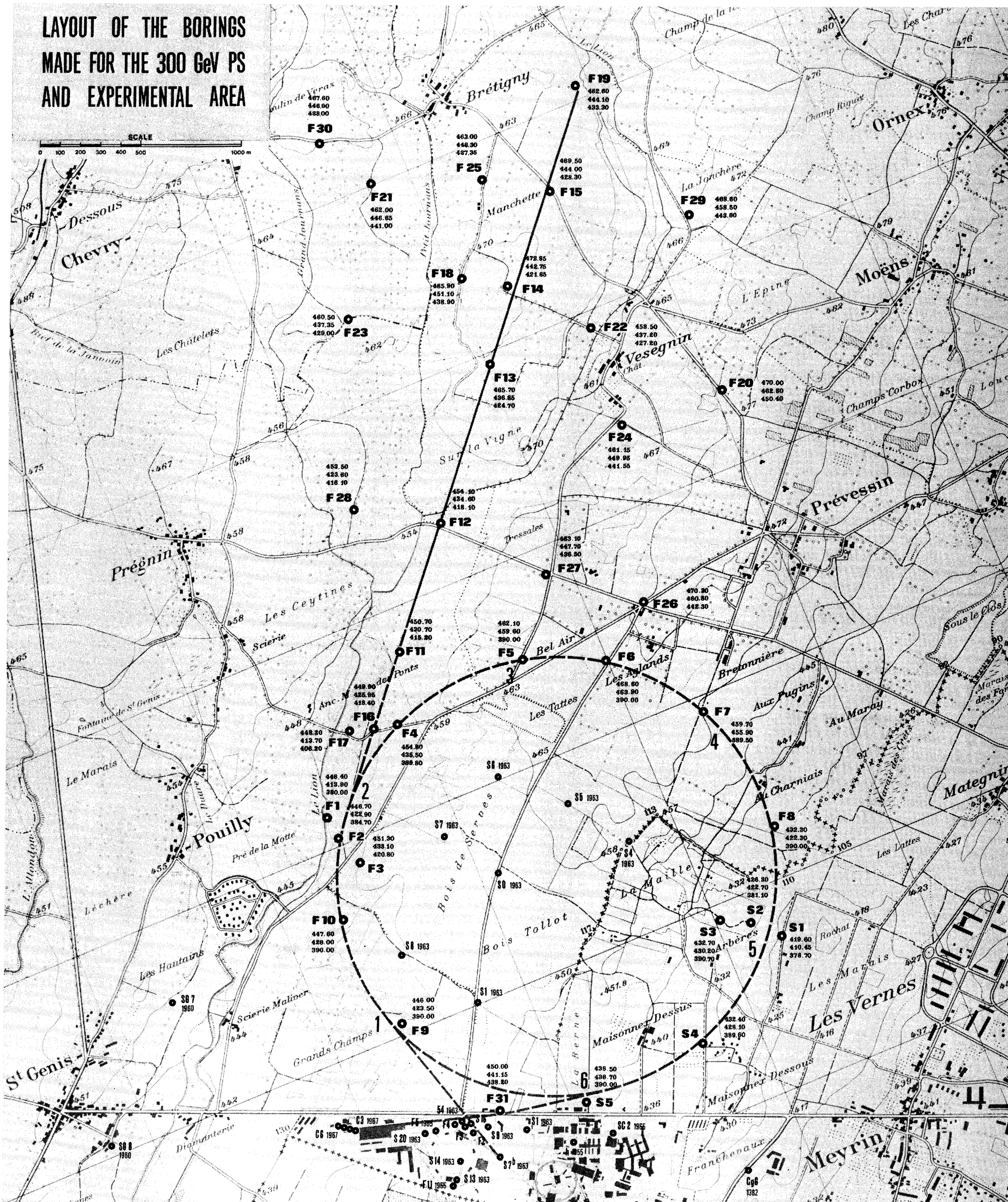
LAYOUT OF THE BORINGS MADE FOR THE 300 GeV PS AND EXPERIMENTAL AREA
SCALE
Brétigny
Ornex
Chevry-Dessous
Moëns
Vesegnin
Prévessin
Prégnin
Pouilly
Mategnin
Les Vernes
St Genis
Meyrin
Bois Tollot
Bois de Serves
Grands Champs
Maisonnex Dessus
Maisonnex Dessous
Les Ceytines
Bel Air
Les Tattes
Champs Corbox
Les Châtelets
Sur la Vigne
Tressales
Manchette
Bretonnière
Aux Pugins
Au Maray
Charniais
La Maille
Arbères
Le Marais
Pré de la Motte
Les Hautains
Scierie Maliver
Diamanterie
Sous les Vignes
Franchebeaux
L'Epine
La Jonchère
Champ Riguz
Scierie
Les Aglands
Les Maisis
Rochat
Sous le Clos
Les Lattes
F1 F2 F3 F4 F5 F6 F7 F8 F9 F10 F11 F12 F13 F14 F15 F16 F17 F18 F19 F20 F21 F22 F23 F24 F25 F26 F27 F28 F29 F30 F31
S1 S2 S3 S4 S5
1 2 3 4 5 6

Fig. 14.1

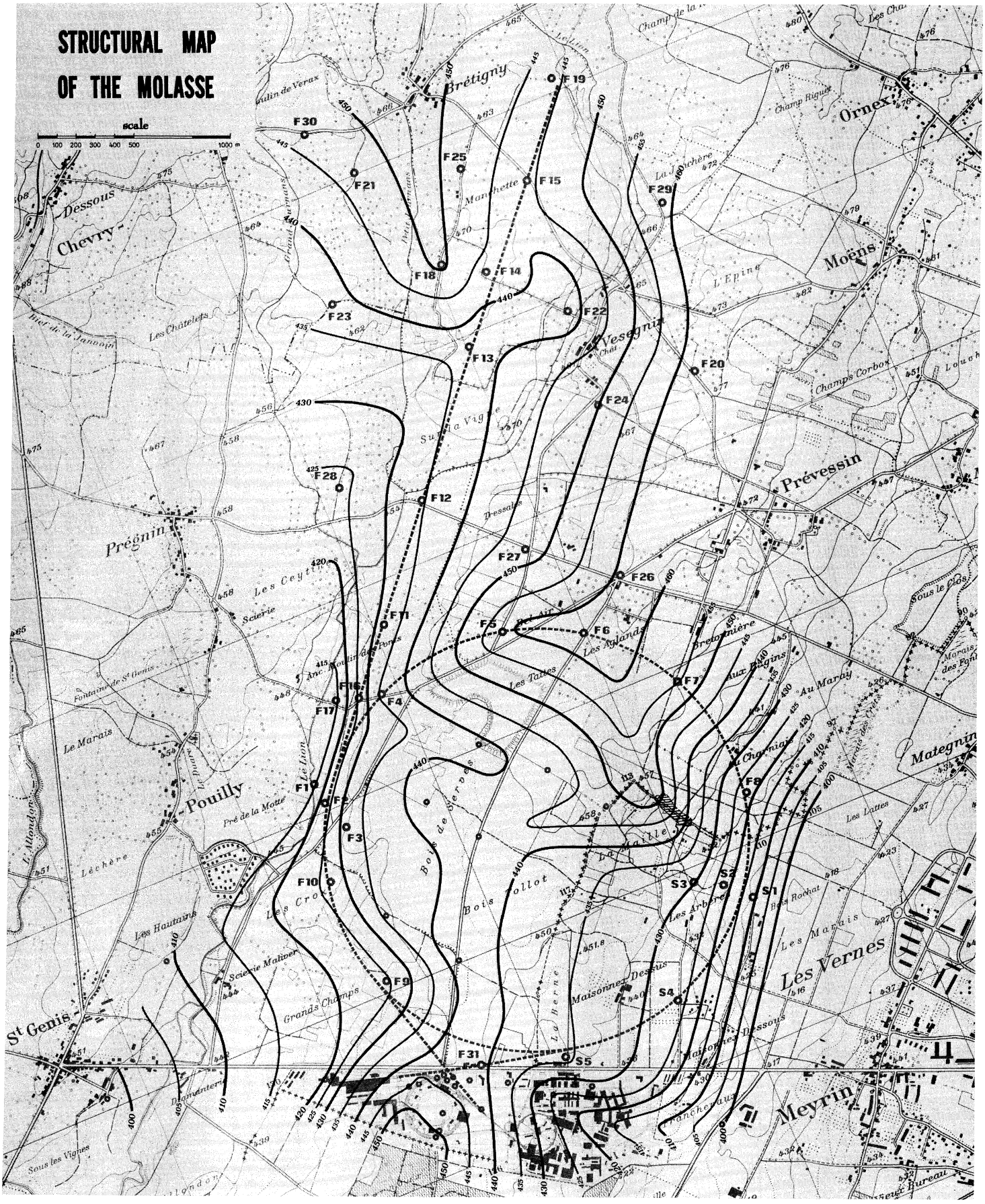
STRUCTURAL MAP
OF THE MOLASSE
scale
0 100 200 300 400 500 1000 m
Bretigny
Ornex
Chevry
Dessous
Moëns
Vesegnin
Prévessin
Prégnin
Pouilly
St Genis
Meyrin
Les Vernes
Mategnin
F1
F2
F3
F4
F5
F6
F7
F8
F9
F10
F11
F12
F13
F14
F15
F16
F17
F18
F19
F20
F21
F22
F23
F24
F25
F26
F27
F28
F29
F30
F31
S1
S2
S3
S4
S5

Fig. 14.3

The 36 borings, representing more than 1,400 m of cores, have provided detailed information on the material encountered on the path of the SPS and the North Experimental area. The structural map (Fig. 14.3), which gives the contours of the roof of the molasse, shows that the SPS ring is situated right on the axis of the isoclinal structure of the molasse. Unfortunately, the North Experimental area is located on the left bank of a fossile valley; Thus the thickness of the moraine overburden exceeds 20 m over the entire length of the beam trajectory (Fig. 14.4).

14.4 Seismology

On April 17, 1936, the epicentre of the Frangy-Chaumont earthquake -- one of the strongest felt in France in 1936 -- was at a point mid-way between these two villages. The intensity fell sharply, however, around the epicentral area and, for an intensity of VII to VIII at the epicentre, the total macro-seismic area was only 1900 km^2 (see Fig. 14.5). The area of intensity V is longer in the N-S direction, 35 km as opposed to only 20 km in the E-W direction. Generally, it includes the whole plateau of molasse from the Vuache to the first chain of the Jura. On the eastern side, the isoseists do not coincide with the limits of any geological units; a sharp damping of the movements was, however, observed on the molasse plateau. This was so marked that, at the site of the proposed laboratory, the recorded intensity of the earthquake was only III, although the epicentre was no further away than 25 km. The molasse plateau also serves to damp the microseismic waves which affect the ground in this region. These are natural waves caused by the ocean lapping against the continental shelf with a frequency of between 3 and 7 seconds, and industrial microseismic waves having a frequency of the order of a 10th of a second. The plateau also serves to damp the effects of intercontinental earthquakes.

14.5 Hydrology

When the ISR were constructed, only a limited water table was found in the moraine. It was not, in fact, located at the moraine/molasse interface; in the alluvial deposits there are discontinuous clayey layers which prevent the water from reaching the molasse on the new site; this was confirmed by all the borings.

The molasse encountered during excavation of the ISR and transfer tunnels was found to be dry. The permeability values recorded by oedometer are extremely low, of the order of 10^{-10} to 10^{-11} m/s, sometimes less than 10^{-11} m/s, after which they become impossible to measure. The average permeability values of the molasse in this area were calculated from the rate at which the water rose in the boring tubes of the piezometers: this is of the order of 10^{-9} m/s. This average value assumes that the molasse in which the boring was made, or in which the piezometers were inserted, was homogeneous as far as permeability was concerned. This is clearly not the case, but whenever water did penetrate the molasse it was through fissures; the permeability values in this area are low, since the amount of water passing through the fissures is not great. The 'cut and fill' method was used when building the 15 m wide tunnel. In the whole length of the 1 km-long excavation, which in some points was 22 m deep, only a few fissures were discovered, and the amount of water passing through was very small.

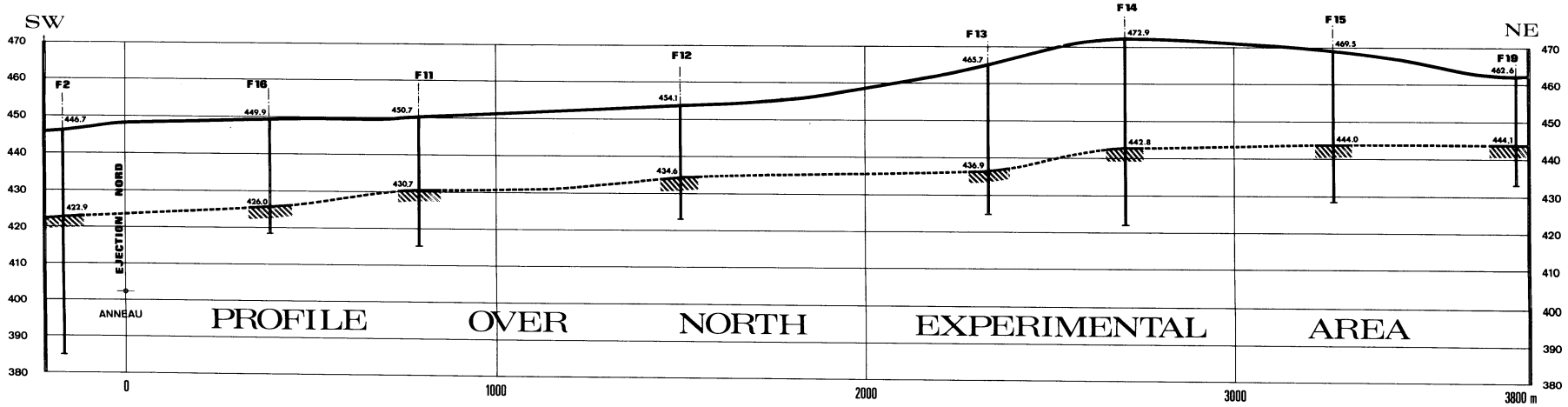
SW
NE
F2
F16
F11
F12
F13
F14
F15
F19
446.7
449.9
450.7
454.1
465.7
472.9
469.5
462.6
422.9
426.0
430.7
434.6
436.9
442.8
444.0
444.1
EJECTION NORD
ANNEAU
PROFILE OVER NORTH EXPERIMENTAL AREA
0
1000
2000
3000
3800 m

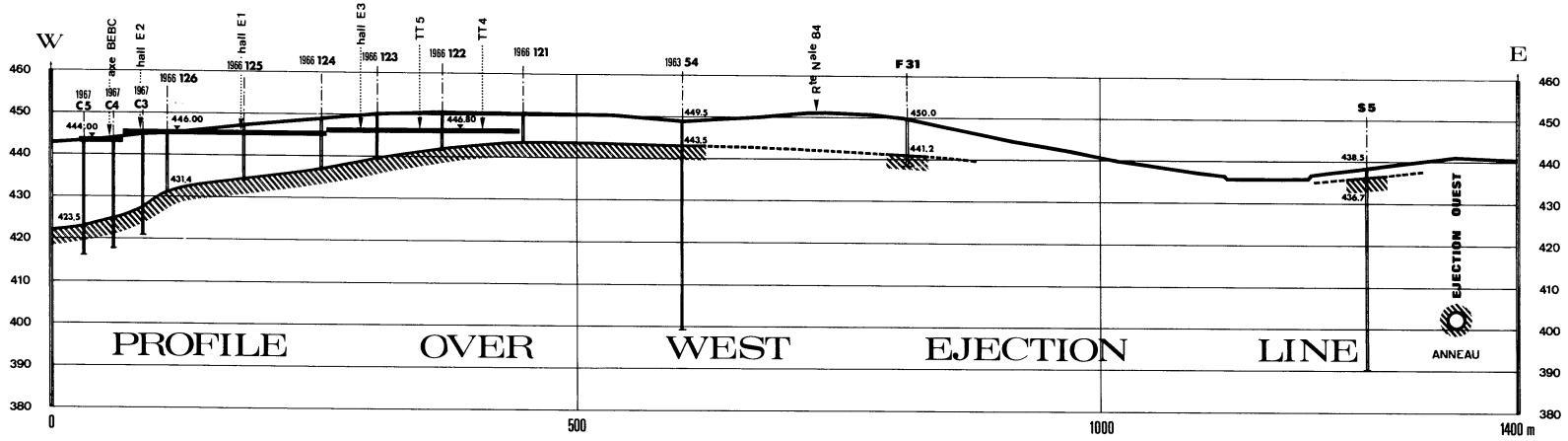
W
E
axe BEBC
hall E2
hall E1
hall E3
TT 5
TT 4
1967 C5
1967 C4
1967 C3
1966 126
1966 125
1966 124
1966 123
1966 122
1966 121
1963 54
Rte Nale 84
F 31
S5
444.00
446.00
446.80
449.5
450.0
443.5
441.2
438.5
436.7
431.4
423.5
EJECTION OUEST
ANNEAU
PROFILE OVER WEST EJECTION LINE
0
500
1000
1400 m

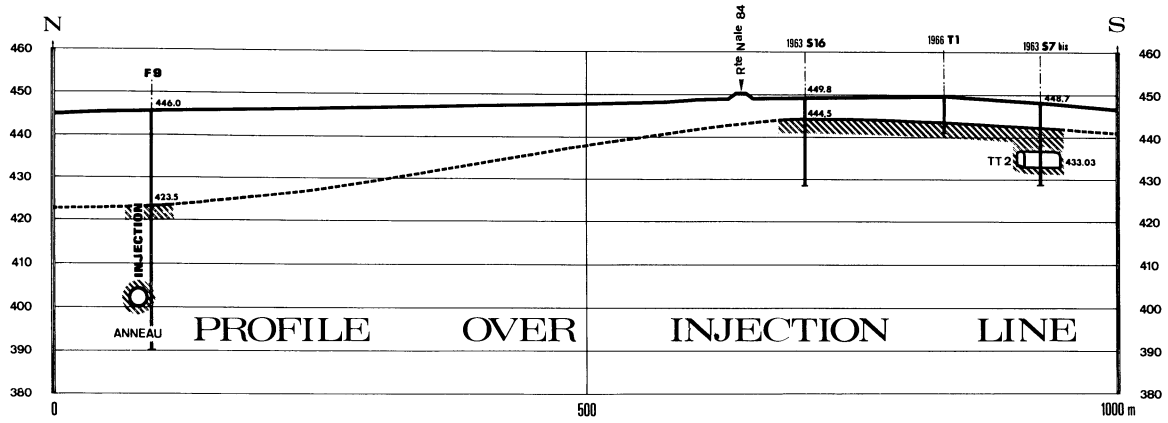
N
S
F9
Rte Nale 84
1963 S16
1966 T1
1963 S7 bis
446.0
449.8
448.7
444.5
TT2
433.03
423.5
INJECTION
ANNEAU
PROFILE OVER INJECTION LINE
0
500
1000 m

Fig. 14.4

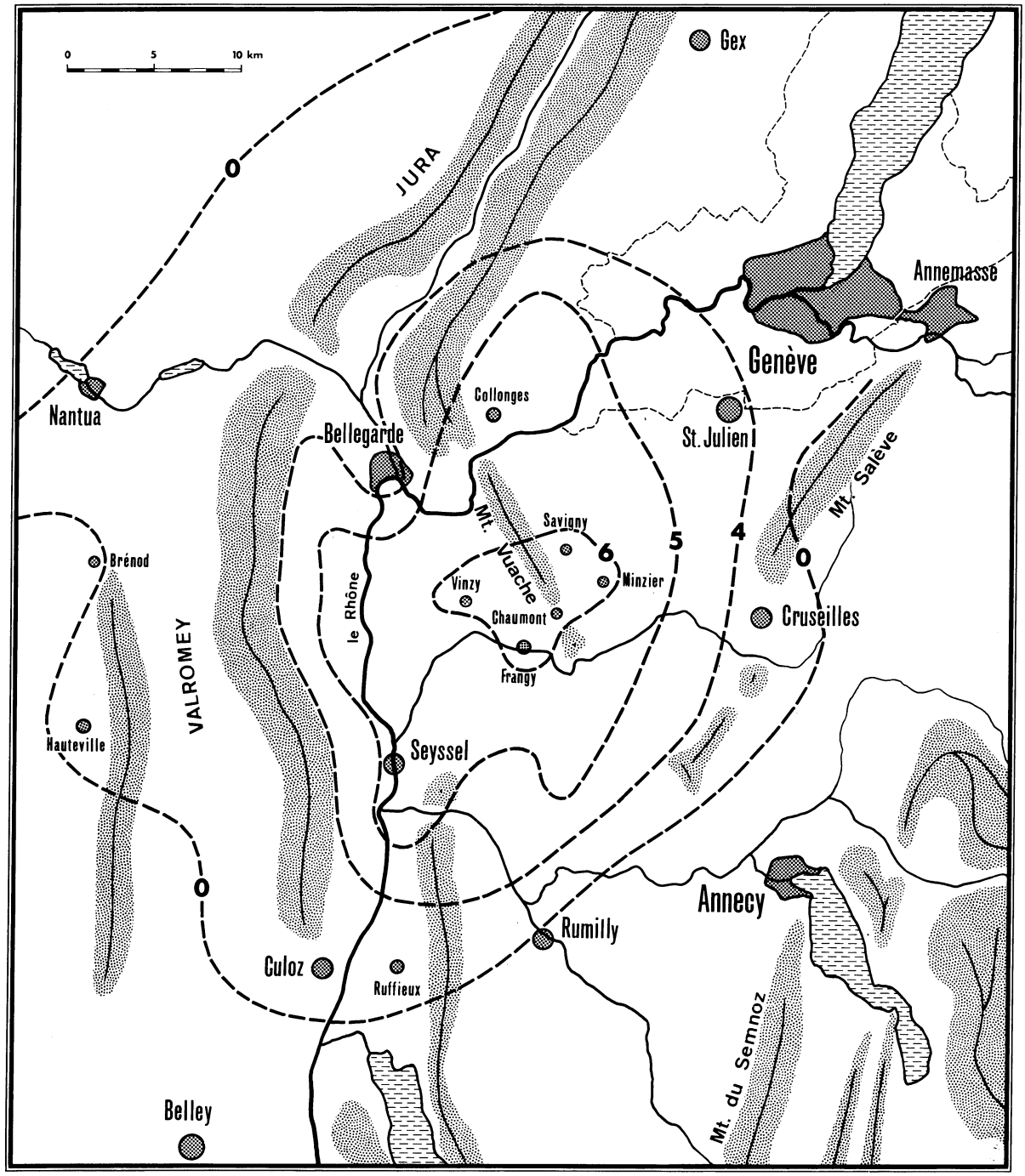

Fig. 14.5 Isoseists of Haute-Savoie earthquake which occurred on 17 April 1936 (after E. Rothé, 1942)

The majority of the transfer tunnels between the 28 GeV PS and the ISR were blasted out of the molasse. At only four points in the 600 m of tunnelling was water seen to enter, and only then at a low flow-rate; it was not a source of serious difficulty when the tunnel was being lined. A service tunnel 1.60 m in diameter and 600 m long was also blasted in the molasse; there was no inflow of water whatsoever.

Thirteen piezometers were installed in borings S1, F1, F2, F4, F5, F10, F11, F12, F14, F15, F16, F17 and F28, and the level of the water was measured over six months with no significant movements.

In none of the 36 borings was any loss recorded in the molasse. Only at boring F1, near the Lion river and outside the area of the ring was a partial water loss observed, at a depth of between 56.60 and 66.40. A permeability test made at this depth gave $k = 1 \times 10^{-5}$ m/s.

The Lugeon tests made at borings S2, S3, S4 and S5 in the molasse at 2, 4 and 7 atmospheres showed no absorption whatsoever.

Borings F1, F4, F10, F13, F14, F16, F17 along the edge of the St Genis molasse fossile valley, and boring F28 along the axis of this valley, showed slight water losses and flows in the quarternary overburden. At boring F28 an artesian water flow of about 20 ℓ/m was observed at depth of between 13.30 and 29.00 metres.

14.6 Rock mechanics

Although samples show the molasse to be heterogeneous, it is, when considered on a large scale, relatively homogeneous as far as its overall geotechnical characteristics are concerned. The sedimentary formations of this molasse are of continental and detrital origin, and they possess all of the characteristics of this type of material. The values obtained for the modulus of deformability measured in the laboratory vary according to the sample, but the values obtained for layers of a given thickness, show less scatter. Tests carried out during the construction of the ISR showed the average value of the modulus of deformability to be 14.5 kbar for the marl samples and 21.5 kbar for the sandstone samples.

In the ISR, the deformability of the molasse was measured in the region of the supports of the concrete beams on which the magnets were to be installed. The jack-test measurements were made with a 0.30 m diameter plate on a molasse which was decompressed, due to the fact that the width of the tunnel foundations was about 20 metres. The modulus of deformability for the 162 tests made proved to be 12.3 kbar.

No special problems were encountered during the boring of the transfer tunnels, and it was not felt necessary in the constructional stage to make any jack-tests.

The samples from the borings on the new site fell into four main categories: variegated marls, non-sandy marls or partly sandy marls, sandstone marls and sandstones. Borings S1

and S2 revealed a layer of fine to medium sandstone, which was marly, soft, slightly and partly impregnated with hydrocarbons (with a porosity of about 30%). Samples of all the above materials have been examined in the laboratory.

Table 14.1 gives the wet density, unconfined compression strength and modulus of deformability for each type of molasse.

Table 14.1

	Samples of molasse	Wet density	Rc (bar)	E (kbar)
VM	variegated marls	2.25	33	6.6
PSM	non-sandy or partly sandy marls	2.30	65.6	9.1
SM	sandstone marls	2.33	109.3	16.7
S	sandstones	2.40	233.0	43.9
HS	soft sandstones with hydrocarbons	2.20	50.0	7.1

Table 14.2 gives the average modulus of deformability of the molasse, measured along the ring between 400 m and 405 m above sea-level.

Table 14.2

Boring	Type of material	%	R_c	E	E'
S1	S 2.20 VM 1.60 PSM 1.20	44 32 24	129.2	12.6	23.6
S2	VM 2.05 PSM 2.95	41 59	52.7	3.4	8.1
S4	VM 1.95 PSM 2.65 S 0.40	39 53 8	66.8	5.1	10.9
S5	VM 1.85 PSM 1.00 S 2.15	37 20 43	126.0	12.3	23.1
F2	VM 0.15 PSM 3.30 S 1.55	3 66 31	116.6	11.2	19.8
F4	PSM 0.40 S 4.60	8 92	219.6	23.0	41.1
F5	S 5.00	100	233.0	24.7	43.9
F6	VM 2.90 PSM 2.10	58 42	47.4	3.1	7.7
F7	PSM 4.20 S 0.80	85 16	92.4	7.6	14.7
F8	PSM 2.10 S 2.90	42 58	162.7	16.1	29.3
F9	PSM 3.40 S 1.60	68 32	119.2	10.8	20.2
F10	VM 0.30 PSM 3.20 S 1.50	6 64 30	113.9	10.3	29.4
Average value			123.3	11.7	22.7

14.7 Stability

It should not be forgotten that for the last fifteen years measurements have been carried out on the molasse supporting the CERN I Laboratory with a view to determining its stability and deformation under load.

Figure 14.6 shows the vertical movement of the pillars of the 28 GeV PS over a period of ten years. The pillars are anchored into the molasse, which remains absolutely stable as long as it is not deformed by a change in the loading, such as: removal or addition of earth

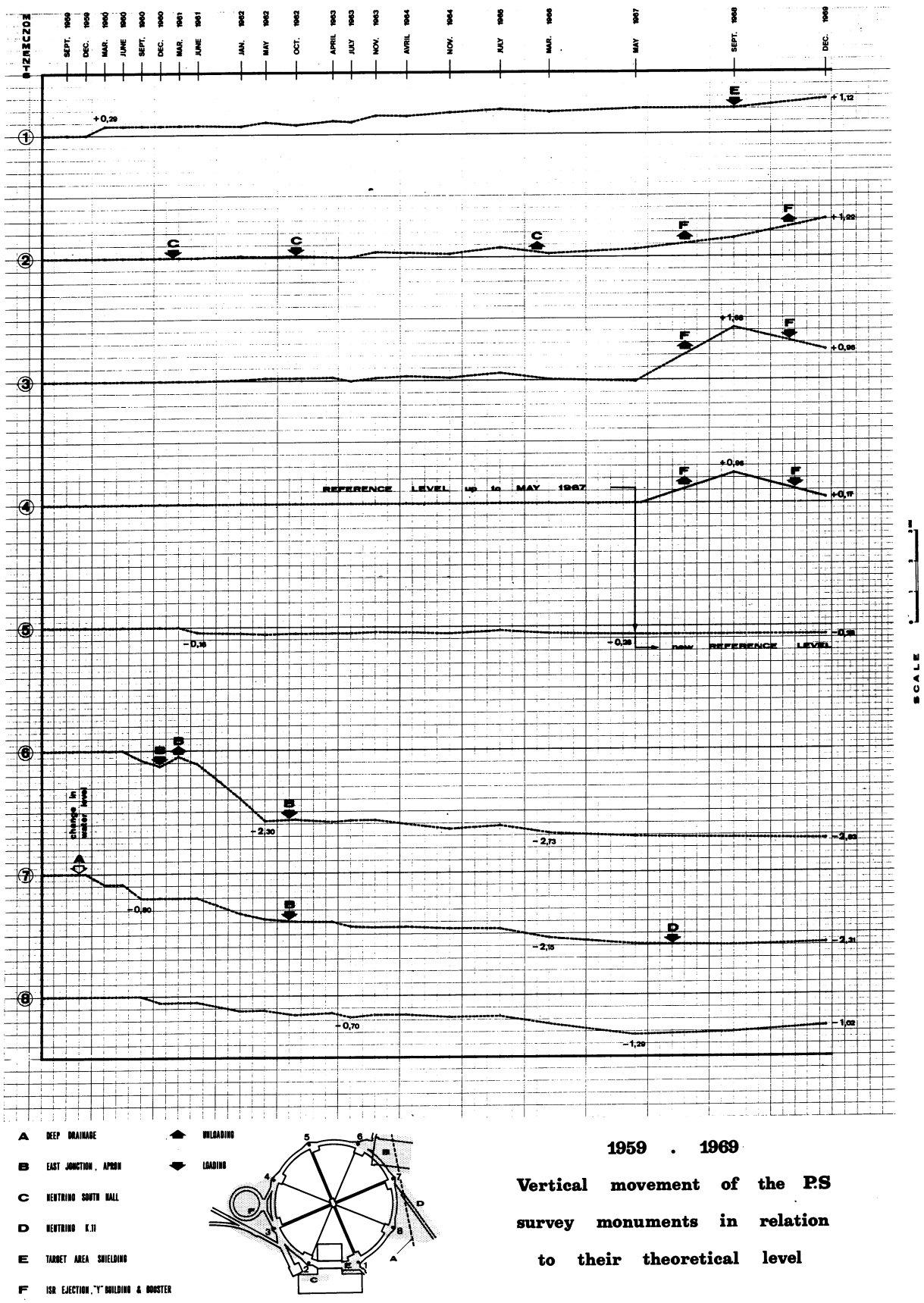

1959 . 1969

Vertical movement of the P.S survey monuments in relation to their theoretical level

Fig. 14.6

above the accelerator tunnel, construction work on the experimental areas near the synchrotron, experiments, such as those on the neutrino, which require considerable alteration in the amount of shielding. Results of measurements on pillars 3, 4 and 5 show a vertical stability of ±0.2 mm. The graphs for pillars 3 and 4 show that the deformations are elastic.

The reference figure for the metrology of the 28 GeV PS was a regular octagon with a central point. Repeated measurements showed the horizontal stability to be 0.1 mm per 100 m per year.

A measurement carried out independently of any triangulation confirmed these figures. From 24 August 1965 to 13 February 1968 a pair of Marussi horizontal pendulums were mounted on the centre pillar of the synchrotron. These instruments measure the variation in the inclination of the vertical, and therefore that of the support on which the instrument is mounted. It will be seen from Fig. 14.7 that the movement of the molasse and of the pillar itself has not exceeded 0.2 mm in two and a half years.

It is too early to predict the stability of the molasse and of the foundations of the ISR magnets, since the components have only just been installed. Nevertheless, measurements have been carried out repeatedly since May 1970 in transfer tunnels TT1 and TT2, which were bored through the rock, and results have shown the stability to be identical to that of the pillars of the 28 GeV PS. The measurements were made on pillars erected on the floor of the tunnel and on brackets set into the walls. The pillar/bracket combination showed that, over the last five months, both the horizontal and vertical stability was ±0.1 mm over distances of the order of 100 metres.

14.8 Conclusion

The results obtained from measurements in the 28 GeV PS were, in fact, used as a basis for drawing up the technical requirements for the 300 GeV project; in particular, the specification stated that a rock with a modulus of deformability greater than 10 kbar would offer the two-fold advantage of reducing construction costs and improving operational reliability. The experience already gained in the construction of the transfer tunnels of the PS/ISR complex confirms that the natural stability of the molasse is adequate for the construction and proper exploitation of the machine in the near future.

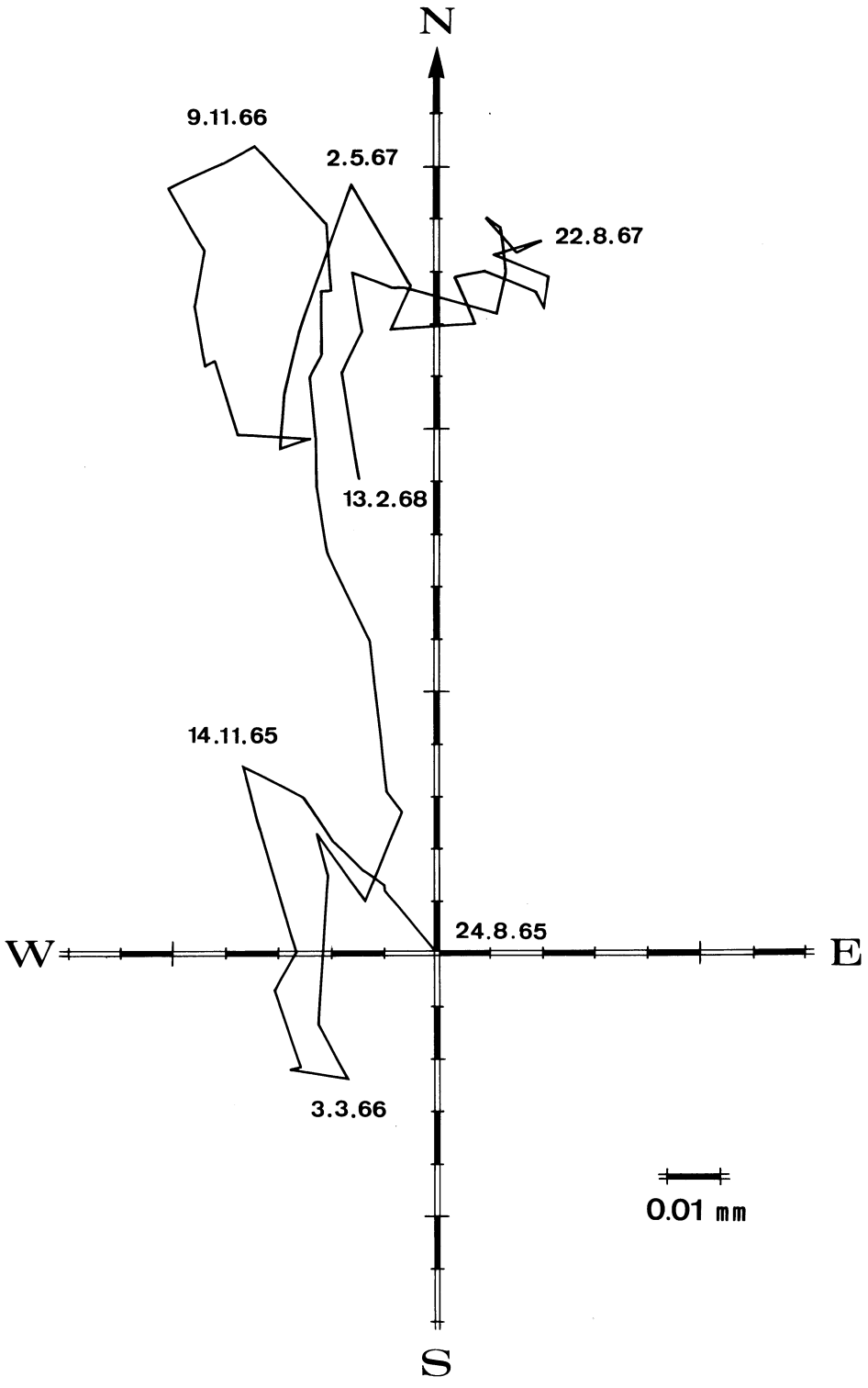

Fig. 14.7 Movement detected in the monument at the centre of the PS, according to measurements with horizontal pendulums over the period 24 August 1965 to 13 February 1968.

Chapter 15

SITE INSTALLATIONS AND BUILDINGS

15.1 General

The layout of the synchrotron has been dictated by the injection and the two ejection beam lines. The ring diameter has been fixed to a maximum value compatible with the useful extent of the site and underlying molasse, at the depth required by radiation shielding.

Most careful attention has been paid in the design to avoid spoiling the rural setting of the site: this implies, among other things, limiting the use of overhead electric lines, making maximum use of existing roads together with careful design and landscaping of buildings.

The way in which we expect the laboratory to develop has been considered in the design of the overall plan presented here. The locations of the main parts of the project are shown in Fig. 15.1.

The construction of the main Laboratory centre has already started: located at the North of the ring, close to the future North Experimental Area, it includes several multi-purpose cross-shaped buildings containing offices, laboratories, shops etc. and one large assembly hall ($\sim$ 11000 m^2).

The construction of this centre will extend over several years: in the first phase (end of the second year of the project) there will be enough space to accommodate about 400 people.

The underground ring tunnel (at an average depth of 40 m below the surface) will have six access shafts: three of these will be equipped as cable and pipe ducts, plus personnel and light equipment access while three will also permit the handling of the heaviest machine components. At the top of every access shaft there will be an auxiliary equipment building, containing power distribution, rectifier banks, local controls, water pumps and heat exchangers etc. Where appropriate, these buildings will also house the injection (Nr. 1) and ejection power supplies (Nrs. 2 and 6) and the radio-frequency equipment (Nr. 3). This last auxiliary building, the closest to the main laboratory centre and to the North Experimental Area, will include the main control room.

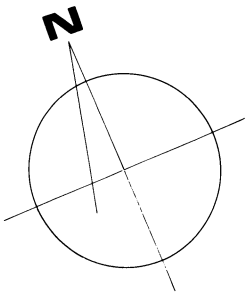

- Ⓐ Main Ring
- Ⓑ Injection tunnel (TT 10)
- Ⓒ Ejection tunnel (TT 60) to west exp. area
- Ⓓ Ejection tunnel (TT 20) to north exp. area
- Ⓔ Main control room
- Ⓕ Main electrical sub-station
- Ⓖ Power House
- Ⓗ Laboratories and Offices buildings
- Ⓘ Assembly hall
- Ⓛ Water reservoir and pumping station
- Ⓜ Lake water pipeline
- ①②③④⑤⑥ Auxiliary buildings and access pits
- ⑦ Civil engineering shaft

Fig. 15.1 General site layout

Two beam transfer tunnels will link the ring to laboratory I: one is a branch of the existing ISR and West Area Line (TT2), and will be used for injection while the other will return the high energy protons to the West Area.

The new laboratory is conveniently close to the existing highways and traffic centres:

6.7 km from the Geneva Airport and autoroute Geneva-Lausanne
3.4 km from the Geneva-Lyon highway
9.7 km from the Geneva main railway station

Good road connections with Laboratory I and with the main road network are needed for the staff and for the delivery of goods and supplies. An extensive use has been made of the existing road system. It will not be necessary to ask for new public road works, apart from improvement, widening and development of crossroads on the existing network. Some new secondary roads are of course needed to serve some of the buildings of the new project (see Fig. 15.1). A new entrance will be opened in Laboratory I's fence to connect it directly to Laboratory II (2.7 km).

15.2 Accelerator buildings

These include the main ring tunnel, together with its access pits and auxiliary buildings, and also the injection tunnel from PS and ejection tunnels to West and North Experimental Areas (see Fig. 15.1). This programme has been launched.

15.2.1 Main ring tunnel

Of an average diameter of 2.2 km, the main ring will have a developed length of 6910 m consisting of:

6450m of normal cross-section (see Fig. 15.2)
460m of enlarged cross-section where the injection and ejection tunnels join the main ring (see Fig. 15.3)

The bottom level of the main ring is at an elevation of 400 m above sea level, corresponding to a depth below the surface which varies between 23 m and 65 m. The main ring tunnel will be entirely built in the molasse rock, with a minimum of 11 m of molasse cover on top, plus the layer of moraine up to the surface.

The normal cross-section (see Fig. 15.2) will have a net internal diameter of 4m corresponding to a diameter of 4.80 m for the boring allowing a concrete lining thickness of about 30 cm. This lining will consist of two parts: an external shell made of precast concrete slabs 15 cm thick fixed to the rock by means of cement injection and an internal shell of the same thickness made of cast concrete. A metal liner placed between the two shells will ensure

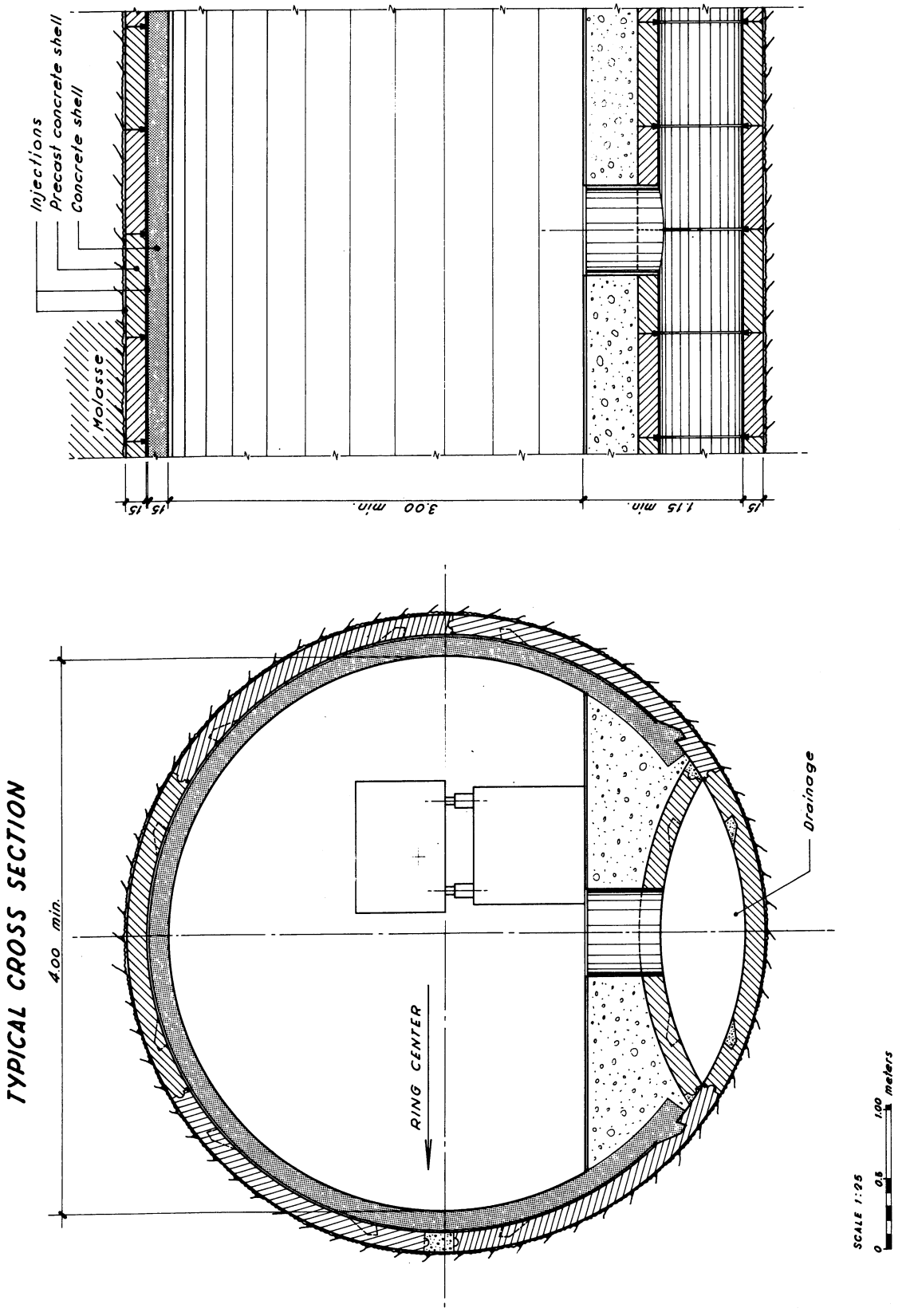

Fig. 15.2 Main tunnel

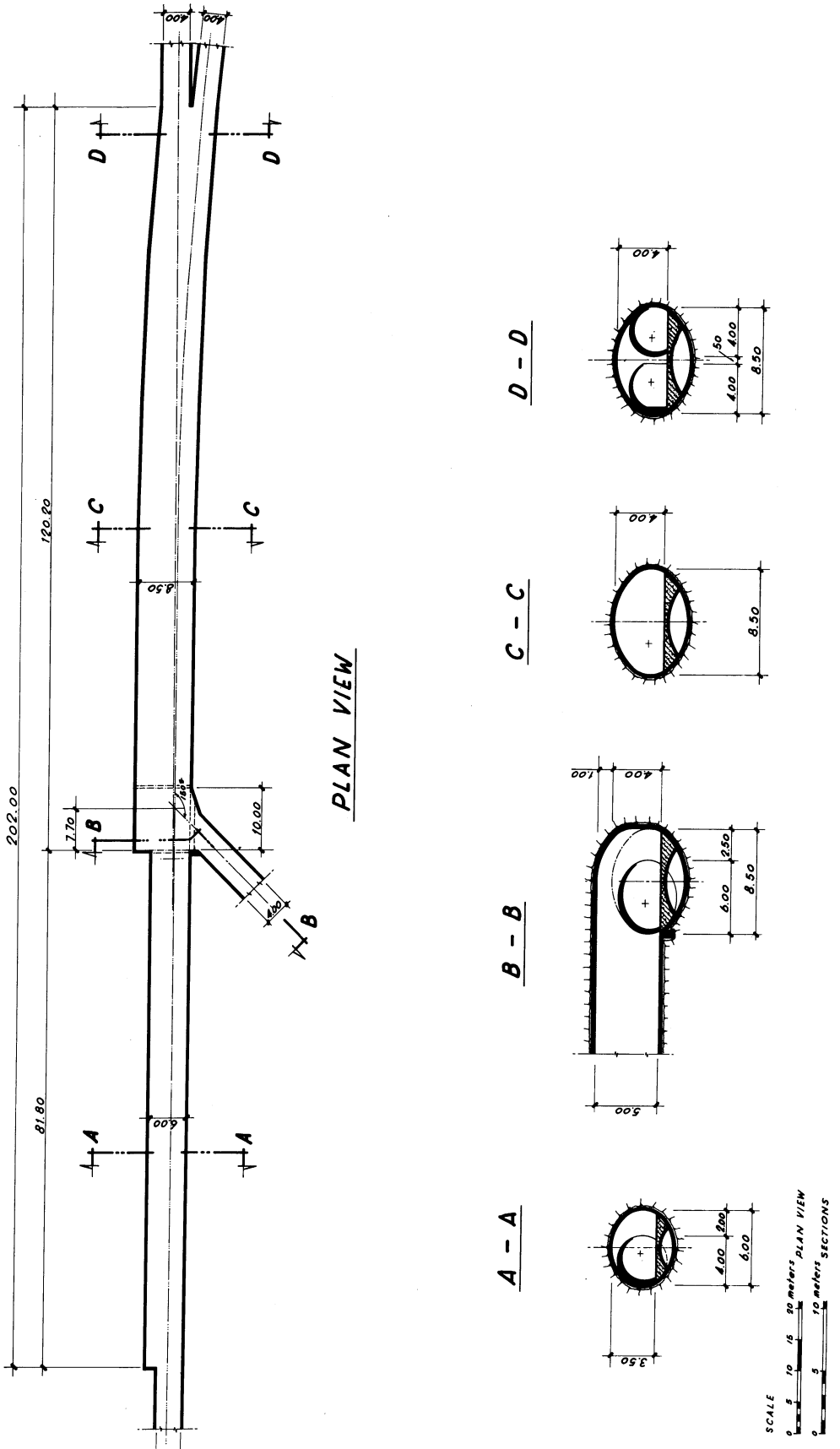

Fig. 15.3 Ejection regions LSS.2 and LSS.6

the water tightness . The second shell is also secured to the first and to a floor beam by cement injection, so that the whole system is rigidly jointed to the rock, in order to guarantee a perfect stability.

The excavation procedure will avoid disturbing the molasse layers and the use of explosives will be prohibited in the vicinity of the tunnel. The excavation of the tunnel will be executed by means of a full face boring machine of a type which has been extensively used especially in molasse.

The regions of the main tunnel which correspond to the three enlarged cross-sections joining to the injection and ejection tunnels (see Fig. 15.3) will be bored at first by the same machine used for the normal cross-section. In a second phase, a moving head boring machine will enlarge them to their final shape. Metal hoops and sprayed concrete will provide for a first shell completed by a second one made of cast concrete. The exact profile and the thickness of the liner and of the floor will be determined after more precise calculations.

15.2.2 Access pits (see Fig. 15.4)

The main ring tunnel will have six access points of similar design. At each point a 5 m wide pit will connect the auxiliary building on the surface to the machine level. This pit will be equipped with a 1 ton lift, emergency ladders and working platforms and will allow both personnel access and cable and pipe ducts. The pits will also serve as air-conditioning ducts, for either air inlet or outlet. Moreover, three pits (P2, P3 and P6) will be equipped with a shaft permitting the transport of the machine magnets by means of a crane (or a mobile gantry crane) and a special lifting device guided by means of rails fixed to the walls of the shaft.

The bottom of the pits will be connected to the main ring tunnel by a short tunnel (about 30 m long) of horse-shoe section to be constructed with the moving head boring machine. The connection between these access galleries and the main ring tunnel have to be shaped so that the large number of cables and pipes coming from the ground level can pass over the machine magnets to the trays installed on the opposite wall of the main tunnel.

15.2.3 Auxiliary buildings

Six such buildings will be constructed on the access pits in order to house the rectifiers, power supplies, power sub-stations, beam controls and other control equipment, air-conditioning and ventilation equipment, heat exchangers etc. These buildings will not be identical, their dimensions vary according to the equipment to be housed at each point. The average dimension of the auxiliary buildings should be of the order of 1000 m^2. The construction type is assumed to be light, with steel structure and metal cladding. A double floor

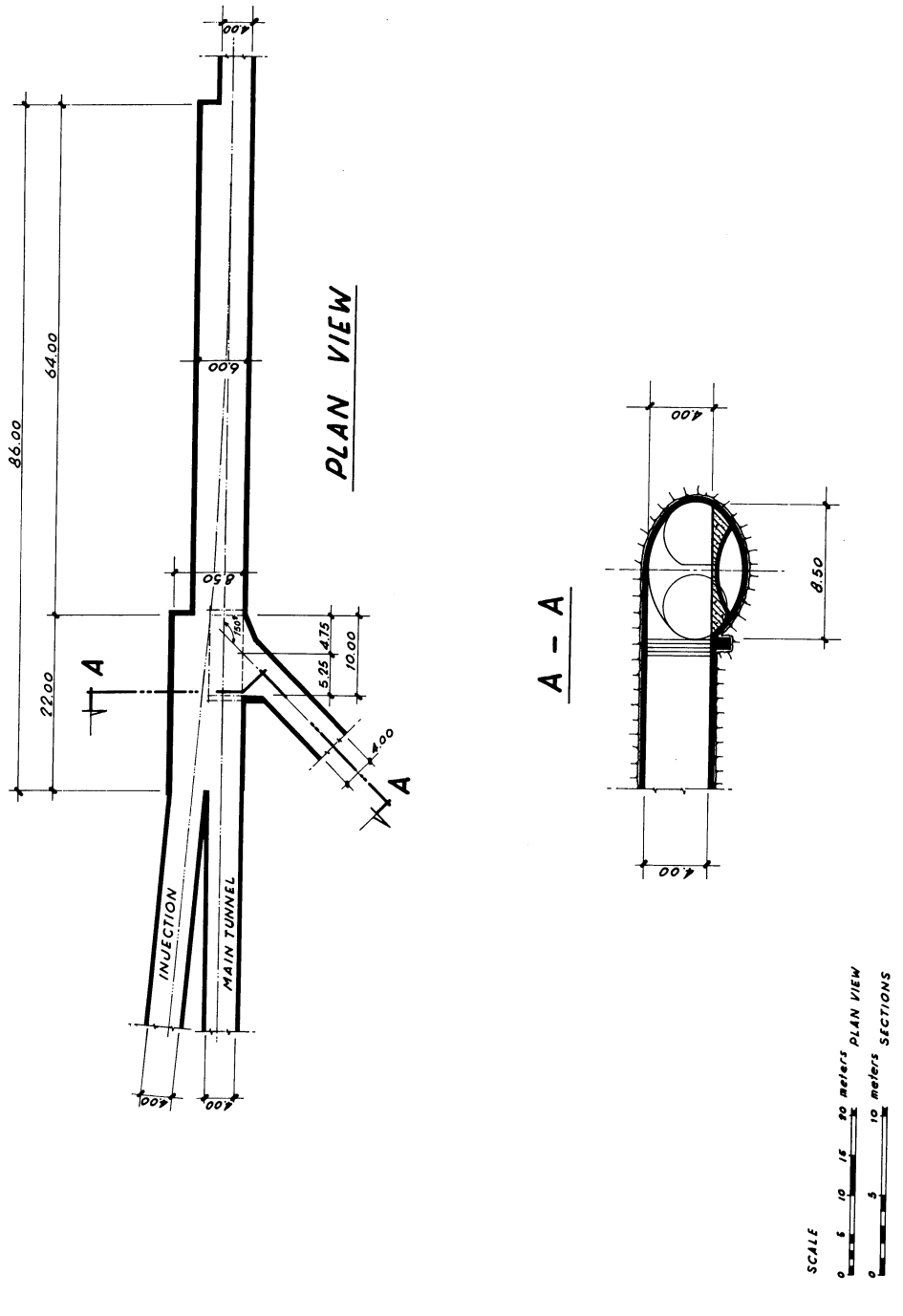

Fig. 15.4 Injection region

is planned, to allow the laying of cables and pipes connecting the equipment to the main ring tunnel. One of the six auxiliary buildings (P3, the one nearest to the main laboratory complex) will be combined with the Main Control Room.

The supply of water and electric power to these buildings and the controls coming from the Main Control Room will be provided by pipes and cables buried in the ground. Heating and air-conditioning will be independent for each building.

15.2.4 Injection and ejection tunnels (see Fig. 15.5)

There will be three tunnels:

(i) The 720 m long TT10 injection tunnel connecting the transfer tunnel TT2 of the ISR to the main ring tunnel;
(ii) the 709 m long TT60 ejection tunnel connecting the main ring tunnel to tunnel TT4 of the ISR towards the West Area;
(iii) the 420 m long TT20 ejection tunnel to the North Experimental Area, having a slope around 10%.

The cross-section of these tunnels is of the horse-shoe type, 4 m wide. The first tunnel, which is entirely contained in the molasse, will be dug with the moving head machine. It includes a shaft called Civil Engineering Shaft (PGC) placed at around 200 m from the injection point in the main ring tunnel. This shaft will be used to extract the material excavated from half of the ring and to bring in the precast elements and the concrete for the whole ring.

In the second tunnel, TT60, a switchyard has been added for splitting the EPB between slow EPB and r.f. The design of the switchyard is such that an underground neutrino facility may be linked to it if required. The precise design of such a facility is under study. In the tunnel the slow EPB and an r.f. separated beam run side by side.

In the case of the second and the third tunnels, the sections crossing the moraine layer will be excavated by classical means. Metal hoops, sprayed concrete and cast concrete will be used in a similar way to the one used for the enlarged sections.

15.3 Experimental areas

The utilisation of the synchrotron will be based upon two main experimental areas, which will come into operation at different times. Their development is discussed in Chapter 13.

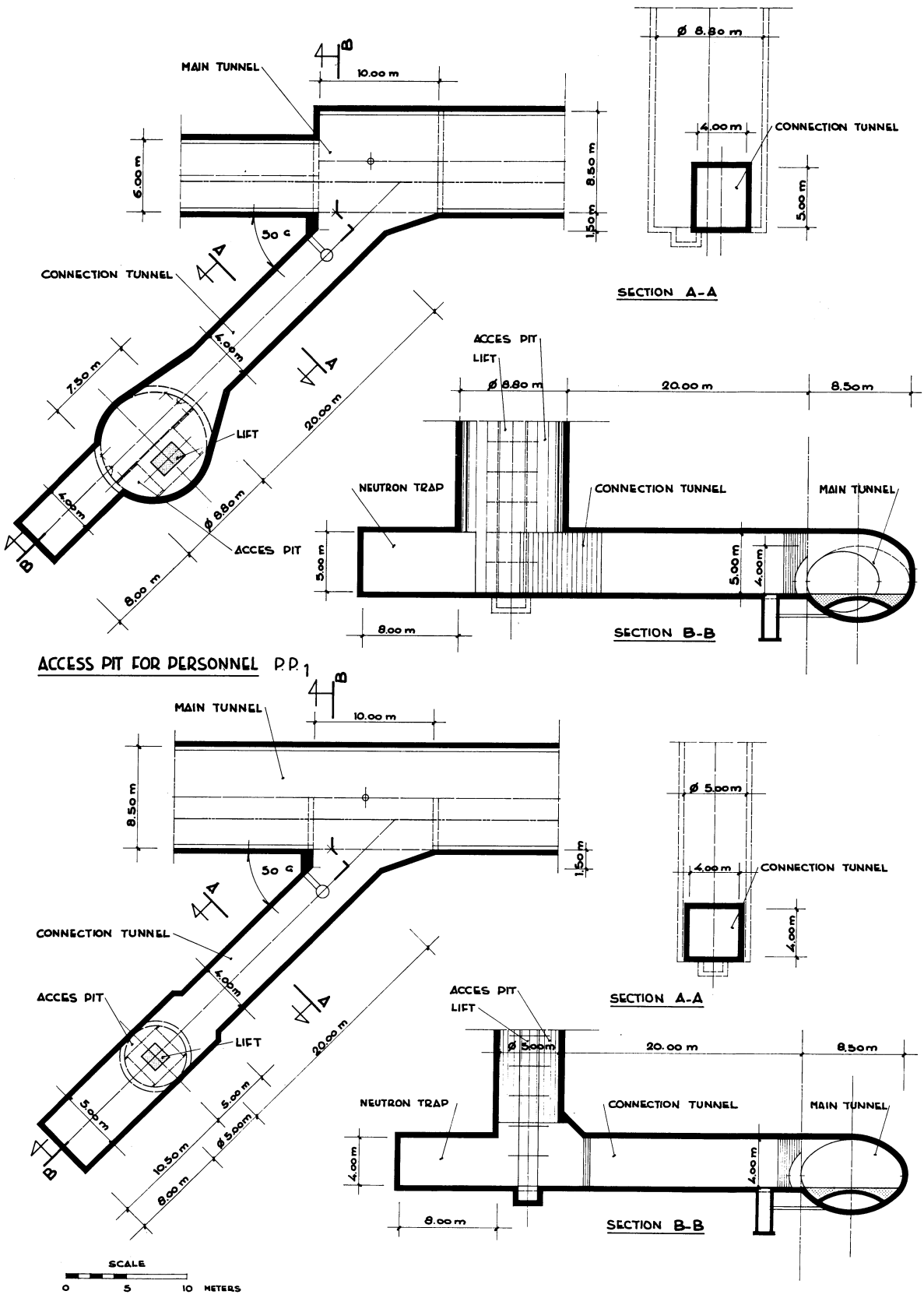

Fig. 15.5 Access pit for magnets and personnel

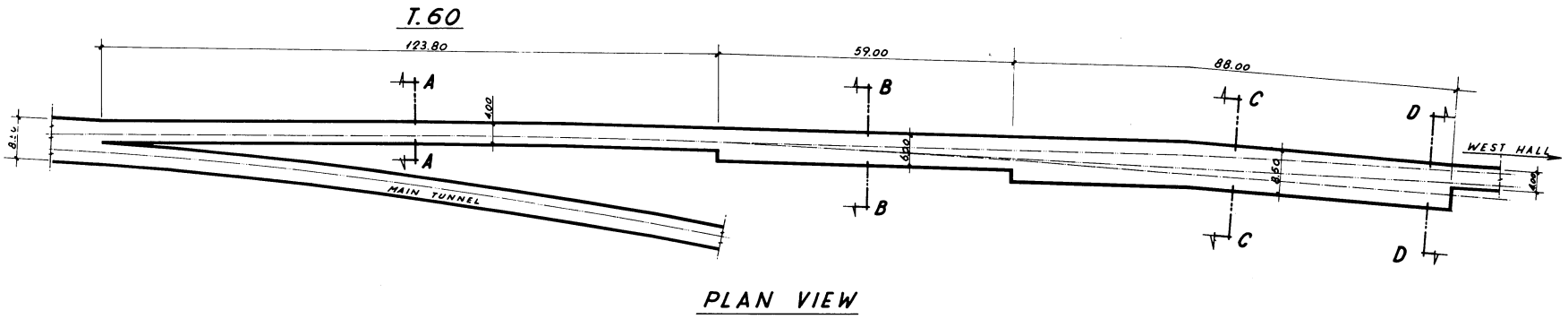

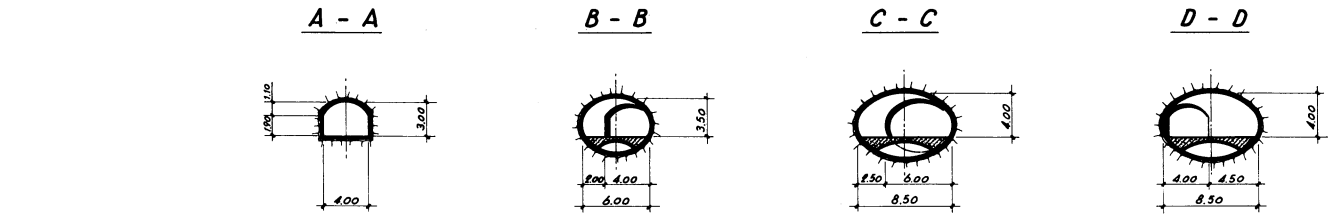

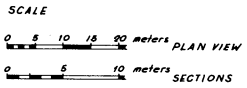

Fig. 15.6 West ejection tunnel

15.3.1 West experimental area

This area is the existing complex of buildings and facilities where 25 GeV physics with the CPS extracted beam will start in 1972. By the time of the commissioning of the 300 GeV synchrotron, the area will house two large experimental facilities, the 3.5 m hydrogen bubble chamber (BEBC) and the magnetic spark chamber system (Omega).

The area will be fed by a proton beam from the SPS, ejected along the transfer tunnel TT60 and emerging in the TT4 and the West Hall at an angle of 60 mrad (see Fig. 15.6).

The chain of three experimental halls totals about 15000 m^2 and these are surrounded by aprons, roads, service buildings of various kinds.

The Main Experimental Hall (Hall E1) has a floor area of 10000 m^2, 65 m wide in a single span and about 150 m long, and is equipped with two large cranes (40 tons and 60 tons) with a 9.5 m high hooks.

15.3.2 North experimental area

The devlopment of this area is assumed to take place in the seventh and eight year of the Programme. For this reason, the design of this area isstill in a preliminary stage and only some general ideas can be presented here. The proton beam will be ejected along TT20, a tunnel reaching the ground some 430 m from the ring.

The proton EPB will be kept at 5 to 10 m below the ground surface, running in a shielded duct. The target stations too will be underground with relevant earth cover for shielding.

Because the length required for their separation and analysis is of the order of several hundred meters, the secondary beams should also run underground tunnels until they reach the experimental area. This area could consist of an apron 30 m x 250 m, and situated several meters below ground for shielding reasons.

Extensive studies of the new experimental facilities will be made, to minimize the civil engineering and the distribution costs.

15.4 Laboratories, offices and other facilities

15.4.1 Laboratory complex

Fig. 15.7 indicates general layout of these various buildings which would consist of five buildings of 2 floors above ground floor, totalling 25000 m^2 gross surface and an assembly hall of 11000 m^2.

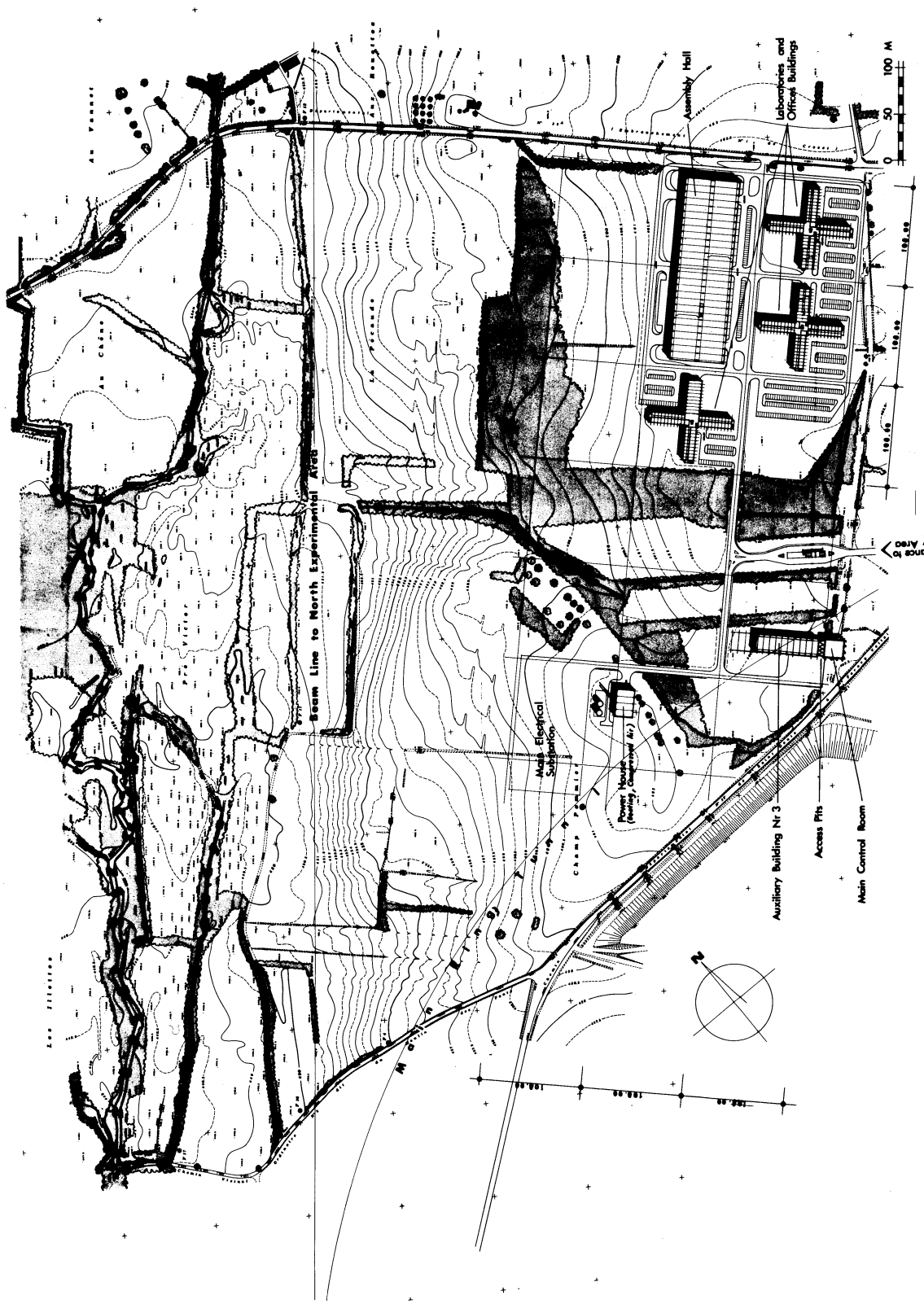

Fig. 15.7 Layout of laboratory area

In the first stage, three buildings and the assembly hall will be built, the remainder of the construction being spread out over the 8 years of the Programme. The buildings will be located according to a rectangular regular network enabling them to be connected up by a simple network of straight service tunnels and roads.

The layout of the premises (see Fig. 15.8) will be such that offices, laboratories, small workshops, computer rooms, small assembly halls, library, conference rooms, canteen etc., can find their place without the need for any external modifications. These low buildings (about 10 m high) will ensure harmony with the existing trees in the area, which will be preserved.

Construction methods for these buildings will use prefabrication for the obvious reasons of speed of construction and economy due to standardization.

The assembly hall will be of a conventional construction and will have the same height as the five-office laboratory buildings. It will consist of two bays of 29 metres equipped with three cranes, one of 30 tons and two of 15 tons (lifting height 6 m). It will be used for the tests and assembly of all the major components of the machine, but also the general stores and goods delivery.

15.4.2 Other facilities

Fig. 15.7 shows the other constructions in the same area and in particular:

(i) main electrical sub-station
(ii) main house
(iii) contractor's site

These three facilities are planned to serve the North Experimental Area as well as, in the first stage of the construction, to provide temporary electricity and heating supplies for the first three office buildings, the assembly hall and the contractor's site installations. The latter will be located so as to spoil as little as possible the general appearance of the site.

15.5 Supplies and services

15.5.1 Electricity

Power to the new laboratory will be provided by means of a single 380 kV line about 30 km long linking CERN to Génissiat, the nearest production and distribution centre of Electricité de France. Both the pulsed power supply for the ring magnet and the steady load for conventional consumers can be supplied from this single line without inconvenience.

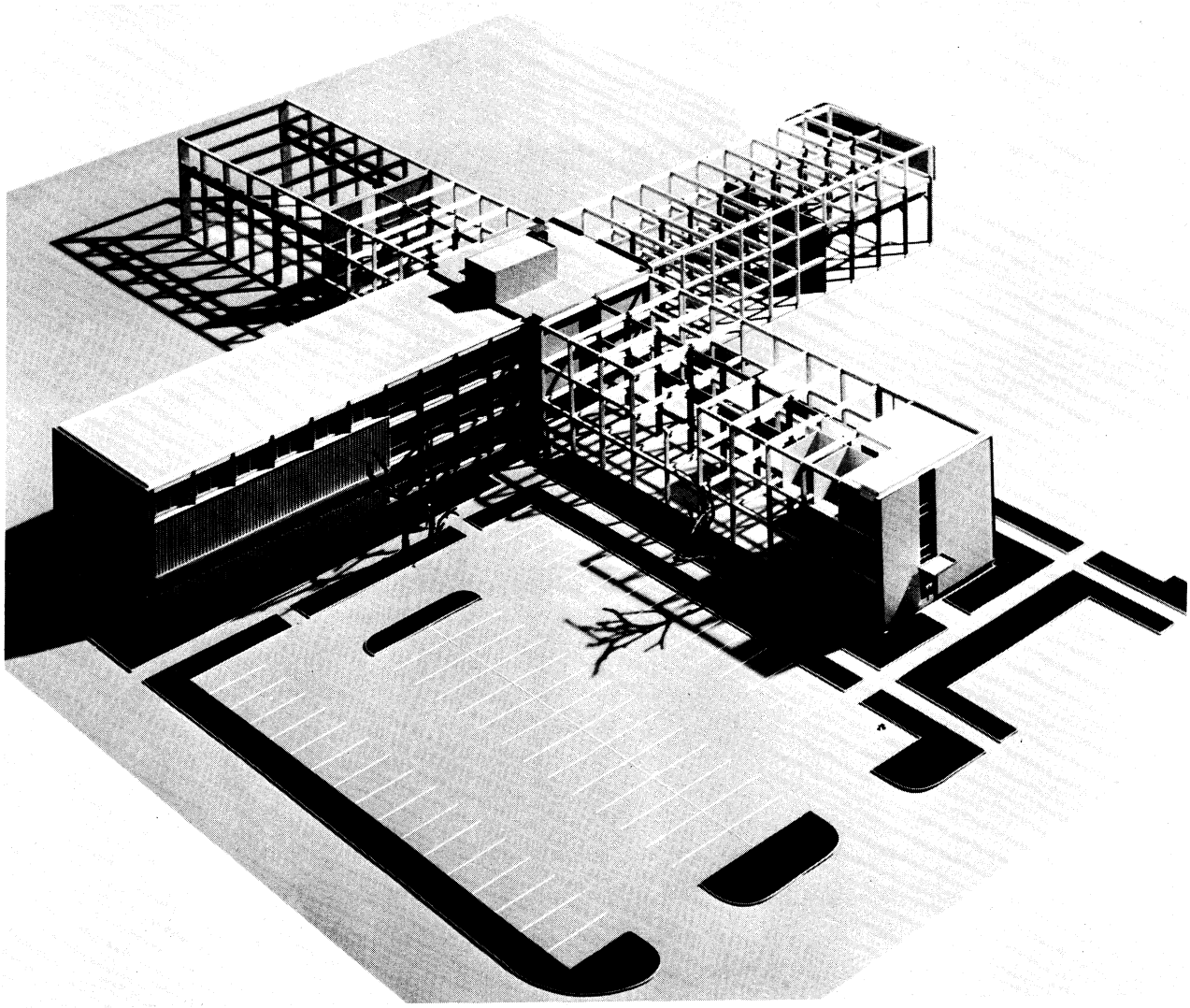

Fig. 15.8 Laboratories and offices building

In the first stage two transformers will be installed, their main parameters being:

unit output	80 MVA
voltage ratio (without load)	380 ± 11% / 19 KV
coupling	star-delta
with on-load tap changer	

The space for a third transformer is foreseen.

As far as the medium voltage is concerned, 18 kV has been adopted, i.e. the same voltage as in Lab. I, as this simplifies the interchanging of equipments between the two laboratories. Each unit will feed one separate single busbar system, transformer No. 1 supplying the machine magnets and the RF pulsed power while transformer No. 2 will feed the general facilities, laboratory installations and the future North Experimental Area. In case of a breakdown of one transformer or for maintenance purposes the other one will feed both busbars at a reduced rate.

Since the completion of the main sub-station is only foreseen in 1974, an 18 kV cable between the two laboratories will be installed in 1972 in order to supply laboratory II with 10 MVA as an interim measure. Later on this cable could operate as an emergency link.

The 18 kV distribution schemes to the machine are different for the two busbar systems.

While each one of the 12 main magnet power supplies located in 6 auxiliary buildings around the ring is linked directly to the distribution board No. 1, the 6 conventional power sub-stations located in the same buildings will be fed by a loop coming from distribution board No. 2. This loop will also energize the pumping station beneath the water reservoir and the equipment for the beam transfers via sub-stations No. 1 (injection), 6 (ejection to Lab. I facilities) and 2 (ejection to the North Experimental Area).

Later on, the North Area itself may be energized by another loop coming from the same distribution board, which will also feed the office and laboratories zone via an independent cable.

Important features of the distribution system are the type of 18 kV cables and the way they will be installed. Cross-linked polyethylene insulated, single conductor aluminium cables are foreseen. They will be buried in trenches except in the zone of general facilities where they will be laid on cable trays in the galleries.

15.5.2 Water supply and cooling

A draft design, studied in collaboration with the Services Industriels de Genève, envisages a supply of water from the Geneva lake with the following characteristics:

The water flow required will be 1000 ℓ/s of which 700 ℓ/s will be needed for cooling machine components (magnets and their power supplies, RF equipment, etc.) and 300 ℓ/s will be for general use in the laboratories, the assembly hall and the power house.

The water intake will be at 40 m depth in the lake, about 3 km off "Le Vengeron" in the Canton of Geneva, where the temperature is 12° C or less for as much as 95% of the year. It will be filtered and chemically treated in a water treatment and pumping station to be built near the shore of the lake at "Le Vengeron", thus excluding all contamination of piping and equipment. The treated water will be pumped through approximately 9300 m of cast iron or steel pipeline into an underground reservoir of a volume of 10000 m^3 situated on Swiss territory near one of the access pits of the ring (see Fig. 15.1).

Another pumping station installed on or near this reservoir will feed into a buried pipe network which will supply the water to each of the 6 auxiliary buildings and to the office and laboratory complex. At each of the hexagonal points of the ring, either in the auxiliary building or at the bottom of the access pit, the primary water will flow through appropriate type of heat exchangers to cool the secondary, demineralized water to be circulated through the magnet coils and other components. By-passing through these heat exchangers the primary water will be heated to a temperature of 28° C maximum. Part of it will then be reused as cooling tower make-up for experimental equipment cooling. All waste water only thermally polluted will be collected on the site by a separate piping system and conveyed to the Rhône river.

15.5.3 Telephones

By a special agreement between the French and Swiss Telecommunication Offices, CERN has been allowed to extend the Laboratory I exchange to accommodate 800 lines for Laboratory II uses. A cable will be installed connecting the two Laboratories.

The system will be brought to 1500 lines in the future when needed.

15.5.4 Heating of offices, laboratories and assembly hall

A central medium temperature water heating plant near the west end of the office and laboratory area (labelled Power House in Fig. 15.7) will be equipped, in a first phase, with two boilers of 4 Gcal/h capacity each. From this plant water at 160° C will be distributed to the office and laboratory buildings, the assembly hall and to the main control room.

In each of these buildings appropriate heat exchangers, as well as mixing stations will ensure the supply of hot water at adequate temperature for the different services, namely:

(i) heating of offices and laboratories by hot water radiators,
(ii) heating of the assembly hall by radiant panels and unit heaters,
(iii) heating for air-conditioning in the main control room.

Hot water for sanitary purposes will be prepared locally by electric boilers.

15.5.5 Air-conditioning of the main ring tunnel

It turns out that the heat loss through the tunnel walls, at moderate air temperature and stabilized conditions, will be almost negligible and just about enough to compensate the heat gain due to lighting. It is thus obvious that all the heat liberated by machine components (magnets and their connections, RF equipment, cables, etc) must be conveyed to the surface by some heat-carrying medium (water or air).

It is envisaged to extract heat exclusively via the cooling water. In addition, an air-conditioning system will then be installed for air renewal, filtration of the air introduced into and extracted from the tunnel and for control of temperature and humidity of the air introduced into the tunnel.

Air treatment plants will be located in three of the six auxiliary buildings. Each of these plants will comprise a refrigeration system, an outside air fan, air filters, a cooling and dehumidifying coil and heating coils. Outside air will be brought into the tunnel through these plants and through the adjoining access pits. The air, upon leaving the apparatus, will have approximately room temperature and a dew point low enough to compensate moisture gain due to uncontrolled infiltration of humid outside air, diffusion of water vapour through walls and accidental spilling of water inside the tunnel. Heating in the winter will be done electrically and the condensers of the refrigeration systems will be used for reheating the cooled and dehumidified air in the summer.

Extraction fans and filters will be located at the top of the three remaining access pits.

The air conditions in the tunnel aimed at are:

dry bulb temperature : max. 25° C
dew point temperature : max. 12° C

Care will be taken to keep temperature gradients along the tunnel axis to a minimum.

Chapter 16

TIME SCHEDULES, MANPOWER REQUIREMENTS AND COST ESTIMATES

16.1 Introduction

At the time of writing the programme has been in operation for close to one year and it is therefore useful to compare the original forecasts with the present situation. Any new forecast for the coming years will obviously be more accurate than the one made one year ago.

During 1971 the staff has grown from 4 to 100 staff members, and another 39 posts have been committed. All the appointments to the Group Leaders posts were made by June, in September all the Group Leaders were working full time at CERN, the Selection Board system for recruiting other staff began in June. This rapid build-up of staff undoubtedly reflects the great interest taken in the new Laboratory by European phycisists and engineers working in this field.

The groups now formed on the site have taken over the activity carried out in 1970 by the 300 GeV Machine Committee, a body which consisted of staff members of CERN and of the European national Laboratories who worked part time on the project. It is rewarding to note that the leading parameters are now frozen, a number of various technical solutions have been analysed and final choices have been made. At the same time some component models have been built and are in the process of being tested. It appears therefore that the original forecast for the progress to be achieved in the first year of the programme has in fact been completed.

The boundary conditions have remained unchanged :

(i) The duration of the programme is 8 years and runs from February 19th 1971 to February 19th 1979.

(ii) The total cost of the programme cannot exceed 1150 MSF at 1970 costs and fixed prices. However, due to the late start of the programme compared with what was expected, the yearly budgetary profile has had to be adjusted and is now estimated as the following in 1970 prices (see CERN/FC/1408) :

1971	1972	1973	1974	1975	1976	1977	1978	1979	Total
28.0	86.1	159.0	180.0	175.0	165.0	165.0	165.0	26.9	1150

(iii) The operating energy of the machine will be at least 300 GeV with an intensity of at least 10^{12} protons per second.

(iv) A 200 GeV proton beam will become available for research in the West Hall during the sixth year of the programme, but it could be of 300 GeV energy, depending on the decision to be taken in 1973-1974.

(v) The energy of the beam feeding the North Experimental Area shall have a value of at least 300 GeV and be available for research at the end of the programme, i.e. at the end of the eighth year.

16.2 Time Schedules

The method used in defining the schedules is essentially an iterative procedure. The first step in this process consists in an attempt to identify those components, procedures or operations which are most likely to be on the critical path of the programme. Secondly, the possible component schedules of the other elements are analysed, in order to check that they fit into the time scale set by the critical activities. During this part of the process it becomes increasingly important to find the points of interaction between the various functional elements. These "interfaces" are indeed important events in that they may interfere with the "normal" development of the different functional components. As a result of such an analysis, it may appear that other elements than those first considered are in fact imposing their own time scale and thus creating a new critical path. A new evaluation has then to be carried out and the process is repeated until a coherent picture emerges. It must however be pointed out that this picture is always changing, because of the essentially dynamic nature of the scheduling process. The results obtained at any given time must be fed back into the programme activities in order to modify priorities, reduce the duration of critical activities etc..

At present a number of conclusions can be drawn:

Firstly, as indicated in MC/60, it appears that the magnet is the component defining the critical path. This is due in part to the long lead-time for procurement of raw-materials, tooling and prototype testing, the essential feature being the sheer number of elements that have to be manufactured, assembled, checked and tested. It is expected that the following time scale will be possible :

- prototype construction and testing during the first half of 1972,
- contract awarded by autumn 1972,
- first magnet delivered at the beginning of third quarter 1973,
- first magnet installed in the tunnel by the end of 1973,
- last magnet in place in the tunnel during second quarter of 1975.

The functional elements most closely correlated with the magnet schedule are : the civil engineering construction programme (main assembly hall, tunnel complex), the vacuum system, the cooling water and power supplies and the control system.

These elements have been analysed and it appears that they can be fitted into the magnet time schedules. However, it also appears that the amount of slack is very limited, so that careful control will have to be maintained throughout the programme.

The other components are less dependent on the magnet programme, but are all tightly related to the civil engineering construction programme and the Control system. It thus appears that it is these two elements together with the magnet that will impose their time scale to the whole programme.

Finally, it is planned that beam tests will be possible during the second part of 1975 and that a 200 GeV proton beam will become available for research in the West Hall during 1976.

16.3 Manpower requirements and Cost estimates

In describing the scheduling process no mention has been made of the limitations which could be imposed by the available resources. These limitations could be due either to the available manpower, or to the annual expenditures now agreed for the Programme. It can however be seen that during the first part of the Programme - covering the construction and installation processes - the staff expenses are relatively small and increasing regularly with time. During this period, however, the capital expenditure is very great. It is therefore to be expected that the budgetary profile could impose limitations if the rate of required capital expenditure is too high, or irregular. The limitations imposed by lack of sufficient staff is likely to be due to recruiting difficulties rather than to budgetary considerations. It has however already been mentioned that no difficulties of such a nature have yet been met. The expected build-up of staff working for the Programme is given in Fig. 16.1

It is to be pointed out that a significant part of the required man-years will be provided by Laboratory I staff, especially in the administrative and services groups.

The cost estimates of the programme are given in the table of Fig. 16.2, which indicates the breakdown according to functional elements. During 1971, as the design of the different components proceeded, the costs of these elements was constantly revised. The new costs are more reliable both because of the greater amount of detailed work and of continuous contacts with industry during the initial enquiry processes. The detailed costs of the elements have had to be revised, but the general costs of the functional units have changed remarkably little.

They can therefore be considered as reasonably reliable and are given in Fig. 16.2 rather than the more detailed costs which might be more easily subject to fluctuations.

A check was carried out and it was ascertained that, with the proposed time schedule it will indeed be possible to avoid annual over-expenditures with respect to the profile given in CERN/FC/1408.

16.4 Conclusions

As required by the time scale of the programme, the first two large civil engineering contracts have been awarded, and the staff of the new laboratory has been built up at a rapid rate during the first year. The design and studies carried out by the new groups, while leading to modifications of some aspects of the scheduling and cost estimates, do not change the overall forecasts in a significant manner.

Staff at the end of each year

	1971	1972	1973	1974	1975	1976	1977	1978	1979
Machine Group	82	270	365	400	450	475	475	500	500
"Services" Group	44	145	197	215	242	255	255	270	270
Total	126	415	562	615	692	730	730	770	770
Man-years	63	270	488	588	653	711	730	750	100 *

* The programme covers man-years in 1979 up to 19 February 1979

Fig. 16.1

Cost Estimates (1970 costs and constant prices)

		Stage A (200 GeV)	Stage B (300 GeV)
1.	Machine Equipment	201.1	271.5
2.	Civil Engineering, Aux. Equip. & Installation	138.6	140.6
3.	North Experimental Area development	-	143.2
4.	Lab. Equipment & Tools	24.0	50.0
5.	Personnel (Staff & Régie)	178.0	311.1
6.	Machine operating costs	10.0	100.0
7.	Contingency	82.0	133.6
	Total (MSF)	633.7	1'150.0

Fig. 16.2

ANNEX I - LIST OF PARAMETERS

Lattice and Orbit Parameters

	A	B	C	
Maximum momentum	200	300	400	GeV/c
Maximum bending field	1.8	1.8	1.8	T
Magnetic bending radius	370.6	555.9	741.3	m
Mean radius	1100	1100	1100	m
Injection momentum	10	10	10	GeV/c
Injection field	0.090	0.060	0.045	T
Number of bending magnets per normal period	4	6	8	
Quadrupole gradient for Q = 28.75 F	10.0	14.9	19.9	T/m
D	9.9	14.9	19.9	T/m
Quadrupole gradient for Q = 27.75 F	9.7	14.5	19.4	T/m
D	9.7	14.5	19.4	T/m
Nominal length of quadrupoles			3.220	m
Nominal length of bending magnets			6.260	m
Length of inter-magnet gap			0.400	m
Length of short straight section			2.225	m
Free length between quadrupoles			28.78	m
Length of period			63.994	m
Structure of a period			FODO	
Number of periods			108	
Number of superperiods			6	
Gamma transition (Q = 27.75)	23.78	23.33	24.08	
Gamma transition (Q = 28.75)			24.95	
Nominal working point			27.75	
Lattice functions for Q = 27.75				
Phase advance per period			92.50	deg.
Maximum β in F quadrupole			108.9	m
Maximum β in D quadrupole			109.0	m
Minimum β in D quadrupole			18.0	m
Minimum β in F quadrupole			18.0	m
Maximum of momentum compaction function			4.25	m
Minimum of momentum compaction function			-0.03	m

Tolerances (r.m.s.)

Misalignment of quadrupoles	0.15	mm
Random error in bending field ($\Delta B/B$)	5.10^{-4}	
Random tilt in median plane of magnets	0.2	mrad
Stray horizontal field (Bx)	0.12	G
Stray vertical field (By)	0.28	G
Unocrrected closed orbit distortion amplitude (horizontal)	33.0	mm
(vertical)	18.7	mm
Probability of this amplitude being exceeded	2	%
Random error in quadrupole strength ($\Delta K/K$)	2.10^{-3}	
Increase in beam size due to $\Delta K/K$	3	%
Systematic error in field of bending magnets (half width)	3.10^{-4}	
Systematic error in gradient of quadrupoles (half width)	4.10^{-3}	
Horizontal half aperture at β_{max} and α_{max}	62.5	mm
Vertical half aperture at β_{max}	24.5	mm

Magnet System

Magnets	B1	B2	
Nominal peak field	1.8	1.8	T
Magnetic length	6.260	6.260	m
Aperture height	39	52	mm
Aperture width	129	92	mm
Core length	6.220	6.200	m
Lamination height	2×225	2×225	mm
Lamination width	800	800	mm
Packing factor	0.96	0.96	
Core weight	16	15.5	ton
Coil length (overall)	6.507	6.476	m
Number of turns	12	16	
Conductor inner coil	24×33	32×22.5	mm^2
Conductor outer coil	32×32	33.5×33.5	mm^2
Cooling hole inner coil	6.5	10.2	mm
Cooling hole outer coil	10	11	mm
Number of water circuits	3	3	
Amount of cooling water	1.9	2.59	m^3/h
Temperature rise	14	14	^oC
Copper weight	1.38	1.88	ton

Peak ampere turns	58.8	78.4	kA
Peak current	4.9	4.9	kA
R.m.s. current	3.1	3.1	kA
R.m.s. current density	3.42	3.36	A/mm^2
Resistance at $20^{\circ}C$	3.23	4.42	mΩ
Inductance (maximum)	7.73	9.9	mH
Losses	31.1	42.3	kW
Peak stored energy	88.2	113	kJ
Ampere turns in iron (1.8 T)	5	5	%

Quadrupoles (QF, QD)

Peak gradient	19.9	T/m
Magnetic length	3.220	m
Radius of inscribed circle	44	mm
Core length	3.130	m
Lamination height	800	mm
Lamination width	800	mm
Packing factor	0.96	
Core weight	9.6	ton
Coil length (overall)	3.300	m
Number of turns per pole	11	
Conductor dimensions	26×20	mm^2
Cooling hole diameter	6.2	mm
Copper weight	1.35	ton
Pressure drop	6	atm
Temperature rise	15	$^{\circ}C$
Peak current (Stage C)	1500	A
Peak ampere turns in iron	7	%
R.m.s. current density	1.95	A/mm^2
Resistance at $20^{\circ}C$	11.4	mΩ
Losses	10.24	kW
Peak stored energy	30	kJ

Number of magnet units required	A	B	C
B1 magnets	180	360	360
B2 magnets	192	192	384
Half length of B2 magnet	0	12	0
Quadrupoles (QF, QD)	216	216	216

Magnet Power Supply

Bending Magnets	A	B	C	
Number of rectifier stations	12	12	12	
Total peak voltage	21070	23540	25600	V
Peak current	4886	4886	4886	A
R.m.s. current	3102	3102	3102	A
Peak power	100	113	123	MW
Losses	16.7	22.6	30.4	MW
Total maximum magnet inductance	3.31	4.76	6.60	H
Total magnet resistance	1.44	2.35	2.86	Ω
Cable resistance	0.30	0.30	0.30	Ω
Quadrupoles (F + D)				
Peak voltage	6150	7370	8175	V
Peak current	700	1055	1501	A
R.m.s. current	450	659	947	A
Peak power	4.2	7.6	12.1	MW
Losses	0.7	1.5	3.1	MW
Total maximum magnet inductance	6.5	6.5	6.5	H
Total magnet resistance	2.48	2.48	2.48	Ω
Cable resistance	0.98	0.98	0.98	Ω
Public Supply Load				
R.m.s. load on EDF	48	57	70	MVA
Mean power from EDF	17.4	24.1	33.5	MW
Peak power from EDF	104	121	135	MW
Nominal Excitation Profile				
Injection and debunching	0.20	0.20	0.20	s
Front porch	0.19	0.19	0.19	s
Rise with round off	1.11	1.71	2.35	s
Flat top	0.70	0.70	0.70	s
Decay with round off	0.62	0.83	1.07	s
Recovering time	0.54	0.46	0.26	s
Peak dB/dt	1.50	1.00	0.75	T/s
Total cycle time	3.36	4.09	4.77	s
Peak (dB/dt)/B	8.33	8.33	8.33	s^{-1}
Minimum cycle time with 2 s flat top	6.59	7.31	8.00	s

Tolerances (half width)

on B field, injection	3.10^{-4}	
on B field, flat top	1.10^{-4}	
on quadrupole field, injection	3.10^{-4}	
on quadrupole field, flat top	1.10^{-4}	

Accelerating System

Number of r.f. cavities	3	
Total r.f. power per cavity	500	kW
Harmonic number	4620	
Frequency at gamma transition	200.225	MHz
Frequency swing (10 GeV/c injection)	0.44	%
Peak volts/turn (1.10^{13} ppp)	5.4	MV
Peak r.f. volts at injection	4.0	MV
Synchrotron frequency (injection)	2.0	kHz
Front porch bucket limit	0.22	rad
Maximum $\Delta p/p$ in PS beam (half)	$1.64.10^{-3}$	
Maximum $\Delta p/p$ after trapping (half)	$2.4.10^{-3}$	
Maximum rate of rise of momentum	166.7	GeV/s
Maximum beam loading	270	kW
Phase angle (nominal maximum)	45	deg.
Phase angle (start front porch)	1.1	deg.
Front porch time	190	ms
Momentum at end of front porch	19.63	GeV/c
Interaction length of cavity	18.70	m
Diameter of cavity	0.80	m
Cells per cavity	50	
Phase advance per cell (transition)	$\pi/2$	
R/Q	650	Ω/m
Cavity shunt impedance (effect)	11	MΩ
Group velocity/c	0.088	
Beam phase slip (injection)	-180	deg.
Beam phase slip (porch end)	-14	deg.
Beam phase slip (β = 1)	44	deg.
Cavity temperature for γ = 24	27	^{o}C
$d(\gamma)/dt$	-0.2	^{o}C

CPS Extraction System

General parameters with bunch by bunch extraction		
Transfer momentum	10.0	GeV/c
CPS cycle time for 10 GeV/c	700	ms
CPS minimum acceleration time	250	ms
CPS beam intensity	1.10^{13}	ppp
CPS beam momentum spread (half)	$1.3.10^{-3}$	
CPS beam emittance (H × V)	$7\times3.4\times\pi$	mm mrad
CPS beam bunch frequency	9.5	MHz
Bunch by bunch extraction		
Number of bunches	20	
Transfer time (upper limit)	4	ms
Transferred momentum spread (half)	$1.3.10^{-3}$	
Transferred emittance (H × V)	$7\times3.4\times\pi$	mm mrad
Debunching time in main ring	130	ms
Fast kicker rise time	70	ns
Fast kicker fall time	73	ns
Fast kicker pulse length	105	ns
Fast kicker deflection	1.5	mrad
Fast kicker length overall	2.30	m
Magnetic septum deflection	30	mrad
Magnetic septum length	2.30	m
Extraction of a debunched or prebunched beam		
Transfer time	23	µs
Maximum transferred $\Delta p/p$ (half)	$0.5.10^{-3}$	
Transferred emittance (H × V)	$2.3\times3.4\ \pi$	mm mrad
Fast kicker rise time per step	100 to 250	ns
Fast kicker pulse length	23	µs
Fast kicker deflection	0.5	mrad
Fast kicker length (each)	0.80	m
Electrostatic septum deflection	0.7	mrad
Electrostatic septum length	0.80	m
Magnetic septum deflection	30	mrad
Magnetic septum length	2.30	m

Injection into SPS (10 GeV/c)

Inflector		
Number of magnets	2	
Magnet length	1.40	m
Magnet aperture (H × V)	50×48	mm
Magnet inductance	1.83×10^{-6}	H
Magnetic field	0.054	T
Total deflection	4.5	mrad
Septum magnet		
Number of units	2	
Magnet length	2.00	m
Magnet aperture (H × V)	140×47	mm
Magnetic field	0.347	T
Total deflection	41.6	mrad

SPS Extraction System

SPS Beam before extraction	200	300	400	GeV
Betatron amplitude at maximum β_H	8.1	7.0	6.2	mm
Betatron amplitude at maximum β_V	6.2	5.0	4.5	mm
Half momentum spread × 10^{-3}	0.5	0.35	0.3	
Semi-aperture for Δp at α_{max}	2.4	1.9	1.41	mm

Extraction channel (400 GeV)

Electrostatic septum		
Thickness	0.15	mm
Length	9.0	m
Unit length	3.0	m
Units per tank	1	
Number of tanks	3	
Field strength	100	kV/cm
Aperture (H × V)	20×25	mm
Deflection	0.225	mrad

Correction Elements

Sextupoles			
Number		2×12(2×36)*	
Length of core		0.85	m
Strength		150	T/m^2
Overall length		1.0	m
Octupoles			
Number		(2×36)	
Length of core		0.55	m
Strength		12000	T/m^3
Overall length		0.7	m
Quadrupoles			
Number		(36)	
Length of core		0.2	m
Strength		21	T/m
Overall length		0.3	m
Dipoles			
Number		2×108	
Length of core		0.25	m
Strength	0.07	0.17	T
Overall length		0.4	m
Correcting Power Supplies			
Number		4	
Power each		300	kW
Beam Position Indicators			
Number		216	
Overall length		0.2	m
Observation error		0.5	mm
Centre line tolerance (r.m.s.)		1.0	mm

---

* The initial installation will be 2×12 units but space is reserved for up to 72 units.

Vacuum System

Vacuum Chamber Magnets	B1	B2	
Number (Stage A)	180	192	
Length	6.5	6.5	m
Thickness	2.0	1.5	mm
Tolerance on thickness (full band)	0.05	0.05	mm
Outside height	42.2	55.8	mm
Outside width	149.4	124.8	mm
Permeability	1.004	1.004	
Resistivity	74.10^{-6}	74.10^{-6}	Ωcm

Vacuum Chamber Quadrupoles	QF	QD	
Number	108	108	
Length	3.3	3.3	m
Thickness	2.0	1.5	mm
Tolerance on thickness	0.05	0.05	mm
Outside height	47		mm
Outside width	160		mm
Outside radius		43	mm
Permeability	1.004	1.004	mm
Resistivity	74.10^{-6}	74.10^{-6}	Ωcm

Pumping System		
Main ring pressure	10^{-7}	Torr
Ion pumps (50 ℓ/s)	432	
Rotary pumps	108	
Rotary pumps pressure	10^{-4}	Torr
Ion pumps (500 ℓ/s)	60	
Sublimation pumps (1000 ℓ/s)	27	
Turbomolecular pumps	21	
Number of gauge heads	250	
Number of gate valves	24	

Main Ring Tunnel

Standard Sections		
Total length	6.9	km
Diameter before lining	4.8	m
Lining thickness	0.3	m
Radius of curved sections (tunnel axis)	946.76	m
Beam height above floor	1.0	m
Centre line ASL	402.2	m

Long Straight 1 (Injection)	Sect. 1	Sect. 2	
Length	27	60	m
Width	4	8.5	m
Height	3	4.6	m
Rock cover		20	m
Earth cover		22	m
Access pit section		5×5	m
Long Straight 2 (North Extraction)			
Length	80	122	m
Width	6	8.5	m
Height	4	4.6	m
Rock cover		19	m
Earth cover		24	m
Access pit section	Magnet Pit		
Long Straight 3 (r.f.)			
Length		64	m
Width		6	m
Height		4	m
Rock cover		34	m
Earth cover		2	m
Access pit section	Magnet Pit		
Long Straight 4 (Dump)			
Length	80	122	m
Width	6	8.5	m
Height	4	5	m
Rock cover		48	m
Earth cover		5	m
Access pit section		5×5	m
Long Straight 5 (Spare)			
Length		128	m
Width		4	m
Height		3	m
Rock cover		12	m
Earth cover		7	m
Access pit section		5×5	m

Long Straight 6 (West Extraction)	Sect. 1	Sect. 2	
Length	80	122	m
Width	6	8.5	m
Height	4	4.6	m
Rock cover		32	m
Earth cover		4	m
Access pit section	Magnet Pit		